CALIX[4]PYRROLE AND PORPHYRIN-BASED MOLECULAR ASSEMBLIES.

Virginia Valderrey Berciano

Dipòsit Legal: T 1672-2014

Ph.D. Thesis

CALIX[4]PYRROLE AND PORPHYRIN-BASED MOLECULAR ASSEMBLIES

Virginia Valderrey Berciano

Supervised by Prof. Dr. Pablo Ballester Balaguer

Tarragona

November 2013

UNIVERSITAT ROVIRA I VIRGILI

ICIQ
Institut Català d'Investigació Química

Av. Països Catalans,16
43007, Tarragona, Spain
Tel +34 977920200 (Ext. 316)
Fax +34 977920221

UNIVERSITAT ROVIRA I VIRGILI
DEPARTAMENT DE QUIMICA ANALITICA I QUIMICA ORGANICA
C/ Marcel·lí Domingo s/n
Campus Sescelades
43007 Tarragona
Tel. 34 977 55 97 69
Fax 34 977 55 84 46
e-mail: secqaqo@urv.net

Prof. Dr. PABLO BALLESTER BALAGUER, Group Leader of the Institute of Chemical Research of Catalonia (ICIQ) and Research Professor of the Catalan Institution for Research and Advanced Studies (ICREA).

CERTIFIES that the research work entitled "Calix[4]pyrrole and Porphyrin-based Molecular Assemblies" that Virginia Valderrey Berciano presents to obtain the Ph.D. degree in Chemistry, has been carried out under my supervision in the ICIQ and fulfils all the requirements to be awarded with the "Doctor Europaeus" Mention.

Tarragona, November 2013

Prof. Dr. Pablo Ballester Balaguer

UNIVERSITAT ROVIRA I VIRGILI
CALIX[4]PYRROLE AND PORPHYRIN-BASED MOLECULAR ASSEMBLIES.
Virginia Valderrey Berciano
Dipòsit Legal: T 1672-2014

A mis padres,

Acknowledgements

Quiero comenzar esta tesis agradeciendo a todas las personas que de muy diversas maneras han contribuido a ella.

En primer lugar quiero agradecer al Profesor Pablo Ballester la oportunidad que me dio hace cuatro años de formar parte de su grupo de investigación. Por ayudarme primero a entender y después a participar en la construcción del maravilloso "mundo que va más allá de la molécula". Muchas gracias Pau por tu excepcional labor didáctica, tu comprensión y dedicación durante todo este tiempo.

Por otra parte, mi más especial agradecimiento a los presentes y pasados miembros de su grupo porque su apoyo y compañía a lo largo de estos años ha sido indispensable. A **Mónica Espelt**, con quien afortunadamente he compartido la totalidad del camino porque siempre me ha transmitido optimismo y tranquilidad. Echaré de menos nuestras conversaciones; ojalá algún día España se dirija hacia donde soñamos. A **Marcos Chas**, muchas gracias por tu amistad y tus consejos fuera y dentro del lab. A las chicas que pusieron la chispa de alegría a estos años: mi compañera del "Dúo Cómico" **Inmaculada Pintre**, **Moira Ciardi** y **Laura Hernández**. También a los que con su trabajo, han contribuido a los resultados de esta tesis. A **Gemma Aragay**, en particular por ayudarme a desvelar los entresijos de las porfirinas y en general por su ayuda incondicional al resto de la gente del grupo. A **Albano Galán** por aquellos fines de semana escuchando a Paco Ibañez mientras hacíamos flotar submarinos en la pecera del PB4. A **Louis Adriaenssens** a quien le agradezco sus enseñanzas en el laboratorio y su ayuda en el proyecto calixpirrol-porfirina. Y a todos los demás miembros y visitantes del grupo porque ha sido un placer trabajar con ellos: **Eddy**, **Dani**, **Nelson**, **Frank**, **Sasha**, **Carmela**, **David**, **Kilian** y **Martina**. Gracias a **Leti** y a **Ramón** que han llegado al final con nuevos aires de diversión para grupo. Finalmente, muchas gracias a **Beatriz Martín** por estar siempre ahí haciendo nuestro trabajo más sencillo. Mi más sincero agradecimiento también a todas las unidades de soporte a la investigación del ICIQ.

Gracias al Profesor **Christoph A**. **Schalley** por darme la oportunidad de hacer una estancia en su grupo y por su ayuda para llevar mi química a la fase gas. A **Dominik**

UNIVERSITAT ROVIRA I VIRGILI
CALIX[4]PYRROLE AND PORPHYRIN-BASED MOLECULAR ASSEMBLIES.
Virginia Valderrey Berciano
Dipòsit Legal: T 1672-2014

Sattler y **Luca Cera** por su ayuda y amistad durante aquellos fantásticos meses en Berlín.
Mi agradecimiento es también para mis profesores de la Universidad de Valladolid de quienes aprendí las bases necesarias para realizar esta tesis.

Muchas gracias a todos los amigos que desde la distancia me han apoyado durante estos años. A **Carmen Berciano** por compartir conmigo su sensibilidad moral. Cada una de nuestras conversaciones me llena de alegría y esperanza. A **Mayca**! por su apoyo durante la carrera y estos últimos años. A **Yannis**!, ragazzo dell`Europa y odioso siempre. Añoro nuestro tiempo en Italia, muchas gracias por las buenas palabras que siempre tienes para mí!.
Haber llegado hasta aquí ha sido únicamente posible gracias al amor y apoyo incondicional de mi familia. A **mis padres** porque siempre me habéis impulsado a seguir adelante y habéis creído en mí mucho antes de que yo misma lo hiciera. Gracias por darme siempre la libertad de ir por la vida a mi manera. A mi **hermana**, persona dulce de carácter fuerte, muchas gracias por tus consejos y por tu apoyo. A mi **abuela**, a mis **tíos** y **primos**. A mi tío **Fidel**, ejemplo de humildad y valentía. A la memoria de mi Abuelo **Tomás** porque nunca olvidaré tus manos cálidas y la sensación de pasear contigo por el monte de Destriana. Por último, quiero agradecer a **Tony Stüke**r su continua presencia durante este tiempo a pesar de estar a tantos kilómetros de distancia. Gracias por compartir conmigo tu manera tan especial de ver el mundo, tu sencillez y tu pasión por la naturaleza y la ciencia.

El trabajo recogido en esta tesis doctoral ha sido posible gracias a concesión de una Beca Predoctoral de Formación del Personal Investigador (FPI: BES-2009-029602) por parte del Ministerio de Economía y Competitividad y a la financiación del Institut Català d´Investigació Química (ICIQ) y de la Generalitat de Catalunya.

"In the preparation of receptors of these types, the imagination of the chemist is limited only by her or his synthetic ability"

J.W. Steed and J.L. Atwood, Supramolecular Chemistry,
J. Wiley & Sons: Chichester, 2000.

Table of contents

Chapter 1

General Introduction*

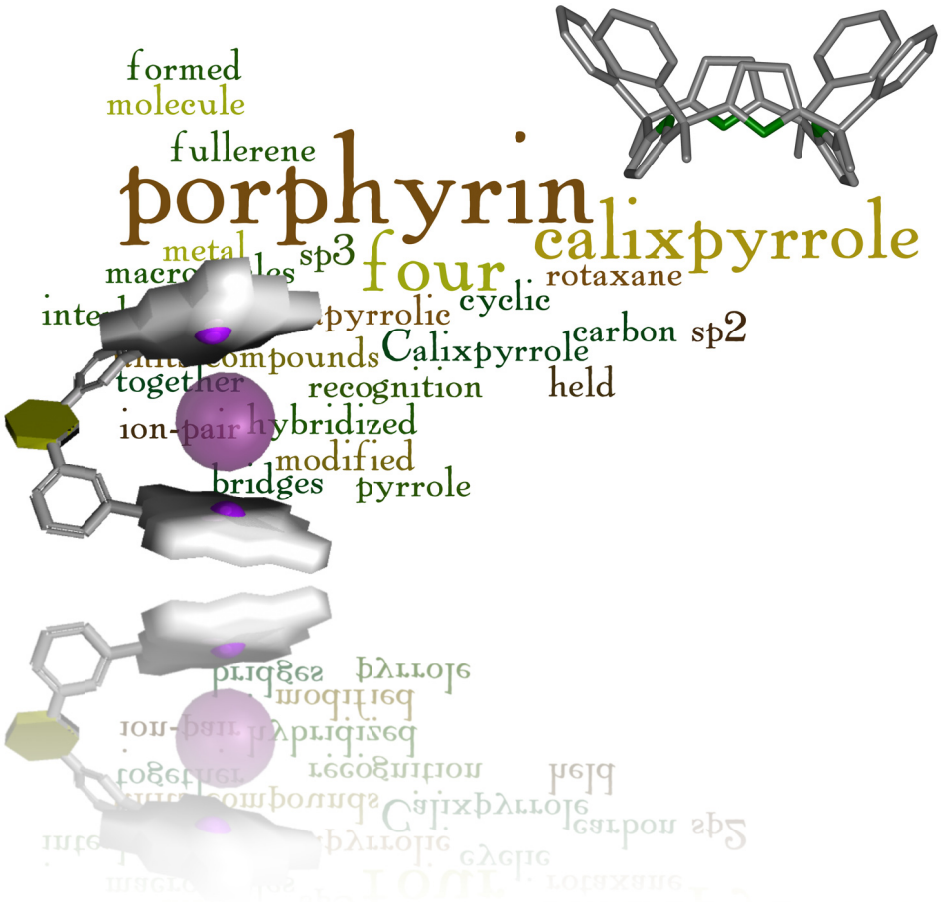

*Part of the content of this chapter is included in the publication:

Valderrey,V.; Aragay, G; Ballester, P. *Coord. Chem. Rev.* 258–259, **2014**, 137–156

1.1 General Introduction

1.1.1 Tetrapyrrolic macrocycles: calix[4]pyrroles and porphyrins

Calix[4]pyrroles and porphyrins are cyclic compounds formed by four modified pyrrole units held together by four sp^3 or sp^2 hybridized carbon bridges (*meso*-carbons), respectively. The macrocycles can be synthesized by an acid catalyzed condensation of pyrrole and an aldehyde[1,2] in the case of porphyins or a ketone[3], in the case of calix[4]pyrroles. The alkyl substituents at the *meso*-carbons of the resulting porphyrinogen in the latter prevent its further oxidation to the aromatic flat porphyrins. As a consequence calix[4]pyrroles are structurally similar to porphyrins but present different electronic properties (Scheme 1.1).

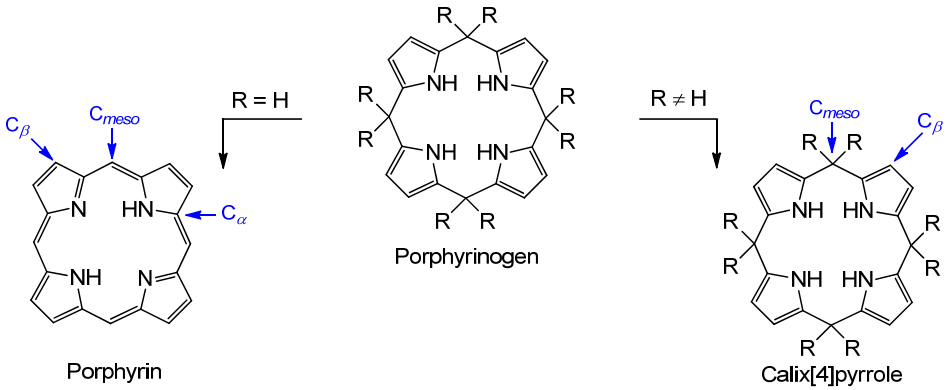

Scheme 1.1 Representation of the different behavior under oxidative conditions of porphyrinogens depending on the nature of its *meso* substituents (R = H or R ≠ H).

1.1.1.1 Calix[4]pyrroles

Calix[4]pyrroles are usually colorless and highly conformationally flexible molecules. The conformations arise on the basis of the relative orientation of the pyrrole units in the macrocycle: *cone, partial cone*, *1,3-alternate* and *1,2-alternate* conformation (Figure 1.1). In non-polar solvents the most favored conformation is the *1,3-alternate* conformation, while in more polar solvents the *1,2-alternate* conformation is the most populated.

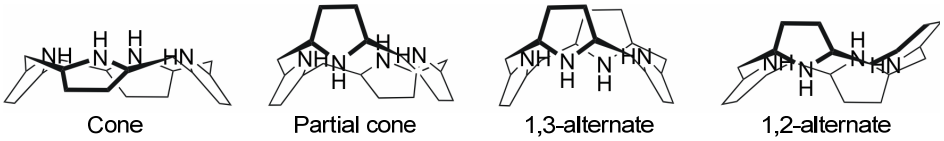

Figure 1.1 Representation of the possible conformations adopted by a calix[4]pyrrole core.

The *cone* conformation is generally the major conformation adopted upon the binding of electron-rich molecules (i.e anions, *N*-oxides) by means of hydrogen-bond interactions.[4] Then, considering the *meso*-octamethylcalix[4]pyrrole, the simplest calix[4]pyrrole, the binding of a ligand is dependent on the strength of the ligand-receptor interaction and also on the energetic cost require to arrange the calix[4]pyrrole core in the *cone* conformation. Both aspects are well known to be solvent dependent.[4] Calix[4]pyrroles can be functionalized at *meso*- and *β*-positions. Sessler has studied how the binding ability of *β*-functionalized calix[4]pyrrole receptors can be tuned according to the electronic nature of the *β* substituents.[5] Functionalization at the *meso*-positions allows the modification of the calix[4]pyrrole binding properties and simultaneously constitutes an additional binding site in the receptor.

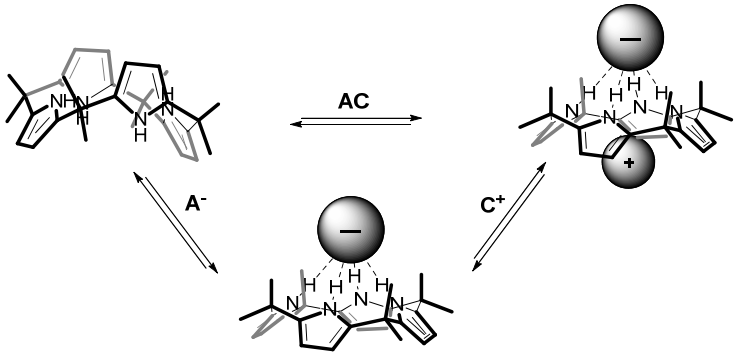

Figure 1.2 Ion-pair binding sequence by a calix[4]pyrrole receptor as it was proposed by Sessler.[6]

Calix[4]pyrroles have been used in different applications.[7,8,9] They are known heteroditopic receptors for ion pairs[10,11] displaying a *host-separated* binding geometry. In the mechanism proposed by Sessler[6], the anion of the ion pair is initially bound by the pyrrolic NHs. Such interaction stabilizes the calixpyrrole core in the *cone* conformation creating a cavity opposite to the hydrogen bond donor NHs which is electron rich and presents a bowl-shape. This cavity is able to recognize cations that are complementary in size and shape.

1.1.1.2 Porphyrins

Porphyrins are highly colored compounds found in many life processes. This relevant class of compounds has been widely employed as building blocks in supramolecular chemistry. Thanks to the convergence of electronic donor properties of the inner-ring periphery, porphyrins are easily functionalized by metallation. A wide variety of metals have been incorporated into the porphyrin ring. During the metallation process the porphyrin loses two protons from the pyrrole nitrogen atoms and behaves as a dianionic ligand. The two remaining nitrogen atoms coordinate to the inserted metal ion using their lone pairs. Metallated porphyrins can be considered as acceptor building blocks having at least one axial binding site available for coordination with different ligands containing nitrogen or oxygen donor atoms. The physico-chemical properties of porphyrins can also be tuned *via* functionalization at the *meso*- and *β*-pyrrolic positions (Scheme 1.1). Free-base and metallated porphyrins display a characteristic intense band (the *Soret* band) with a maximum between 380 and 420 nm in their UV-Vis spectrum. This band corresponds to a π-π* transition from the ground state to the second excited singlet state. The maximum of this absorption band is extremely sensitive to changes in the electronic environment of the porphyrin unit. Two or four additional bands (for metalated or free-base porphyrins, respectively) between 480 and 700 nm (*Q*-bands) can typically be observed in the electronic absorption spectra of porphyrins. They correspond to π-π* transitions from the ground state to the first excited singlet state. In many cases, porphyrins also exhibit fluorescent properties. Fluorescence is only detected from the first exited state due to a rapid interconversion process. The fluorescence properties of the porphyrins can be used to detect binding events at very low concentration for diagnostic detection purposes.[12] Other relevant features of these relative electron-rich macrocycles are their redox properties. In this sense, porphyrins have been extensively exploited as molecular components in natural and synthetic light harvesting systems. The absorption of light by the porphyrin unit provokes its involvement in highly efficient photo-induced electron and energy transfer processes.[13] While host-guest chemistry of free-base porphyrins is mainly dominated by weak π-π interactions, the formation of coordination bonds between electron-rich atoms of the guests and the metal center in metalloporphyrins confers a strong driving force to the

interaction. Free-base porphyrin and metalloporphyrin units are both ideal binding sites for many different guests ranging from neutral organic molecules[14] to carbon nanomaterials[15,16] (e.g. fullerene, carbon nanotubes CNTs) and many more besides.[17,18,19,20] The type of metal inserted into the porphyrin core has an important role on the thermodynamic and kinetic binding properties of the porphyrin complexes. Likewise, the inserted metal can be used to direct the selective coordination of different Lewis basic centers that are commonly present in mono- and ditopic ligands i.e. N *vs* O or P complexation.

1.1.2 Templating strategies in the assembly of pseudorotaxanes

Rotaxanes are mechanically interlocked molecules containing at least one macrocycle threaded by a linear molecule with bulky end groups. To prevent the dissociation of the components the end groups have to be big enough to avoid the passage of the linear component through the annulus of the macrocycle. In the first synthetic examples of rotaxanes[21] the threading of the linear molecule through the macrocycle was simply based in statistical approaches. Consequently, the rotaxane structures were produced in very low yields. To overcome this problem, the association of the rotaxane units can be directed by the design of cyclic and linear components that present mutual recognition properties. In general terms the host-guest complex that results from the non-covalent interaction of a cycle threaded by a linear molecule is a [2]pseudorotaxane. Due to the lack of bulky stoppers at the end of the linear component, a reversible process between the free and the complex pseudorotaxane units is always observed in solution. Pseudorotaxanes are considered key intermediates in the synthesis of rotaxanes.[22] Thus, the development of strategies to self-assemble pseudorotaxanes is a topic of current interest. [2]Pseudorotaxanes can be assembled considering two general approaches (Figure 1.3). The first approach is based in the functionalization of the macrocyclic ring and the linear component with mutual recognition moieties that direct the formation of the interwoven structure (Figure 1.3a). Examples that follow this approach have been widely used taking advantage of donor-acceptor and hydrogen-bond interactions besides others. The assembly of pseudorotaxanes through donor-acceptor interactions has been firstly described by Stoddart *et al*.[23,24,25,26,27]

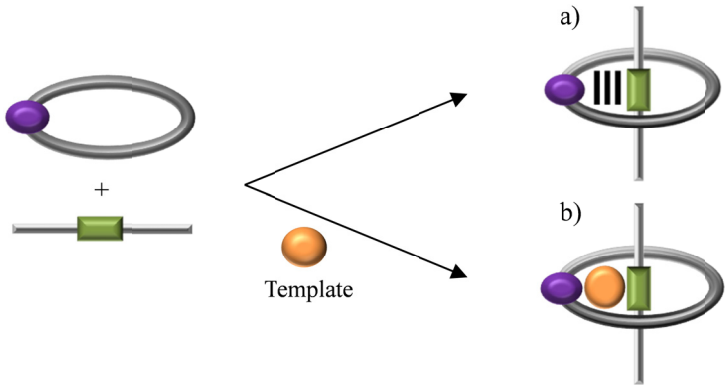

Figure 1.3 Self-assembly strategies for the formation of pseudorotaxanes: based on a mutual recognition process a) or mediated by a chemical template b).

For example, the macrocyclic tetracation formed by two units of *p*-phenylene and paraquat is able to form weak inclusion complexes stabilized by charge transfer interactions with dimethoxybenzenes in acetonitrile (Figure 1.4a).[28] Several donating and accepting hydrogen-bond groups have been employed to self-assemble pseudorotaxane entities. Stoddart and co-workers developed a templating strategy based on the well-known macrocyclic crown ethers and secondary dialkylammonium hexafluoro-phosphate salts (Figure 1.4b).[29] In that case, the self-assembly of both units is driven by the formation of hydrogen-bond interactions and, in some instances, by aryl-aryl interactions. Different examples were reported by the groups of Leigh and Schalley with the design of macrocycles that contain multiple hydrogen-bond amide donor units directed towards the interior of the macrocyclic cavity. It was proven that such macrocycles can be effectively threaded by using linear diamide components[30] (Figure 1.4c) or phenolate anions[31] through the formation of N-H···O interactions.

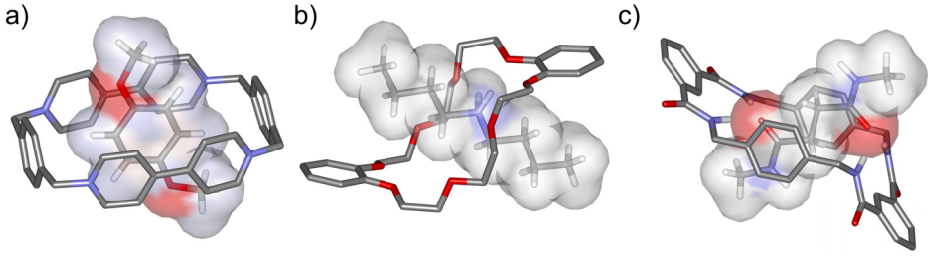

Figure 1.4 Energy-minimized structures[32] of 1:1 inclusion complexes displaying pseudorotaxane topology where the two components are self-assembled by donor-aceptor interactions a) and hydrogen-bonding interactions b), c).

In contrast, the second strategy to form [2]pseudorotaxanes requires the presence of an external chemical template (Figure 1.3b). Here, the macrocycle and the linear component are self-assembled due to the simultaneous recognition of a template. Most of the examples of this kind are using metals as templates due to its ability to for coordinate bonds in a preferred geometry with several ligands. In doing so, Sauvage and co-workers envisaged that the tetrahedral coordination geometry of ligands to Cu(I)[33] could be useful for the self-assembly of molecules with pseudorotaxane topology. To accomplish this, phenanthroline macrocyclic derivatives were designed.[34,35] Cu(I)-templated pseudorotaxanes can be formed by mixing equimolar quantities of the macrocycle with a linear bis-pyridine and $Cu(MeCN)_4PF_6$ complex (Scheme 1.2).[36] Besides bis-pyridine ligands other linear molecules functionalized with bis-nitrile[34] and bis-poshine[35] ligands have been proven to be effective in the quantitative assembly of Cu(I)-templated pseudorotaxanes.

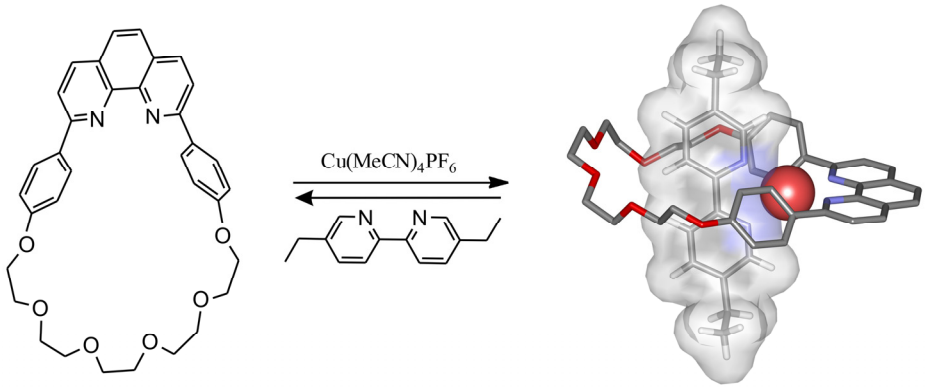

Scheme 1.2 Representation of the Cu(I)-template strategy for the formation of [2]pseudorotaxanes described by Sauvage *et al.* Energy-minimized model[32] of the ternary metallic complex with pseudorotaxane topology where the copper metal is shown as CPK model.

In a similar manner of using metal coordination bonds, an anion templating strategy that combines the two synthetic approach for pseudorotaxane formation was described by Beer *et al.* (Scheme 1.3).[37,38] In this particular case, the macrocyclic unit was equipped with three different binding sites. Hydroquinone and polyether units were introduced to recognize the cationic pyridinium rod-like molecule. Additionally, an isopthalamide group was attached to the macrocycle to interact with electron-rich molecules by means of hydrogen-bond interactions. The linear component consisted in a pyridinium cation

functionalized with two amide groups in order to form strong ion-pairing complexes with chloride in non-competitive solvents.[39] The pseudorotaxane formation is based on a first recognition event where the pyridinium cation threads the macrocycle. Simultaneously to this process the anion is recognized by the macrocyclic ligand resulting in an orthogonal orientation of the pyridinium cation. In brief, the pyridinium nicotinamide cation-chloride is recognized as an intimate ion pair by the macrocyclic unit thanks to the combination of two effects: anion recognition and ion-pairing.

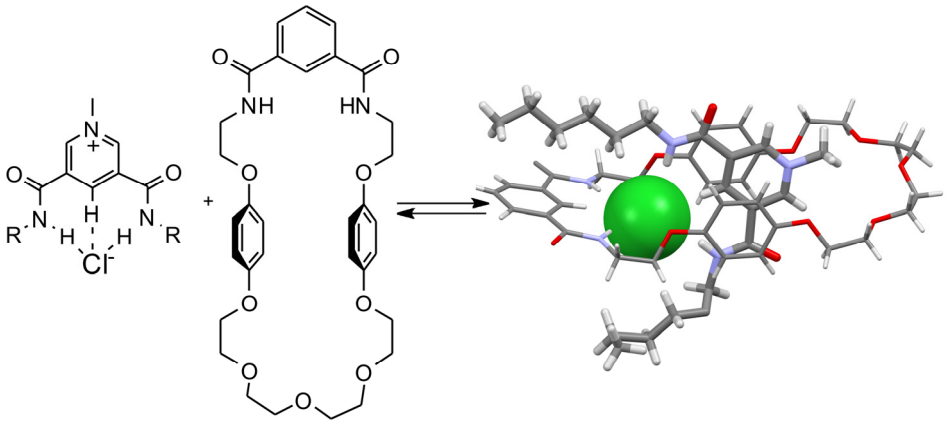

Scheme 1.3 Representation of the [2]pseudorotaxane equilibrium between pyridinium nicotinamide cation-chloride and a hydroquinone-polyether functionalized macrocycle. X-ray structure of the interwoven structure where the chloride anion is represented as CPK model.

This templating strategy is applicable to other cations containing 1,2,3-triazolium[40], benzimidazolium[38], guanidinium[38] and imidazolium[38] functionalities. More recently halogen-functionalized imidazolium threading components have been used in the self-assembly of pseudorotaxanes by chloride ion templation.[41] Interestingly, it was demonstrated that halogen bonding enhances the strength of the chloride anion templating formation of pseudorotaxanes compared with the related ones templated with hydrogen-bonds.

1.1.3 Ion-pair recognition

The recognition of ion pairs by synthetic receptors offers important advantages in terms of selectivity and sensitivity, when compared with simple cation or anion versions.[42,43]

In general, receptors designed for anion recognition contain hydrogen bonding donor functional groups.[44,45,46] In contrast, cation recognition is mainly achieved by molecules containing crown ethers or π-electron donor binding sites.[47,48] Those receptors that contain covalently attached anion and cation binding sites are the so called heteroditopic receptors.[43] Its classification can be done on the bases of the limiting modes in which the ion pair is bound to the receptor: *close*-contact[49,50,51], *solvent*-separated and *host*-separated[52,53,54] binding modes (Figure 1.5a).

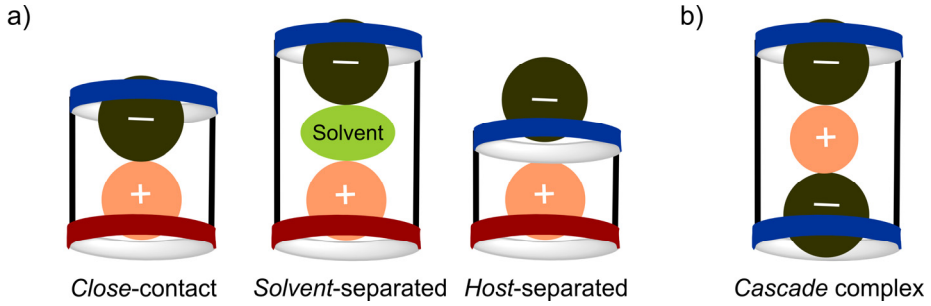

Figure 1.5 Schematic representations of the limiting binding modes displayed by heteroditopic receptors modes a) and a homoditopic receptor displaying a cascade complex arrangement of the ions b).

Probably, one of the best examples to illustrate these limiting binding modes was described by Seesler *et al.*[55] A cyclic dimer that contains a heteroditopic ion-pair calix[4]pyrrole receptor covalently linked to a homotopic calix[4]arene cation receptor binds ion pairs in the three limiting binding modes (Figure 1.6). Interestingly, the size of the receptor cavity in relation with the size of the ion pair determines the receptor binding mode. For a common cation (Cs^+) the size of the ion pair is determined by the anion: fluoride, chloride or nitrate. In all the cases, the calix[4]pyrrole unit binds the anion by establishing four hydrogen bonds. When CsF is used, the ion pair is recognized through a *solvent*-separated binding mode and only takes places when both ions are present in solution (Figure 1.6a). The caesium cation is selectively included in the aromatic cavity of the calix[4]arene macrocycle by establishing cation-π interactions. Additionally, the size of the cavity that is formed between the cesium cation and the fluoride anion is adequate to include a molecule of water. In striking contrast, the coordination of CsCl is achieved through a host-separated binding mode (Figure 1.6b) where the calix[4]pyrrole unit is acting as heteroditopic ion-pair receptor.

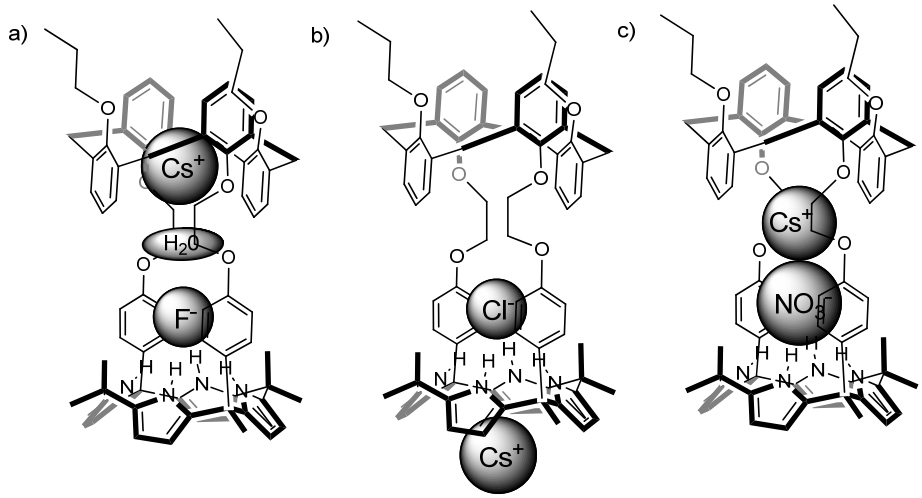

Figure 1.6 Molecular structures of the three different binding modes displayed by a single ion-pair receptor: a) *solvent*-separated, b) *host*-separated and c) *close*-contact binding modes.

Simple molecular modelling studies indicate that the size of the ion pair is too small to display a *close*-contact binding mode but too large to include a solvent molecule between the ion pair. Finally, by using the largest nitrate anion the recognition of the ion-pair is achieved through a *close*-contact binding mode.

Cooperative effects together with the strength of the ion pairing can benefit or difficult the ion-pair recognition. Additionally, the ion-pair binding can occur in a concurrent or in a sequential way.[43] In the first case the ion pair is simultaneously recognized by the receptor. By contrast, in the second case the ion-pair recognition occurs in a step-wise fashion. In particular, the sequential binding of one ion may produce conformational changes in the receptor which enhances the binding of the second ion (allosteric effects). In reality, cooperative and allosteric effects often exist together in the same system.[56] Another strategy for the recognition in a sequential manner of ion pairs consists in the formation of *cascade* complexes. In this case a homoditopic receptor binds two anions or two cations to form a double charged supramolecular assembly which possess a cavity able to recognize geometric and electrostatic complementary ions. This term was initially introduced by Lehn *et al*. with the formation of inclusion complexes of the binuclear cationic copper (II) cryptate (Figure 1.7).[57] The cationic

metal acts as Lewis acid and the insertion of an anion compatible in terms of size between the two cations results in a triplet of ions in *close*-contact binding mode.

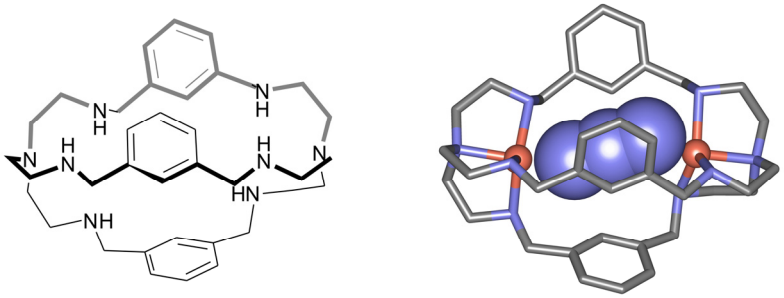

Figure 1.7 Left: molecular structure of the cyclic octaazaphane. Right: energy-minimized structure[32] of the cascade di-copper (II) complex with azide. The anion is represented in CPK model and the receptor in stick representation.

1.1.4 Porphyrin-based tweezers

In general terms, "molecular tweezer" receptors consist of two binding sites (BS) separated by a more or less conformationally-flexible spacer. When the two binding sites converge, they define a binding cavity opened at three sides, a molecular cleft. The nature of the binding site plays a key role in substrate recognition.

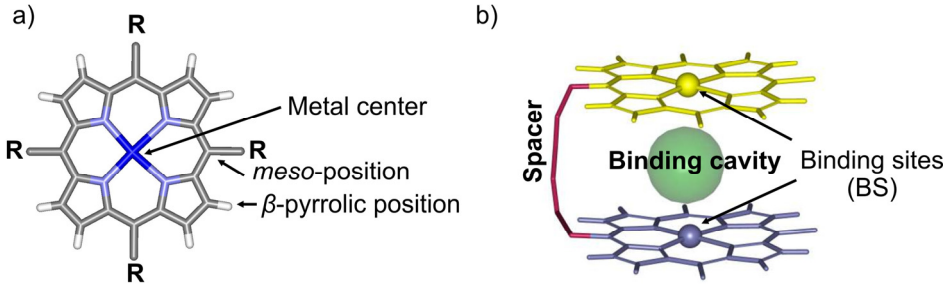

Figure 1.8 a) Metallated porphyrin scaffold indicating the main functionalization sites: *meso* and *β*-positions; b) schematic representation of a porphyrin tweezer receptor highlighting the main components.

Many different types of binding sites have been used in the synthesis of molecular tweezers. These include for example anthracene, acridine, cyclohexyl rings or tetrathiofulvalene (TTF) moieties. Consequently, molecular tweezers can act as receptors for a wide variety of substrates ranging from carbon materials[58,59], anions[60,61,62], organic[63] and inorganic cations[64] and neutral organic guests[65]. The

physicochemical properties of porphyrins permit the use of a varied number of techniques for the study of their recognition/binding properties compared to other binding units also employed in the synthesis of molecular tweezer receptors. The use of free-base or metalloporphyrin units as binding sites of tweezer receptors has a strong impact on the type of guest that can be recognized. As a general trend, guest recognition by porphyrin tweezers is governed by establishing non-covalent interactions with the porphyrin units, mainly metal-ligand coordination bonds and π-π interactions. The molecular spacer serves to hold together the two porphyrin binding units and to constrain them within certain proximity in space. When the spacer is conformationally locked the distance between binding sites is more or less fixed, and their precise relative orientation is achieved. The nature of the spacer used to hold together the two binding units of the tweezer receptors, and most importantly, its conformational flexibility are key factors in controlling the binding affinity.

1.2 Aim of the thesis

The objective of this thesis has to do mainly with the design, synthesis and characterization of molecules and supramolecules containing calix[4]pyrrole or/and porphyrin units that are able to recognize other molecules by means of non-covalent interactions. The study of the resulting supramolecular aggregates also falls into the scope of the thesis.

In line with this general objective, this thesis covers two specific topics. The first one is related to the preparation of bis-calix[4]pyrrole macrotricycles and the study of their supramolecular applications. The goals of this project are listed below:

1. Design and synthesis of bis-calix[4]pyrrole macrotricycles.
2. Use of bis-calix[4]pyrrole macrotricycles as the “cyclic component” in self-assembly processes leading to [2]pseudorotaxanes. Polyatomic anions in combination with bis-amide pyridyl *N*-oxides and bis-pyridyl bis-*N*,*N*´-oxides will be used as linear components of the pseudorotaxane assembly.

3. Synthesis of interlocked molecules such as [2]rotaxanes taking advantage of the same templating strategies used for the assembly of the previous [2]pseudorotaxanes.
4. Exploring the recognition of ion-pair dimers and ion quartets with a bis-calix[4]pyrrole macrotricyclic receptor. Evaluation of the cooperative factors involved in the recognition processes. Our efforts will also be directed towards the study of the effect that the structural nature of the cation in the ion pair has in the magnitude of the cooperativity factors exhibited by the self-assembly processes and the final geometry of the resulting multimolecular aggregates.
5. Another important objective of this work will be to study the modifications of the racemization energy barriers for *ortho*-disubstituted bispyridine bis-*N*,*N*′-oxide ligands when included within a bis-calix[4]pyrrole macrocyclic receptor.

In the second part of the thesis, we will focus our attention on the synthesis and the study of the binding properties of metallated bis-porphyrin receptors. Within this particular topic the following objectives will be pursued:

1. Synthesis of porphyrin tweezer receptors containing calix[4]pyrroles units as spacers. Study of the binding properties of the prepared receptors towards alkylammonium salts derived from [6,6]-phenyl-C_{61}-butyric carboxylic acid.
2. Preparation and characterization of self-assembled macrocycles based on Rh(III) bis-porphyrin units and bis-amidopyridyl ligands. Formation of [2]rotaxanes and [2]pseudorotaxanes-like structures by the threading of linear diamides into the pre-formed supramolecular macrocycles. Finally, the kinetic and thermodynamic stability of the assembled [2]rotaxane-like structures based on Rh(III) metallated porphyrins will be compared with those of their Zn(II) counterparts.

1.3 Outline of the thesis

The use of polyatomic anions for the quantitative assembly of ion-paired complexes displaying [2]pseudorotaxane topology is described in *Chapter 2*. This approach

exploits the unique ion-pair recognition properties exhibited by non-covalent neutral receptors assembled through hydrogen-bonding interactions between a bis-calix[4]pyrrole macrocycle and linear bis-amidepyridyl-*N*-oxides. The complexation of bidentate polyatomic anions that are complementary in size and shape to the receptor's cavity, in which six NH hydrogen-bond donors converge, induces the exclusive formation of four particle-threaded assemblies. In *Chapter 3*, we reported the binding properties of two bis-calix[4]pyrrole macrocyclic receptors and bispyridine bis-*N,N´*-oxides. In addition, we described how the structural characteristics of a bis-calix[4]pyrrole macrocyclic receptor affects the racemization barrier of *3,3´*-disubstituted bipyridine bis-*N*,*N*′-oxide ligands. The elongation of the bipyridine bis-*N*,*N*′-oxides at the *3,3´*-position provide the possibility to synthesize fairly linear molecules that can be used in the synthesis of interlocked molecules. We present our attempts towards the synthesis of [2]rotaxanes by following this templating strategy. In *Chapter 4* we described the unprecedented binding properties towards two ion pairs featured by the macrotricyclic receptor which is equipped with two convergent calix[4]pyrrole units. A highly cooperative binding process is observed for pairs of tetrabutylammonium (TBA) salts. The complexes have a structure with a cascade-like arrangement of the ion pairs. One ion-pair is bound in a close contact geometry while the other in a receptor-separated arrangement. Additionally, the exclusive and quantitative formation of the ion-pair hetero-dimers is detailed.

Chapter 5 deals with the synthesis of two structurally different nickel bisporphyrins containing *aryl*-extended calix[4]pyrroles as spacers. Moreover, the recognition properties of this porphyrin-based tweezers towards alkylammonium salts derived from [6,6]-phenyl-C_{61}-butyric carboxylate are introduced.

In 2002 our group described[66] the construction of [2]pseudorotaxane and [2]rotaxane structures using a series of self-assembled heterodimeric tetralactam macrocycles. The macrocycles were assembled by the formation of two kinetically labile zinc porphyrin-pyridine interactions. Zn(II) porphyrins and *N*-donor ligands are known to form complexes which have weak thermodynamic stability and are kinetically quite labile. In consequence, the chemical exchange between the free and the bound states of the molecular components of the rotaxane assembly structure is fast on the ^{1}H NMR

timescale. The existence of a fast exchange process complicates the analysis of the assemblies using NMR spectroscopy. One of the motivations of our work with rhodium porphyrins as building blocks is to make use of the high thermodynamic and kinetic stability of the Rh(III)-porphyrin-nitrogen bond compared to the Zn(II) analogs. Hence, kinetically and thermodynamically more stable rotaxane-like structures will be assembled. In *Chapter 6* we described our findings on the construction of pseudorotaxane and rotaxane assemblies based on Rh(III) bisporphyrins. The Rh(III) centers are basic interaction sites for the assembly of supramolecular macrocycles through the formation of two coordination bonds with suitable pyridyl ditopic ligands. Subsequently, the results obtained in the study of the threading process of linear diamides through the macrocyclic supramolecular assembly are also discussed.

1.4 References and notes

[1] Rothemund, P. *J. Am. Chem. Soc.* **1935**, *57*, 2010.
[2] Rothemund, P. *J. Am. Chem. Soc.* **1936**, *58*, 625.
[3] Baeyer, A. *Ber. D. D. Chem. Gesell*. **1886**, 19, 2184.
[4] Blas, J. R.; Lopez-Bes, J. M.; Marquez, M.; Sessler, J. L.; Luque, F. J.; Orozco, M. *Chem-Eur. J.* **2007**, *13*, 1108.
[5] Gale, P. A.; Sessler, J. L.; Allen, W. E.; Tvermoes, N. A.; Lynch, V. *Chem. Commun.* **1997**, 665.
[6] Gross, D. E.; Schmidtchen, F. P.; Antonius, W.; Gale, P. A.; Lynch, V. M.; Sessler, J. L. *Chem-Eur. J.* **2008**, *14*, 7822.
[7] Sessler, J. L.; Gale, P. A.; Genge, J. W. *Chem-Eur. J.* **1998**, *4*, 1095.
[8] Tong, C. C.; Quesada, R.; Sessler, J. L.; Gale, P. A. *Chem. Commun.* **2008**, 6321.
[9] Nishiyabu, R.; Anzenbacher, P. *J. Am. Chem. Soc.* **2005**, *127*, 8270.
[10] Custelcean, R.; Delmau, L. H.; Moyer, B. A.; Sessler, J. L.; Cho, W. S.; Gross, D.; Bates, G. W.; Brooks, S. J.; Light, M. E.; Gale, P. A. *Angew. Chem., Int. Ed.* **2005**, *44*, 2537.
[11] Wintergerst, M. P.; Levitskaia, T. G.; Moyer, B. A.; Sessler, J. L.; Delmau, L. H. *J. Am. Chem. Soc.* **2008**, *130*, 4129.
[12] Rana, A.; Panda, P. K. *RSC Advances* **2012**, *2*, 12164.
[13] Panda, M. K.; Ladomenou, K.; Coutsolelos, A. G. *Coord. Chem. Rev.* **2012**, *256*, 2601.
[14] Berova, N.; Pescitelli, G.; Petrovic, A. G.; Proni, G. *Chem. Commun.* **2009**, 5958.
[15] Bottari, G.; Trukhina, O.; Ince, M.; Torres, T. *Coord. Chem. Rev.* **2012**, *256*, 2453.
[16] Tashiro, K.; Aida, T. *Chem. Soc. Rev.* **2007**, *36*, 189.
[17] D. Beer, P.; G. B. Drew, M.; Jagessar, R. *Dalton Trans.* **1997**, *0*, 881.
[18] Shelton, A. H.; Rodger, A.; McMillin, D. R. *Biochemistry* **2007**, *46*, 9143.
[19] Allard, M.; Dupont, C.; Muñoz Robles, V.; Doucet, N.; Lledós, A.; Maréchal, J.-D.; Urvoas, A.; Mahy, J.-P.; Ricoux, R. *ChemBioChem* **2012**, *13*, 240.
[20] Wienkers, M.; Ramos, J.; Jemal, H.; Cardenas, C.; Wiget, P.; Nelson, A.; Free, S.; Wu, J.; Roach, R.; Vulcan, M.; Waynant, K.; Fort, K.; Vladimirova, A.; Sun, J.; Hunt, S. E.; Rudkevich, D. M.; Starnes, S. D. *Org. Lett.* **2012**, *14*, 1370.
[21] Harrison, I. T.; Harrison, S. *J. Am. Chem. Soc.* **1967**, *89*, 5723.
[22] Vickers, M. S.; Beer, P. D. *Chem. Soc. Rev.* **2007**, *36*, 211.
[23] Allwood, B. L.; Colquhoun, H. M.; Doughty, S. M.; Kohnke, F. H.; Slawin, A. M. Z.; Stoddart, J. F.; Williams, D. J.; Zarzycki, R. *J. Chem. Soc., Chem. Commun.* **1987**, 1054.
[24] Allwood, B. L.; Shahriarizavareh, H.; Stoddart, J. F.; Williams, D. J. *J. Chem. Soc., Chem. Commun.* **1987**, 1058.
[25] Allwood, B. L.; Spencer, N.; Shahriarizavareh, H.; Stoddart, J. F.; Williams, D. J. *J. Chem. Soc., Chem. Commun.* **1987**, 1061.
[26] Allwood, B. L.; Spencer, N.; Shahriarizavareh, H.; Stoddart, J. F.; Williams, D. J. *J. Chem. Soc., Chem. Commun.* **1987**, 1064.
[27] Asakawa, M.; Ashton, P. R.; Brown, G. R.; Hayes, W.; Menzer, S.; Stoddart, J. F.; White, A. J. P.; Williams, D. J. *Adv. Mater. (Weinheim, Ger.)* **1996**, *8*, 37.

[28] Ashton, P. R.; Odell, B.; Reddington, M. V.; Slawin, A. M. Z.; Stoddart, J. F.; Williams, D. J. *Angew. Chem., Int. Ed.* **1988**, *27*, 1550.
[29] Ashton, P. R.; Chrystal, E. J. T.; Glink, P. T.; Menzer, S.; Schiavo, C.; Spencer, N.; Stoddart, J. F.; Tasker, P. A.; White, A. J. P.; Williams, D. J. *Chem-Eur. J.* **1996**, *2*, 709.
[30] Gatti, F. G.; Leigh, D. A.; Nepogodiev, S. A.; Slawin, A. M. Z.; Teat, S. J.; Wong, J. K. Y. *J. Am. Chem. Soc.* **2001**, *123*, 5983.
[31] Ghosh, P.; Mermagen, O.; Schalley, C. A. *Chem. Commun.* **2002**, 2628.
[32] Geometries of the complexes were refined by performing an optimize geometry calculation with Molecular Mechanics using augmented MM3 parameters as implemented in the software CAChe WorkSystem Pro Version 6.1.12.33, Fujitsu Limited. A conjugate gradient method was used for energy minimization with a convergence energy criterion of 0.001 kcal/mol.
[33] Dietrichbuchecker, C. O.; Sauvage, J. P.; Kern, J. M. *J. Am. Chem. Soc.* **1984**, *106*, 3043.
[34] Sakellariou, E. G.; Collin, J. P.; Dietrich-Bucheker, C. O.; Sauvage, J. P. *Eur. J. Inorg. Chem.* **2004**, 575.
[35] Mohankumar, M.; Holler, M.; Nierengarten, J. F.; Sauvage, J. P. *Chem-Eur. J.* **2012**, *18*, 12192.
[36] Mobian, P.; Collin, J. P.; Sauvage, J. P. *Tetrahedron Lett.* **2006**, *47*, 4907.
[37] Wisner, J. A.; Beer, P. D.; Drew, M. G. B. *Angew. Chem., Int. Ed.* **2001**, *40*, 3606.
[38] Wisner, J. A.; Beer, P. D.; Berry, N. G.; Tomapatanaget, B. *Proc. Natl. Acad. Sci. U. S. A.* **2002**, *99*, 4983.
[39] Vickers, M. S.; Beer, P. D. *Chem. Soc. Rev.* **2007**, *36*, 211.
[40] Mullen, K. M.; Mercurio, J.; Serpell, C. J.; Beer, P. D. *Angew. Chem., Int. Ed.* **2009**, *48*, 4781.
[41] Serpell, C. J.; Kilah, N. L.; Costa, P. J.; Felix, V.; Beer, P. D. *Angew. Chem., Int. Ed.* **2010**, *49*, 5322.
[42] Kim, S. K.; Sessler, J. L. *Chem. Soc. Rev.* **2010**, *39*, 3784.
[43] McConnell, A. J.; Beer, P. D. *Angew. Chem., Int. Ed.* **2012**, *51*, 5052.
[44] Kang, S. O.; Llinares, J. M.; Powell, D.; VanderVelde, D.; Bowman-James, K. *J. Am. Chem. Soc.* **2003**, *125*, 10152.
[45] Kang, S. O.; VanderVelde, D.; Powell, D.; Bowman-James, K. *J. Am. Chem. Soc.* **2004**, *126*, 12272.
[46] Kang, S. O.; Hossain, M. A.; Powell, D.; Bowman-James, K. *Chem. Commun.* **2005**, 328.
[47] Gokel, G. W.; Leevy, W. M.; Weber, M. E. *Chem. Rev. (Washington, DC, U. S.)* **2004**, *104*, 2723.
[48] Kim, J. S.; Quang, D. T. *Chem. Rev. (Washington, DC, U. S.)* **2007**, *107*, 3780.
[49] Mahoney, J. M.; Beatty, A. M.; Smith, B. D. *J. Am. Chem. Soc.* **2001**, *123*, 5847.
[50] Suksai, C.; Leeladee, P.; Jainuknan, D.; Tuntulani, T.; Muangsin, N.; Chailapakul, O.; Kongsaeree, P.; Pakavatchai, C. *Tetrahedron Lett.* **2005**, *46*, 2765.
[51] Chae, M. K.; Lee, J. I.; Kim, N. K.; Jeong, K. S. *Tetrahedron Lett.* **2007**, *48*, 6624.
[52] Savage, P. B.; Holmgren, S. K.; Gellman, S. H. *J. Am. Chem. Soc.* **1993**, *115*, 7900.
[53] Scheerder, J.; vanDuynhoven, J. P. M.; Engbersen, J. F. J.; Reinhoudt, D. N. *Angew. Chem., Int. Ed.* **1996**, *35*, 1090.

[54] Tozawa, T.; Misawa, Y.; Tokita, S.; Kubo, Y. *Tetrahedron Lett.* **2000**, *41*, 5219.
[55] Kim, S. K.; Sessler, J. L.; Gross, D. E.; Lee, C. H.; Kim, J. S.; Lynch, V. M.; Delmau, L. H.; Hay, B. P. *J. Am. Chem. Soc.* **2010**, *132*, 5827.
[56] Hunter, C. A.; Anderson, H. L. *Angew. Chem., Int. Ed.* **2009**, *48*, 7488.
[57] Lehn, J. M.; Pine, S. H.; Watanabe, E. I.; Willard, A. K. *J. Am. Chem. Soc.* **1977**, *99*, 6766.
[58] Perez, E. M.; Martin, N. *Pure Appl. Chem.* **2010**, *82*, 523.
[59] Romero-Nieto, C.; Garcia, R.; Herranz, M. A.; Ehli, C.; Ruppert, M.; Hirsch, A.; Guldi, D. M.; Martin, N. *J. Am. Chem. Soc.* **2012**, *134*, 9183.
[60] Chen, C. W.; Whitlock, H. W. *J. Am. Chem. Soc.* **1978**, *100*, 4921.
[61] Yoon, H.; Lee, C. H.; Jang, W. D. *Chem-Eur. J.* **2012**, *18*, 12479.
[62] Hermida-Ramon, J. M.; Estevez, C. M. *Chem-Eur J* **2007**, *13*, 4743.
[63] Klarner, F. G.; Kahlert, B. *Acc. Chem. Res.* **2003**, *36*, 919.
[64] Carraro, M.; Modugno, G.; Fiorani, G.; Maccato, C.; Sartorel, A.; Bonchio, M. *Eur. J. Org. Chem.* **2012**, 281.
[65] Hardouin-Lerouge, M.; Hudhomme, P.; Salle, M. *Chem. Soc. Rev.* **2011**, *40*, 30.
[66] Ballester, P.; Costa, A.; Deya, P. M.; Frontera, A.; Gomila, R. M.; Oliva, A. I.; Sanders, J. K. M.; Hunter, C. A. *J. Org. Chem.* **2005**, *70*, 6616.

Chapter 2

Anion Assistance in the Assembly of [2]pseudorotaxanes*

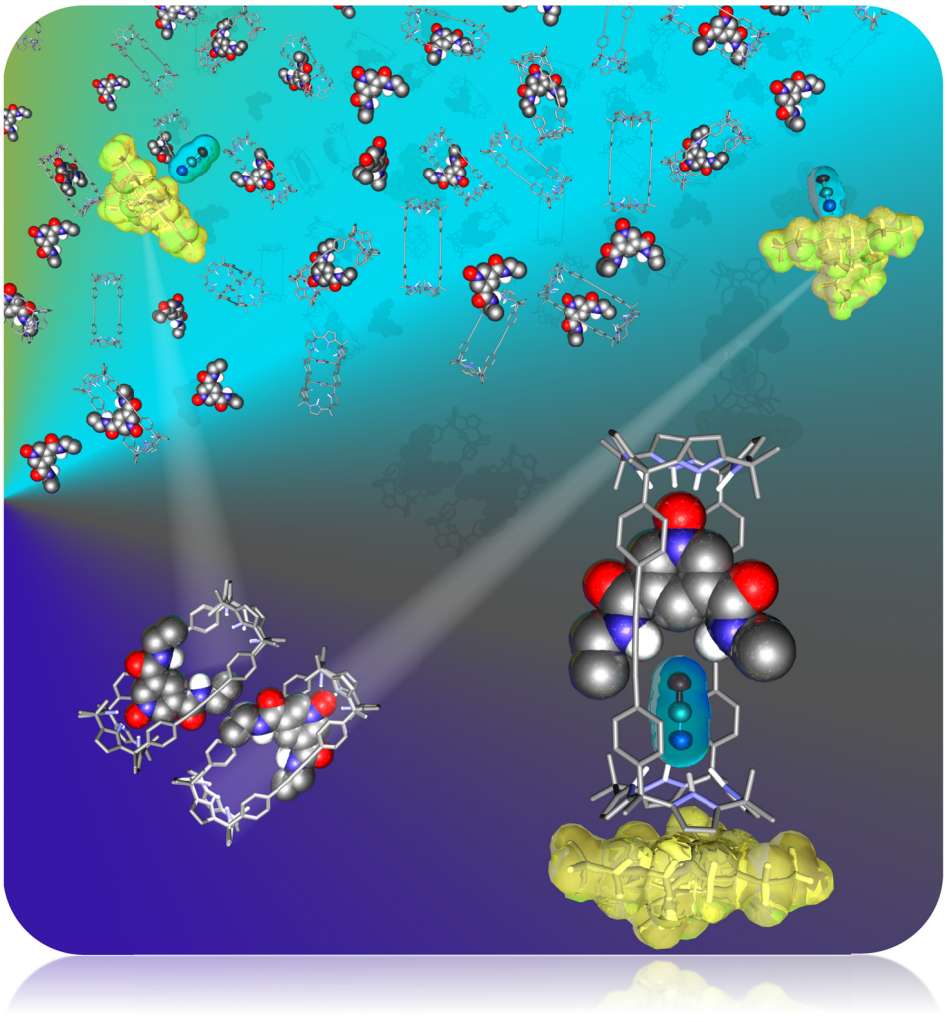

*Part of this Chapter was published in: Valderrey,V.; Escudero-Adan, E. C; Ballester, P. *J. Am. Chem. Soc.* **2012**, 134,10733

2.1 Introduction

Catenanes and rotaxanes are mechanically locked structures with potential application in molecular machinery.[1,2] Supramolecular assistance facilitates the preparation of these interlocked topologies.[3] A key intermediate for their construction is the non-covalent pseudorotaxane, where a linear molecule is threaded through a macrocycle.[4] Thus, the development of new supramolecular strategies and interweaving motifs for the construction of pseudorotaxanes is a topic of current interest.[5, 6] Specifically, examples of template assistance for the formation of rotaxanes, catenanes, and pseudorotaxanes using cations,[7,8,9,10] anions,[11,12,13] hydrogen bonds,[14,15,16] hydrophobic interactions,[17,18] and π–π interactions[19,11,12] have all been reported. A general templating strategy for the construction of threaded assemblies that combines halide recognition by the macrocyclic component with strong ion-pairing of the linear component has been developed.[20] Then the efficacy of the [2]pseudorotaxane assembly is most of all dependent on the strength of the properties of the ion pair linear component.

In this chapter, we describe the use of anions for the quantitative construction of pseudorotaxane-like assemblies, which does not involve ion-pairing with the linear component[21]. Rather, the anion of the ion pair is recognized by the supramolecular complex that results when a neutral heteroditopic linear component threads a homoditopic macrocycle. The counter ion is coordinated externally to the macrocyclic structure. In sort, the approach described herein exploits the exceptional ion-pair recognition properties[22] of a self-assembled ditopic interwoven receptor. The versatility of this templating strategy for the formation of pseudorotaxanes is evidence with the use of different linear components and through the study of a pool of different alkylammonium ion pairs. We demonstrate that both, the nature of the cation and the anion have a strong influence in the thermodynamic and kinetic stability of the pseudorotaxane structures.

2.2 Results and discussion

2.2.1 Design and synthesis

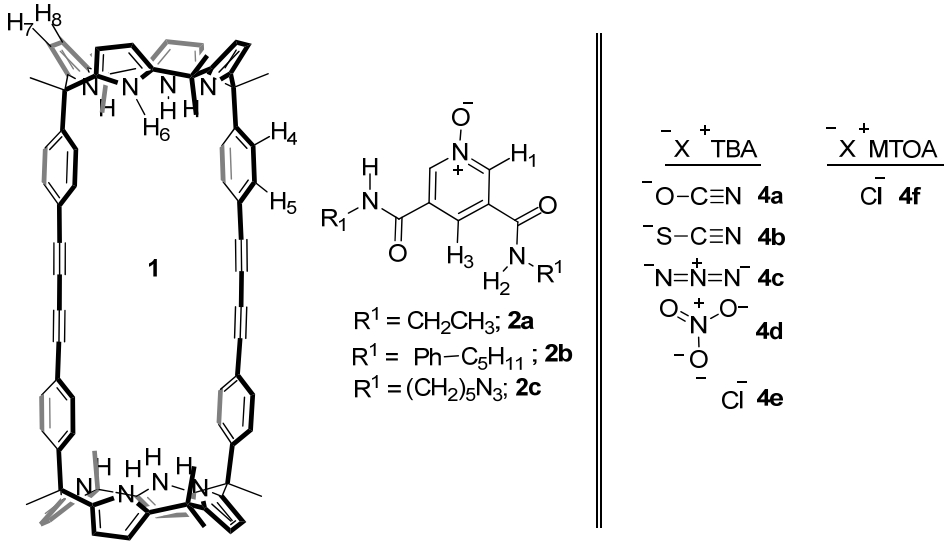

Figure 2.1 Structures of macrotricycle **1**, the bis-amidepyridyl-*N*-oxides **2** and ion pairs of monoatomic and polyatomic anions **4** with TBA and MTOA cations used in our studies.

The bis-calix[4]pyrrole macrotricyclic receptor **1** was synthesized following the synthetic procedure depicted in Figure 2.2, Figure 2.5 and Figure 2.7. Initially, the acid catalysed condensation of the commercially available 4-iodoacetophenone with an excess of freshly distilled pyrrole afford the 5-methyl-5´-(4-iodophenyl)dipyrromethane **5** in a 57 % of yield. Next, the dipyrromethane **5** is reacted in acetone in the presence of boron trifluoride ethyl ether affording two calix[4]pyrrole stereoisomers α,α-**6** and α,β-**6** depending on the relative orientation of the 1,3-*meso* phenyl substituents. Highly dilution conditions are desired in this reaction step to favour the formation of the macrocyclic products and minimize the polymeric pyrrolic undesired subproducts. The two isomers were isolated by column chromatography obtaining the α,α-**6** and α,β-**6**, in 6 and 8% yield, respectively.

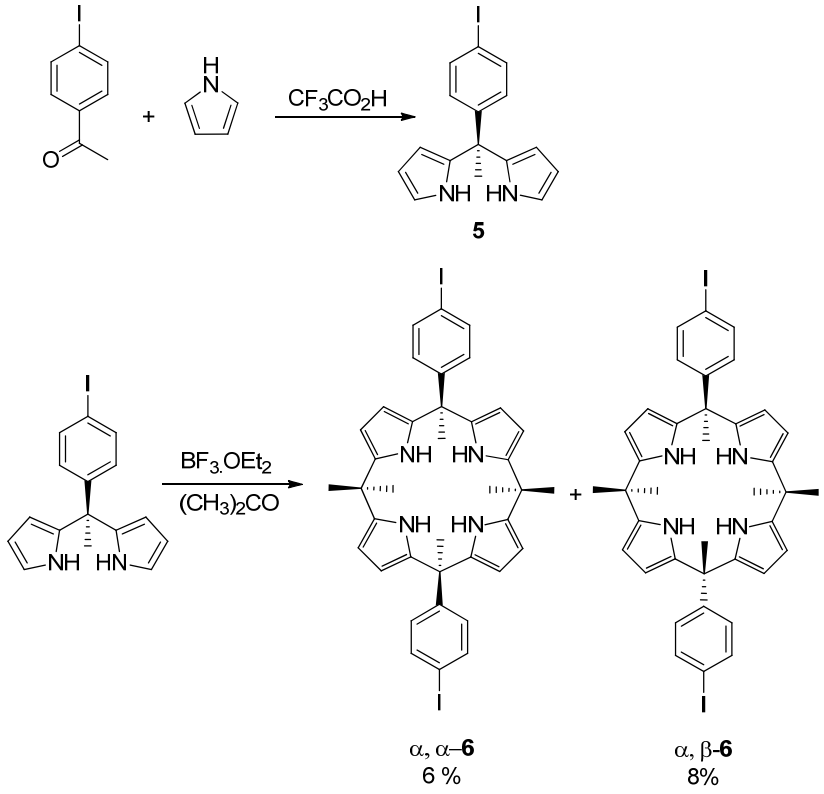

Figure 2.2 Synthetic scheme outlining the synthesis of 5-methyl-5´-(4-iodophenyl)-dipyrromethane **5** and the two possible isomers of the di-iodo *aryl*-extended calix[4]pyrrole **6**.

The ^{1}H NMR spectra of the calix[4]pyrroles **6** display two different signals corresponding to the two β-pyrrolic protons (Hc and Hb) (Figure 2.3). In non-polar solvents as $CHCl_3$, the favoured conformation for the calix[4]pyrrole core is the *1,3-alternate* conformation. In that conformation the β-pyrrolic protons Hb appear upfield shifted compared with Hc due to the ring current influence of the aromatic ring. The α,β **-6** isomer present C_{2h} symmetry resulting the six methyl protons m_1 chemical and magnetically equivalents (Figure 2.3a). Contrary, the α,α-**6** isomer presents C_{2v} symmetry and three singlets are detected due to the magnetically inequivalence of m_1 and m_3 (Figure 2.3b).

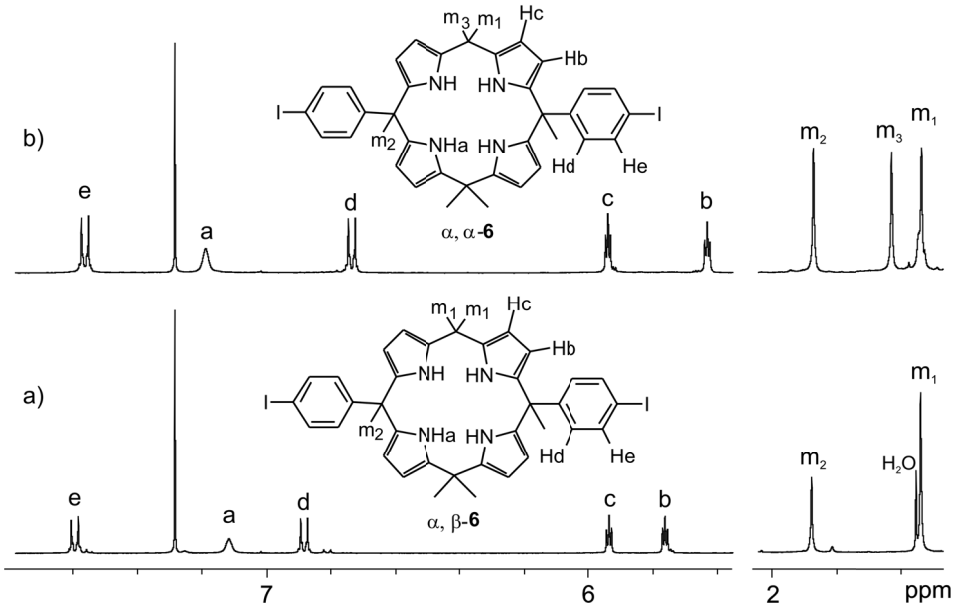

Figure 2.3 Selected regions of the ^{1}H NMR spectra (500 MHz, $CDCl_3$, 298 K) of the two isomers of the di-iodocalix[4]pyrrole **6**, a) α,β-isomer and b) α,α-isomer.

The structure of the desired α,α-**6** stereoisomer was confirmed in the solid state by X-ray diffraction analysis. The crystals were obtained from a saturated acetonitrile solution by slow evaporation. Even in this polar solvent, the α,α-**6** calix[4]pyrrole feature a *1,2-alternate* conformation and there is not any molecule of solvent interacting with the four NHs pyrrolic protons.

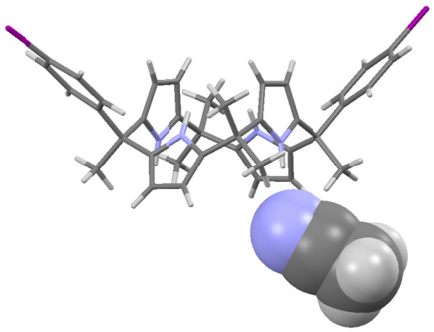

Figure 2.4 X-ray structure of the α,α-isomer of the di-iodocalix[4]pyrrole. The acetonitrile solvent molecule is depicted as space-filling representation.

Later, the α,α-di-iodocalix[4]pyrrole **6** was functionalized in the upper rim with dimethyl propargylic alcohol by a palladium catalysed Sonogashira coupling to afford

the calix[4]pyrrole **7** in a 90% yield. The further deprotection of the propargylic alcohol groups of **7** in strong basic media provides the calix[4]pyrrole **3** in a 98% yield.

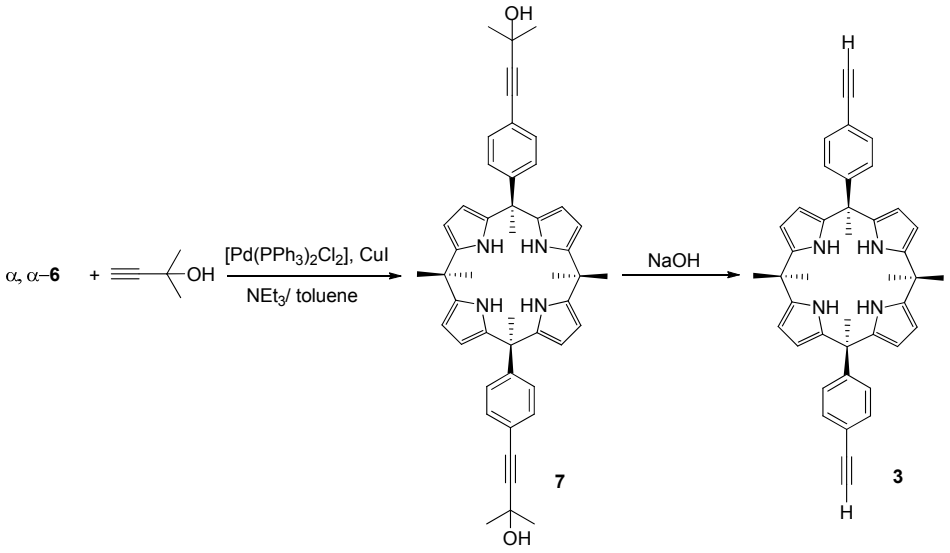

Figure 2.5 Schematic representation of the synthetic pathway used to obtain the calix[4]pyrrole **7** direct precursor of the homoditopic receptor **3**.

Calix[4]pyrrole **3** was selected as starting material in the synthesis of macrotricycle **1**. We envisaged that the formation of a macrocyclic derivate of **3** could be achieved in good yields through the formation of molecular capsules. The idea is to favour the self-assembly of the two calix[4]pyrrole units and dispose their reactive sites close in the space thought templation effects during the reaction. Inspired in the work developed in our group for the self-assembly of dimeric tetraureas calix[4]pyrroles capsules[23] we selected as template the 4,4′-bipyridine bis-*N*,*N*′-oxide **8**. It is well known that calix[4]pyrroles interact with electron rich neutral molecules through the formation of four hydrogen bonds established between the NH pyrrolic protons of the calix[4]pyrrole and the electron rich guest.[24,25] In non-polar solvents, this interaction changes the calix[4]pyrrole conformation from the *1,3-alternate* to the *cone*. Molecular modelling studies revealed that 4,4′-bipyridine bis-*N,N*′-oxide **8** perfectly fits the cavity formed by the two calix[4]pyrrole units freezing the calix[4]pyrrole cores in *cone* conformation.

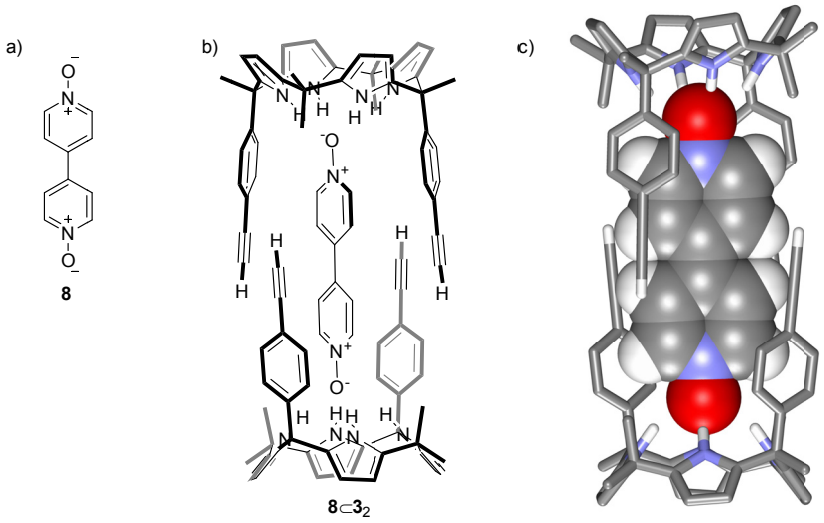

Figure 2.6 a) Molecular structure of the homoditopic 4,4′-bipyridine bis-*N*,*N*′-oxide **8**. b) Molecular structure of the 2:1 assembled capsule **8**⊂**3**$_2$. c) Energy-minimized structure[26] of the dimeric assembly where the encapsulated **8** is hold by eight hydrogen bond interactions. The calix[4]pyrrole units are represented as stick representation where the nonpolar hydrogens are omitted by clarity and the 4,4′-bipyridine bis-*N*,*N*′-oxide **8** is represented as CPK model.

Hay coupling of calix[4]pyrrole **3** templated by 1 equivalent of 4,4′-bipyridine bis-*N*,*N*′-oxide afforded the bis-calix[4]pyrrole macrocycle **1** in 60% yield. The 4,4′-bipyridine bis-*N*,*N*′-oxide **8** coordinated to the macrocycle during the synthesis is removed by column chromatography.

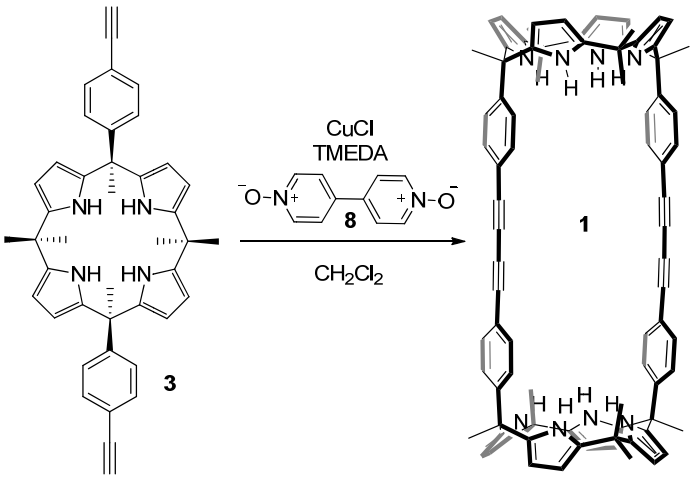

Figure 2.7 . Synthetic scheme for the preparation of macrotricycle **1** through the coupling of two terminal alkynes under standard Hay coupling reaction conditions.

Fortunatelly, single crystals suitable for X-ray diffraction analyses where obtained by slow evaporation of a saturated acetonitrile solution. It is worthy to note, that in this structure one molecule of acetonitrile is establishing four hydrogen bond interactions with the NHs pyrrolic protons locking the calix[4]pyrrole in the cone conformation. This conformational change creates an electron-rich bowl cavity where a second solvent molecule is interacting by means of CH-π interactions. Comparing with the X-ray structure of the α,α-isomer di-iodocalix[4]pyrrole α,α-**6** which displays *1,2-alternate* conformations of the pyrrolic rings (*vide infra*), we conclude that at least in polar solvents, the covalent attachment of the two calix[4]pyrroles induces certain conformational preference of the calix[4]pyrrole cores towards the *cone* conformation.

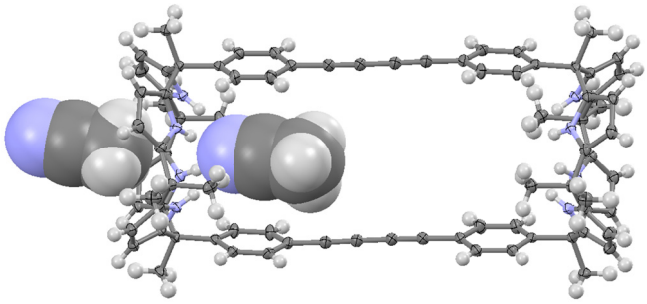

Figure 2.8 X-ray structure of the bis-calix[4]pyrrole macrotricyclic receptor **1** . Thermal ellipsoid are drawn at the 50% probability. The acetonitrile solvent molecules are depicted as CPK representation.

3,5-pyridinecarboxamide-*N*-oxides **2** heteroditopic linear components were prepared following described synthetic procedures for similar compounds[27,28] (Figure 2.1).

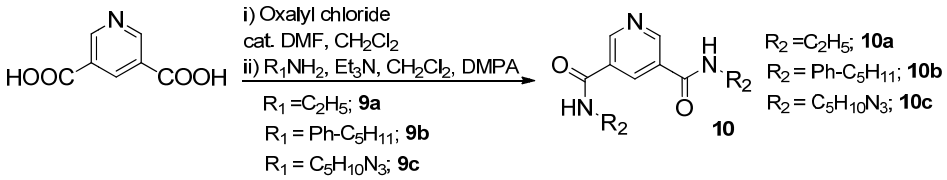

Figure 2.9 Synthetic scheme for the preparation of di-substituted pyridine-3,5-dicarboxamides **10**.

The series of pyridine-3,5-dicarboxamides **10** were prepared from the commercially available 3,5-pyridinedicarboxylic acid by reaction with oxalyl chloride and a catalytic amount of DMF to obtain the 3,5-pyridine acyl chloride. The acyl chloride is immediately subjected to react with the different diamines to afford the amide

derivatives **10a**, **10b** and **10c**. The amines **9a** and **9b** are commercially available and the amine **9c** was synthesized following described procedures.[29,30] Initially, 1,5-diazopentane was prepared by a nucleophilic substitution from the commercially available 1,5-dibromopentane in the presence of sodium azide. Later, the selective reduction of one azide was achieved with a Staudinger reaction using PPh_3 obtaining the monoamine substituted product **9c** in a 57 % yield. Finally, the three pyridine *N*-oxides **2a**, **2b** and **2c** were obtained by reacting **10a** with m-chloroperbenzoic acid and **10b** and **10c** with Oxone®.

2.2.2 Structural and thermodynamic characterization of [2]pseudorotaxanes **4a⊂1•2a** and **4a⊂1•2b**

The hydrogen bonding complementarity that exists between the receptor **1** and the linear component **2a** was proven by means of ^{1}H NMR titration experiments. The initial addition of 0.5 equiv of *N*-oxide **2a** over a millimolar $CDCl_3$ solution of the homoditopic macrotricycle **1** at room temperature produces a dramatic change in the ^{1}H NMR spectrum of **1** (Figure 2.10b).

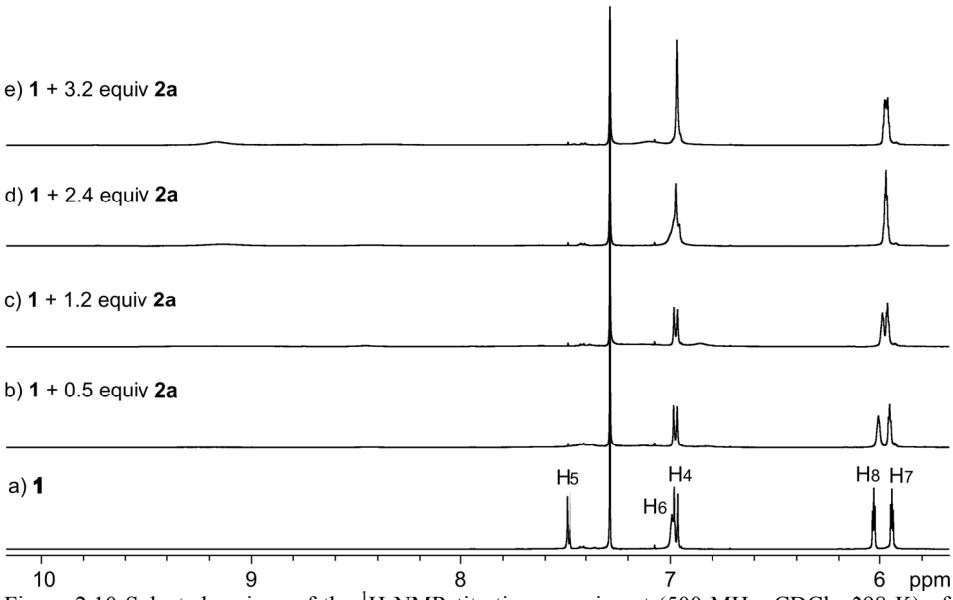

Figure 2.10 Selected regions of the ^{1}H NMR titration experiment (500 MHz, $CDCl_3$, 298 K) of ditopic macrotricycle [**1**]=**3** mM with *N*-oxide **2a**. The concentration of **1** was maintained constant throughout the titration. See Figure 2.1 for proton assignments.

The pyrrolic NHs proton signal becomes broad preventing direct observation but suggesting hydrogen bonding interactions (N-H···O) between the pyrrole NHs and the *N*-oxide oxygen. Likewise, the H_1, H_2, and H_3 proton signals for *N*-oxide **2a** are not detected due to broadening. The doublet corresponding to the H_5 protons of the *meso*-phenyl residues in **1** also broadened beyond detection. In order to calculate the association constant between **1** and **2a**, we analysed the chemical shifts changes of the β-pyrrole and the methyl protons of **1** using the HyPNMR2008 software. To calculate the association constant of the interaction between **2a** and **1** we have to take into account the formation of secondary species that could have an influence in the equilibrium under study. In the present case, **2a** *N*-oxide is able to dimerize/oligomerize by establishing hydrogen bond interactions. Figure 2.11b shows the putative structure for a trimeric species.

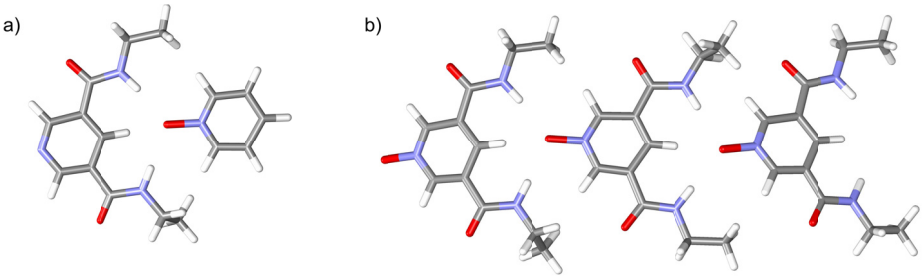

Figure 2.11 Energy-minimized structure[26] of a) dimer of N^3,N^5-diethylpyridine-3,5-dicarboxamide and pyridine *N*-oxide stabilized through hydrogen bond interactions and used as model system and b) trimer aggregate of **2a**.

If we consider isodesmic processes, this means the bonds that are broken and formed in every oligomer are equal, we can use a model system to evaluate a single pair of hydrogen bond interactions (Figure 2.11a).The association constant of the dimer formed by one *N*-oxide and one diamide through two hydrogen bond interactions was evaluated by ^{1}H NMR titrations (experimental section: Figure 2.42) of the commercially available pyridine *N*-oxide and the N^3, N^5-diethylpyridine-3,5-dicarboxamide. The microscopic association constant of the dimeric interaction resulted to be $K_{dimer} = K_{\mathbf{10a}\cdot pyridine.N\text{-}oxide} = 36.0\ M^{-1}$ (Figure 2.43 a). We evaluated the dimerization/oligomerization process of **2a** performing ^{1}H NMR dilution experiments (Figure 2.12). A 17 mM solution of ligand **2a** was diluted by the incremental addition of $CDCl_3$. The upfield shift experienced by the

signal of the amide NH groups upon dilution of the sample is indicative of the diminution of the amount of **2a** involved in hydrogen bonding aggregates.

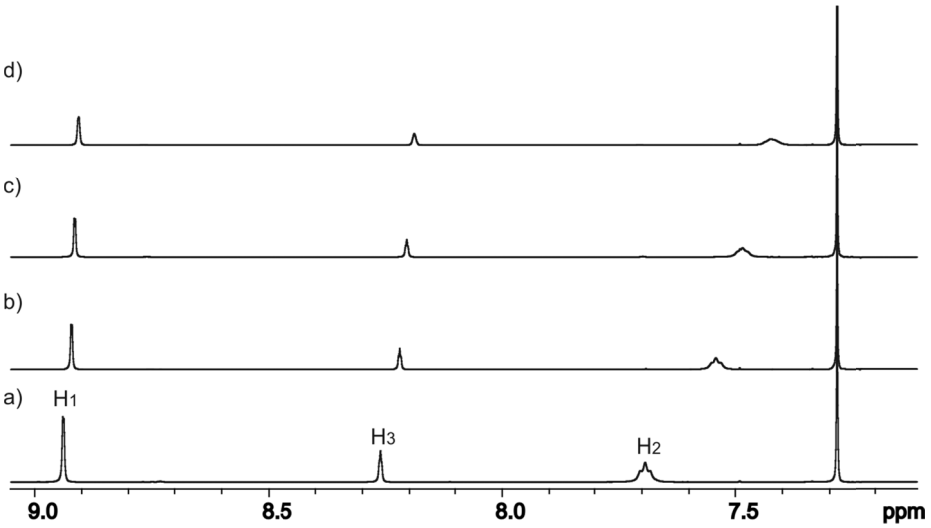

Figure 2.12 Downfield region of the ^{1}H NMR selected spectra (500 MHz, $CDCl_3$, 298 K) acquired during the dilution experiments of a 17 mM solution of **2a** by the incremental addition of $CDCl_3$.a) [**2a**] = 17 mM. d) [**2a**] = 5 mM.

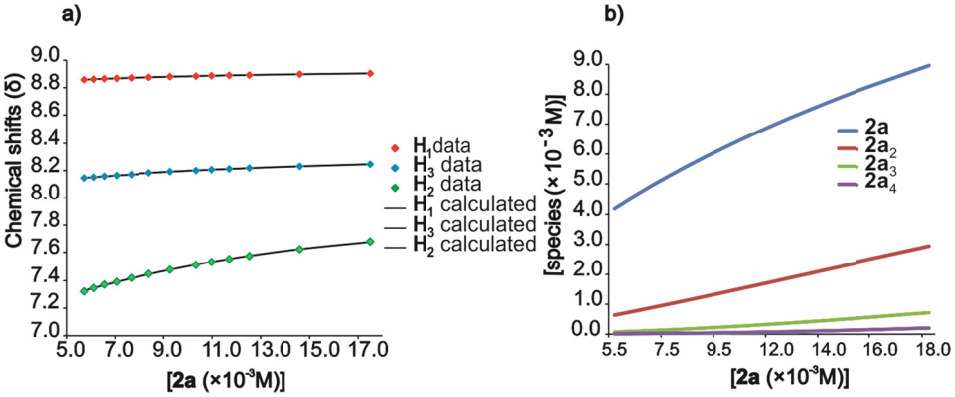

Figure 2.13 a) Fit of the chemical shift changes experienced by the proton signals of **2a** in the ^{1}H NMR dilution experiments to a theoretical binding model of an isodesmic oligomerization process that includes from dimeric to tetrameric species. $K_{dimer} = k_{m}$ =36.0 M^{-1}, b) speciation profile of the dilution experiment showing that tetrameric species is formed in almost negligible levels in the studied range of concentrations.

Fitting the data of the titrations and considering an isodesmic process we calculated the association constants of the species involved in the oligomerization process: the dimerization constant presents the same value that the microscopic constant, the

trimerization constant $K_{trimer} = K_m^2 = 1.2 \times 10^3\ M^{-2}$ and the tetramerization process $K_{tetramer} = K_m^3 = 4.6 \times 10^4\ M^{-3}$. Additionally, the species distribution profile at these experimental conditions indicates that the tetramer is not representative. Taking in consideration this results we conclude that at the working concentrations range, the tetramer and trimer of the **2a** *N*-oxide are almost not present in solution. Then, we did not consider this species in the calculation of the stability constant for the interaction between **2a** and **1** where we only considered the **2a** dimer formation.

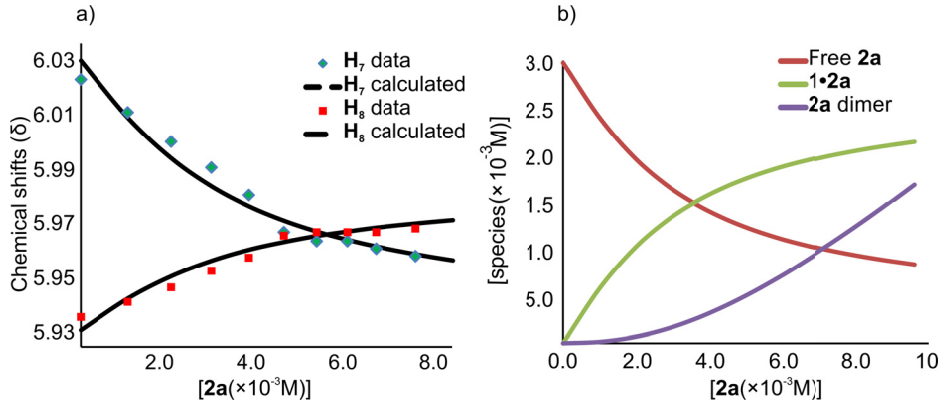

Figure 2.14 a) Fit of the chemical shift changes experienced by the signals of protons H_7 and H_8 of **1** during the titration with **2a** using a simple 1:1 binding model (lines) and the HyPNMR2008 software, b) Speciation diagram of the titration experiment.

The fit of the experimental data of the **1•2a** complex formation was performed using a simple 1:1 binding model. The apparent association constant value calculated for the **1•2a** was $K_{1•2a} = 800\ M^{-1}$. Although macrocycle **1** presents two identical binding sites, molecular modelling studies indicate that the size of the cavity is not big enough to allow the inclusion of two molecules of **2a**. Lowering the temperature of a sample containing **1** and 0.5 equiv of **2a** to 233 K enabled the observation of two well resolved downfield doublets corresponding to the *meso*-phenyl aromatic protons of free **1** (H_4, H_5) and two broad signals that were assigned to the same protons in the bound macrocycle (Figure 2.15). The integral ratio of free and bound signals is 1:1. Taken together these observations suggested the formation of a kinetically stable 1:1 complex between **1** and **2a** with a stability constant higher than $10^4\ M^{-1}$ at 233K.

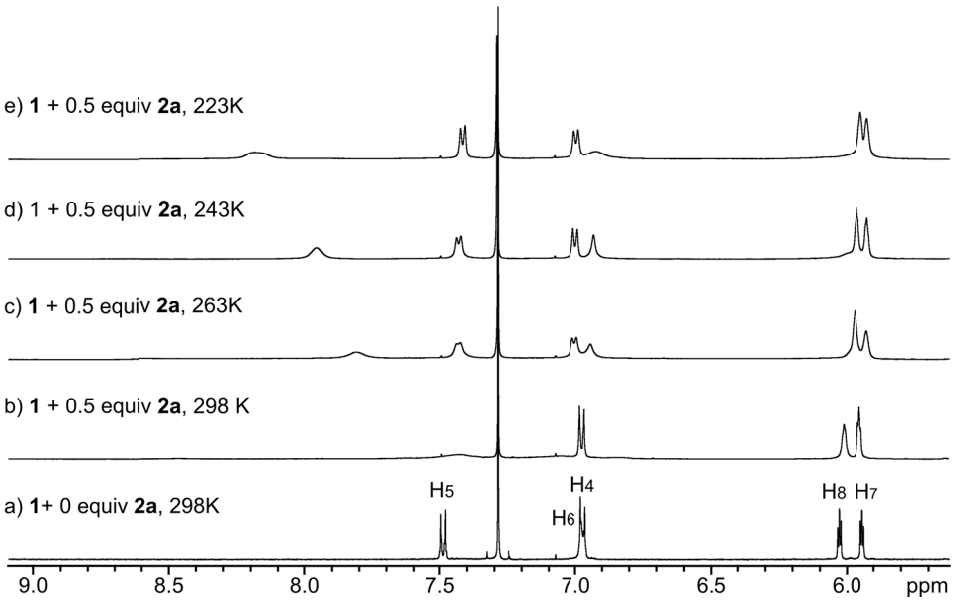

Figure 2.15 ^{1}H NMR spectra (500 MHz) acquired in a variable temperature experiment of a $CDCl_3$ solution containing macrocycle **1** and 0.5 equivalents of the lineal component **2a**.

We assigned a pseudorotaxane topology to the **1•2a** complex based on the chemical shift changes observed at 243 K for the *meso*-phenyl protons in free and bound **1**. We interpreted the dissimilar exchange dynamics for the two sets of *meso*-phenyl protons as the result of the interweaving geometry assigned to the **1•2a** complex. At 243K the threading-dethreading process becomes slow producing separate signals for the aromatic protons of free and bound macrocycle **1**. However, the pirouetting process of the linear component **2a** occurring at an intermediate rate on the ^{1}H NMR timescale within the **1•2a** complex produced broadening of the aromatic protons of bound **1**.

An interwoven structure for the **1•2a** complex was also observed in the solid-state (Figure 2.16b) where *N*-oxide **2a** is threaded through **1** showing disorder between two equivalent positions.

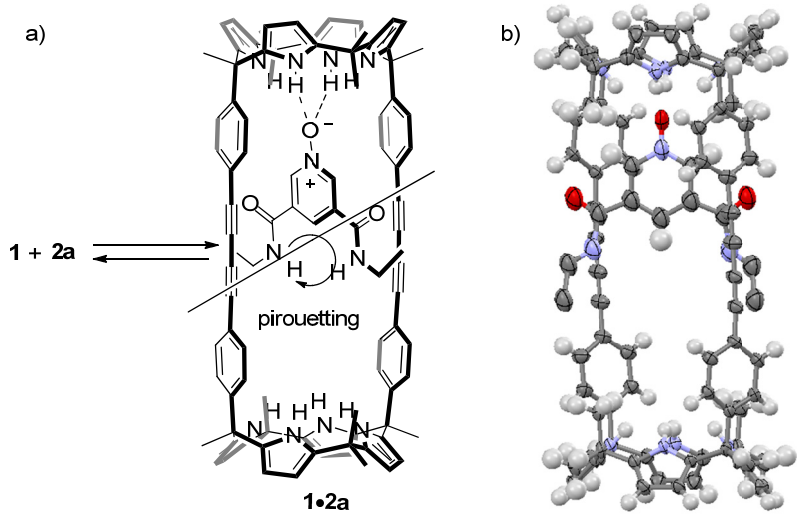

Figure 2.16 a) Self-assembly of **1•2a** where it is represented the pirouetting movement between the two equivalent positions of the *N*-oxide **2a** threaded through the annulus of the homoditopic bis-calix[4]pyrrole macrocycle **1**, b) X-ray structure of **1•2a** in acetonitrile. The disorder that **2a** showed in the solid state between the two equivalent calix[4]pyrrole interacting sites and the solvent molecules were removed for clarity.

It is worth highlighting that the amide functional groups of **2a** are positioned with a relative orientation of the two carbonyl groups pointing "up", what we called the α,α-conformation. Optimized geometries (Figure 2.17) and total energies were calculated for the three conformational isomers of the bis-amidepyridyl-*N*-oxide **2a** by the B3LYP method of theory using the 6-311G* basis set.

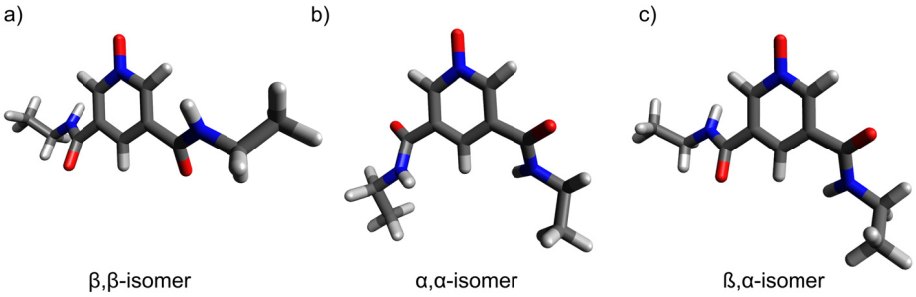

Figure 2.17 Conformational isomers of the bis-amidepyridyl-*N*-oxide **2a**: β,β-isomer a), α,α-isomer b) and β,α-isomer.

The calculated total energies are represented in Table 2.1 and indicate that the conformation with the lower energy of **2a** is the α,β conformation b).

Isomer	Total energy [E_h]	ΔE^* [E_h]	ΔE^* [Kcal.mol^{-1}]
β,β	-818,2988	0,0012	0,80075
α,α	-818,2981	0,0019	1,21103
β,α	-818,3000		

* The stabilities of the isomers a) and b) have been related as ΔE to the isomer c).

Table 2.1 Calculated total energies and relative stability of the conformational isomers.

The β,β-isomer and the α,α-isomer are 0,801 kcalmol^{-1} and 1,211 kcalmol^{-1} less stable than the β,α-isomer, respectively. Molecular modelling studies of the complex that results from the interaction between the more stable β,α-isomer of **2a** and **1** indicated that when the carbonyl group of the pyridine *N*-oxide is pointing "down", the ethylamide substituents brought their electron clouds close to the ones of the methyl-substituents of **1** (Figure 2.18). Probably the energetic cost of this unfavourable interaction is higher than the 1,211 kcalmol^{-1} energetic penalty that *N*-oxide **2a** has to pay when changing from the more stable β,α- to the α,α-conformation. Additionally, a molecule of solvent is hydrogen bound to both pyridine NHs as revealed the X-ray structure of the complex in acetonitrile. Such interaction also contributes to the stabilization of the less stable α,α-conformation of the bis-amidepyridyl-*N*-oxide.

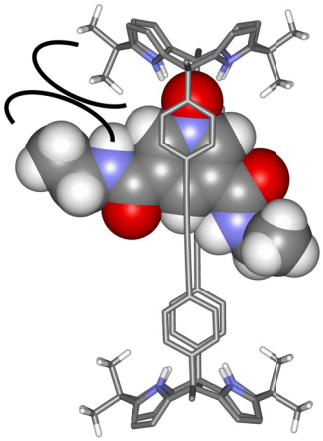

Figure 2.18 Energy-minimized[26] structure of the complex between **1** and the β,α conformational isomer of **2a** where it is marked the stearic hindrance between the methyl protons of receptor **1** and the ethyl amide substituents in the *N*-oxide **2a**.

The addition of 1 equivalent of tetrabutylammonium cyanate **4a** to an equimolar $CDCl_3$ solution of **1** and **2a** produced a dramatic change in the ^{1}H NMR spectrum of the

mixture (Figure 2.19 d). All proton signals for **1** and **2a** became sharp, well defined and were easily assigned. Two different and highly downfield shifted signals for the pyrrole NH protons (H_{11} and H_{19}) of **1** indicate participation in distinct hydrogen bonding interactions. Four different sets of proton signals were observed for the aromatic and β-pyrrole protons. These findings point to an unsymmetrical assembly (Figure 2.20). All the proton signals of the bis-amidepyridyl-*N*-oxide **2a** are broad and experienced significant chemical shift changes with respect to those observed for **2a** alone. In addition, the multiplet of the methylene protons *alpha* to the nitrogen atom of the tetrabutylammonium cation in the free **4a** become broad and it was upfield shifted.

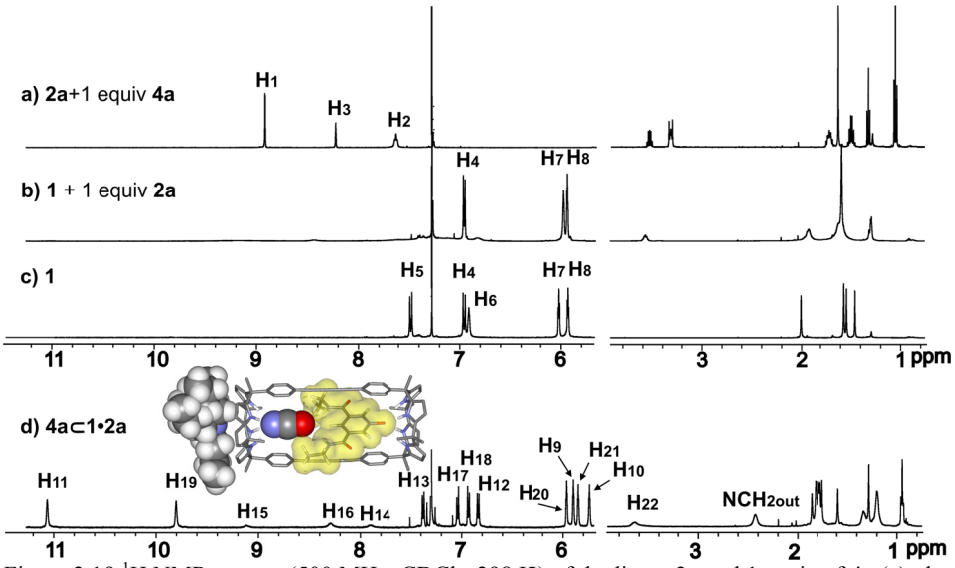

Figure 2.19 ^{1}H NMR spectra (500 MHz, $CDCl_3$, 298 K) of the linear **2a** and 1 equiv of **4a** (a), the macrotricycle **1** and 1 equiv of linear **2a** (b), cyclic free **1** (c) and the solution containing the three components **1**, **2a** and **4a** in a 1:1:1 ratio (d). Inset: Energy minimized structure[26] of ion-paired [2]pseudorotaxane complex **4a⊂1•2a**. See Figure 2.1 and Figure 2.20 for proton assignments.

Taken together these observations, give strong support for the quantitative formation of an unprecedented four component pseudorotaxane-like complex between macrocycle **1**, linear component **2a** and ion pair **4a** (Figure 2.19d). Accordingly, the ditopic linear component **2a** threads into **1** and hydrogen bonds its *N*-oxide group to one of the calix[4]pyrrole caps of macrotricycle **1** as described for the **1•2a** complex. Furthermore, the polyatomic anion guest hydrogen bonds simultaneously to the amide NHs of **2a** at one end and to the opposing calix[4]pyrrole unit of **1**. The cyanate anion is included in

the three dimensional cavity defined by the macrotricycle and the linear component of the pseudorotaxane, in which up to six hydrogen-bond donors converge, whereas the tetrabutylammonium counter-ion is located in the shallow external cavity defined by the pyrrole rings opposite to the included anion. Thus, pseudorotaxane-like complex **4a⊂1•2a** displays a *host*-separated ion-pair arrangement. In short, ion pair **4a** acts as a template capable of driving the equilibria towards the quantitative assembly of a four-particle aggregate with pseudorotaxane topology. The cyanate anion is ambidentate. Most likely, in solution the sandwiched anion rotates freely within the complex. In addition, the stability constant of the [2]pseudorotaxane complex can be estimated as $K_{\mathbf{4a\subset 1\bullet 2a}} > 10^8\ M^{-2}$.

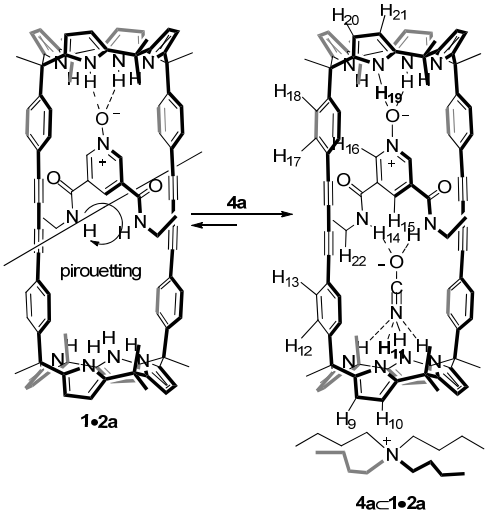

Figure 2.20 Molecular structures involved in the quantitative self-assembly of **4a⊂1•2a** from the thermodynamically labile complex **1•2a**.

Bidimensional ^{1}H NMR experiments COSY and ROESY were used to assign the proton signals of **4a⊂1•2a** and revealed close intermolecular contacts as expected from the described pseudorotaxane topology (Figure 2.21). Intermolecular cross-peaks indicating spatial proximity are observed between the NHs proton signal H_{19} of one calix[4]pyrrole hemisphere and the protons *alpha* H_{16} to the pyridine *N*-oxide ligand **2a** (Figure 2.21a). Moreover, close contacts peaks between the methylene protons *alpha* to the nitrogen of the TBA cation and the β-pyrrolic protons H_9 and H_{10} are also detected ratifying the placement of the TBA cation in the aromatic shallow external cavity defined by the

pyrrole rings opposite to the included anion. The cross-peaks in the ROESY experiment (Figure 2.22a) between the two NH pyrrolic protons H_{11} and H_{19} indicating chemical exchange confirm the interconversion of the two chemically magnetically inequivalent hemispheres of the macrotricycle **1** when is forming the **4a⊂1•2a** complex.

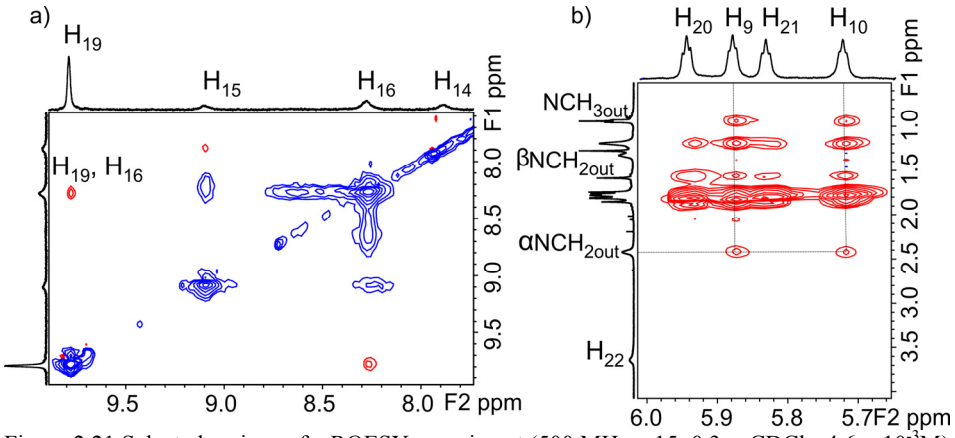

Figure 2.21 Selected regions of a ROESY experiment (500 MHz, p15: 0.3 s, $CDCl_3$, 4.6 × 10^{-3}M) of the 1:1:1 [2]pseudorotaxane complex **4a⊂1•2a** showing a) cross-peaks indicating intermolecular close contacts between the *ortho*-protons of the pyridyl-*N*-oxide **2a** (H_{16}) and the NH pyrrole signal at 9.8 ppm of **1** (H_{19}). The chemical exchange that exists between bound **2a** and a small excess of the free component is also detected. b) cross-peaks indicating intermolecular close contacts between the methylene protons *alpha* to the nitrogen of the TBA cation and the β-pyrrolic protons H_9 and H_{10}.

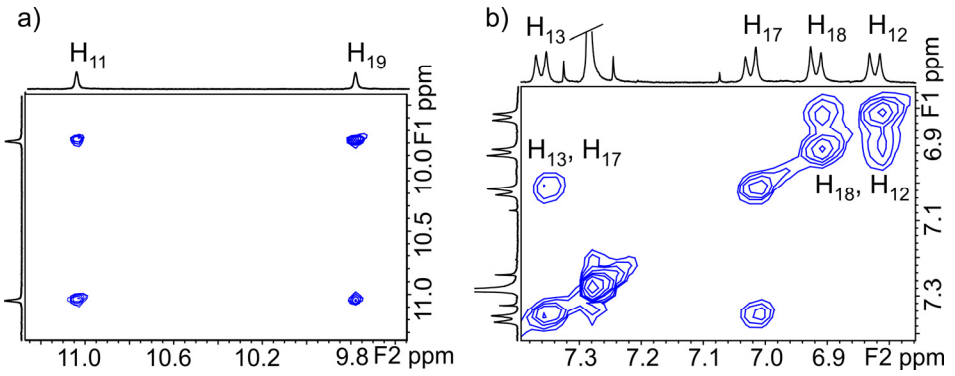

Figure 2.22 Selected regions of the ROESY experiment (500 MHz, p15: 0.3 s, $CDCl_3$, 4.6 × 10^{-3} M) of the [2]pseudorotaxane complex **4a⊂1•2a** showing cross-peaks indicating chemical exchange between the β-pyrrolic protons and the aromatic protons of the two non-equivalent hemispheres of the receptor **1**.

We also ascribed the broadness of the proton signals corresponding to the *N*-oxide ligand when is forming the complex **4a⊂1•2a** to the pirouetting of the included **2a·4a** between the two equivalent positions of the macrotricycle **1**. Since the longitudinal size of the linear component **2a** is smaller than the distance between the two calix[4]pyrrole cores in macrotricycle **1**, the freely rotation of the included **2a•4a** components inside the macrocycle is a plausible mechanism. However, it is also possible that such equilibrium involves the dissociation of the two species included within the receptor **1**. To gain more insight about this process, we decided to investigate the binding properties of the longer *N*-oxide **2b** (Figure 2.1). In complete agreement with the results obtained for the **4a⊂1•2a** assembly (*vide supra*); upon addition of an equimolar mixture of **2b** and **4a**, all the chemically equivalent pyrrolic and aromatic protons of **1** became magnetically inequivalent giving rise to the splitting of their signals. These results point out again to an asymmetrical assembly (Figure 2.23).

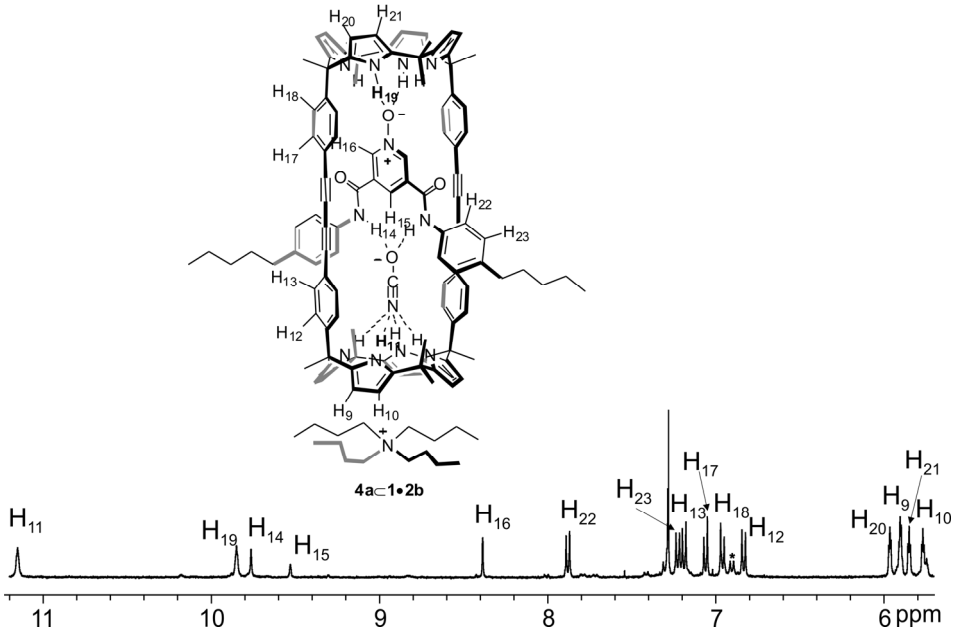

Figure 2.23 Top: Molecular structure of the **4a⊂1•2b** pseudorotaxane. Bottom: downfield region of the ^{1}H NMR spectrum (500 MHz, $CDCl_3$, 298 K) of the solution containing the three components **1**, **2b** and **4a** in a 1:1:1 ratio and quantitatively assembled.*= impurity.

According to that, two different downfield shifted signals are observed for the pyrrolic NH protons that are participating in two distinct hydrogen bond interactions. Four

different aromatic and β-pyrrolic signals are observed corresponding to the two magnetically inequivalent hemispheres of the macrocycle. H_{14}, H_{15} and H_{16} signals of the coordinated *N*-oxide **2b** are sharp and downfield shifted compared with the ones of free **2b**. ROESY experiments allowed the assignment of all proton signals of the assembly. Interestingly, no chemical exchange cross peaks were observed in the bidimensional ROESY experiment between the two calix[4]pyrrole hemispheres. This results indicate that the longer *N*-oxide **2b** prevent the mechanism that is responsible of the chemical exchange cross-peaks in the case of **4a⊂1•2a**. Most likely, it involves the pirouetting movement of **1** or **2a•4a** around to each other.

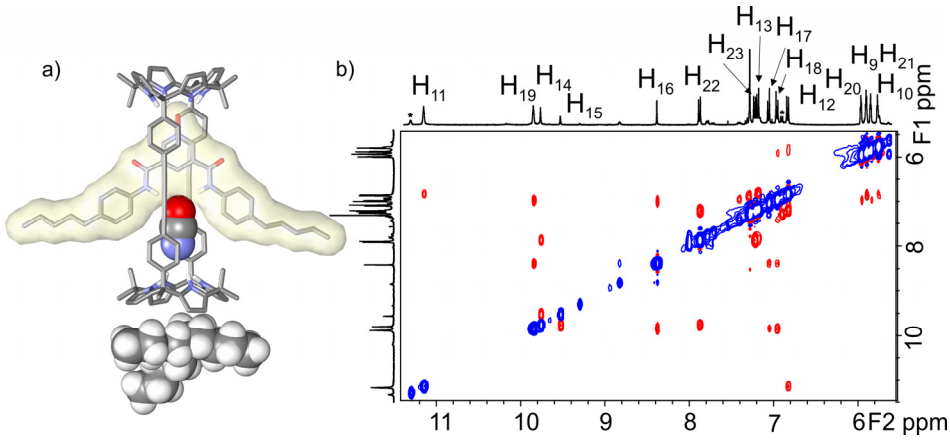

Figure 2.24 a) Energy-minimized structure[26] of [2]pseudorotaxane **4a⊂1•2b**. b) ROESY experiment (500 MHz, p15: 0.3 s, $CDCl_3$, 4.6×10^{-3} M) of the [2]pseudorotaxane complex **4a⊂1•2b** not showing any cross-peaks indicating chemical exchange between the β-pyrrolic protons and the aromatic protons of the receptor **1**. The signals marked with * correspond to the complex $\mathbf{4a_2}\subset\mathbf{1}$ due to a small excess of **4a**.

DOSY experiments also supported the formation of the pseudorotaxane-like complex **4a⊂1•2a** in solution. The values of the diffusion coefficients in $CDCl_3$ solutions of **2a** and **4a** are larger (7.5 and 8.2×10^{-10} m^2s^{-1}, respectively) than for **1** (5.0×10^{-10} m^2s^{-1}). This is expected based on their relative molecular weights and sizes. A 2D DOSY experiment performed of an equimolar mixture of **1**, **2a** and **4a** showed similar diffusion profiles for the three components supporting their participation in a common aggregate (Figure 2.25a). We also determined the diffusion coefficient value of the formed supramolecular entity **4a⊂1•2a** as 4.5×10^{-10} m^2s^{-1}. Not surprisingly, this value is only slightly lower than the one calculated for the free component **1**. This is because,

although the change in molecular weight of **1** *vs.* **4a⊂1•2a** is considerable, this is not the case for the values of the hydrodynamic radii.

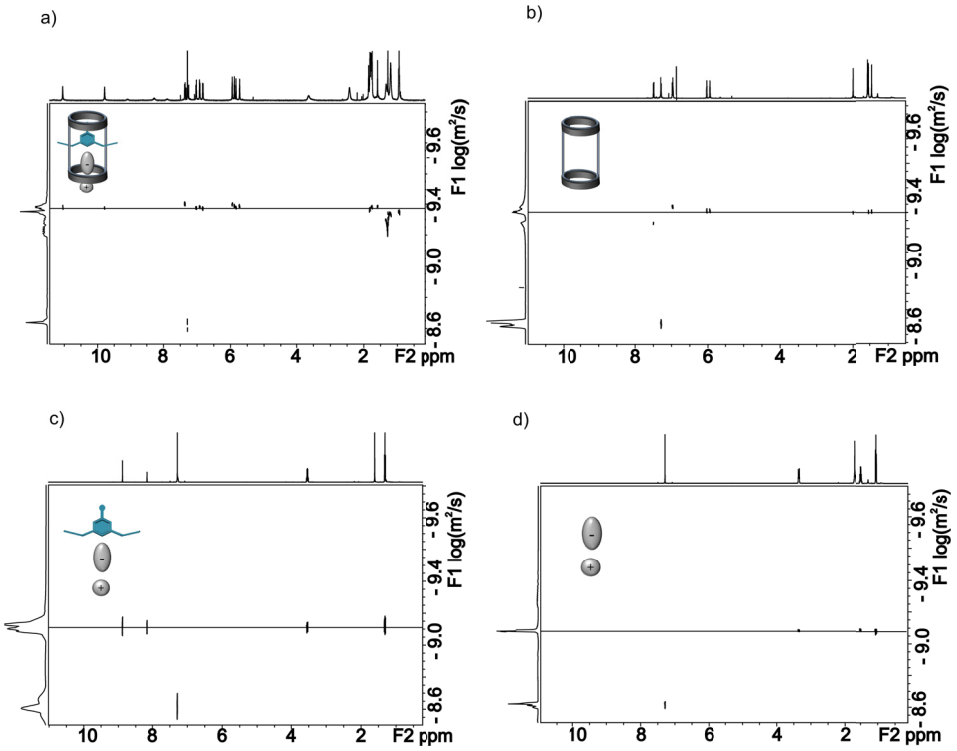

Figure 2.25 DOSY ^{1}H NMR experiments processed as 2D spectra (500 MHz, 298K, 4.9×10^{-3} M) a) **4a⊂1•2a**; b) **1**; c) **2a•4a** and d) **4a**.

To study the thermodynamic stability of the **4a⊂1•2a** pseudorotaxane-like complex, we determined the binding constant of every interaction involved in the assembly. The association constant of linear component **2a** and tetrabutylammonium cyanate **4a** was determined by ^{1}H NMR titration experiments. To a chloroform solution of ligand **2a** increasing quantities of tetrabutylammonium cyanate **4a** salt were added. The solution of **4a** was prepared using as a solvent a solution of ligand **2a** in $CDCl_3$ to keep the concentration of the *N*-oxide constant during the titration and avoid dilution processes. Selected spectra of the titration increasing the number of equivalents of tetrabutylammounium cyanate salt are depicted in Figure 2.26. Upon addition of tetrabutylammonium cyanate **4a** the proton signal corresponding to the NHs of the

amides of **2a** is downfield shifted suggesting hydrogen bond interactions with the cyanate anion.

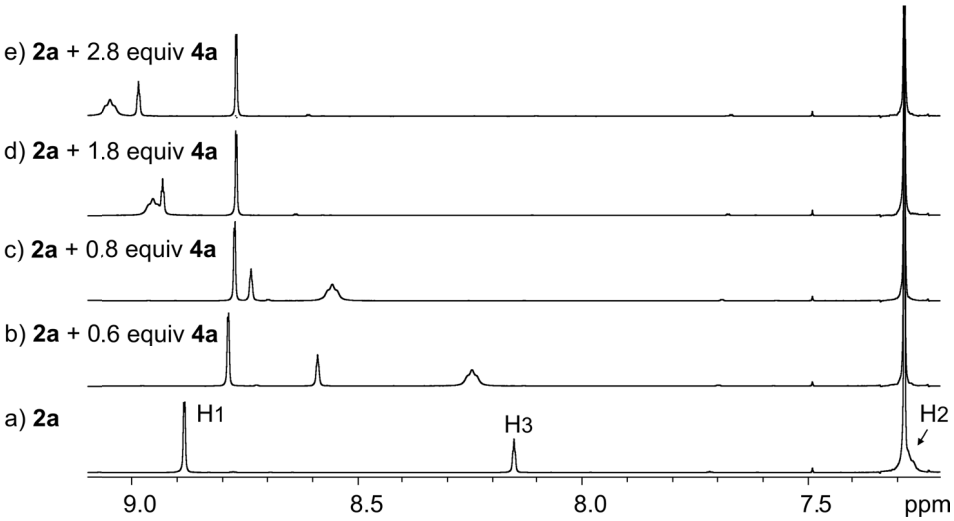

Figure 2.26 Downfield region of selected ^{1}H NMR spectra (500 MHz, 298 K, $CDCl_3$) acquired during the titration of N^3,N^5-diethylpyridine-3,5-dicarboxamide *N*-oxide [**2a**] = 4.3 mM with tetrabutylammonium cyanate **4a**. See Figure 2.1 for proton assignments.

The data fitting of the titration (Figure 2.27) was done using the HypNMR2008 program and based on the chemical shift changes of the protons H_1, H_2 and H_3 of **2a** (Figure 2.26). It was done considering the presence of five species in solution: free **4a** and **2a**, dimer $\mathbf{2a}_2$, trimer $\mathbf{2a}_3$ and **2a•4a**. The association constants of dimer $\mathbf{2a}_2$ and trimer $\mathbf{2a}_3$ are already known from the **2a** dilution experiment and were calculated as $K_{dimer} = k_m = 36.0\ M^{-1}$ and $K_{trimer} = k_m^2 = 1.2\times10^3\ M^{-2}$ (Figure 2.13). With this considerations the program returned a binding constant for the interaction between **4a** and **2a** of $K_{\mathbf{4a\cdot 2a}} = 1.6\times10^3\ M^{-1}$. The species distribution profile shows that the presence of the dimer and trimer of **2a** is negligible at the working concentrations (Figure 2.27b). As mentioned above the ^{1}H NMR spectrum of an equimolar mixture of **1**, **2a** and **4a** showed slow chemical exchange on the NMR time scale between the free and components forming the **4a⊂1•2a** pseudorotaxane-like complex (Figure 2.19).

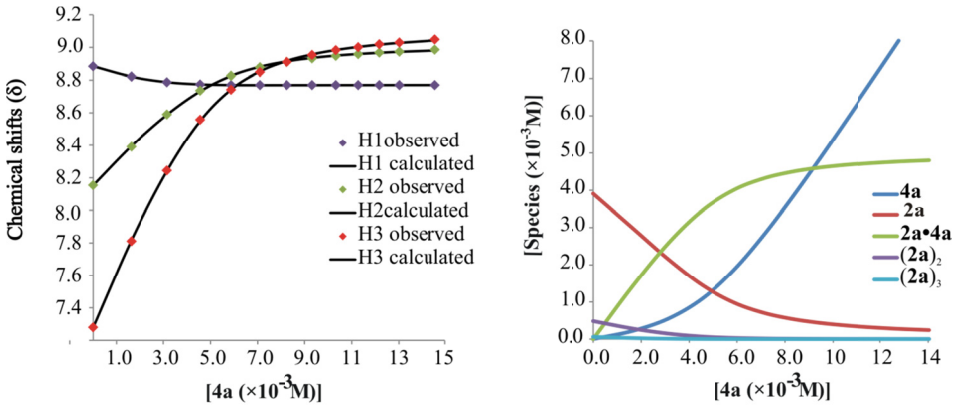

Figure 2.27 Left: Fit of the data obtained in the ^{1}H NMR titration of **2a** with **4a** to a theoretical binding model that considers the formation of the 1:1 complex **2a•4a** and the oligomerization (dimer and trimer) of **2a** (*vide infra*): $K_{4a\cdot 2a} = 1.6 \times 10^3$ M^{-1}. Right: Speciation profile of the titration.

This suggests that the pseudorotaxane-like assembly present an association constant higher than 10^8 M^{-2}. Since association constants higher than 10^4 cannot be determined by ^{1}H NMR titration experiments we used isothermal titration calorimetry (ITC) to quantify the thermodynamic stability of the **4a⊂1•2a** pseudorotaxane-like complex. A $CHCl_3$ solution of *N*-oxide **2a**, [**2a**]=0.6 mM, was added to an equimolar mixture of **1** and **4a** , [**1**]=[**4a**]=0.06 M that produced a gradual release of heat due to the exothermic binding process (Figure 2.28). The mathematical analysis of the titration data was performed using the HypΔH software which allows handling systems with any number of reagents and complexes of any stoichiometry.[31] In the formation of **4a⊂1•2a** pseudorotaxane-like complex we have to consider the presence of other complexes that can be form due to the interaction of the biscalix[4]pyrrole macrocycle **1** and the ion pair **4a**. Since receptor **1** holds two equivalent binding sites, one can expect the coordination of one or even two ion pairs within it, resulting the complexes **1•4a** and **1•4a**$_2$, respectively. Then, the resulting binding isotherm (normalized integrated heat *vs.* molar ratio [**2a**]/[**1•4a**]) (Figure 2.28) was analysed using a binding model that considered the formation of the following species: **4a⊂1•2a**, **1•4a** and **1•4a**$_2$. The value of the stability constants and enthalpies of the **1•4a** and **1•4a**$_2$ species were calculated in an alternative experiment.

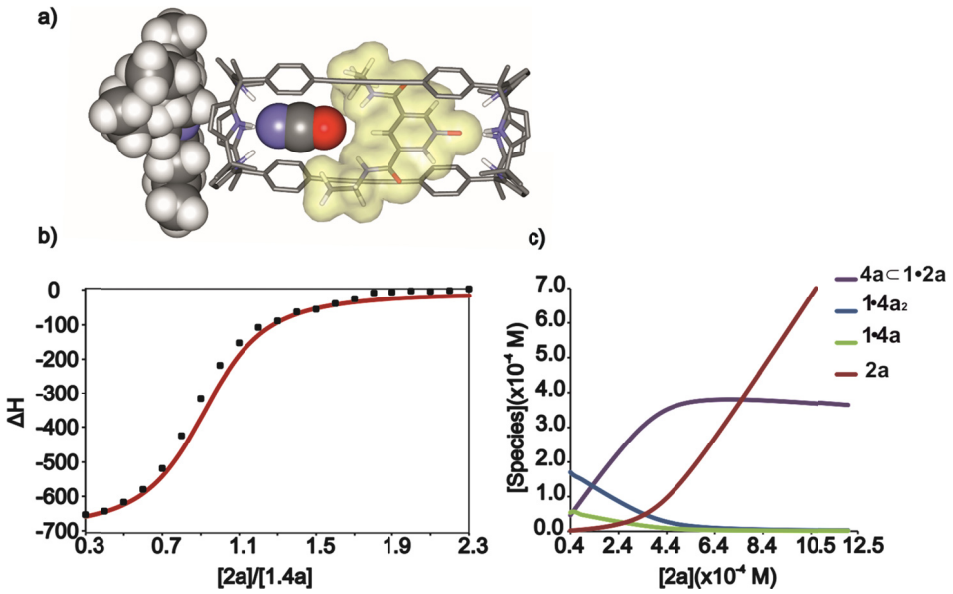

Figure 2.28 a) Energy-minimized structure[26] of the [2]pseudorotaxane **4a⊂1•2a.** The polyatomic anion used to template the assembly is tetrabutylammonium cyanate b) Data points obtained in the ITC experiment of an equimolar $CHCl_3$ solution of **1** and **4a** with **2a**. Fit to the theoretical binding isotherm (red line) using a binding model that considers the formation of three different aggregates: **4a⊂1•2a**, **1•4a**, and **1•4a$_2$**. Conditions: [**2a**] = 0.6 mM syringe and [**4a**] and [**1**] = 0.06 mM calorimeter cell, c) Simulated speciation diagram of the titration experiment. The determined thermodynamic variables were: $K_{\mathbf{4a\subset 1\cdot 2a}} = 9.1\times10^{10}$ M^{-2}, ΔH = - 1.4 kcal/mol. The thermodynamic variables for the formation of the complexes **1•4a** and **1•4a$_2$** were fixed to the values obtained in a previous experiment.

The stepwise injection of a $CHCl_3$ solution of receptor **1** to a solution of **4a** in the same solvent produces a highly exothermic process (Figure 2.29). The thermodynamic characterization of these complexes is deeply analysed in *Chapter 4*. The calculated thermodynamic variables derived from the fit were: $K_{\mathbf{1\cdot 4a}} = 1\times 10^5$ M^{-1}, ΔH = -5 kcal/mol, $K_{\mathbf{1\cdot 4a2}} = 1\times 10^{11}$ M^{-2}, ΔH = -13 kcal/mol. These values were fixed in the mathematical treatment of the experimental results for the thermodynamic characterization of the **4a⊂1•2a** pseudorotaxane-like complex (Figure 2.28). The best fitting of the experimental data was achieved using the following values for the thermodynamic variables $K_{\mathbf{4a\subset 1\cdot 2a}} = 9.1\times 10^{10}$ M^{-2}, ΔH = - 1.4 kcal/mol. It is surprising that the values of the calculated association constants of the formation of the **1•4a$_2$** complex and the pseudorotaxane **4a⊂1•2a**, are very similar. Fortunately, we can corroborate experimentally that the formation of the pseudorotaxane is favourable.

As general consideration, it is important to remark that the stability constants values of the complexes involving ion pair **4a** should be considered as apparent because ion pair dissociation and ion-paired complex formation equilibria are not taken in consideration in the mathematical analysis of the titration data.

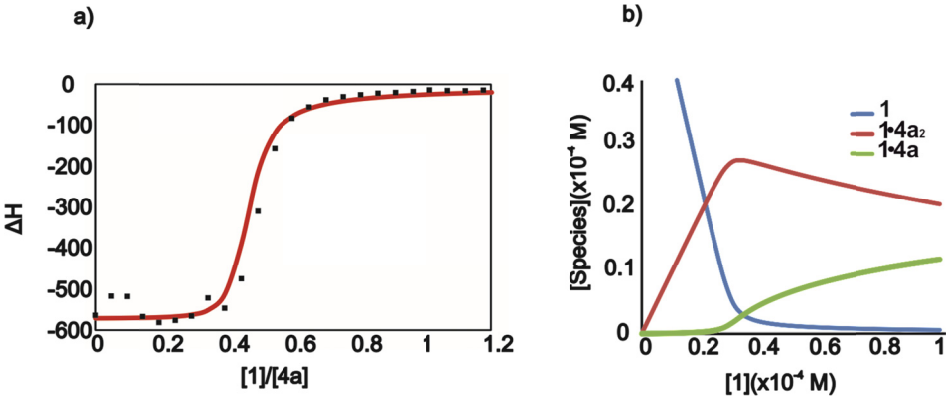

Figure 2.29 a) Data points (squares) obtained in the ITC experiment of **4a** with **1**. The fit to the theoretical binding isotherm (red line) was performed using the HypΔH software and a binding model that considers the formation of two aggregates. Conditions: [**1**] = 6.4 mM syringe and [**4a**] = 0.64 mM calorimeter cell, c) Speciation diagram of the titration.

The quantitative assembly of pseudorotaxane **4a⊂1•2** was also independent of the order of addition of its components. During the experimental investigations of the different addition strategies for the assembly of pseudorotaxane **4a⊂1•2a**, we also determined the stability constants of all the intermediate species. We performed simulated speciation's using the SPECFIT software program of the three possible addition alternatives for a two-step formation of **4a⊂1•2a** (Figure 2.30). The stability constants used in the simulation are those calculated for all the intermediate species by ^{1}H NMR and ITC experiments. In complete agreement with experimental observations, the simulated profiles showed that working under strict stoichiometric conditions (1 equivalent of each component) the pseudorotaxane **4a⊂1•2a** is quantitatively assembled independently of the order of addition of the components. However, the simulated speciation profiles indicated that when ion pair component **4a** is added incrementally, pseudorotaxane **4a⊂1•2a** disassembles in favour of the formation of **1•4a**$_2$ in the presence of more than 1 equivalent of ion pair. In contrast, self-assembled

pseudorotaxane **4a⊂1•2a** remains stable in the presence of excess of either of the two other components: macrocycle **1** or *N*-oxide **2a**.

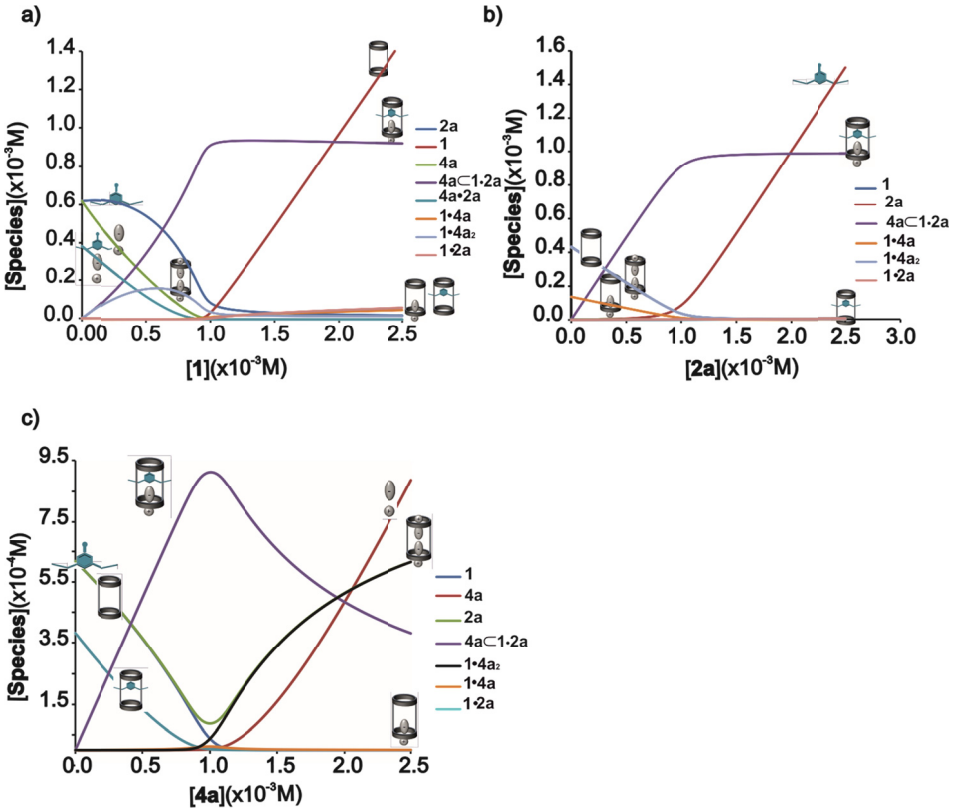

Figure 2.30 a) Speciation profiles of the addition of increasing quantities of **1** over an equimolar mixture of **2a** and **4a**. b) Speciation profiles of the addition of increasing quantities of **2a** over an equimolar mixture of **1** and **4a**. c) Speciation profiles of the addition of increasing quantities of **4a** over an equimolar mixture of **1** and **2a**. Notice when more than one equivalent of **4a** is added [2]pseudorotaxane **4a⊂1•2a** disassembles in favour of the formation of **1•4a**$_2$.

Experiments were in complete agreement with the simulated speciation profiles. In the presence of excess macrocycle **1** or *N*-oxide **2a**, pseudorotaxane **4a⊂1•2a** remained intact. The addition, at room temperature, of one equivalent of **2a** to a $CDCl_3$ solution of the [2]pseudorotaxane **4a⊂1•2a** produced broad and separated proton signals for the free and the coordinated ligand (Figure 2.31b). All the diagnostic signals corresponding to the intact [2]pseudorotaxane **4a⊂1•2a** were also observed. Lowering the temperature of the sample produced chemical shift changes in the signals of the protons for free and bound **2a** with a concomitant sharpening effect especially for those of bound **2a** (Figure

2.31 c, d, e). These observations suggest that the chemical exchange processes in which free and bound **2a** are involved become slower on the NMR timescale owing to the temperature.

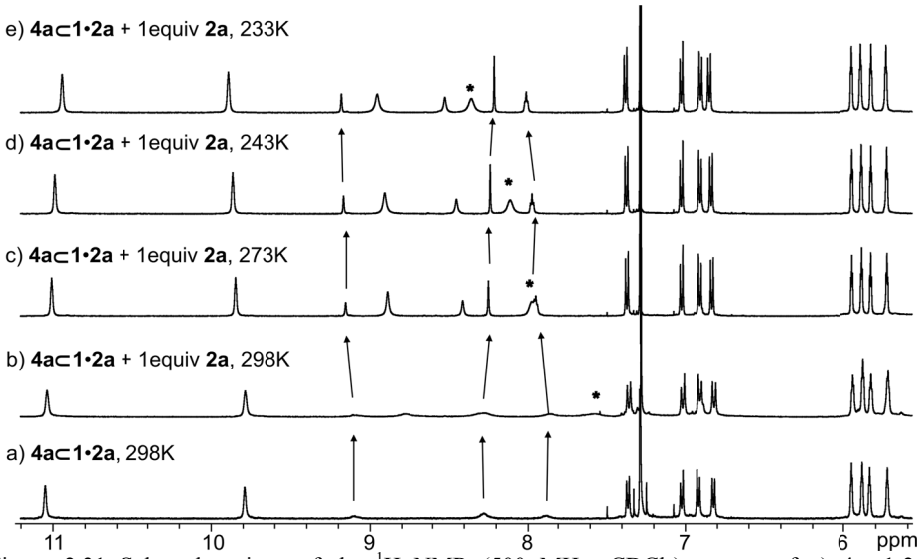

Figure 2.31 Selected regions of the ^{1}H NMR (500 MHz, $CDCl_3$) spectra of a) **4a⊂1•2a**, [**4a⊂1•2a**] = 3mM at 298 K, b) **4a⊂1•2a** + 1 equivalent of **2a** at 298K and **4a⊂1•2a** + 1 equivalent of **2a** at 273 K c), 243 K d), 233 K e). The chemical shift changes experienced by the proton signals of bound **2a** are indicated with arrows. The NH proton of free **2a** is signalled with an asterisk.

In contrast, the addition of excess of **4a** induced the emergence of proton signals assigned to **1•4a**$_2$ at the expense of those corresponding to **4a⊂1•2a** when an excess of **4a** was added to the solution containing the intact pseudorotaxane and free **2a** (

Figure 2.32). The presence of the singlet resonating at δ = 11.3 ppm indicates the formation of **1•4a**$_2$ to the expense of **4a⊂1•2a**.

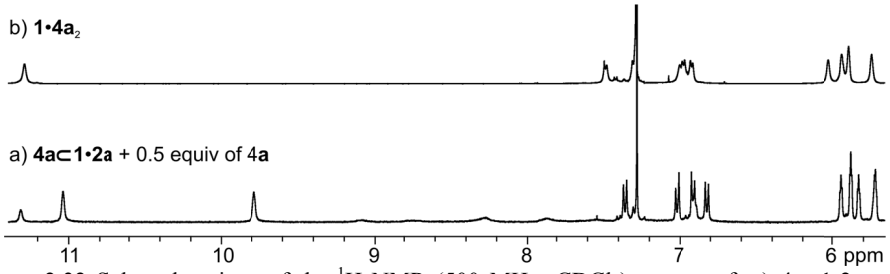

Figure 2.32 Selected regions of the ^{1}H NMR (500 MHz, $CDCl_3$) spectra of: a) **4a⊂1•2a** with excess of **4a**, the release of **2a** owing to pseudorotaxane disassembly is also visible; b) **1•4a**$_2$ complex.

2.2.3 Other ion pairs used as templates in the formation of [2]pseurotaxanes

The three-dimensional cavity of the **1•2a** supramolecular receptor possessing six convergent hydrogen-bond donors complements the hydrogen-bond acceptor guests as anions. Anions are represented in a wide range of shapes and geometries i.e. spherical (halides), linear (SCN and N_3) or trigonal planar (NO_3) among others. Since the receptor cavity presents fix dimensionality, a suitable geometry of the anion is a requirement to template the quantitative assembly of **4⊂1•2a** [2]pseudorotaxanes. Together, hydrogen bonding characteristics and the shape and size of the polyatomic anions are key parameters for the quantitative assembly of the **4⊂1•2** aggregates. Firstly, we decided to compare the formation of [2]pseudorotaxanes templated with ion pairs having an identical cation (TBA) but anions of different size, shape or polarizability. Secondly, by using ion pairs containing the same anion, the influence of different cations was investigated.

The anion recognition properties of self-assembled neutral heteroditopic receptor **1•2a** towards different tetrabutylammonium salts of polyatomic anions (azide **4c**, thiocyanate **4b** and nitrate **4d**) were studied. The azide anion **4c** provided parallel results to those observed for **4a**. The ^{1}H NMR spectrum of an equimolar mixture of **1**, **2a** and **4c** gives rise to the characteristic signals expected for an asymmetrical assembly that corresponds to the quantitative assembly of **4c⊂1•2a** [2]pseudorotaxane (Figure 2.33 c). The stability constant of this complex can be estimated as $K_{\mathbf{4c\subset 1\cdot 2a}} > 10^8$ M^{-2}. We observed two different signals for the pyrrolic NHs indicating its participation in different kind of hydrogen-bond interactions. Similarly to the **4a⊂1•2a** spectrum and based on bidimensional experiments, we assigned the most downfield signal to the NHs (H_{11}) that are charge-assisted hydrogen bound to one extreme of the linear azide anion.

The NH pyrrolic protons H_{11} resonate at 10.8 ppm (11.1 ppm when cyanate is involved in the assembly). The difference in chemical shift (0.3 ppm) reveals that azide is bound to the **1•2a** receptor through weaker hydrogen-bond interactions compared with cyanate. One explanation could be the different nature of the hydrogen-bond interactions (NH···N *vs.* NH···O) or as it is more probable in the present case, that the azide anion does not complement the host cavity as good as the cyanate.

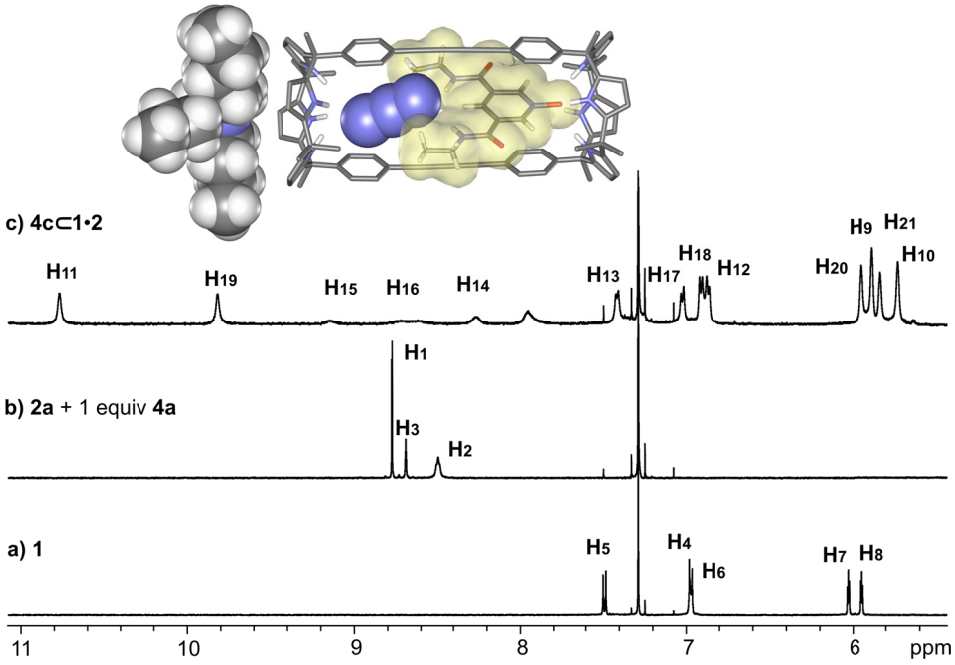

Figure 2.33 Bottom: ^{1}H NMR spectra (500 MHz, $CDCl_3$, 298 K) of a) **1**, b) **2a•4c** and c) **4c⊂1•2a** where it is observed a small excess of 2a. Top: Energy-minimized structure[26] of the pseudorotaxane **4c⊂1•2a** with tetrabutylammonium azide **4c** as template. See Figure 2.1 and Figure 2.20 for proton assignments.

To gain insight into the features of the hydrogen bond interactions established between the azide and the bis-amide *N*-oxide ligand, we determined the stability constant of the interaction between **2a** and **4c** by means of ^{1}H NMR titrations (see experimental section Figure 2.45). For the sake of comparison, the titration was performed using identical experimental conditions than in the case of tetrabutylammonium cyanate **4a**. The treatment of the data was performed using HypNMR2008 software and considering also the possible formation of dimeric and trimeric species of **2a** (see experimental section Figure 2.46). The association constant resulted to be $K_{\mathbf{4c•2a}} = 2\times 10^3$ M^{-1}. The similar magnitude for the association constant of TBAOCN ($K_{\mathbf{4a•2a}} = 1.6\times 10^3$ M^{-1}) and $TBAN_3$ with **2a** make us to conclude that the intrinsic nature of the hydrogen bonds is not the factor which explains the differences observed in the ^{1}H NMR spectra of **4c⊂1•2a** compared with **4a⊂1•2a**. Molecular modelling studies indicated that azide is too large (0.42Å larger than cyanate) to perfectly fit the **1•2a** receptor cavity (Figure 2.31 top).

The most reported examples of hydrogen bonding hosts for the recognition of polyatomic anions are tested for those containing elements of the first row of the periodic table such as N, O, and F as hydrogen bond acceptors.[32, 33, 34] The recognition of anions formed by second row elements such as S as hydrogen bond acceptors are scarce. Here, we studied the templating properties of the ambidentate polyatomic anion thiocyanate **4b** as tetrabutylammonium salt in the assembly of [2]pseudorotaxanes. In striking contrast with the results observed for **4a** and **4c**, the addition of 1 equivalent of the linear thiocyanate **4b** to an equimolar $CDCl_3$ solution of **1** and **2a** did not produce ^1H NMR spectra with sharp or well resolved signals. Several proton signals in **1** and **2a** were not even observable due to broadening (Figure 2.34 a). However, lowering the temperature to 213 K results in a ^1H NMR spectrum which contains the diagnostic proton signals expected for the quantitative assembly of the pseudorotaxane-like complexes **4b⊂1•2a**. Ion pair **4b** templates the partial formation of the corresponding **4b⊂1•2a** complex. The exchange dynamics that exist between free and bound components resulted in broadening of the proton signals. At low temperature the thermodynamic and kinetic stability of the **4b⊂1•2a** complexes is increased, enabling their detection as the predominant species in solution. This lower kinetic stability at r.t. can be ascribed to at least two different factors. On one hand, similarly to the azide **4c**, the longitudinal size of the thiocyante **4b** is 0.238 Å higher than the one of the cyanate **4a** causing a slightly worse fit of the anion within the supramolecular receptor cavity. On the other hand, the nature of the hydrogen bond interaction NH···S is certainly different than the NH···N and NH···O ones due to the higher polarizability of the S atom.

Interestingly, the structure of the **4b⊂1•2a** complex was confirmed in the solid-state from X-ray diffraction of a single crystal grown from an equimolar $CDCl_3$ solution of **1**, **2a** and **4b** (Figure 2.34 top). The X ray structure evidence the interweaving nature of the four component assembled structure able to chelate anions. It is worthy to note that in the solid state the thiocyanate is preferentially oriented. The sulphur atom is interacting with the amide moieties of the *N*-oxide **2a** and the nitrogen with the pyrrolic protons of the calix[4]pyrrol.

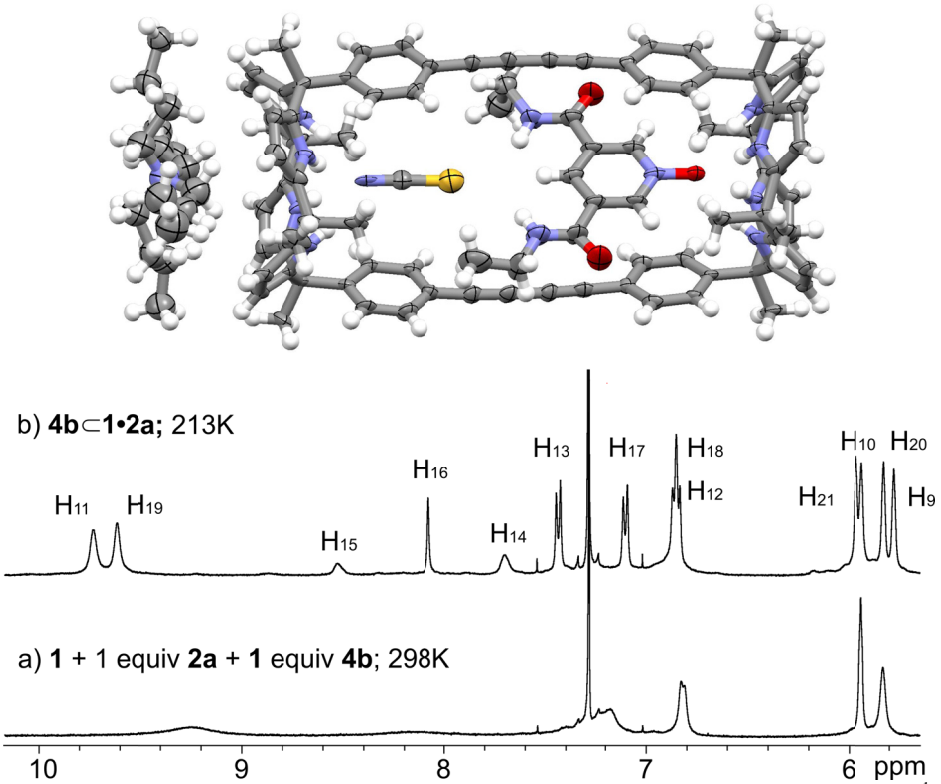

Figure 2.34 Top: Single crystal X-ray structure of **4b⊂1•2a**. Bottom: downfield regions of the ^{1}H NMR spectra of the $CDCl_3$ solution containing an equimolar mixture of **1**, **2a** and tetrabutylammonium thiocyanate **4b** recorded at a) 298 K and b) 213 K.
[**1**] =[**2a**]=[**4b**]= 4.6×10^{-3} M. See Figure 2.1 and Figure 2.20 for proton assignments.

The **1•2a** cavity is not symmetrical and it seems to be more sterically hindered in the calix[4]pyrrole hemisphere due to the proximity of the two aromatic walls. Since the polarizability and size of the sulphur atom is higher than the one of nitrogen it is plausible the preferential placement of the sulphur pointing to the less hindered hemisphere of the cavity. However, the freely rotation of the ambidentate ligand within the cavity is probable in solution. The X-ray structure also suggests that the components of the quaternary complex are preorganized by the establishment of a number of non-covalent interactions. Beside the network of ten hydrogen bond interactions established between the macrotricyclic receptor and both included guests (*N*-oxide and anion), the whole assembly also presents other weaker interactions. Cation-π interactions between the tetrabutylammonium and the aromatic electron rich cavity of the calipyrrole, as well

as π-π interactions between the aromatic walls of the receptor and the pyridine *N*-oxide can also be found.

In complete agreement with the later experiments, it was not surprising that the larger and highly polarizable triiodide as tetrabutylammonium salt did not template the formation of [2]pseudorotaxanes even at low temperatures.

Polyatomic anions with different geometry were also investigated. For anions with the same charge, structural effects became important and symmetry matching has to be considered. Nitrate possesses a diameter of 3.58 Å (considering it spherical) and a trigonal planar geometry. Due to the directional nature of the hydrogen bond interactions, a trigonal geometry of the anion would complement perfectly the also trigonal geometry of the cavity of **1•2a**. Molecular modelling studies (Figure 2.35 top) indicated that the two NHs of the pyridine converge with an angle slightly smaller than 120º but adequate to bind two oxygens of the nitrate. The third oxygen atom is held by the four NHs of the calix[4]pyrrole. Despite this topological complementarity, the size of the nitrate seems to be too small to give proper interactions with both sides of the cavity. This fact can be corroborated by ^{1}H NMR studies (Figure 2.35).

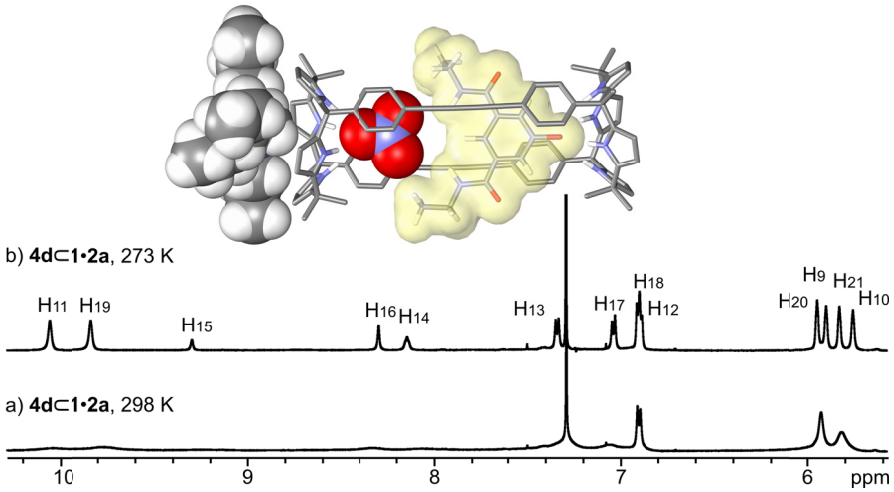

Figure 2.35 Top: Energy-minimized structure[26] of the pseudorotaxane **4d⊂1•2a** with tetrabutylammonium nitrate **4d** as template. Bottom: Selected region of the ^{1}H NMR spectra (500 MHz, $CDCl_3$) of **4d⊂1•2a**: a) 298 K), b) 273 K. See Figure 2.1 and Figure 2.20 for proton assignments.

The addition of 1 equivalent of the $TBANO_3$ ion pair **4d** to a $CDCl_3$ solution containing equimolar amounts of **1** and **2a** produced a ^1H NMR spectrum with broad signals that were not possible to be assigned to the [2]pseudorotaxane structure (Figure 2.35 bottom). Increasing the kinetic stability of the assembly by lowering the temperature at 273 K, we observed a ^1H NMR spectrum containing the diagnostic proton signals expected for the quantitative assembly of the pseudorotaxane-like complexes **4d⊂1•2a**. Similarly to the experiments using thiocyanate anion, the kinetic and thermodynamic stability of the pseudorotaxane assembly was significantly reduced compared to cyanate anion due to a lower complementarity between the guests and the supramolecular host.

Taking into consideration the studies performed with polyatomic anions and especially the ones concerning to $TBANO_3$, monoatomic anions seems to be too short to interact with both extremes of the **1•2a** cavity and template the quantitative assembly of [2]pseudorotaxanes at room temperature. For example, chloride presents a diameter of 3.62 Å which is similar to the one of nitrate. As expected, the addition of 1 equivalent of the tetrabutylammonium ion pair **4e** (TBACl) to $CDCl_3$ solution containing equimolar quantities of **1** and **2a** produced the broadening of most of the ^1H NMR spectrum signals (Figure 2.36 a). As explained in *Chapter 1*, it is well documented that calix[4]pyrroles are heteroditopic receptors able to coordinate ion pairs in a *host*-separated binding mode. Sessler and co-workers determined the existence of a cation dependence on the anion binding affinities in halogenated solvents; this means a cooperative or allosteric ion pair effect.[35] We envisaged the positive cooperative effect of a cation over the binding of an anion would also contribute to increase the anion template effect in the **1•2a** [2]pseudorotaxane formation. The addition of 1 equivalent of the ion pair **4f** (MTOACl) to an equimolar mixture of **1** and **2a** produces the quantitative formation of the **4f⊂1•2a** [2]pseudorotaxane at room temperature with an estimated association constant $K_{\mathbf{4f\subset 1\bullet 2a}}>10^8 M^{-2}$ (Figure 2.36 b). In general terms, the ^1H NMR spectrum of **4f⊂1•2a** shows the characteristic signals of the previous interwoven assemblies. However, some differences are worthy to mention. The two NHs of the *N*-oxide amide groups (H_{14}) appear as a broad hump at δ= 7.2 ppm. This is the same chemical shift for the corresponding protons in the free *N*-oxide **2a** at this concentration.

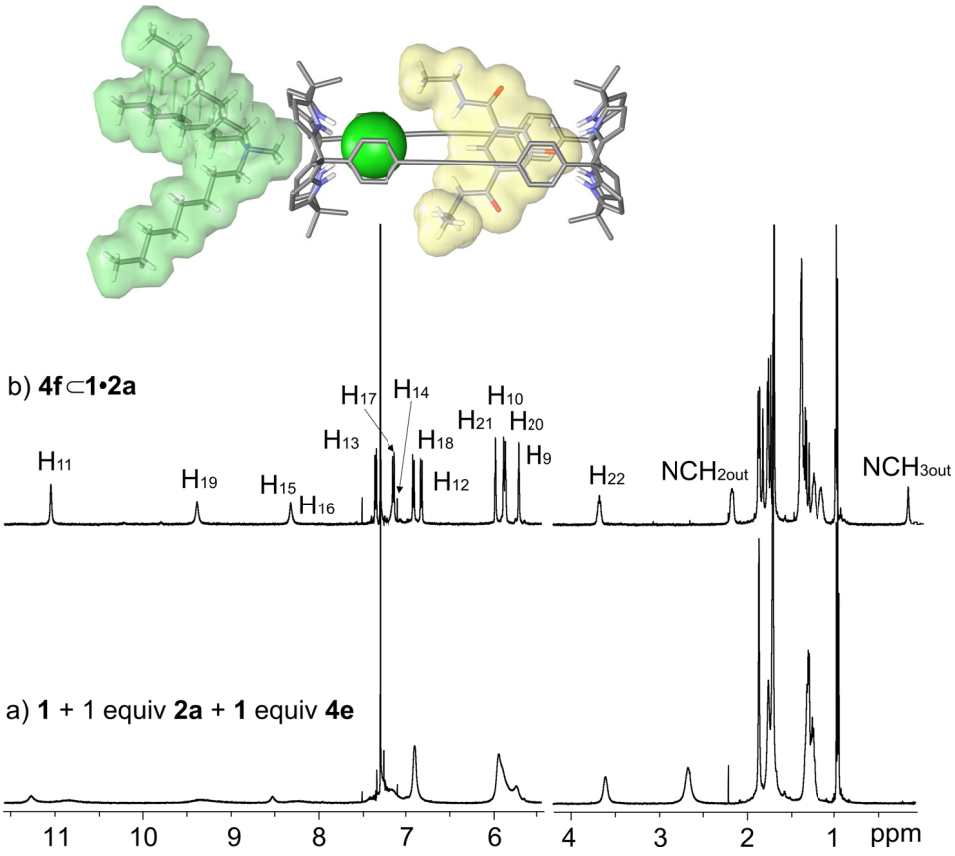

Figure 2.36 Top: Energy-minimized structure[26] of the pseudorotaxane **4f⊂1•2a** with methyltrioctylammonium chloride **4f** as template. Bottom: ^{1}H NMR spectra (500 MHz, $CDCl_3$, 298K) of: a) equimolar mixture of **1**, **2a** and TBACl **4e** and b) equimolar mixture of **1**, **2a** and TMOACl **4e**. See Figure 2.1 and Figure 2.20 for proton assignments.

The proton signal for H_{15} appears at δ= 8.16 ppm that coincide with the chemical shift of the same protons in the free *N*-oxide **2a**. Only the protons H_{16} α to the *N*-oxide were shifted upfield respect to the one in the free *N*-oxide. Together this results indicate that once the *N*-oxide interacts with one calix[4]pyrrole hemisphere of **1**, the two amide moieties are too far away from the bound chloride anion. In complete agreement, molecular modelling studies indicate that the chloride anion is bound to one calix[4]pyrrole hemisphere of **1** but it is not large enough to rich the amide moieties of the *N*-oxide **2a** (Figure 2.36 top).

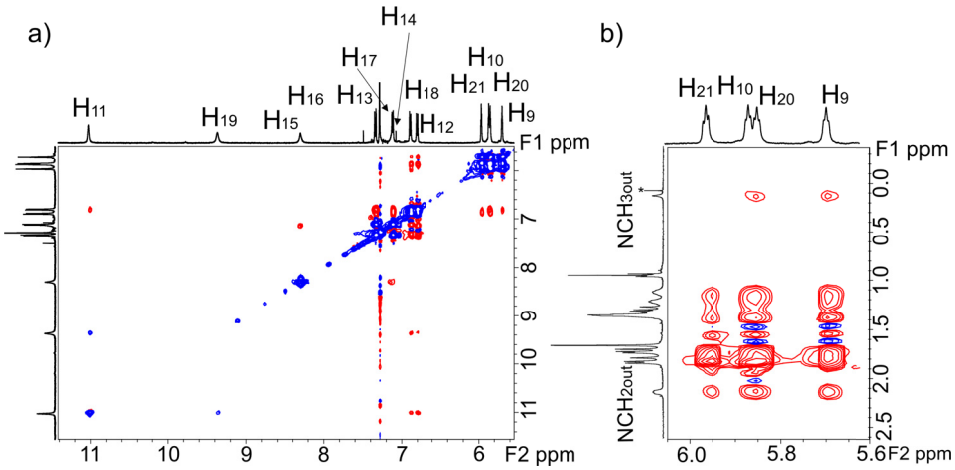

Figure 2.37 Selected regions of a ROESY experiment (500 MHz, p15: 0.3 s, $CDCl_3$, 2.5 × 10^{-3}M) of the 1:1:1 [2]pseudorotaxane complex **4f⊂1•2a** showing a) cross-peaks indicating chemical exchange between the protons corresponding to the two NHs (H_{11} and H_{19}) of the two different hemispheres of the macrocycle, b) cross-peaks indicating intermolecular close contacts between the methyl (NCH_{3out}) and methylene (NCH_{2out}) protons *alpha* to the nitrogen of the MTOA cation and the β-pyrrolic protons of the calix[4]pyrrole of the **4f⊂1•2a** assembly.

The methyl and methylene protons α to the nitrogen of the methyltrioctylammonium, named as NCH_{2out} and NCH_{3out}, appear upfield shifted (δ = 2.2 ppm and δ = 0.2 ppm, respectively) respect to the same ones in the free salt (δ = 3.49 ppm and δ = 3.38 ppm, respectively). This results together with exclusive intermolecular close contacts in the ROESY experiment between NCH_{2out} and NCH_{3out} and the β-pyrrolic protons of the calix[4]pyrroles (Figure 2.37b) indicate that the MTOA cationic is bound to the bowl-shaped external cavity of the calix[4]pyrrole. Upon the binding of chloride anion, the calix[4]pyrrole is locked in the *cone* conformation creating a cavity able to include a cation with a suitable size and shape. The magnitude of this interaction is highly structure dependent on the cation structure. Alkylammonium salts possessing long alkyl chains are too big to fit in the pyrrolic aromatic cavity of the calix[4]pyrrole. Contrary, the presence of at least one methyl group in the alkylammonium salt produces the better fit of the cation in the shallow aromatic cup opposite to the bound anion.[35] In brief, by changing the structural features of the cation it is also possible to increase the thermodynamic and kinetic stability of the **4⊂1•2a** [2]pseudorotaxanes.

2.2.4 Gas-phase characterization of **4⊂1•2** [2]pseudorotaxanes

The study of supramolecular assemblies in the gas phase provide a better understanding of the intrinsic nature of non-covalent intermolecular interactions due to the absence of solvent molecules. Electrospray ionization (ESI) is a soft ionization method that allows transferring molecules from solution to the gas phase without significant signs of fragmentation. For this reason ESI-MS is very useful in the characterization of supramolecular structures. By Electrospray Fourier-transform ion-cyclotron-resonance mass spectrometry, we observed that [2]pseudorotaxane structures **4⊂1•2** containing different anions of TBA remain assembled in the gas-phase after being formed in solution. Previous experiments in solution and in solid state indicated that tetrabutylammonium cation TBA is bound to the external shallow aromatic cup of one calix[4]pyrrole in the [2]pseudorotaxane structures **4⊂1•2** through weak cation-π interactions. Contrary, it was proven that the *N*-oxide and anion are stabilized inside the macrotricyclic receptor **1** through a net of stronger hydrogen bond interactions. Consecuently, we expected the detection of negatively charged ternary complexes by losing the bound TBA cation during the transition of the supramolecular assembly from solution to gas phase. ESI-FTICR mass spectrum of the free **1** in negative mode exhibited a signal at m/z 1231.6 corresponding to the adduct $[\mathbf{1}+Cl]^-$ (see experimental section Figure 2.47). The presence of chloride anion cannot be avoided since it is present in the capillary used to inject the sample. Fortunately, the ESI mass spectrum of an equimolar solution containing **4d**, **2a** and **1** showed only one peak corresponding to the negatively charged ternary complex $[NO_3⊂\mathbf{1•2a}]^-$ at m/z 1496,7 (Figure 2.38). The experimental isotope pattern matches the theoretical one on the basis of the natural isotope abundances. Other tetrabutylammonium salts such as **4b** or **4c** were tested for the formation of **4⊂1•2** [2]pseudorotaxanes in the gas phase. In both cases, supramolecular ions of the ternary complexes were detected. When using tetrabutylammonium thiocyanate salt **4b** the peak corresponding to the ternary complex $[SCN⊂\mathbf{1•2a}]^-$ was selectively formed (see experimental section Figure 2.48).

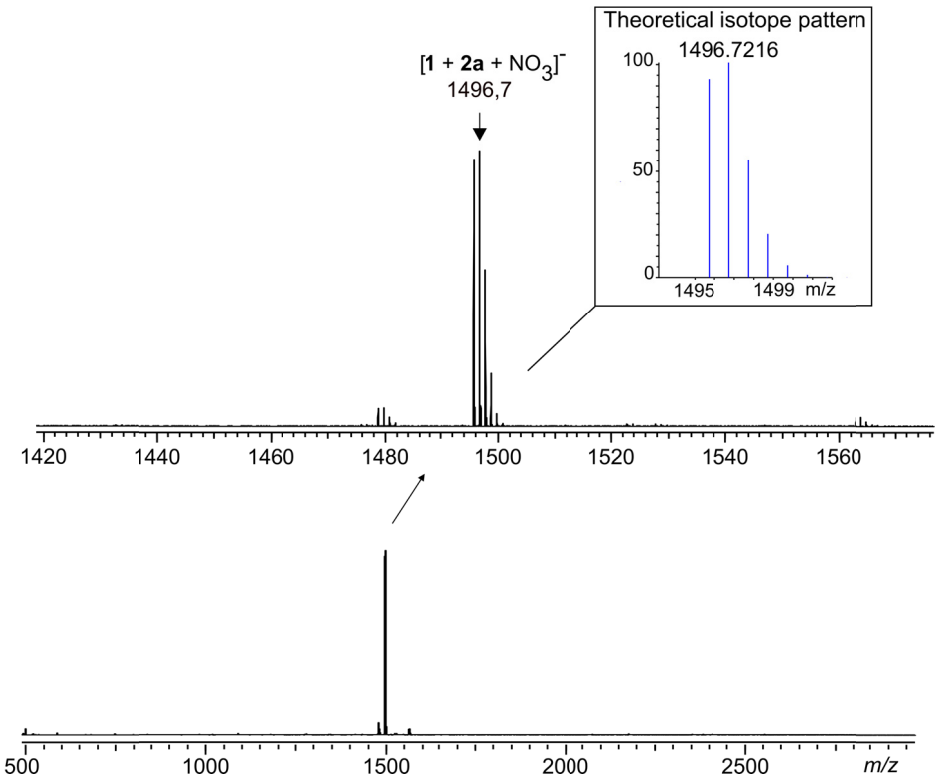

Figure 2.38 ESI-FTICR mass spectrum in negative mode of an equimolar mixture of **2a**, **1** and **4d**.

However, in the case of the tetrabutylammonium azide **4c**, we observed the formation of $[N_3TBACl\subset\mathbf{1}]^-$ and $[(N_3)TBA\subset\mathbf{1{\bullet}2a}]^-$ in a representative extent a part of $[N_3\subset\mathbf{1{\bullet}2a}]^-$ (see experimental section Figure 2.49). According to the simulated speciation profiles of the three possible addition alternatives for a two-step formation of **4a⊂1•2a** (Figure 2.30 c), the presence of this two ionic species is easy to explain. In solution it was shown that the addition of an excess of salt induced the formation of more stable species **1•4a** at the expense of those corresponding to **4a⊂1•2a**.

2.2.5 Ion pairs used as templates in the synthesis of [2]rotaxanes

Due to the biological importance of anions, the development of non-covalent anion receptors have been attracted the attention of many scientists during the last 50 years. More recently, interlocked molecules as rotaxanes or catenanes have been also

employed as very sensitive and selective anion receptors.[36] The design and the study of pseudorotaxane structures as intermediates for the synthesis of interlocked molecules is hugely important. Interlocked molecules can be synthesized taking advantage of the supramolecular templating effects used to assemble pseudorotaxanes. If a template is required to achieve the formation of an interlocked molecule, upon its removal, it is obtained a molecule with a three-dimensional, geometrically fixed and functionalized cavity. Such rotaxane structures possess complementary binding sites that allow the sensitive and selective interaction of guests that are of similar nature than the template used to achieve its synthesis. In previous sections of this chapter we described a versatile anion templating strategy to build [2]pseudorotaxanes. The evolution from this interpenetrated **4⊂1•2** [2]pseudorotaxanes to interlocked rotaxane structures would provide unprecedented examples of polyatomic anion receptors. Then, we selected a "capping" strategy to covalently attach bulky stoppers to both ends of the linear pyridine bis-amide *N*-oxide component previously threaded into macrotricycle **1**.

The copper(I)-catalysed azide–alkyne cycloaddition, the so called 'click' reaction, is described in literature to be effective for the synthesis of covalent interlocked molecules.[37] The reaction is selective for the azide and terminal alkynes involved and secondary reactions are not produced. More important, the experimental conditions are mild being compatible with the weak character of the non-covalent interactions that are necessary to template the assembly of the rotaxane components. Then we designed a linear heteroditopic component **2c** (Figure 2.39) which presents; on the one hand, the functional groups necessary to achieve the interactions required to be assembled with macrotricycle **1** based on anion template effects. On the other hand, azide functionalized linear aliphatic chains that provide solubility in non-polar solvents and also position the azide functional group at an enough distance to avoid stearic hindrance effects between the macrocycle **1** and the bulky stoppers. Based on molecular modelling studies, the stoppers were selected to be bulky enough to prevent the dissociation of both components of the assembly. The stopper **11** is widely used in the synthesis of rotaxane structures and it was synthesized following described procedures.[38,39,40]

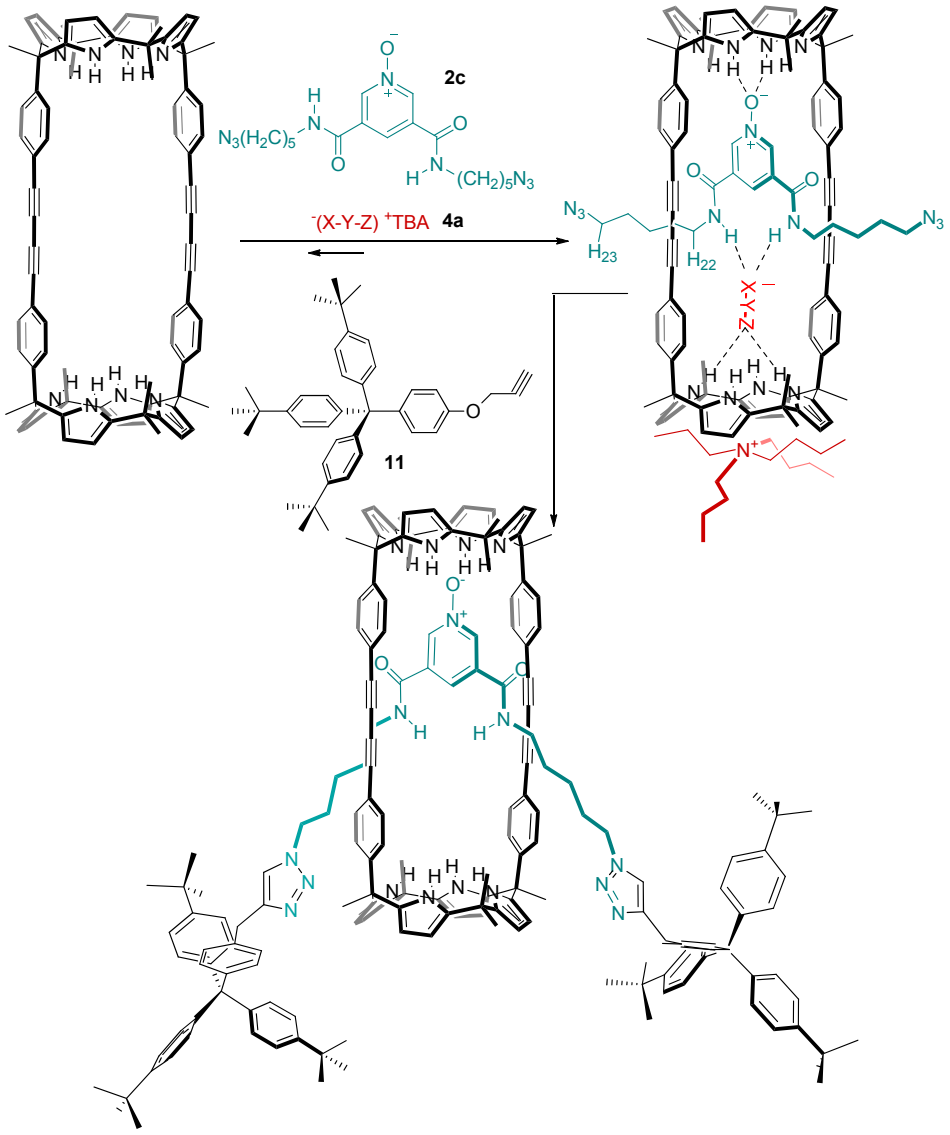

Figure 2.39 Polyatomic anion template synthesis of [2]rotaxanes by a copper(I)-catalysed azide–alkyne cycloaddition between the linear component **2c** and stopper **11**.

Initially, the interaction between macrotricycle **1** and linear component **2c** in the presence of tetrabutylammonium cyanate **4a** was probed. An equimolar mixture of the three components showed the quantitative formation of the **4a**⊂**1**•**2c** [2]pseudorotaxane (Figure 2.40 a). It is worthy to mention that the proton signal corresponding to the methylene protons H_{23} *alpha* to the azide substituents appears slightly broad but at

identical chemical shift than the same protons of free **2c**. This result suggests that the azide moieties are not involved in any kind of interaction in the **4a⊂1•2c** [2]pseudorotaxane assembly and are potentially available to react with the two terminal alkynes of the stoppers.

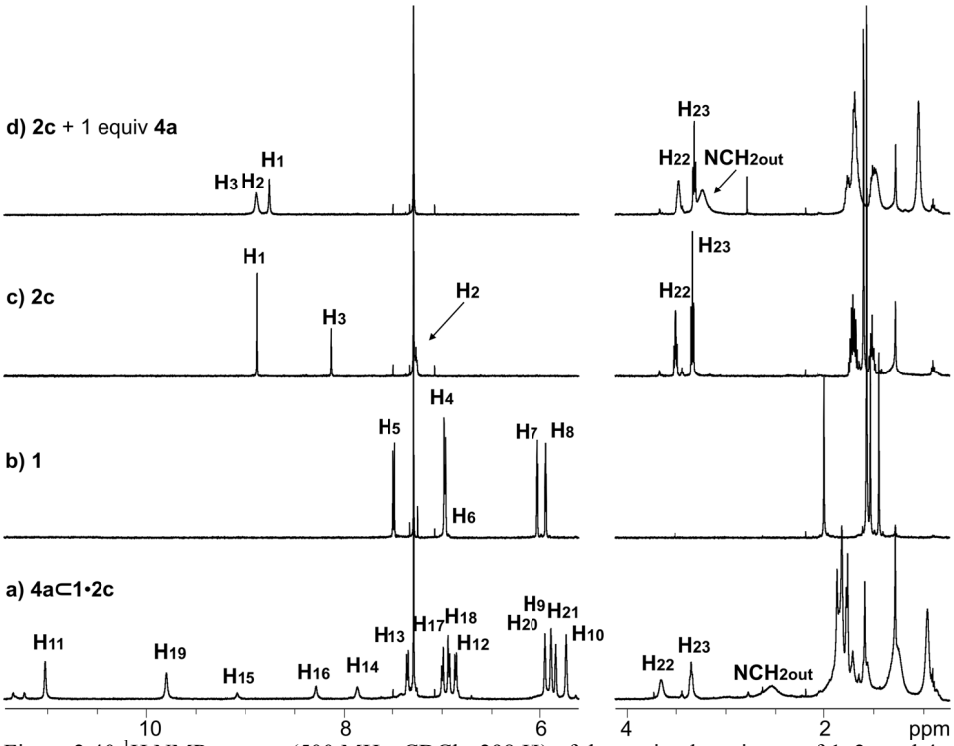

Figure 2.40 ^{1}H NMR spectra (500 MHz, $CDCl_3$, 298 K) of the equimolar mixture of **1**, **2c** and **4a** (a), macrotricycle **1** (b), linear component **2c** (c) and the solution containing an equimolar mixture of **2c** and **4a** (d). See Figure 2.1, Figure 2.20 and Figure 2.39 for proton assignments.

In order to select the most adequate reaction conditions to obtain the [2]rotaxanes we starting studying model reactions. We tested different copper(I)-catalysed azide–alkyne cycloaddition reaction conditions to obtain the *N*-oxide **12** (Figure 2.41) that will constitute the axle of the rotaxane. The best conditions were achieved using $[Cu(CH_3CN)_4]PF_6$ as catalyst in a mixture of dichloromethane and acetonitrile 2:2 which affords the desired product in a 67.7% yield. Unfortunately, when using the same conditions in the presence of an equimolar mixture of **2c**, **4a** and macrotricycle **1** the [2]rotaxane structure was not isolated and only the product of the "click" reaction **12** was recovered.

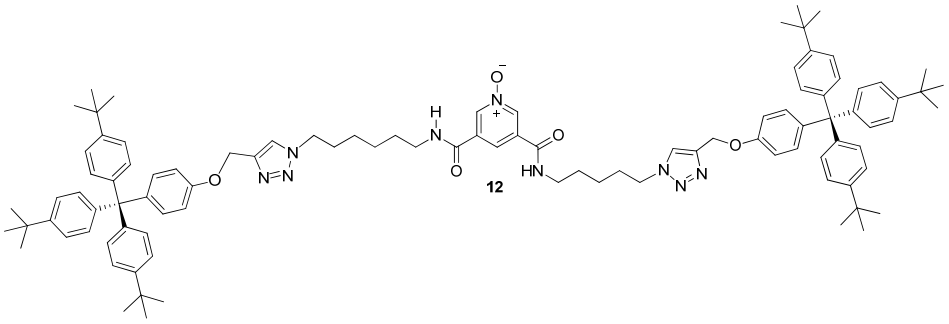

Figure 2.41 Molecular structure of *N*-oxide **12**.

Most likely, the aliphatic chains of the *N*-oxide **2c** are not long enough to avoid the stearic hindrance between the stoppers **11** and the macrocyclic structure.

2.3 Conclusion

In conclusion, we have synthesized a homoditopic bis-calix[4]pyrrole macrocycle **1**. We have used its topology and binding properties to develop a general strategy for the quantitative self-assembly of pseudorotaxane-like complexes. These structures are unprecedented examples of four particles aggregates with interwoven topology. At room temperature, in $CDCl_3$ solution an equimolar combination of tetrabutylammonium cyanate **4a** or azide **4c** with **1** and a linear bis-amidepyridine *N*-oxide **2a** induces the quantitative formation of the ion-paired pseudorotaxane-like complex **4a,c⊂1•2a** independently of the addition order of the components. This [2]pseudorotaxanes are structural and thermodynamically fully characterized. The same template strategy can be used with other bis-amidepyridine *N*-oxide derivatives obtaining similar self-assembled structures. Other polyatomic anions derivate from tetrabutylammonium salts were used to template the assembly of analogous [2]pseudorotaxanes. The quantitative formation of such structures at room temperature is extremely dependent on the size, shape and electronic characteristics of the polyatomic anions that have to be included in the fixed dimensional cavity of **1•2a**. In addition, we achieved the quantitative formation of [2]pseudorotaxanes templated with monoatomic anions at room temperature taking advantage of the positive cooperative effects that govern the recognition of ion pairs by calix[4]pyrrole units. Finally, we presented our attempts in

exploiting the anion templated assembly of [2]pseudorotaxanes to the synthesis of mechanically interlocked molecules (i.e. rotaxanes).

2.4 Experimental section

2.4.1 General information and instrumentation

All reagents were obtained from commercial suppliers and used without further purification. Anhydrous solvents were obtained from a solvent purification system SPS-400-6 from Innovative Technologies, Inc. All solvents were of HPLC grade quality, commercially obtained and used without further purification.

Routine ^{1}H NMR spectra were recorded on a Bruker Avance 400 (400.1 MHz for ^{1}H NMR) and Bruker Avance 500 (500.1 MHz for ^{1}H NMR) ultrashield spectrometer. The deuterated solvents (Aldrich) used was in all the experiments $CDCl_3$; chemical shifts are given in ppm, relative to TMS. Isothermal titration calorimetry experiments were performed using a Microcal VP-ITC Microcalmeter.

Crystal structure determinations were obtained by slow evaporation of an acetonitrile solution of α,α-**6** and **1** and by slow evaporation of a chloroform solution containing an equimolar mixture of **1**, **2a** and **4b**. The measured crystals were unstable under atmosphere conditions; they were prepared under inert conditions immersed in perfluoropolyether as protecting oil for manipulation. Measurements were made on a Bruker FR591 diffractometer equipped with an APPEX 2 4K CCD area detector, a rotating anode with $Mo_{K\alpha}$ radiation and an Oxford Cryostream 700 low temperature device (T = 100K). Full-sphere data collection was used with ω and φ scans. Programs used: Data collection Apex2 V2010.7-0 (Bruker AXS 2010), data reduction Saint + Version 7.60A (Bruker AXS 2008) and absorption correction SADABS V. 2008-1 (2008). Crystal structure solution was done using methods implemented in SHELXTL version 6.14 (Sheldrick, G.M. (2008).

Electrospray ionization Fourier-transform ion-cyclotron resonance (ESI-FTICR) MS experiments were performed with an Ionspec QFT-7 FTICR mass spectrometer (Agilent Technologies, Lake Forest, CA, USA), equipped with a 7 T superconducting magnet and a Micromass Z-spray ESI source (Waters Co., Saint-Quentin, France).

2.4.2 Synthetic procedures

5-methyl-5´-(4-iodophenyl)dipyrromethane **5**

To a suspension of commercially available 4-iodoacetophenone (5g, 20.3 mmol) in 37.5 mL of pyrrole freshly distilled, trifluoroacetic acid (5mL, 61.0 mmol) was added over a period of 30 minutes at 0ºC. The reaction mixture was stirred at room temperature for 3 hours. The mixture was poured into 20 mL of distilled water and neutralized with KOH 2M (pH=7). The crude was extracted with CH_2Cl_2 (2x40 mL) and dried over $MgSO_4$. The solvent was concentrated under reduced pressure to remove the dichloromethane and the excess of pyrrole. The reaction mixture was purified using silica column chromatography and hexanes/ethylacetate (75:25) as eluent. The first eluted fraction corresponds to the starting material and the second one corresponds to the desired dipyrromethane (4.2 g, 57.5%).

^{1}H NMR (400 MHz, CD_3CN) δ (ppm) 1.96 (s, 3 H), 5.79 (m, 2 H), 6.02 (m, 2H), 6.65 (m, 2 H), 6.95 (d, J_{H-H} ~ 8.7 Hz, 2H), 7.42 (d, J_{H-H} ~ 8.7 Hz, 2H), 8.74 (s, broad 2H).

10α,20α-bis(4-iodophenyl)calix[4]pyrrole α,α-**6**. Synthetized by applying similar reaction conditions to the ones described in the reference[41]

To a solution of dipyrromethane **5** (1 g, 2.76 mmol) in 75 mL of acetone, $BF_3.OEt_2$ (370 µL, 3.0 mmol) was drop wise added over a period of 30 minutes at 0ºC. After the addition, the reaction was stirred at room temperature for 12 hours. Next, 65 mL of distilled water were added. The acetone was removed under reduced pressure to obtain a residue which was neutralized (KOH 2M to pH = 7). The mixture was extracted with dichloromethane (3× 50 mL). The collected organic layers were dried over Na_2SO_4 and concentrated under reduced pressure. The crude solid obtained was subjected to a column chromatography (SiO2, ethyl acetate/hexane 5:95) (140 mg, 6.26% yield).

^{1}H NMR (400 MHz, $CDCl_3$) δ (ppm) 1.54 (s, 6 H), 1.63 (s, 6 H), 1.87 (s, 6H), 5.63 (dd, $^3J_{H-H}$ ~ 3.5 Hz, $^4J_{H-H}$ ~ 3.0 Hz, 4 H), 5.94 (dd, $^3J_{H-H}$ ~ 3.5 Hz, $4J_{H-H}$ ~ 3.0 Hz, 4 H), 6.74 (d, $^3J_{H-H}$ ~ 8.7 Hz, 4H), 7.23 (s, broad, 4H), 7.57 (d, $^3J_{H-H}$ ~ 8.7 Hz, 4H).

MS (ESI +ve) m/z calculated for $C_{38}H_{38}I_2N_4$ $[M+H]^+$ 805.1, found $[M+H]^+$ 805.0, $[M+Na]^+$ 827.0

10α,20α-Bis(4-[(3-Methyl-3-hydroxybut-1-yn-1-yl)phenyl]calix[4]pyrrole **7**

10α, 20α-bis(4-iodophenyl)calix[4]pyrrole (50 mg, 0.062 mmol), $Pd(PPh_3)_2Cl_2$ (6.11 mg, 8.7 μmol) and CuI (1.65 mg, 8.7 μmol) were placed in a *schlenk* flask. The flask was purged with argon and later, 6 mL of dry toluene were added. The reaction was stirred under Ar and a yellow suspension was formed. Next, 6 mL of freshly distilled triethylamine were added and finally, the propargylic alcohol (156 mg, 1.86 mmol). The reaction was stirred at 40ºC under Ar during 2h. The crude obtained was subjected to a column chromatography (silica, from CH_2Cl_2 to CH_2Cl_2/ethyl acetate (9:1)). A white solid was recovered as the desired product (39 mg, 89% yield)

^{1}H NMR (400 MHz, $CDCl_3$) δ (ppm) 1.54 (s, 6 H), 1.62 (s, 12 H), 1.63 (s, 6 H), 1.89 (s, 6H), 1.99 (s, 2H) 5.62 (dd, $^3J_{H\text{-}H}$ ~ 3.5 Hz, $^4J_{H\text{-}H}$ ~ 3.0 Hz, 4 H), 5.94 (dd, $^3J_{H\text{-}H}$ ~ 3.5 Hz, $^4J_{H\text{-}H}$ ~ 3.0 Hz, 4 H), 6.93 (d, $^3J_{H\text{-}H}$ ~ 8.2 Hz, 4H), 7.23 (s, broad, 4H), 7.3 (d, $^3J_{H\text{-}H}$ ~ 8.7 Hz, 4H).

HR-MS (ESI +ve) m/z calculated for $C_{48}H_{52}N_4O_2$ $[M+H]^+$ 717.4169, found 717.4174.

10α, 20α-Bis(4-[ethynylphenyl]calix[4]pyrrole **3**

A solution of 10α,20α-Bis(4-[(3-Methyl-3-hydroxybut-1-yn-1-yl)phenyl]calix[4]pyrrole **7** (105 mg, 0.14 mmol) in toluene (12 mL) was treated with powdered NaOH (117 mg, 2.93 mmol) under reflux (128ºC). After 3.5 h, TLC analysis showed the complete consumption of the starting material. The reaction mixture was subjected to a column chromatography (CH_2Cl_2/hexane 9:1). Removal of the solvent led to a white solid (88.2 mg, 100%).

^{1}H NMR (400 MHz, $CDCl_3$) δ (ppm) 1.55 (s, 6 H), 1.63 (s, 6 H), 1.89 (s, 6H), 3.05 (s, 2H), 5.63 (dd, $^3J_{H\text{-}H}$ ~ 3.5 Hz, $^4J_{H\text{-}H}$ ~ 3.0 Hz, 4 H), 5.94 (dd, $^3J_{H\text{-}H}$ ~ 3.5 Hz, $^4J_{H\text{-}H}$ ~ 3.0 Hz, 4 H), 6.74 (d, $^3J_{H\text{-}H}$ ~ 8.7 Hz, 4H), 7.23 (s, broad, 4H), 7.57 (d, $^3J_{H\text{-}H}$ ~ 8.7 Hz, 4H).

^{13}C {H} NMR (125.7 MHz, $CDCl_3$, 298K) δ (ppm) 148.5 (C), 138.5 (C), 136.0 (C), 131.5 (CH), 127.4 (CH), 120.1 (C), 106,0 (CH), 103.3 (CH), 83.6 (C), 76.8 (C), 44.7 (C), 35.3 (C), 30.0 (CH_3), 27.8 (CH_3), 27.6 (CH_3).

HR-MS (ESI +ve) m/z calculated for $C_{42}H_{40}N_4$ $[M+H]^+$ 601.3331, found 601.3326

Bis-calix[4]pyrrole macrotricyle **1**

10α,20α-Bis(4-[ethynylphenyl]calix[4]pyrrole **3** (88.0 mg, 0.148 mmol) and one equivalent of 4,4´-bipyridine bis-*N*,*N*´-oxide. $2H_2O$ (27.8 mg, 0.148 mmol) were placed in a 100mL round bottom flask and suspended in 55 mL of CH_2Cl_2 and the mixture was stirred at room temperature during 15 minutes. Later, copper (I) chloride (1.02 g, 10.3 mmol) and N^1,N^1,N^2,N^2-tetramethylethane-1,2-diamine (1.12 g, 10.36 mmol) were added to the suspension and stirred in O_2 atmosphere during three hours. The mixture was washed three times with water and the organic phases were dried with Na_2SO_4 and concentrated. A short silica column was done with CH_2Cl_2 as mobile phase and a white solid (48, 3 mg, 60% yield) was recovered.

^{1}H NMR (400 MHz, CD_2Cl_2) δ (ppm) 1.44 (s, 12 H), 1.54 (s, 12 H), 1.99 (s, 12H), 5.94 (dd, $^3J_{H\text{-}H}$ ~ 2.93 Hz, $^4J_{H\text{-}H}$ ~ 3.63 Hz, 8 H), 6.03 (t, $^3J_{H\text{-}H}$ ~ 3.01 Hz, 8 H), 7.00 (d, $^3J_{H\text{-}H}$ ~ 8.23 Hz, 8H), 7.03 (s, broad, 8H), 7.51 (d, $^3J_{H\text{-}H}$ ~ 8.23 Hz, 8H).

MS (MALDI +ve) m/z calculated for $C_{84}H_{77}N_8^{+\cdot}$: 1197.6, found: 1197.8, m/z calculated for $C_{84}H_{76}N_8^{+}$: 1196.6, found: 1196.7 (complex isotopic pattern obtained as mixture of $M^{+\cdot}$ and M-H)$^+$. Structure confirmed by X-ray diffraction studies.

N^3, N^5-diethylpyridine-3, 5-dicarboxamide **10a**

Pyridine-3,5-dicarboxylic acid (1.27 g, 7.62 mmol) was suspended in dry CH_2Cl_2 (150 mL). The white suspension was stirred under Ar at room temperature and oxalyl chloride (2.0 mL, 22.8 mmol) and a catalytic amount of dry DMF were added. The mixture was stirred under Ar for 2 h. The solvents were removed *in vacuum* and the white residue redissolved in 100 mL of dry CH_2Cl_2. This solution was added slowly to a solution of 9.5 mL of $EtNH_2$ 2M in THF and 2.8 mL of NEt_3 and a catalytic amount of DMAP. After 1 hour the reaction was complete and it was purified by column chromatography (silica; 1:1 ethyl acetate/MeOH) to yield a white solid (730 mg, 43%).

^{1}H NMR (400 MHz, $CDCl_3$) δ (ppm) 1.30 (t, $^3J_{H\text{-}H}$ ~ 5.7 Hz, 6 H), 3.55 (q, $^3J_{H\text{-}H}$ ~5.7 Hz, 2 H), 3.57 (q, $^3J_{H\text{-}H}$ ~5.7 Hz, 2H), 6.32 (broad s, 2H), 8.47 (t, $^4J_{H\text{-}H}$ ~2.08 Hz, 1H), 9.11 (d, $^4J_{H\text{-}H}$ ~2.08 Hz, 2H). ^{13}C {H} NMR (300.1 MHz, $CDCl_3$, 298K) δ (ppm) 164.9 (CH), 150.3 (CH), 133.5 (C), 130.1 (C), 35.1 (CH_2), 14.7 (CH_3).

HR-MS (ESI +ve) m/z calculated for $C_{11}H_{15}N_3O_2$ $[M+H]^+$ 222.1243, found 222.1235.

N^3, N^5-diethylpyridine-3,5-dicarboxamide *N*-oxide **2a**

To a solution of N^3, N^5-diethylpyridine-3,5-dicarboxamide (100 mg, 0.452 mmol) in CH_2Cl_2 (6 mL) was added m-chloroperbenzoic acid (200 mg, 1.15 mmol). The solution was stirred during 3 hours and the reaction crude was filtered through a basic aluminoxide column eluting with CH_2Cl_2 to give the desired product (50 mg, 46% yield).

^{1}H NMR (400 MHz, $CDCl_3$) δ (ppm) 1.31 (t, $^3J_{H-H}$~ 5.7 Hz, 6 H), 3.51 (q, $^3J_{H-H}$~5.7 Hz, 2 H), 3.53 (q, $^3J_{H-H}$ ~5.7 Hz, 2H), 7.65 (broad t, 2H), 8.25 (t,$^4J_{H-H}$ ~1.30 Hz, 1H), 8.94 (d, $^4J_{H-H}$ ~1.30 Hz, 2H). ^{13}C {^{1}H} NMR (300.1 MHz, $CDCl_3$, 25ºC) δ (ppm) 162.1 (CH), 140.1 (CH), 134.0 (C), 124.9 (C), 35.5 (CH_2), 14.5 (CH_3).

HR-MS (ESI +ve) m/z calculated for $C_{11}H_{15}N_3O_3$ $[M+Na]^+$ 260.1011, found: 260.0999.

N^3,N^5-bis(4-pentylphenyl)pyridine-3,5-dicarboxamide **10b**

Pyridine-3,5-dicarboxylic acid (400 mg, 2.39 mmol) were suspended in dry CH_2Cl_2 (50 mL). The white suspension was stirred under Ar at room temperature and oxalyl chloride (0.6 mL, 7.18 mmol) and a catalytic amount of dry DMF were added. The mixture was stirred under Ar for 2 h. The solvents were removed *in vacuum* and the white residue redissolved in the minimum quantity (4 mL) of dry CH_2Cl_2. This solution was added slowly to a solution of (960 mg, 5.88 mmol) of 4-pentylaniline and 0.83 mL of NEt_3 and a catalytic amount of DMAP. After 1 h the reaction was complete and it was purified by column chromatography (silica; 1:1 CH_2Cl_2/ethyl acetate 3:7) to yield a white solid (908 mg, 84%).

^{1}H NMR (400 MHz, $CDCl_3$) δ (ppm) 0.91 (t, $^3J_{H-H}$ ~ 6.63 Hz, 6 H), 1.34 (m, 8 H), 3.57 (q, 4H), 2.63 (t, $^3J_{H-H}$ ~ 8.22 Hz, 4H), 7.21 (d,$^3J_{H-H}$ ~8.81 Hz, 4H), 7.69 (d, $^4J_{H-H}$ ~8.81 Hz, 4H),. 8.70 (s, 2H), 8.88 (s, 1H), 9.31 (d, 2H).

HR-MS (ESI -ve) m/z calculated for $C_{29}H_{35}N_3O_2$ $[M-H]^-$ 456.2651, found: 456.2657.

N^3,N^5-bis(4-pentylphenyl)pyridine-3,5-dicarboxamide *N*-oxide **2b**. Adapted from the procedure for similar compounds.[42]

N^3,N^5-bis(4-pentylphenyl)pyridine-3,5-dicarboxamide (57 mg, 0.12 mmol) was suspended in 12 mL of a 1:1 mixture H_2O/2-butanone. After that, $NaHCO_3$ (314 mg, 3.74 moL) was added and the solution was stirred vigorously. To this suspension Oxone® (306 mg, 0.49 mmol) was slowly added. After two hours (0.41 mg, 7.10 μmoL) of sodium chloride were added and the product was extracted with $CHCl_3$, dried under Na_2SO_4 and concentrated to yield a white solid (50 mg, 84% yield)

^{1}H NMR (500 MHz, DMSO-d_6) δ (ppm) 0.87 (t, $^3J_{H\text{-}H}$ ~ 7.2 Hz, 6 H), 1.30 (m, 8 H), 1.58 (m, 4H), 7.20 (d,$^3J_{H\text{-}H}$ ~8.47 Hz, 4H), 7.68 (d, $^3J_{H\text{-}H}$ ~ 8.47 Hz, 4H), 8.79 (t, $^4J_{H\text{-}H}$ ~ 2.11 Hz, 1H), 9.25 (d, $^4J_{H\text{-}H}$ ~ 2.11 Hz, 2H),10.52 (s, 2H).

HR-MS (ESI -ve) m/z calculated for $C_{29}H_{35}N_3O_3$ $[M\text{-}H]^-$ 472.2600, found: 472.2605.

N^3,N^5-bis(5-azidopentyl)pyridine-3,5-dicarboxamide **10c**

Pyridine-3,5-dicarboxylic acid (200 mg, 1.197 mmol) were suspended in dry CH_2Cl_2 (0 mL). The white suspension was stirred under Ar at room temperature and oxalyl chloride (0.314 mL, 3.59 mmol) and a catalytic amount of dry DMF were added. The mixture was stirred under Ar for 2 h until the suspension was dissolved. The solvents were removed *in vacuum* and the white residue redissolved in the 50 mL of dry CH_2Cl_2. This solution was added slowly to a solution of (337.0 mg, 2.63 mmol) of 5-azidopentylamine **9c** and 0.605 mL of NEt_3 and a catalytic amount of DMAP. The reaction mixture was stirred two hours and after this the solvents were. The residue was redissolved in approximately 50 mL CH_2Cl_2 that was washed three times with a 20 mL each time of HCl 0.1 N. Later it was washed ones with a basic solution of $NaHCO_3$ and finally with brine. The organic solution was dried under Na_2SO_4 and the solvent evaporated to obtain a brown oil. The oil was purified by column chromatography eluting with a gradient from CH_2Cl_2 to CH_2Cl_2/MeOH 10% to yield a white solid (369.5 mg, 80.0 % yield).

^{1}H NMR (500 MHz, $CDCl_3$) δ (ppm) 1.52 (m, 4 H), 1.34 (m, 8 H), 1.70 (m, 8H), 3.33 (t, $^3J_{H\text{-}H}$ ~ 6.67 Hz, 4H), 3.54 (q,$^3J_{H\text{-}H}$ ~ 7.0 Hz, 4H), 6.34 (m, 2H), 8.46 (d, $^4J_{H\text{-}H}$ ~ 2.16 Hz, 1H), 9.12 (d, $^4J_{H\text{-}H}$ ~ 2.16 Hz, 1H).

HR-MS (ESI +ve) m/z calculated for $C_{17}H_{25}N_9O_2$ $[M+H]^+$ 388.2209, found: 388.2217.

N^3,N^5-bis(5-azidopentyl)pyridine-3,5-dicarboxamide *N*-oxide **2c**

N^3,N^5-bis(5-azidopentyl)pyridine-3,5-dicarboxamide (247.0 mg, 0.63 mmol) was suspended in 60 mL of a 1:1 mixture H_2O/ 2-butanone and (1.60 mg, 19.13 mmoL) of sodium hydrogencarbonate were added and the solution was stirred vigorously. To this suspension it was added (1.27 mg, 2.04 mmol) of Oxone®. After two hours (2.124 mg, 0.036 mmoL) of sodium chloride were added and the product was extracted with $CHCl_3$, dried under Na_2SO_4 and concentrated to yield a white solid (227.9 mg, 89% yield).

^{1}H NMR (500 MHz, $CDCl_3$) δ (ppm) 1.50 (m, 4 H), 1.34 (m, 8 H), 1.70 (m, 8H), 3.33 (t, $^3J_{H\text{-}H}$~ 6.67 Hz, 4H), 3.50 (q, $^3J_{H\text{-}H}$~7.0 Hz, 4H), 7.15 (m, 2H), 8.10 (m, 1H), 9.96 (d, $^4J_{H\text{-}H}$~ 2.16 Hz, 1H). ^{13}C {^{1}H} NMR (300.1 MHz, $CDCl_3$, 25ºC) δ (ppm) 162.3 (CH), 140.0 (CH), 134.1 (C), 124.6 (C), 51.3 (CH_2), 40.3 (CH_2), 28.8 (CH_2), 28.5 (CH_2), 24.11 (CH_2).

HR-MS (ESI +ve) m/z calculated for $C_{17}H_{25}N_9O_3$ $[M+H]^+$ 404.2159, found: 404.2177.

Linear component with bulky stoppers **12**

N^3,N^5-bis(5-azidopentyl)pyridine-3,5-dicarboxamide *N*-oxide **2c** (20 mg, 0.050 mmol), stopper **11** (81 mg, 0.149 mmol) were dissolved in 3mL of a mixture 2:1 CH_2Cl_2/ACN. Later, $NaHCO_3$ (3.15 mg, 0.030 mmol) and $Cu(CH_3CN)_4PF_6$ (13 mg, 0.03 mmol) were added. The reaction mixture was stirred at room temperature overnight. After that, the solvent was evaporated and the reaction crude subjected to a column chromatography eluting with a mobile phase $CHCl_3$/MeOH 5% obtaining the desired product in 67.7% yield.

^{1}H NMR (500 MHz, THF-d_8) δ (ppm) 1.32 (s, 36 H), 1.37 (m, 4 H), 1.63 (m, 4H), 1.92 (m, 4H), 3.34 (m, 4H), 4.36 (t, 4H), 5.09(broad, 4H), 6.85 (d, $^3J_{H\text{-}H}$ ~ 8.17 Hz, 4H), 7.06 (d, $^3J_{H\text{-}H}$ ~ 8.17 Hz, 4H), 7.08 (d, $^3J_{H\text{-}H}$ ~ 8.17 Hz, 12H), 7.24 (d, $^3J_{H\text{-}H}$ ~ 8.17 Hz, 12H), 7.89 (s, 2H), 7.92 (broad, 2H), 8.08 (broad, 2H), 8.47 (broad, 1H).

MS (ESI +ve) m/z calculated for $C_{97}H_{117}N_9O_5$ $[M+Na]^+$ 1511.9, found: 1511.8.

2.4.3 Experimental section: Figures

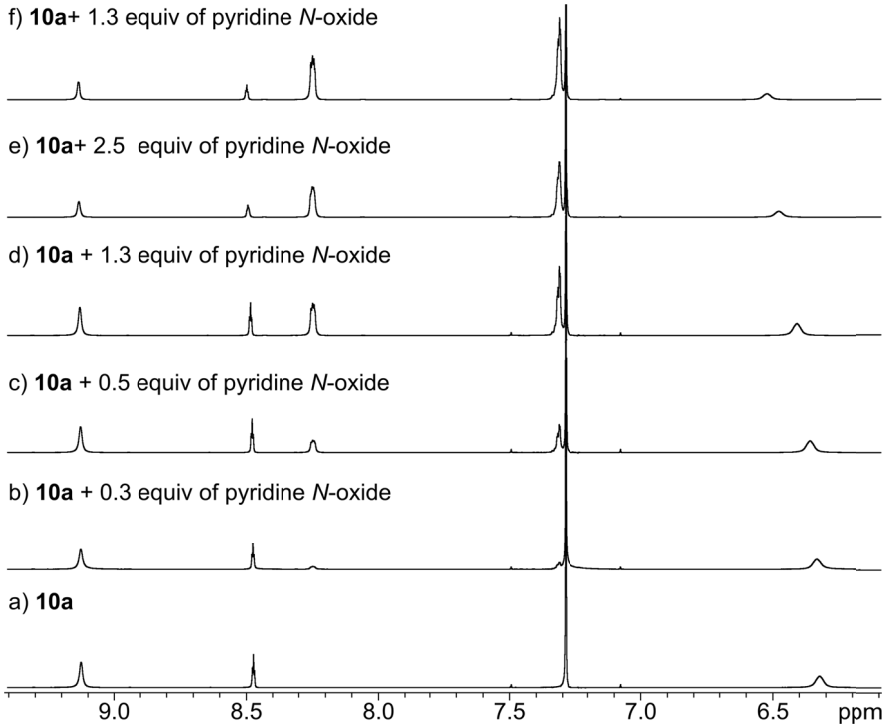

Figure 2.42 Downfield region of selected ^{1}H NMR spectra (500 MHz, 298 K, $CDCl_3$) acquired during the titration of N^3,N^5-diethylpyridine-3,5-dicarboxamide [**10a**] = 5.3 mM with pyridine *N*-oxide.

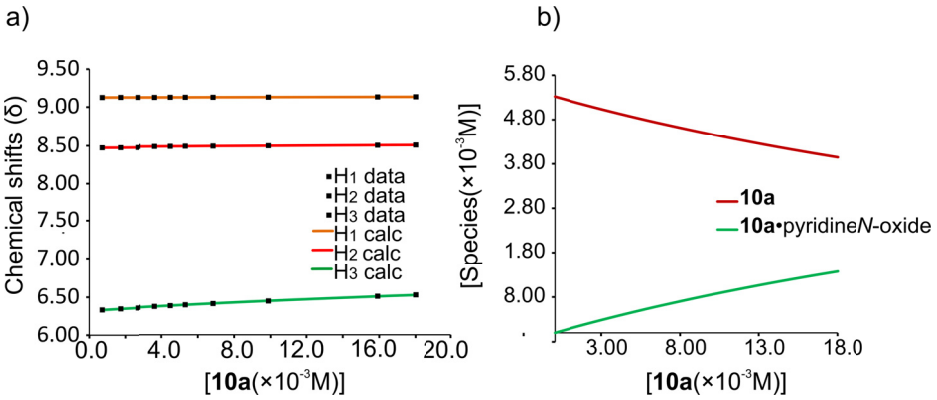

Figure 2.43 a) Fit of the data obtained in the ^{1}H NMR titration experiment of **10a** with pyridine *N*-oxide. $K_{\mathbf{10a}\cdot\text{pyridine }N\text{-oxide}}$ =36.0 M^{-1}, b) speciation distribution profile during the titration.

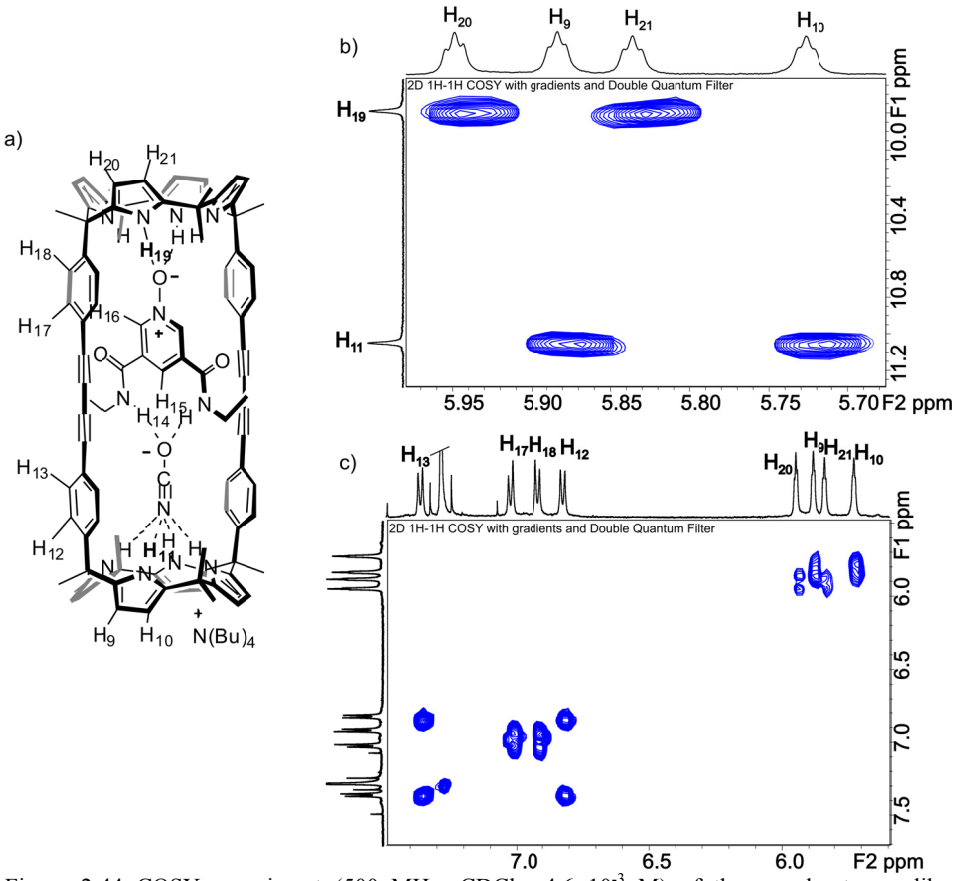

Figure 2.44 COSY experiment (500 MHz, $CDCl_3$, 4.6×10^{-3} M) of the pseudorotaxane-like complex **4a⊂1•2a** showing the assignment of the most relevant signals.

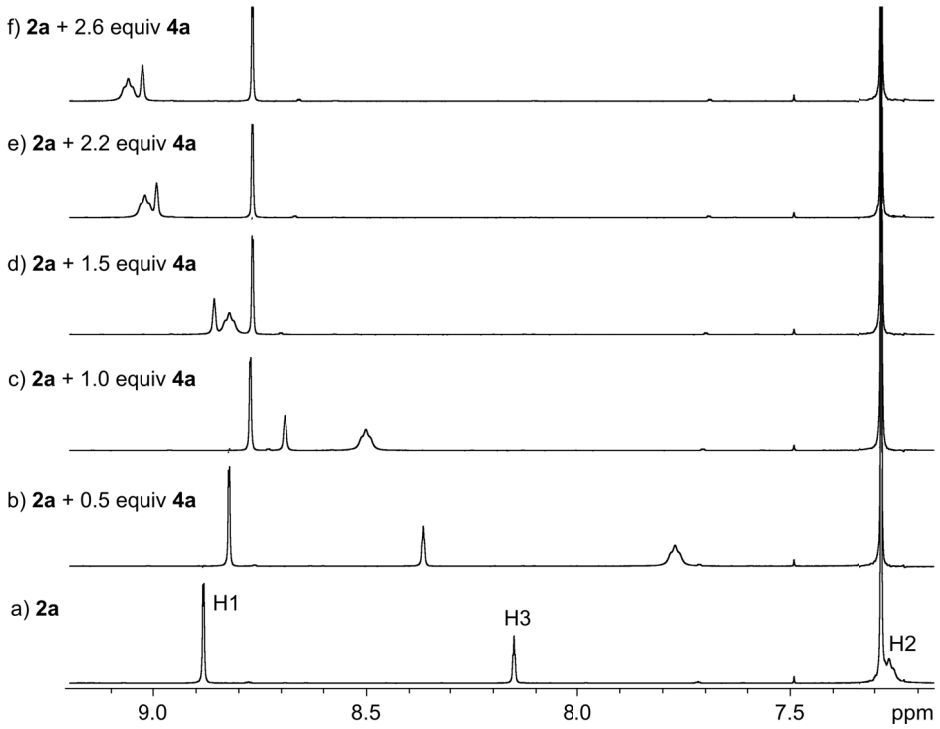

Figure 2.45 Downfield region of selected ^{1}H NMR spectra (500 MHz, 298 K, $CDCl_3$) acquired during the titration of N^3,N^5-diethylpyridine-3,5-dicarboxamide *N*-oxide [**2a**] = 4.3 mM with tetrabutylammonium cyanate **4a**. See Figure 2.1 for proton assignments.

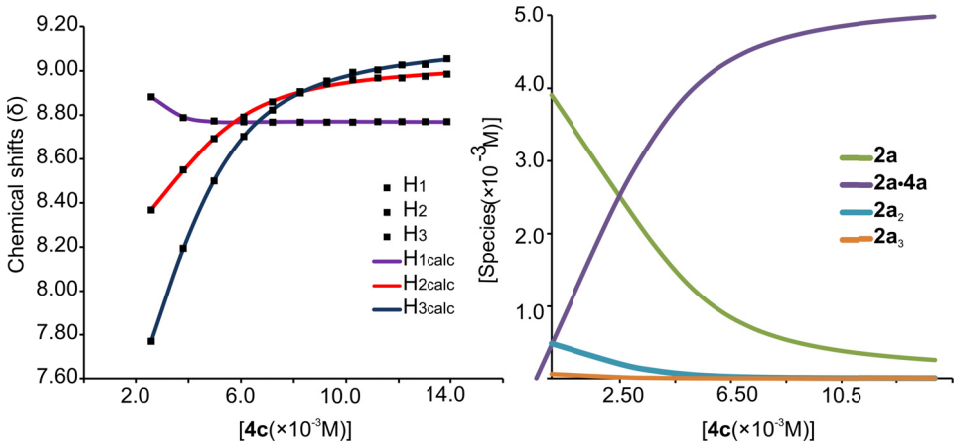

Figure 2.46 Left: Fit of the data obtained in the ^{1}H NMR titration of **2a** with **4c** to a theoretical binding model that considers the formation of the 1:1 complex **2a•4c** and the oligomerization (dimer and trimer) of **2a** $K_{4a\cdot 2c} = 2.2 \times 10^3$ M^{-1}. Right: Speciation profile of the titration.

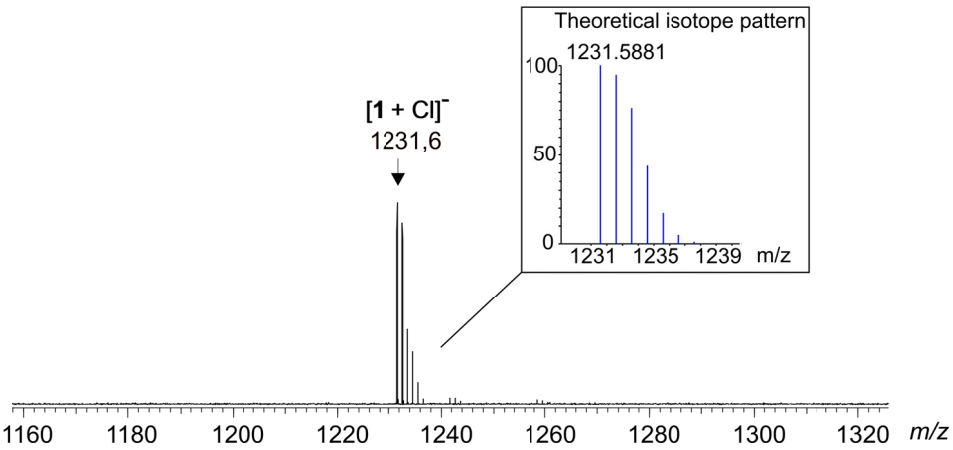

Figure 2.47 ESI-FTICR mass spectrum of **1** in negative mode.

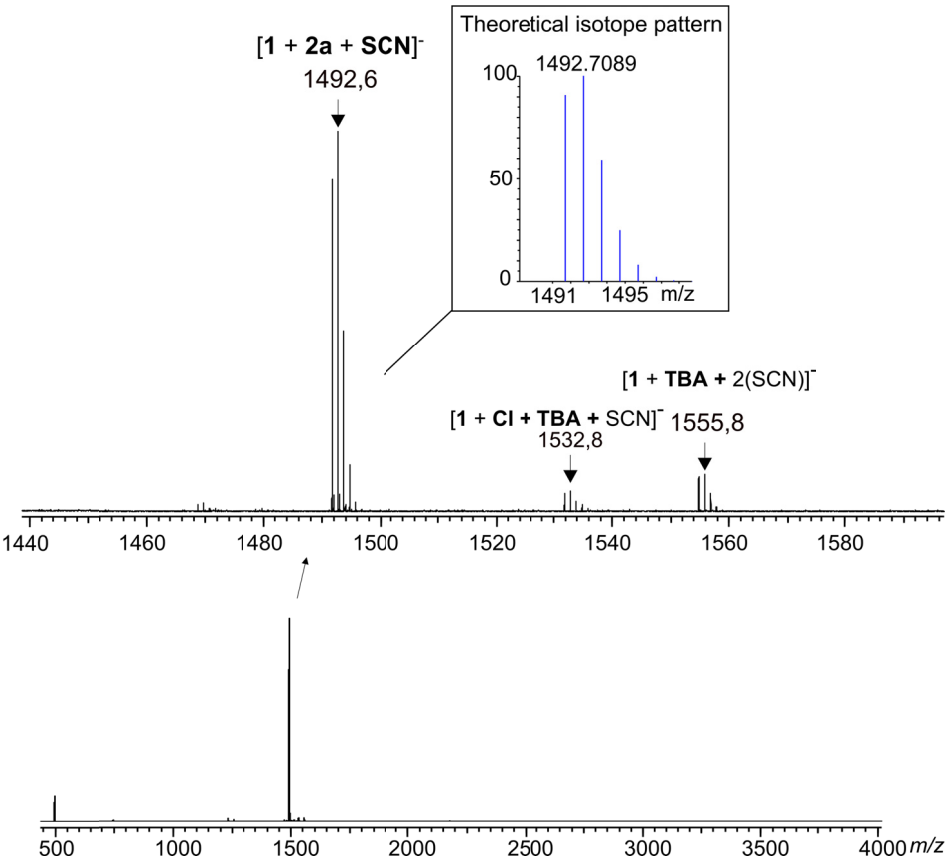

Figure 2.48 ESI-FTICR mass spectrum (negative mode detection) of an equimolar mixture of **1**, **2a** and **4b** injected in dichloromethane solution.

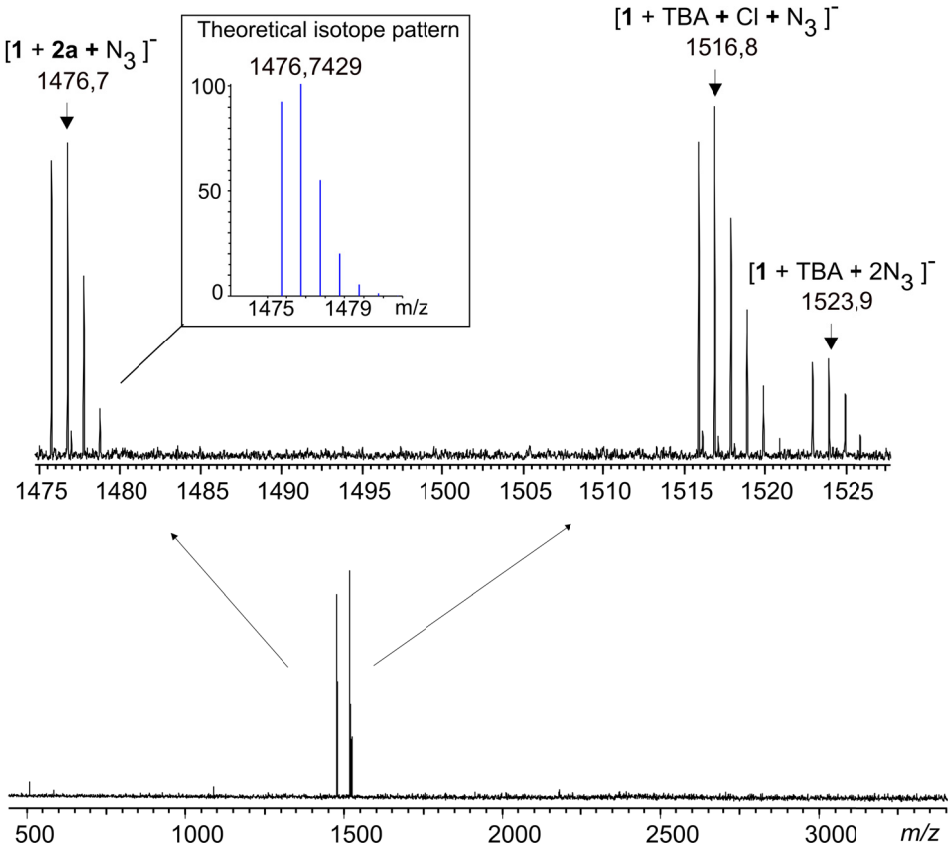

Figure 2.49 ESI-FTICR mass spectrum (negative mode detection) of an equimolar mixture of **1**, **2a** and **4c** injected in dichloromethane solution.

2.5 References and notes

[1] Kay, E. R.; Leigh, D. A. *Pure Appl. Chem.* **2008**, *80*, 17.
[2] Kay, E. R.; Leigh, D. A.; Zerbetto, F. *Angew. Chem., Int. Ed.* **2007**, *46*, 72.
[3] Dietrichbuchecker, C. O.; Sauvage, J. P. *Chem. Rev.* **1987**, *87*, 795.
[4] Breault, G. A.; Hunter, C. A.; Mayers, P. C. *Tetrahedron* **1999**, *55*, 5265.
[5] Gavina, P.; Tatay, S. *Curr. Org. Synth.* **2010**, *7*, 24.
[6] Qu, D. H.; Tian, H. *Chem. Sci.* **2011**, *2*, 1011.
[7] Fuller, A. M.; Leigh, D. A.; Lusby, P. J.; Oswald, I. D. H.; Parsons, S.; Walker, D. B. *Angew. Chem., Int. Ed.* **2004**, *43*, 3914.
[8] Hancock, L. M.; Beer, P. D. *Chem. Commun.* **2011**, *47*, 6012.
[9] Cheng, H. M.; Leigh, D. A.; Maffei, F.; McGonigal, P. R.; Slawin, A. M. Z.; Wu, J. *J. Am. Chem. Soc.* **2011**, *133*, 12298.
[10] Voignier, J.; Frey, J.; Kraus, T.; Budesinsky, M.; Cvacka, J.; Heitz, V.; Sauvage, J. P. *Chem-Eur J* **2011**, *17*, 5404.
[11] Vickers, M. S.; Beer, P. D. *Chem. Soc. Rev.* **2007**, *36*, 211.
[12] Lankshear, M. D.; Beer, P. D. *Acc. Chem. Res.* **2007**, *40*, 657.
[13] Gong, H. Y.; Rambo, B. M.; Karnas, E.; Lynch, V. M.; Keller, K. M.; Sessler, J. L. *J. Am. Chem. Soc.* **2011**, *133*, 1526.
[14] Hunter, C. A. *J. Am. Chem. Soc.* **1992**, *114*, 5303.
[15] Altieri, A.; Aucagne, V.; Carrillo, R.; Clarkson, G. J.; D'Souza, D. M.; Dunnett, J. A.; Leigh, D. A.; Mullen, K. M. *Chem. Sci.* **2011**, *2*, 1922.
[16] Schalley, C. A.; Reckien, W.; Peyerimhoff, S.; Baytekin, B.; Vogtle, F. *Chem-Eur J* **2004**, *10*, 4777.
[17] Wyman, I. W.; Macartney, D. H. *J. Org. Chem.* **2009**, *74*, 8031.
[18] Wenz, G.; Han, B. H.; Muller, A. *Chem. Rev. (Washington, DC, U. S.)* **2006**, *106*, 782.
[19] Amabilino, D. B.; Stoddart, J. F. *Chem. Rev. (Washington, DC, U. S.)* **1995**, *95*, 2725.
[20] Brown, A.; Beer, P. D. *Dalton Trans.* **2012**, *41*, 118.
[21] Valderrey, V.; Escudero-Adan, E. C.; Ballester, P. *J. Am. Chem. Soc.* **2012**, *134*, 10733.
[22] Kim, S. K.; Sessler, J. L. *Chem. Soc. Rev.* **2010**, *39*, 3784.
[23] Ballester, P.; Gil-Ramirez, G. *Proc. Natl. Acad. Sci. U. S. A.* **2009**, 106, 10455.
[24] Chas, M.; Gil-Ramirez, G.; Escudero-Adan, E. C.; Benet-Buchholz, J.; Ballester, P. *Org. Lett.* **2010**, *12*, 1740.
[25] Chas, M.; Gil-Ramirez, G.; Ballester, P. *Org. Lett.* **2011**, *13*, 3402.
[26] Geometries of the complexes were refined by performing an optimize geometry calculation with Molecular Mechanics using augmented MM3 parameters as implemented in the software CAChe WorkSystem Pro Version 6.1.12.33, Fujitsu Limited. A conjugate gradient method was used for energy minimization with a convergence energy criterion of 0.001 kcal/mol.
[27] Chas, M.; Gil-Ramirez, G.; Ballester, P. *Org. Lett.* **2011**, *13*, 3402.
[28] Hancock, L. M.; Beer, P. D. *Chem. Commun.* **2011**, *47*, 6012.
[29] Thomas, J. R.; Liu, X. J.; Hergenrother, P. J. *J. Am. Chem. Soc.* **2005**, *127*, 12434.
[30] Srinivasan, R.; Tan, L. P.; Wu, H.; Yang, P. Y.; Kalesh, K. A.; Yao, S. Q. *Org. Biomol. Chem.* **2009**, *7*, 1821.
[31] Gans, P.; Sabatini, A.; Vacca, A. *J. Solution Chem.* **2008**, *37*, 467.
[32] Fujita, T.; Lehn, J. M. *Tetrahedron Lett.* **1988**, *29*, 1709.
[33] Escuer, A.; Harding, C. J.; Dussart, Y.; Nelson, J.; McKee, V.; Vicente, R. *J. Chem. Soc., Dalton Trans.* **1999**, 223.
[34] Bond, A. D.; Derossi, S. A.; Harding, C. J.; McInnes, E. J. L.; McKee, V.; McKenzie, C. J.; Nelson, J.; Wolowska, J. *Dalton Trans.* **2005**, 2403.

[35] Gross, D. E.; Schmidtchen, F. P.; Antonius, W.; Gale, P. A.; Lynch, V. M.; Sessler, J. L. *Chem-Eur J* **2008**, *14*, 7822.
[36] Spence, G. T.; Beer, P. D. *Acc. Chem. Res.* **2013**, 46, 571.
[37] Hanni, K. D.; Leigh, D. A. *Chem. Soc. Rev.* **2010**, *39*, 1240.
[38] Olsen, J. C.; Fahrenbach, A. C.; Trabolsi, A.; Friedman, D. C.; Dey, S. K.; Gothard, C. M.; Shveyd, A. K.; Gasa, T. B.; Spruell, J. M.; Olson, M. A.; Wang, C.; de Rouville, H. P. J.; Botros, Y. Y.; Stoddart, J. F. *Org. Biomol. Chem.* **2011**, *9*, 7126.
[39] Gibson, H. W.; Lee, S. H.; Engen, P. T.; Lecavalier, P.; Sze, J.; Shen, Y. X.; Bheda, M. *J. Org. Chem.* **1993**, *58*, 3748.
[40] Zhang, W.; Yamamoto, H. *J. Am. Chem. Soc.* **2007**, *129*, 5298.
[41] Mamardashvili, G. M.; Mamardashvili, N. Z.; Koifman, O. I. *Russ. J. Coord. Chem.* **2011**, *37*, 872.
[42] Hancock, L. M.; Beer, P. D. *Chem. Commun.* **2011**, *47*, 6012.

Chapter 3

Coordination of Bipyridine Bis-*N,N´*-oxide Ligands into a Bis-calix[4]pyrrole Macrotricycle

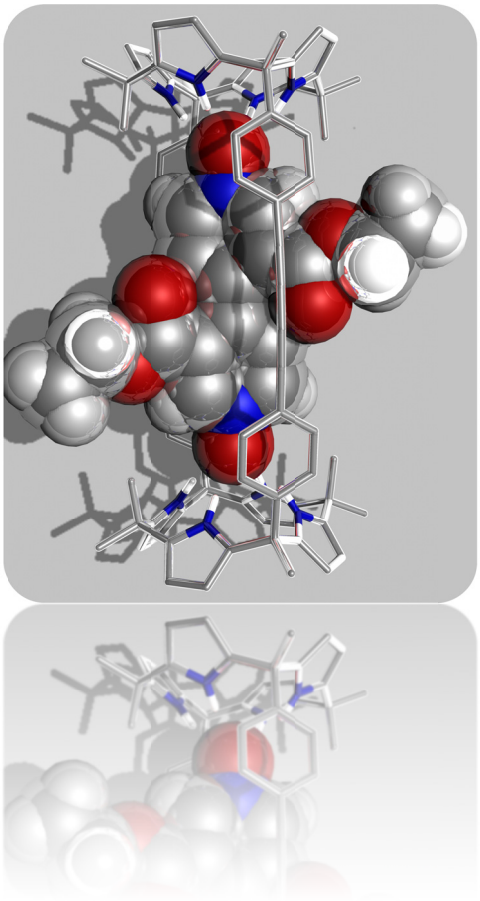

3.1 Introduction

The physico-chemical properties or the reactivity of a substrate can be modified by its specific binding to the catalytic active site of an enzyme.[1] The high specificity that an enzyme possesses towards a substrate is based firstly on their geometrical complementarity according with the "lock and key" theory. Such geometrical complementarity can be increased by additional effects; i.e. the coordinated substrate is able to modulate the flexible binding site of the enzyme by stabilising non-covalent interactions as it was described in the latter "induce-fit" theory. The enzymatic activity is achieved in all the cases by lowering the activation barrier of a determined process. Sometimes this is possible by creating an environment in the active site that produces the stabilization of the reaction transition state. Many examples of synthetic supramolecular receptors have been designed following these considerations. Non-covalent interactions in supramolecular assemblies have been demonstrated to create environments able to modify the guest reactivity[2], produce the stabilization of reactive species[3] or modify its physico-chemical properties.[1,4,5,6,7] Having these examples in mind, we decided to study how the unique structural characteristics of a bis-calix[4]pyrrole macrocyclic receptor affects the racemization barrier of 3,3´-disubstituted 4,4′-bipyridine bis-*N*,*N*′-oxide ligands. We also try to give a rational explanation of the mechanism that is behind the sensible changes in the physico-chemical properties of the guests. Additionally, the elongation of the 4,4′-bipyridine bis-*N*,*N*′-oxide ligands at the 3,3´-position give the possibility to synthesize fairly linear molecules that can be used in the preparation of interlocked molecules. In brief, the self-assembly complementarity that exist between the bis-calix[4]pyrrole macrocycle and the elongated bipyridine bis-*N*,*N*′-oxide ligands is presented as an effective bipyridine bis-*N*,*N*′-oxide templated formation of [2]pseudorotaxanes. Finally, we also present our attempts towards the synthesis of [2]rotaxanes by following this templating strategy.

3.2 Results and discussion

3.2.1 Design and synthesis

The synthesis of the acetylenic-derived bis-calix[4]pyrrole **1** have been described in *Chapter 2*[8]. The tricyclic molecule presents a relatively rigid structure provided by the two 1,3-diynyl linkers that prevent the collapse of its macrocyclic structure and position both calix[4]pyrrole units in a fixed relative distance. As we described in the previous chapter this rigidity allowed the interactions of size and shape complementary guests providing a variety of recognition processes with high association constants.

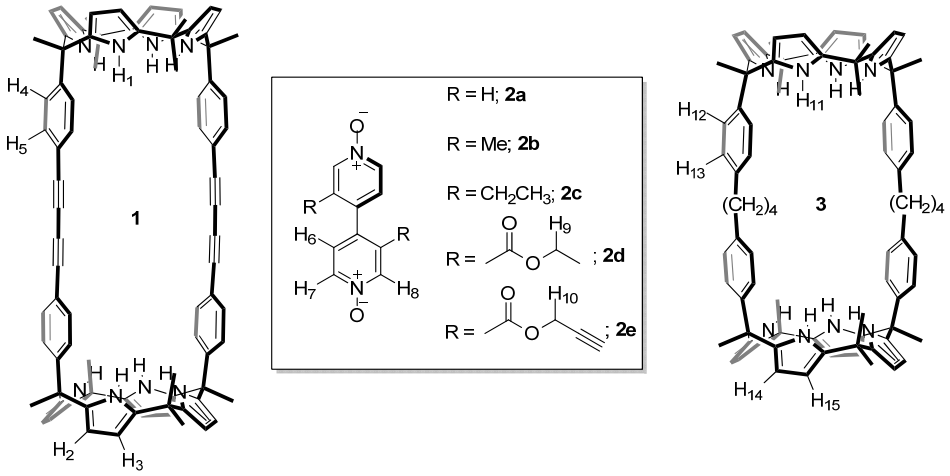

Figure 3.1 Molecular structures of acetylenic-derived bis-calix[4]pyrrole **1** and aliphatic-derived bis-calix[4]pyrrole **3** and 4,4′-bipyridine-*N*,*N*′-dioxide derivatives **2** used in this study.

The catalytic hydrogenation of the acetylenic linkers that connect the calix[4]pyrrole units of macrocycle **1** using Pd/C 10% yielded the bis-calix[4]pyrrole receptor **3** which possess fully saturated aliphatic chains with four methylene units holding both calix[4]pyrroles (experimental section: Figure 3.16). Fortunately, a single crystal structure of **3** was obtained from the slow evaporation of a saturated solution containing a 1:1 mixture of chloroform and methanol. The X-ray structure suggests a flexible macrocycle that in solution is potentially able to exhibit a variety of conformations. We expect that this higher flexibility allows reorganizations processes of both

calix[4]pyrrole units to fit the structural guest requirements opening the applicability of this kind of bis-calix[4]pyrrole macrotricyclic structures.

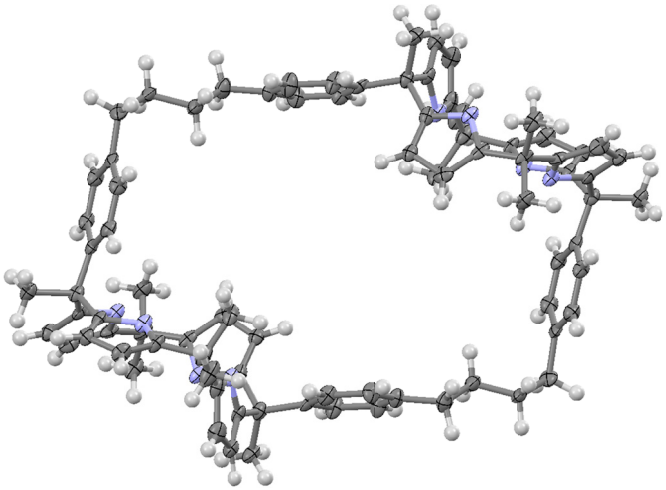

Figure 3.2 X-ray structure of the aliphatic-derived bis-calix[4]pyrrole **3**. Solvent molecules have been omitted for clarity. Thermal ellipsoids are represented at 50% probability.

4,4′-bipyridine bis-*N,N*′-dioxide **2a** is commercially available. The bipyridine bis-*N,N´*-oxide derivatives **2b**, **2c**, **2d** and **2e** were synthesized according to the synthetic scheme represented in Scheme 3.1 and Scheme 3.2. Reductive coupling and subsequent oxidation of the commercially available 3-methylpyridine or 3-ethylpyridine provide the formation of 4,4'-bipyridine derivatives with different alkyl substituents in the 3,3´-position: *methyl* or *ethyl* groups, respectively.[9,10] Next, the oxidation of such 4,4'-bipyridine derivatives afforded the formation of 3,3'-dimethyl-[4,4'-bipyridine] *N,N*'-dioxide **2b** and 3,3'-diethyl-[4,4'-bipyridine] *N,N*'-dioxide **2c** compounds in quantitative yields (Scheme 3.1a). Alternatively, 3,3'-dimethyl-4,4'-bipyridine can be oxidised to 4,4´-binicotinic acid[10] which constitutes our starting material for the synthesis of the bis-*N,N´*-oxides **2d** and **2e** (Scheme 3.1b).

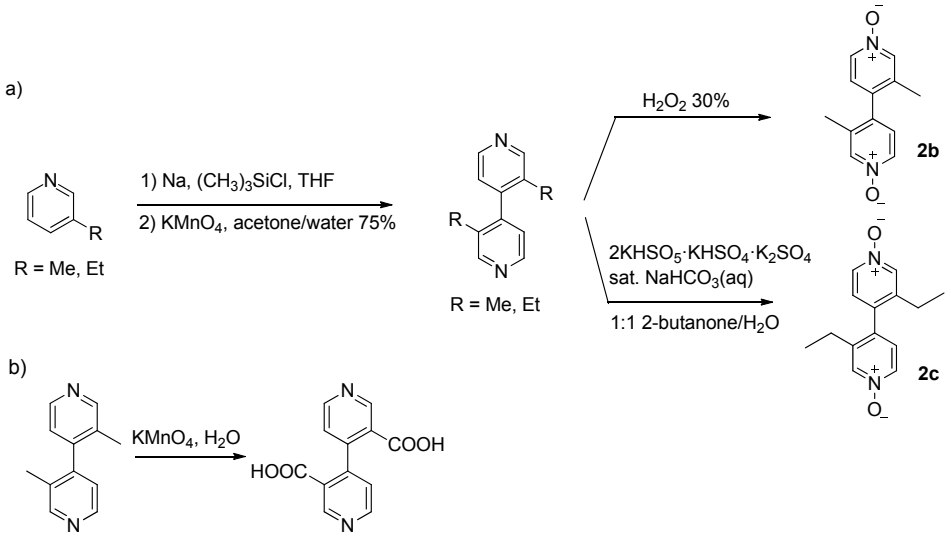

Scheme 3.1 Synthetic scheme for the preparation of a) 4,4′-bipyridine-*N*,*N*′-dioxides **2b** and **2c** and b) 4,4´-binicotinic acid.

3,3´-dicarboxylate- 4,4´-bipyridines were prepared by reacting the 4,4´-binicotinic acid with thionyl chloride and a catalytic amount of DMF to obtain the corresponding acyl chloride derivative. The acyl chloride is immediately subjected to react with ethanol or propargylic alcohol to afford the ester derivatives. Finally, bipyridine bis-*N*,*N*´-oxides **2d** and **2e** were synthesized by reaction of the respective bipyridines with *m*-chloroperbenzoic acid and Oxone®, respectively (Scheme 3.2).

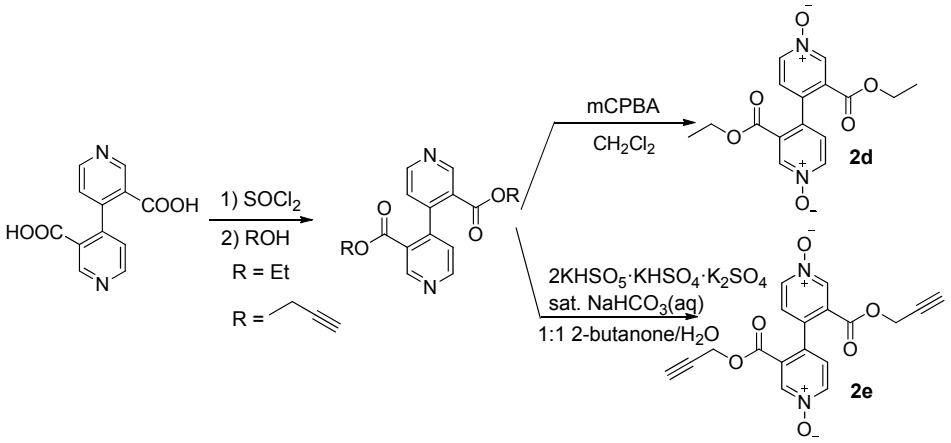

Scheme 3.2 Synthetic scheme for the preparation of 4,4′-bipyridine-*N*,*N*′-dioxides **2d** and **2e**.

Bipyridine *N,N´*-oxide **2e** was immediately used in the synthesis of a rod-like 4,4′-bipyridine bis-*N,N*′-oxide derivative **2f** equipped with bulky end groups. The azide **4** was synthetized following described procedures.[11,12,13] The synthesis of **2f** was achieved in 80% yield by a copper(I)-catalysed azide–alkyne cycloaddition using CuI and triethylammine in DMSO.

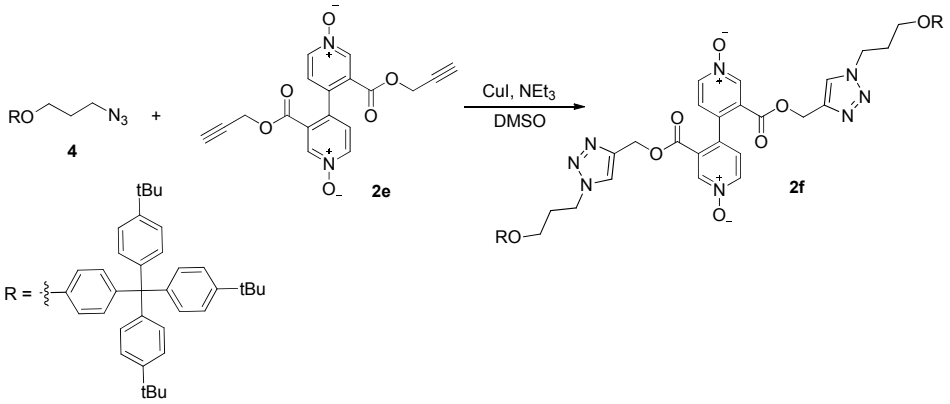

Scheme 3.3 Copper(I)-catalysed azide–alkyne cycloaddition for the preparation of a rod-like 4,4′-bipyridine-*N,N*′-dioxide **2f** having end groups too large to pass through the cavity of macrotricycle **1**.

3.2.2 ^{1}H NMR binding studies

4,4′-bipyridine bis-*N,N*′-oxide **2a** has been described in the previous chapter as an effective template able to bring closer two units of acetylene *aryl*-extended two walls calix[4]pyrrole **3** (see *Chapter 2*, Figure 2.5) and direct the formation of tricycle **1**. Herein, we carried out ^{1}H NMR titration experiments to evaluate the interaction between bis-calix[4]pyrrole **1** and 4,4′-bipyridine bis-*N,N*′-oxide **2a** in dichloromethane. The addition of 0.2 equiv of **2a** to a millimolar dichloromethane solution of **1** produced the appearance of a new set of proton signals sharp and well defined that were assigned to the inclusion complex **2a⊂1**. Additionally, all the proton signals corresponding to free **1** remain at the same chemical shift (Figure 3.3 b). The downfield shift of the NH proton signals (1´) of the **2a⊂1** to 8,8 ppm is consistent with the formation of eight hydrogen bond interaction between the 4,4´-bipyridine bis-*N,N´*-oxide and both

calix[4]pyrrole units of receptor **1**. The appearance of only one signal (1′) of NHs indicates that both hemispheres of receptor **1** are participating in identical interactions as expected for the formation of a complex **2a**⊂**1** with D_{2h} symmetry. New sets of protons signals are observed for the *aryl*-aromatic protons (4′, 5′) and the *β*-pyrrolic protons (3′, 2′). The aromatic protons 4′ appeared upfield shifted compared to the same ones in the free receptor suggesting the presence of π-π interactions between bipyridine bis-*N,N′*-oxide and the aromatic walls of the macrocycle.

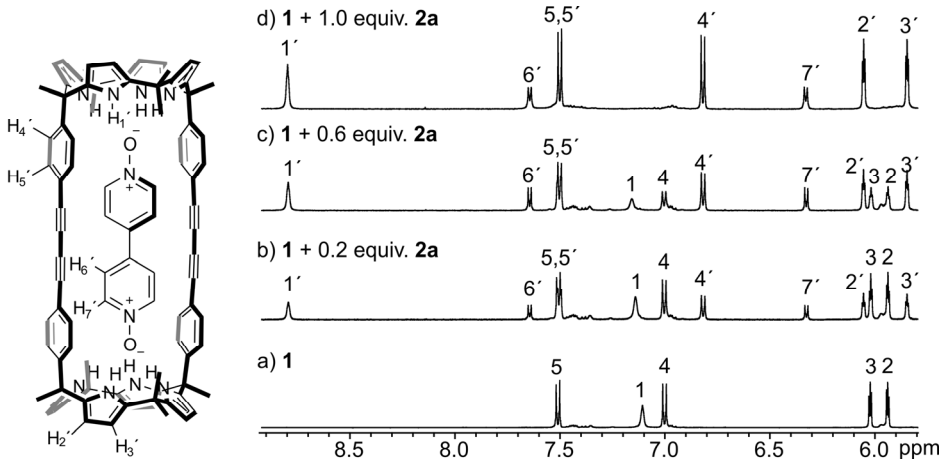

Figure 3.3 Left: Molecular structure of the inclusion complex of ditopic macrotricycle **1** and 4,4′-bipyridine-*N,N′*-dioxide **2a**. Right: Downfield region of the ^{1}H NMR titration experiment (500 MHz, CD_2Cl_2, 298 K) of ditopic macrotricycle [**1**]= 2.2 mM with bipyridine bis-*N,N′*-oxide **2a**. See also Figure 3.1 for proton assignments.

Two different signals are observed for the *β*-pyrrolic protons of **1** that were shifted in opposite directions respect to the unbound receptor. As we commented in *Chapter 2*, the X-ray structure of receptor **1** indicates that the calix[4]pyrrole cores are adopting a *1,2 alternate* conformation even in acetonitrile that is a solvent able to establish hydrogen bonds. In this conformation the *β*-pyrrolic protons 2 are experiencing the shielding effect of the aromatic ring of the macrocyclic linkers. Consequently, when **2a**⊂**1** complex is formed, the calix[4]pyrrole units tend to form hydrogen bond interactions with the guest freezing the calix[4]pyrrole cores in *cone* conformation. Such conformational change positions the *β*-pyrrolic protons (2′) away from the influence of the aromatic ring being the protons (2′) downfield shifted respect to the ones in the free macrocycle **1**. Further evidences for the **2a**⊂**1** complex formation arises from the

observation of two doublets with a characteristic *ortho* coupling at δ = 6.33 and 7.65 ppm (protons 6´and 7´ in Figure 3.3 b) that we assigned to the protons of the included **2a**. The large upfield shift experienced by the pyridyl protons of bound **2a** *alpha* to the *N*-oxide (proton 7´ in Figure 3.3 b Δδ = 1.2 ppm) confirms its interaction with the calix[4]pyrrole units. Together these results indicate that 20% of the receptor **1** is bound to the 4,4′-bipyridine-*N*,*N*′-dioxide **2a** and that the chemical exchange between the free and the bound receptor is slow on the ^{1}H NMR chemical shift timescale. When we add one equivalent of **2a** only the signals of the 1:1 inclusion complex are detected. Such results suggest that complex **2a**⊂**1** is formed with a thermodynamic stability constant estimated to be K(**2a**⊂**1**)>10^4 M^{-1}. Similar ^{1}H NMR titration experiments involving the more flexible macrotricycle **3** and ligand **2a** produced a different dynamic behaviour. The addition of 1 equiv of **2a** to a solution of **3** induced very small shifts of the proton signals of the macrocycle. Moreover, it was necessary to add 3 equiv of ligand **2a** to observe the saturation of the receptor (experimental section: Figure 3.17). This fast exchange regime observed for free and bound receptor suggests that receptor **3** binds 4,4′-bipyridine-*N*,*N*′-dioxide **2a** with a lower association constant than receptor **1**. In short, the acetylenic linkers that connect both calixpyrrole units provide the required preorganization of the host to bind 4,4′-bipyridine-*N*,*N*′-dioxide ligands with high association constants. However, the more flexible aliphatic version of this receptor (receptor **3**), even if contains identical binding sites like **1**, provides lower association constants. This is due to the energetic that has to be paid in order to arrange the two calix[4]pyrrole units in a suitable conformation to bind the bipyridine ditopic ligand. The addition of 0.5 equiv of 3,3'-dimethyl-4,4'-bipyridine bis-*N*,*N´*-oxide **2b** to a chloroform solution of receptor **1** produced the broadening and shifting of the receptor signals. When 1 equiv of **2b** is added, the signals of receptor **1** remain at the same chemical shift. Moreover, the aromatic protons *alpha* to the nitrogen of the pyridyl ligand **2b** were downfield shifted compared to the same ones of the free ligand confirming its inclusion within receptor **1**.

The interaction between **1** and 3,3'-diethyl-4,4'-bipyridine *N*,*N´*-oxide **2c** (Figure 3.5) gave parallel results to the ones obtained for the **2b**⊂**1** complex formation.

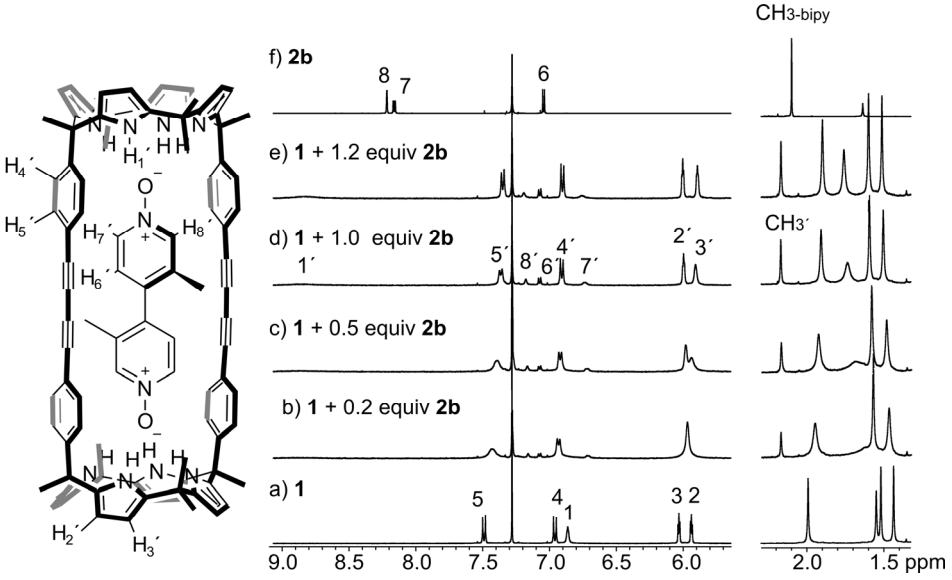

Figure 3.4 Left: Molecular structure of the 1:1 complex formed between macrotricycle **1** and 3,3'-dimethyl-[4,4'-bipyridine] *N*,*N*'-dioxide **2b**. Right: ^{1}H NMR titration experiment (500 MHz, $CDCl_3$, 298 K) of ditopic macrotricycle **1**, [**1**]= 1.0 mM, with **2b**. See also Figure 3.1 for proton assignments.

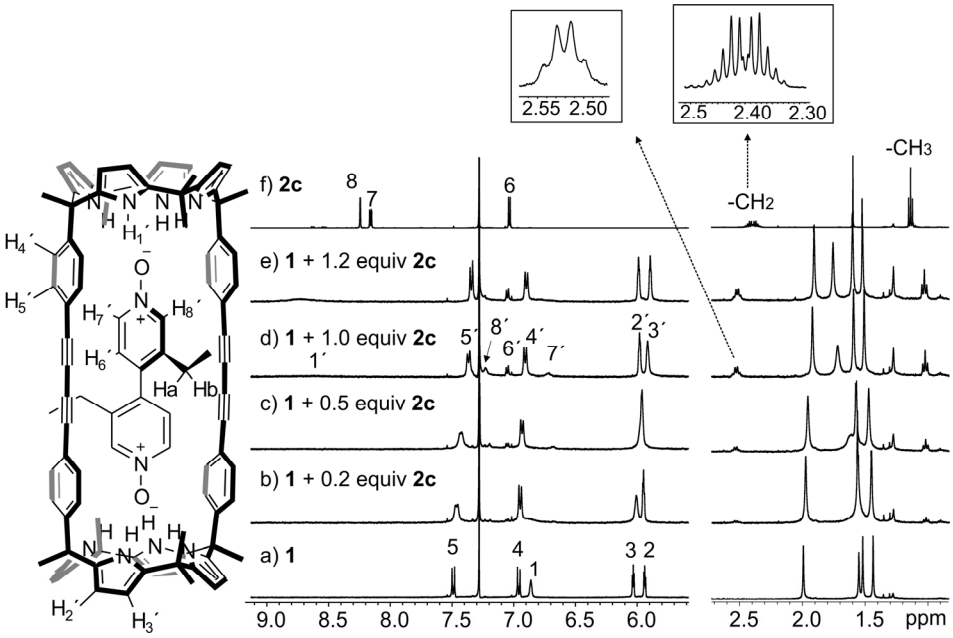

Figure 3.5 Left: Molecular structure of the 1:1 complex of macrotricycle **1** and 3,3'-diethyl-[4,4'-bipyridine] *N*,*N*'-dioxide **2c**. Right: ^{1}H NMR titration experiment (500 MHz, $CDCl_3$, 298 K) of ditopic macrotricycle **1**, [**1**]= 1.0 mM, with **2c**. See also Figure 3.1 for proton assignments.

Both ^{1}H NMR experiments involving **2b** and **2c** indicated than when one equivalent of the *N*-oxides is added, the relative **2⊂1** complexes are quantitatively formed. The addition of higher amounts of *N*-oxides did not produce observable changes in the proton signals of the receptor. These results indicate that the stability constant for these complexes is higher than 10^4 M^{-1}.

The thermodynamic stability constant for the 1:1 complex was determined by isothermal titration calorimetry (ITC) experiments (Figure 3.6).

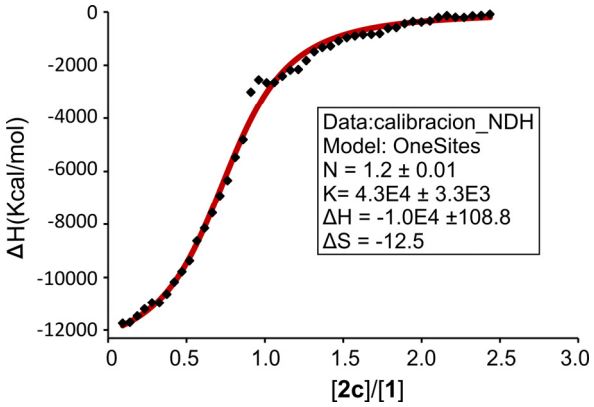

Figure 3.6 Data points (squares) obtained in the ITC experiment of **1** with **2c**. The fit to the theoretical binding isotherm (red line) was performed using the Microcal Origin software and a binding model that considers the formation of one aggregate.

The sample cell was filled with a 0.3 mM solution of receptor **1** in chloroform and the reference cell with a chloroform solution. Later, in a 120 second intervals, aliquots of 10 μL of a ten times more concentrated solution of the **2c** ligand was added into the receptor **1** solution. During a blank experiment it was calculated the heat that corresponds with the dilution of the ligand **2c** in a chloroform solution and at the same concentration. This heat of dilution was later subtracted to the binding heat of the **2c⊂1** complex formation. The complexation process resulted to be exothermic and a single binding isotherm was observed with an inflexion point at a molar ratio approximately 1 confirming the formation of a 1:1 stoichiometry complex. The fit of this binding isotherm was done selecting the "one set of sites" binding model implemented in the Microcal Origin software. The fitting of the data allowed the determination of the thermodynamic variables of the complexation process: ΔG, ΔH and TΔS as well as the

thermodynamic association constant K (Figure 3.6). In agreement with the formation of a complex stabilized by eight hydrogen bond interactions, the process is enthalpically driven ($\Delta H = -1.0\times10^4$ kcal/moL) with an association constant of $K_{\mathbf{2c}\subset\mathbf{1}} = 4.3\times10^4$ M^{-1}. We expect association constants with similar values for the formation of complexes involving similar bispyridyl bis-*N,N´*-oxide ligands like **2b**, **2d** and **2e**.

3.2.3Racemization barriers of chiral 4,4´-bipyridine bis-*N,N´*-oxide derivatives[14]

Due to steric crowding, biaryl systems are not co-planar. The single substitution of one of the two *ortho* position with respect to the single C-C bond of the two pyridyl units in 4,4´-bipyridine bis-*N,N´*-oxide **2a** leads to chiral conformers (axial chirality). The interconversion between this type of conformational enantiomers requires the rotation of the single C-C bond connecting the pyridyl units and produces a higher energy coplanar conformer. The energy required to achieve the coplanar conformation depends on the size of the *ortho* groups (axial chirality). For example, the two enantiomeric conformers of **2b** interconvert readily at room temperature due to a low energy barrier required to access the coplanar conformer. Compound **2b** is isolated as a racemic mixture and even if it was resolved in the two pure conformational enantiomers they would readily racemize. However, when the two *ortho* positions with respect to the C-C single bond in each one of the pyridyl units of 4,4´-bipyridine bis-*N,N´*-oxide are substituents with different groups, the energetic barrier of rotation becomes high enough to avoid the rapid interconversion between enantiomeric conformers at r.t. (spontaneous racemization). If this is the case the isolation of the two enantiopure conformational isomers (atropisomers) is possible by chiral resolution. It is very interesting to consider the use of supramolecular strategies to modify the racemization barrier of such axially chiral 4,4´-bipyridine bis-*N,N´*-oxide derivative ligands. We decided to investigate how the formation of the 1:1 inclusion complex **2⊂1** alters the racemization barrier of ligands **2** compared to the corresponding energy barrier measured for the free substrate in the bulk solution. The studies were performed on the 3,3'-diethyl-4,4'-bipyridine bis-*N,N´*-oxide **2c** as model system. The ^{1}H NMR spectrum of ligand **2c** displays two diastereotopic signals for the protons Ha and Hb of the methylene group (see Figure 3.7a for proton assignments). These signals are well separated at low or rt temperature

and coalesce at higher temperatures (Figure 3.7 c). The rotation of the pyridine-pyridine single bond interconverts the two diastereotopic protons due to the associated racemization (Figure 3.7b). When the rate constant for the interconversion process (chemical exchange) is fast on the ^{1}H NMR timescale a single signal is observed for the diasterotopic protons. In other words, the rate constant of the pyridine-pyridine bond rotation for **2c** can be determined at different temperatures by performing a complete band shape analysis using a set of variable temperature ^{1}H NMR experiments or simply determined at the temperature of coalescence. The use of other 4,4´-bipyridine bis-*N*,*N*´-oxide displaying mono-*ortho* substitution in each pyridyl residue evidenced experimental limitations for the study; i.e. too low racemization barriers, as well as lack of diatereotopic signals for any of their protons. In order to determine how the inclusion of ligand **2c** within the macrotricycle **1** affects the racemization barrier of the ligand, we started calculating the thermodynamic constants for the process in the ligand free in the bulk solution. We performed variable temperature ^{1}H NMR experiments on a millimolar solution of free **2c** in chloroform. The two diastereotopic protons of each methylene group resonate as two separated signals at low temperatures due to the fact that the racemization is a slow chemical exchange process on the ^{1}H NMR timescale. As the temperature is increased the diasterotopic signals shift and broaden until a single and broad signal is observed for both protons at T= 328K (Figure 3.7c). We considered that this temperature coincides or is very close with the value of the coalescence temperature for the racemization process. In 2008 the group of Schalley reported a Tc = 363K for analogues 3,3'-diethyl-4,4'-bipyridine in [D2]-1,1,2,2-tetrachloroethane.[9] The lower racemization barrier in the case of the *N*-oxide compared with its bipyridine precursor is in agreements with previous results obtained for biphenyl ligands.[15] It was demonstrated that as a general trend, the presence of electron-donating groups in the *para* position of axially chiral biphenyl ligands induce an acceleration in the rate of enantiomer interconversion.

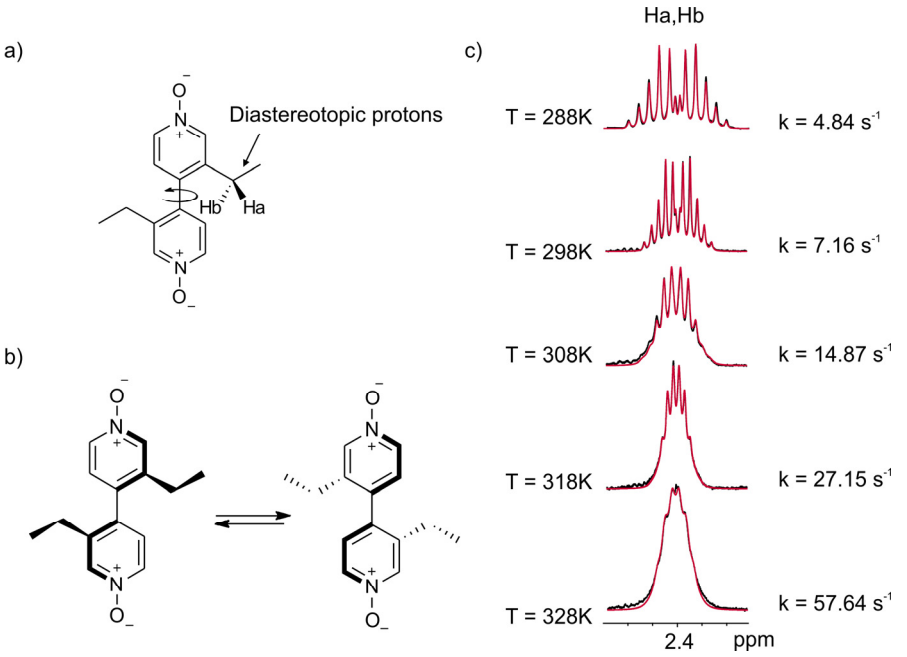

Figure 3.7 a) Molecular structure of 3,3'-diethyl-4,4'-bipyridine *N,N´*-oxide **2c** where the diastereotopic protons Ha and Hb are highlighted. b) Equilibrium between the two enantiomers of 3,3'-diethyl-4,4'-bipyridine bis-*N,N´*-oxide **2c**. c) Selected region of the variable temperature ^{1}H NMR spectra (500 MHz, $CDCl_3$) for the methylene diastereotopic protons (Ha and Hb) of free ligand **2c**. The black line corresponds with the experimental results and the red line represents the theoretical fitting of the experimental data using the Topspin software. k = rate constant (s^{-1}) of the racemization process at each temperature.

The dynamic NMR (DNMR) line shape analysis module implemented in the Topspin software allowed the determination of the exchange rate constants (k) for the diastereotopic protons (Ha and Hb) of ligand **2c** at different temperatures (Figure 3.7c). Ones the rate constant values were available; the Eyring equation [1] was applied to determine the thermodynamic constants of the racemization process.

$$k_r = \frac{kT}{h} e^{\frac{\Delta G^{\ddagger}}{RT}} = \frac{kT}{h} e^{\frac{-\Delta H^{\ddagger}}{RT}} e^{\frac{\Delta S^{\ddagger}}{R}} \qquad [1]$$

$$\ln\frac{k_r}{T} = \ln\frac{k}{h} - \frac{\Delta H^{\ddagger}}{RT} + \frac{\Delta S^{\ddagger}}{R}$$

In equation 1, k_r is the rate constant (s^{-1}), T is the temperature (K), h is the Plank´s constant (Js), k is the Boltzman´s constant (JK) and R the universal constant of gases (JK^{-1} mol^{-1}).

The plot of $\ln(k_r/T)$ vs 1/T shows a nice linear relationship. The linear regression of the plotted data provided as slope the value of $-\Delta H^{\neq}/R$ and as intercept the corresponding value of $\ln(k/h) + \Delta S^{\neq}/R$ (Figure 3.8). The enthalpy of the TS was determined to be $\Delta H^{\neq}$ = 11.14 kcal/mol and the value of the entropy is $\Delta S^{\neq}$ = -0.02 kcal/molK. These results indicate that the energy of the rotational barrier of racemization is dominated by the enthalpic term in all the range of studied temperatures. Entropy also opposes to achieve the geometry of the transition state structure. Finally, the free energy for the TS at 298K is calculated to be $\Delta G^{\neq}$ = 16.2 kcal/mol.

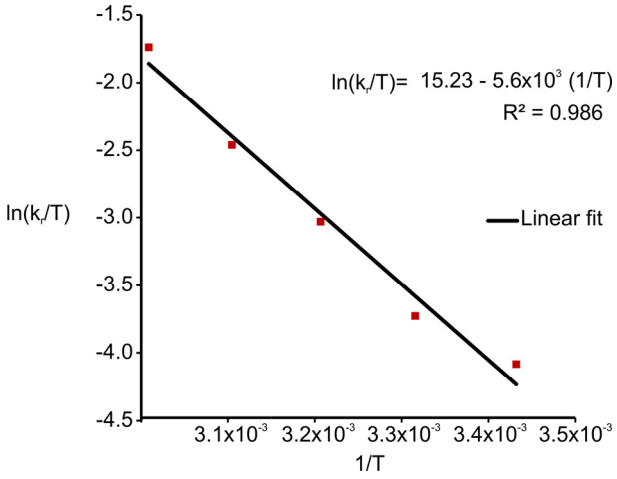

Figure 3.8 Eyring plot used to determine the activation parameters for the racemization barrier of free 3,3'-diethyl-4,4'-bipyridine bis-*N,N´*-oxide **2c** in $CDCl_3$ solution.

To study the effect of the confinement of the ligand **2c** within the macrotricycle **1**, we prepared a solution containing an equimolar mixture of both at millimolar concentration in $CDCl_3$ solution. As described in the previous section a thermodynamically stable **2c⊂1** complex is formed that presents an association constant $K_{\mathbf{2c\subset 1}} = 4.3\times10^4$ M^{-1} determined by ITC experiments (*vide supra*).[16] A variable temperature experiment of the equimolar mixture was performed in chloroform solution. When **2c** is included in receptor **1** the two diastereotopic protons Ha´and Hb´ at each methylene group coalesce at Tc = 278K. The coalescence temperature of the racemization process is drop 50K

when the ligand **2c** is included in receptor **1**. Below this temperature two separated signals are observed for the diastereotopic protons. Interestingly, at temperatures below 278K the NHs pyrrolic proton signal of **1** splits into two signals of equal intensity and the two *β*-pyrrolic protons signals splits into four signals of equal intensity. This observation points out that the responsible of such asymmetry is the slow rotation on the NMR time scale of the bipyridine bis-*N,N´*-oxide rings around the axially chiral axis at low temperatures. In brief, the pyrrolic protons of macrotricycle **1** became diastereotopic at temperatures below the Tc as result of the complexation process and this phenomenon has to be directly related with the racemization energetic barrier of the included guest.

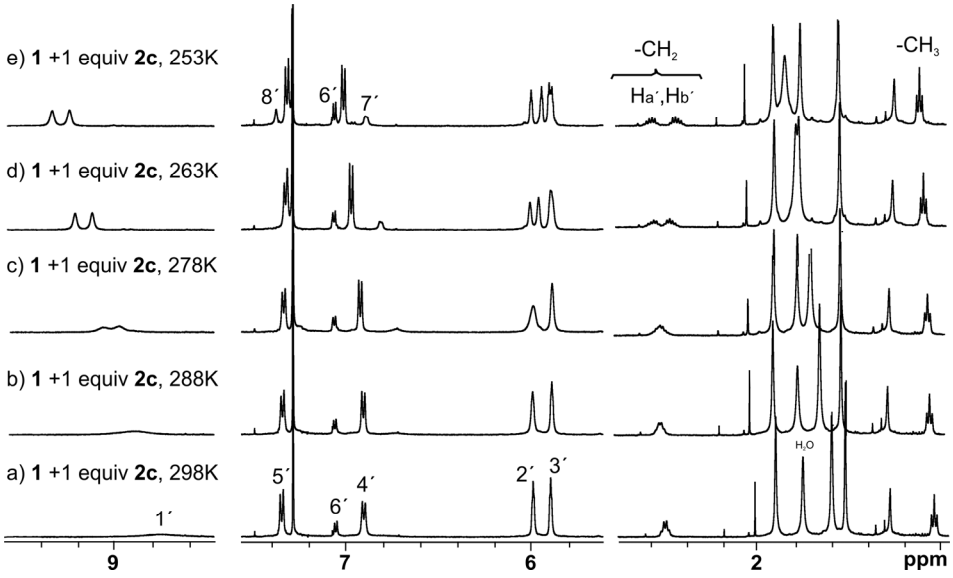

Figure 3.9 Variable temperature ^{1}H NMR spectra (500 MHz, $CDCl_3$) of an equimolar mixture of **1** and **2c**.

A ^{1}H NMR bidimensional ROESY experiment was performed at 253K in order to assign the signals of the complex **2c⊂1**. At this low temperature, EXSY experiments evidenced that diastereotopic NH pyrrolic protons of **2c⊂1** are in chemical exchange and that the calculated rate constant for this exchange is $k_{253K} = 3.9\ s^{-1}$. Additionally, by using dynamic NMR line shape analysis we were able to determine the exchange rates (k) at different temperatures for the diastereotopic protons (Ha´ and Hb´) of the complex **2c⊂1** (Figure 3.10). At 253K the rate constant associated with the racemization barrier

of guest **2c** included into **1** present a higher value than the ones calculated by bidimensional EXSY experiments taking into account the diastereotopic protons of the host. Probably, other processes i.e. the pirouetting of the macrocycle around the ligand or simply the host-guest equilibrium process also has influence in the rate constants.

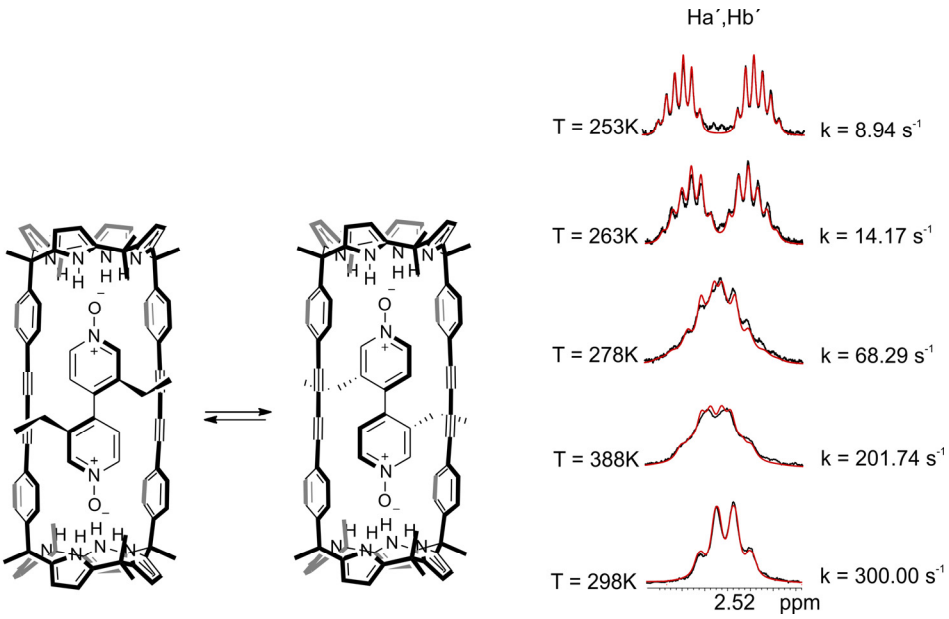

Figure 3.10 Left: Equilibrium between the two enantiomers of 3,3'-diethyl-4,4'-bipyridine *N,N´*-oxide **2c** complex inside receptor **1**. Right: Selected region of the variable temperature ^{1}H NMR spectra (500 MHz, $CDCl_3$) for the methylene diatereotopic protons (Ha´ and Hb´) ligand the bispiridyl *N,N´*-oxide ligand forming the complex **2c⊂1**. The black line corresponds with the experimental results and the red line represents the theoretical fitting of the experimental data using the Topspin software. k = rate constant (s^{-1}) of the racemization process at each temperature.

The plot of $\ln(k_r/T)$ vs 1/T shows again a linear relationship (Figure 3.11). The enthalpy of activation resulted to be $\Delta H^{\neq}$ = 12.1 kcal/mol and the entropy of activation $\Delta S^{\neq}$ = -0.01 kcal/molK. Once more, these results indicate that the rotational barrier of racemization is dominated by enthalpy. The free energy for the transition state at 298 K resulted to be $\Delta G^{\neq}$ = 14.0 kcal/mol. The racemization barrier of the ligand **2c** is reduced 2.2 kcal/mol when it is included into the macrocycle **1** forming the complex **2c⊂1**.

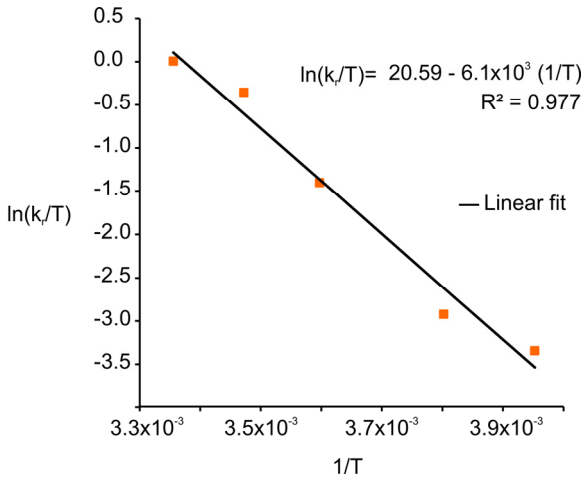

Figure 3.11 Eyring plot used to determine the activation parameters for the racemization barriers of 3,3'-diethyl-4,4'-bipyridine bis-*N*,*N*´-oxide **2c** confined into **1** in $CDCl_3$ solution.

Single crystals suitable for X-ray analysis were obtained from an equimolar chloroform solution of **1** and **2b** by slow evaporation of the solvent (Figure 3.12) providing a direct evidence for the 1:1 inclusion complex formation. The X-ray structure of free receptor **1** described in *Chapter 2* (Figure 2.8) shows that the acetylenic-linkers present a linear character holding both calix[4]pyrrole units at its maximum relative distance. However, X-ray structure of complex **2b**⊂**1** reveals that macrotricyclic receptor **1** is able to reduce its longitudinal size to fulfill the guest size requirements by bending its acetylenic-linkers. The distances N···O corresponding to the hydrogen-bond interaction between the calix[4]pyrrole NHs of **1** and the oxygen of **2b** are in the range of 3.04-3.56 Å. CH···π interactions in the range of 2.6-2.8 Å are also evident between the methyl protons of **2b** and the C≡C triple bond of the linker of receptor **1**. Fortunately, we were able to obtain single crystals of the free bipyridine bis-*N*,*N*´-oxide **2b** by the slow evaporation of a chloroform solution. Interestingly, the dihedral angle of the two pyridine planes of compound **2b** is reduced from 66.3 º to 62.1 º when it is coordinated inside receptor **1**. Additionally, bipiridyl O-O distance is increased 0.071 Å when **2b** is bound to receptor **1**.

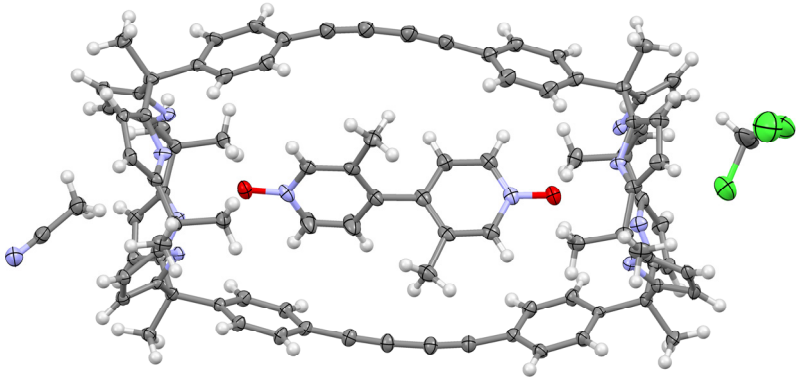

Figure 3.12 X-ray structure of **2b⊂1** complex. Thermal ellipsoids are drawn at the 50% of probability level.

Combining the results in solution and in the solid state, we conclude that the acceleration observed in the bond rotation of bipyridil ligand **2c** included into the macrocycle **1** is due to the non-covalent connectivity in the complex **2c⊂1**. Most likely, the eight NH···O interactions in the complex **2c⊂1** force the elongation of the bispiridyl O-O distance. This elongation stabilizes the transition state of the racemization process by reducing the stearic hindrance between the *ortho* substituents (ethyl or methyl and H groups).

3.2.4 Interlocked molecules: [2]pseudorotaxane and [2]rotaxane structures

The complementarity that exists in terms of size and hydrogen bonds between the 4,4´-bipyridine bis-*N,N´*-oxides and the bis-calix[4]pyrrole macrotricycle **1** can be applied to the synthesis of threaded and interlocked molecules. The association constant of the inclusion 1:1 complex **2a⊂1** was calculated by ITC titration experiments (4.3×10^4 M^{-1}). *Ortho* substituted 4,4´-bipyridine bis-*N,N´*-oxides are expected to present association constants with similar order of magnitude. By the *ortho* functionalization of both pyridine *N*-oxide aromatic rings with alkyl substituted ester moieties it is possible to obtain fairly linear molecules that can be threaded through the macrocyclic ring **1**. Furthermore, the functionalization of such linear components with bulky end groups opens the possibility of [2]rotaxane formation by a “clipping” or “capping” synthetic strategies.

We carried out a ^{1}H NMR study to evaluate the interaction between ligand **2d** and macrotricyclic receptor **1** in chloroform solution (Figure 3.13). Addition of 0.5 equiv of the ligand **2d** to a solution of **1** induced the broadening and shift of the proton signals of **1**. The NHs pyrrolic protons appear at 8.7 ppm as a broad hump. This downfield shift of the NHs pyrrolic protons is consistent with the formation of eight hydrogen bond interactions with both oxygen atoms of the bipyridyl bis-*N,N´*-oxide ligand. Other proton signals of receptor **1** are shifted similarly as it was described in the previous section for **2b,c⊂1** inclusion complexes (*vide supra*). When we add 1 equiv of **2d** only the signals assigned to **2d⊂1** complex are detected.

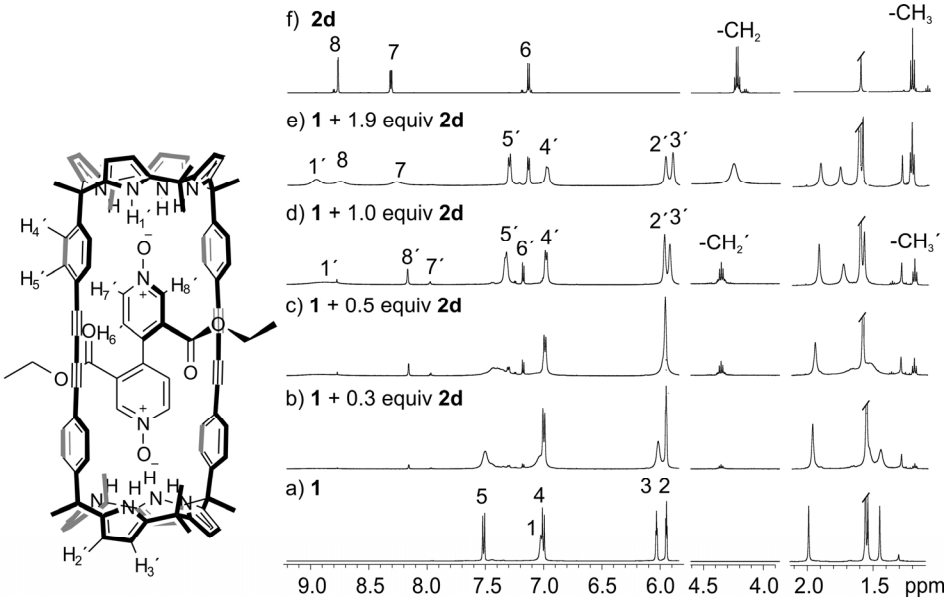

Figure 3.13 Left: Molecular structure of the 1:1 complex of macrotricycle **1** and 4,4'-bipyridine *N,N*'-dioxide derivative **2d**. Right: ^{1}H NMR titration experiment (500 MHz, CD_2Cl_2, 298 K) of ditopic macrotricycle **1**, [**1**]= 2.1 mM, with **2d**. See also Figure 3.1 for proton assignments.

Further evidences for the **2d⊂1** complex formation arises from the upfield shift experienced by the pyridyl protons *alpha* to the *N*-oxide of bound **2d** (protons 8´ and 7´ in Figure 3.13d $\Delta\delta$ = 0.6 ppm and 0.4 ppm, respectively). When more than one equivalent of **2d** is added, the proton signals of the macrocycle **1** remain at the same chemical shift value.

Molecular modelling studies suggest the threading of linear component **2d** through the macrocyclic structure of **1** forming a [2]pseudorotaxane where the pyridine rings possess a dihedral angle of 65º (Figure 3.14).

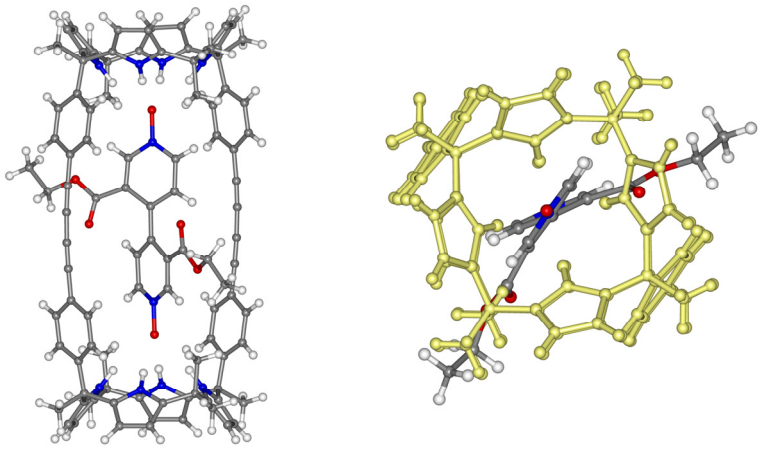

Figure 3.14 Side and top views of the energy-minimized structure[17] of **2d**⊂**1** complex displaying [2]pseudorotaxane topology.

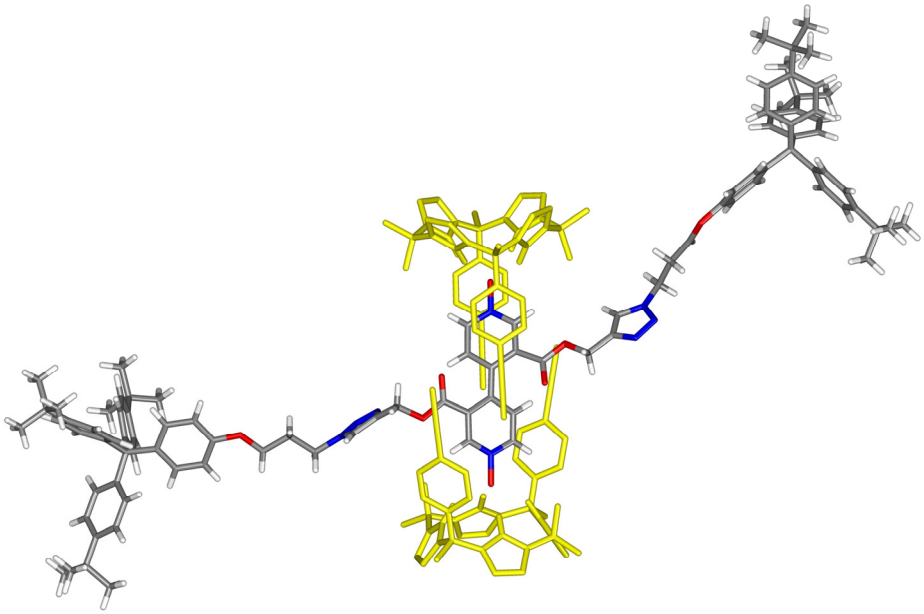

Figure 3.15 Energy-minimized structure[17] of the ternary complex between two units of acetylene α,α-*aryl*-extended calix[4]pyrrole and 4,4'-bipyridine *N*,*N*'-dioxide derivative **2f**.

One strategy for the formation of rotaxanes is the so called "clipping" strategy. It consists in the clipping of a macrocycle around a rod-like molecule that present bulky end groups. Our efforts in the synthesis of [2]rotaxanes were based in the cyclization of two acetylene calix[4]pyrrole units around the bipyridine-*N*,*N*′-dioxide derivative **2f** by using Hay coupling reaction conditions. According to molecular modelling studies (Figure 3.15) the hydrogen-bond complementarity between the calix[4]pyrrole moieties and the bis-*N*,*N*′-oxide position the reactive centres of the calix[4]pyrrole at ideal distance to favour the reaction. Unfortunately, our attempts in the synthesis of the [2]rotaxane have failed.

3.3 Conclusion

We have described the quantitative formation of thermodynamically stable 1:1 inclusion complexes between a biscalix[4]pyrrole macrocycle **1** and a pool of 4.4′-bipyridine bis-*N*,*N*′-oxides **2** in non-polar solvents. By ^{1}H NMR experiments we demonstrated that bis-calix[4]pyrrole macrotricycle **1** binds 4,4′-bipyridine-bis-*N*,*N*′-dioxide **2** ligands with association constants higher than $10^{4}M^{-1}$. However, lower association constants for the interaction between **3** and **2a** are detected. The thermodynamic analysis of the interaction between **2c** and **1** by ITC allows to estimates an association constant of 4.3×10^{4} M^{-1}. Interestingly, it was found that when ligand **2c** is included into receptor **1**, the enantiomer interconversion of the chiral ligand is facilitated by the reduction of its racemization barrier in 2.2 kcal/mol. The structures of the **2b⊂1** inclusion complex and free ligand **2b** were confirmed in the solid state by single crystal X-ray diffraction. Interestingly, the dihedral angle of the two pyridine planes of compound **2b** is reduced from 66.3 º to 62.1 º when it is coordinated inside receptor **1**. Additionally, bipiridyl O-O distance is increased 0.071 Å when **2b** is bound to receptor **1**. The eight NH···O interactions in the complex **2b⊂1** force the elongation of the bipyridine bis-*N*,*N*′-oxide ligand and such elongation stabilizes the transition state of the racemization process.

Finally, we have described a novel strategy for the template formation of [2]pseudorotaxanes. This methodology opens the possibility to use *ortho* substituted 4,4′-bipyridine bis-*N*,*N*′-oxides as linear components for the preparation of different mechanically-interlocked molecular architectures.

3.4 Experimental section

3.4.1 General information and instrumentation

All reagents were obtained from commercial suppliers and used without further purification. Anhydrous solvents were obtained from a solvent purification system SPS-400-6 from Innovative Technologies, Inc. All solvents were of HPLC grade quality, commercially obtained and used without further purification.

Routine ^{1}H NMR spectra were recorded on a Bruker Avance 400 (400.1 MHz for ^{1}H NMR) and Bruker Avance 500 (500.1 MHz for ^{1}H NMR) ultrashield spectrometer. The deuterated solvents (Aldrich) used were $CDCl_3$ and CD_2Cl_2; chemical shifts are given in ppm, relative to TMS.

Isothermal titration calorimetry experiments were performed using a Microcal VP-ITC Microcalmeter.

X-ray structure determinations: Crystals of **2b⊂1** and **2b** were obtained by slow evaporation of chloroform. The measured crystals were unstable under atmosphere conditions; they were prepared under inert conditions immersed in perfluoropolyether as protecting oil for manipulation. Data Collection: Measurements were made on a Bruker Kappa APEX II DUO diffractometer equipped with an APPEX 2 4K CCD area detector, a Microsource with $Mo_{K\alpha}$ radiation and an Oxford Cryostream 700 low temperature device (T = 100K). Full-sphere data collection was used with ω scans. Programs used: Data collection Apex2 V2012.2-0 (Bruker AXS 2010), data reduction Saint + Version 7.60A (Bruker AXS 2008) and absorption correction SADABS V. 2008-1 (2008).

3.4.2 Synthetic procedures

Bis-calix[4]pyrrole **3**

To a 10 ml THF solution of 30 mg of bis-calix[4]pyrrole macrotricycle **1** (1 equivalent, 0.025 mmol) were added 18 mg of Pd/C dissolved in 4 ml of THF. This suspension was stirred under H_2 at 2.5 bar of pressure during 20h and using a 20 ml flask. The reaction

can be followed by silica TLC in CH_2Cl_2/hexane (7/3). The crude was cleaned passing it through celita eluting with THF. Later, a preparative TLC eluting with a CH_2Cl_2/hexane (7/3) mixture allowed obtaining a white-yellow solid (9 mg, 30% yield).

^{1}H NMR (400 MHz, CD_2Cl_2) δ (ppm) 7.35 (s, broad, 8H), 7.08 (d, $^3J_{H-H}$~ 8.37 Hz, 8H), 6.86 (d, $^3J_{H-H}$~ 8.37 Hz, 8H), 5.94 (t, $^3J_{H-H}$~ 3.08 Hz, 8 H), 2.66 (m, 8H), 5.65 (m, 8 H), 1.89 (s, 12H), 1.68 (m, 8H), 1.67 (s, 12 H), 1.56 (s, 12 H).

MS (MALDI +ve) m/z calculated for $C_{84}H_{92}N_8^+$: 1212.7, found: 1212.7 (complex isotopic pattern obtained as mixture of $(M^{+\cdot})$ and $(M-H)^+$. Structure confirmed by X-ray diffraction analysis.

3,3'-dimethyl-4,4'-bipyridine bis-*N*,*N*´-oxide **2b**

3,3'-dimethyl-4,4'-bipyridine (obtained according to described procedures[10]) (50 mg, 0.271mmol) was dissolved in 1 ml of acetic acid and 0,45 ml of H_2O_2 30% were later added. The reaction mixture was heated at 75ºC overnight. The solvent was evaporated and the residue redissolved in 5 ml of water, then washed with 3x5ml of dichloromethane and the organic phase evaporated. A short basic alumina column eluting with $CHCl_3$/MeOH 9:1 afforded a yellowish solid (37.7 mg, 64% yield).

^{1}H NMR (400 MHz, $CDCl_3$) δ (ppm) 8.2 (s, 2H), 8.1 (d, $^3J_{H-H}$ ~ 4.96 Hz, 2H), 7.0 (d, $^3J_{H-H}$ ~ 4.96 Hz, 2H), 2.1 (s, 6H). ^{13}C {^{1}H} NMR (100.6 MHz, $CDCl_3$, 25ºC) δ (ppm) 139.9 (CH), 136.9 (CH), 135.3 (C), 134.8 (C), 125.9 (CH), 16.8 (CH_3).

HR-MS (ESI +ve) m/z calculated for $C_{12}H_{12}N_2$ $([M+Na])^+$ 239.0791, found $([M+Na])^+$ 239.0796.

3,3'-diethyl-4,4'-bipyridine bis-*N*,*N*´-oxide **2c**

3,3'-diethyl-4,4'-bipyridine (obtained according to described procedures[9]) (500 mg, 2.355 mmol) and $NaHCO_3$ (5.9 g, 70.7 mmol) were dissolved in 100 mL H_2O/2-butanone 1:1 and the solution was stirred vigorosly. To this solution it was added in small portions Oxone® (8.6 g, 14.13 mmol). After four hours, we extracted three times with $CHCl_3$ (100 mL), the organic layer was dried over Na_2SO_4 and concentrated. Then passed through a basic alumina column eluting first with CH_2Cl_2 and finally with CH_2Cl_2/MeOH 5% to afford the product as a pale-brown solid, in a 90 % yield.

^{1}H NMR (400 MHz, $CDCl_3$) δ (ppm) 8.3 (s, 2H), 8.1 (d, $^3J_{H-H}$ ~ 4.96 Hz, 2H), 7.0 (d, $^3J_{H-H}$ ~ 4.96 Hz, 2H), 2.4 (m, 4H), 1.1 (t, $^3J_{H-H}$ ~ 7.25 Hz). ^{13}C {^{1}H} NMR (100.6MHz, $CDCl_3$, 25ºC) δ (ppm) 140.7 (CH), 139.9 (CH), 136.77 (C), 134.2 (C), 126.3 (CH), 23.8 (CH_2), 13.9 (CH_3).

HR-MS (ESI +ve) m/z calculated for $C_{14}H_{16}N_2O_2$ $[M+Na]^+$ 267.1104, found $[M+Na]^+$ 267.1112.

3,3´-diethyldicarboxylate-4,4´-bipyridine

4,4'-binicotinic acid (50 mg, 0.205 mmol) was suspended in thionyl chloride (2 ml, 27.4 mmol) and stirred at 78ºC overnight under argon. A white suspension was formed. The excess of thionyl chloride was removed under vacuum washing the residue three times with CH_2Cl_2. The residue was dissolved in the minimum quantity of dry DMSO and an excess of ethanol (1.16 ml, 20 mmol) was added. The reaction mixture was stirred during two hours at 40ºC. Later, we added NEt_3 (57 µL, 0.409 mmol) keeping the stirring for two hours more. Finally, the solvents were removed and a silica column chromatography was performed eluting with ethylacetate. A white–yellow solid 26.3 mg, 42% yield was recovered corresponding to the desired product.

^{1}H NMR (400 MHz, $CDCl_3$) δ (ppm) 9.29 (s, 2H), 8.81 (broad s, 2H), 7.15 (d, $^3J_{H-H}$ ~ 4.96 Hz, 2H), 4.15 (q, $^3J_{H-H}$ ~ 7.24 Hz, 4H), 1.13 (t, $^3J_{H-H}$ ~ 7.24 Hz, 6H).

MS (ESI +ve) m/z calculated for $C_{16}H_{16}N_2O_4$ $[M+H]^+$ 301.1, found $[M+H]^+$ 301.1, $[M+Na]^+$ 323.1.

3,3´-diethyldicarboxylate- 4,4´-bipyridine bis-*N*, *N´*-dioxide **2d**

3,3´-diethyldicarboxylate-4,4´-bipyridine (23.5 mg, 0.078 mmol) was dissolved in 1,8 mL of dry CH_2Cl_2. Later at 0ºC, we added 4 equiv of dry *meta*-chloroperoxybenzoic acid dissolved in 2 mL of dry CH_2Cl_2. The reaction mixture was stirred at room temperature during three hours. A basic aluminoxide filtration was performed recovering 20.3 mg, 78% yield of a white solid corresponding to the desired product.

^{1}H NMR (500 MHz, $CDCl_3$) δ (ppm) 8.83 (d, $^5J_{H-H}$ ~ 1.86 Hz, 2H), 8.35 (dd, $^3J_{H-H}$ ~ 6.69 Hz , $^5J_{H-H}$ ~ 1.86 Hz ,2H), 7.13 (d, $^3J_{H-H}$ ~ 6.65 Hz, 2H), 4.23 (q, $^3J_{H-H}$ ~ 6.88 Hz, 4H), 1.26 (t, $^3J_{H-H}$ ~ 6.88 Hz, 6H).

HR-MS (MALDI +) m/z calculated for $C_{16}H_{16}N_2O_6$ $[M+Na]^+$ 355.0901, found 355.0890.

3,3´-di(prop-2-yn-1-yl)dicarboxylate 4,4'-bipyridine

4,4'-binicotinic acid (1.3g, 5.32 mmol) was suspended in thionyl chloride (52 ml, 7.13 mmol) and stirred at 78ºC overnight. The excess of thionyl chloride was removed under vacuum. The residue was washed three times with CH_2Cl_2 (3x50 mL). The residue was redissolved in 25 mL of propargylic alcohol. Later, triethylammine (2.5 ml, 18.63 mmol) was added slowly. The reaction mixture was stirred at room temperature during three hours. After that the solvents were removed and the residue roughly dried. A silica column eluting with AcOEt as mobile phase was performed to obtain a colourless oil that later crystallized. A white solid 853 mg, 50% yield was recovered corresponding to the desired product.

^{1}H NMR (400 MHz, $CDCl_3$) δ (ppm) 9.32 (s, 2H), 8.84 (d, $^3J_{H\text{-}H}$ ~ 6.50 Hz, 2H), 7.16 (d, $^3J_{H\text{-}H}$ ~ 6.50 Hz, 2H), 4.72 (d, $^4J_{H\text{-}H}$ ~ 2.50 Hz, 4H), 2.45 (t, $^4J_{H\text{-}H}$ ~ 2.51 Hz, 2H).

HR-MS (ESI +ve) m/z calculated for $C_{18}H_{12}N_2O_4$ $([M+Na])^+$ 343.0689, found $([M+Na])^+$ 343.0694.

3,3´-di(prop-2-yn-1-yl)dicarboxylate 4,4'-bipyridine bis-*N,N´*-oxide bis-*N,N'*-oxide **2e**

di(prop-2-yn-1-yl) [4,4'-bipyridine]-3,3'-dicarboxylate (100 mg, 0.312 mmol) and $NaHCO_3$ (0.78 g, 9.37 mmol) were dissolved in 25 mL H_2O/2-butanone 1:1 and the solution was stirred vigorously. To this solution it was added in small portions Oxone® (1.5 g, 2.498 mmol). After 30 minutes, we extracted three times with $CHCl_3$ (10 mL) and the organic layer was dried over Na_2SO_4 and concentrated. A white solid (100 mg, 91% yield) corresponding to the desired product was obtained. This product was directly used in the next reaction.

^{1}H NMR (400 MHz, $CDCl_3$) δ (ppm) 8.86 (d, $^4J_{H\text{-}H}$ ~ 1.93 Hz, 2H), 8.37 (dd, $^3J_{H\text{-}H}$ ~ 6.62 Hz, $^4J_{H\text{-}H}$ ~ 1.93 Hz, 2H), 7.16 (d, $^3J_{H\text{-}H}$ ~ 6.62 Hz, 2H), 4.76 (m, 4H), 2.55 (t, $^4J_{H\text{-}H}$ ~ 2.86 Hz, 2H).

4,4'-bipyridine bis-*N,N*'-dioxide derivative **2f**

3,3´-di(prop-2-yn-1-yl)dicarboxylate 4,4'-bipyridine bis-*N,N´*-oxide bis-*N,N*'-oxide **2e** (41 mg, 0.116 mmol) and azide compound **4** (146 mg, 0.248 mmol) were dissolved in 3mL of DMSO. Copper (I) iodide (8.8 mg, 0.04 mmol) and triethylammine (0.013mL, 0.093 mmol) were added to the previous solution. The heterogeneous mixture was stirred vigorously during one hour, at which point it cleared and TLC analysis indicated complete consumption of **2e**. The reaction mixture was concentrated and the reaction crude redissolved in 10 mL chloroform. The organic phase was washed three times (3x10ml). The organic phase was dried under Na_2SO_4 and concentrated. The residue was purified by column chromatography starting with AcOEt and ending at AcOEt/MeOH 10% to yield a white solid residue (142 mg, 80% yield).

^{1}H NMR (400 MHz, CD_2Cl_2) δ (ppm) 8.60 (d, $^4J_{H\text{-}H}$ ~ 1.77 Hz, 2H), 8.20 (dd, $^3J_{H\text{-}H}$ ~ 6.75 Hz, $^4J_{H\text{-}H}$ ~ 1.77 Hz, 2H), 7.63 (s, 2H), 7.28 (d, $^3J_{H\text{-}H}$ ~ 8.65Hz, 12H), 7.18 (d, $^3J_{H\text{-}H}$ ~ 8.65 Hz, 12H), 7.18 (d, $^3J_{H\text{-}H}$ ~ 8.65 Hz, 4H), 7.03 (d, $^3J_{H\text{-}H}$ ~ 6.75Hz, 2H), 6.79 (d, $^3J_{H\text{-}H}$ ~ 8.65 Hz, 4H), 5.18 (d, $^3J_{H\text{-}H}$ ~ 2.15 Hz, 4H), 4.61 (t, $^3J_{H\text{-}H}$ ~ 6.67Hz, 4H), 4.00 (t, $^3J_{H\text{-}H}$ ~ 5.85Hz, 4H), 2.41 (tt, 4H), 1.33 (s, 54H).

HR-MS (ESI +ve) m/z calculated for $C_{98}H_{110}N_8O_8$ $[M+Na]^+$ 1549.8411, found $[M+Na]^+$ 1549.8339.

3.4.3 Experimental section: figures

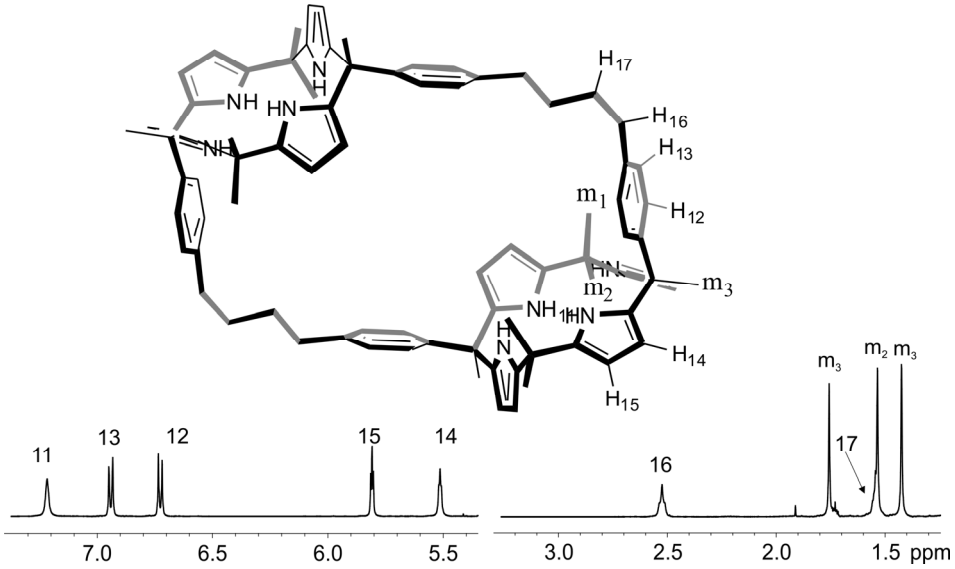

Figure 3.16 ^{1}H NMR spectrum (500 MHz, CD_2Cl_2, 298 K) of ditopic macrotricycle **3**.

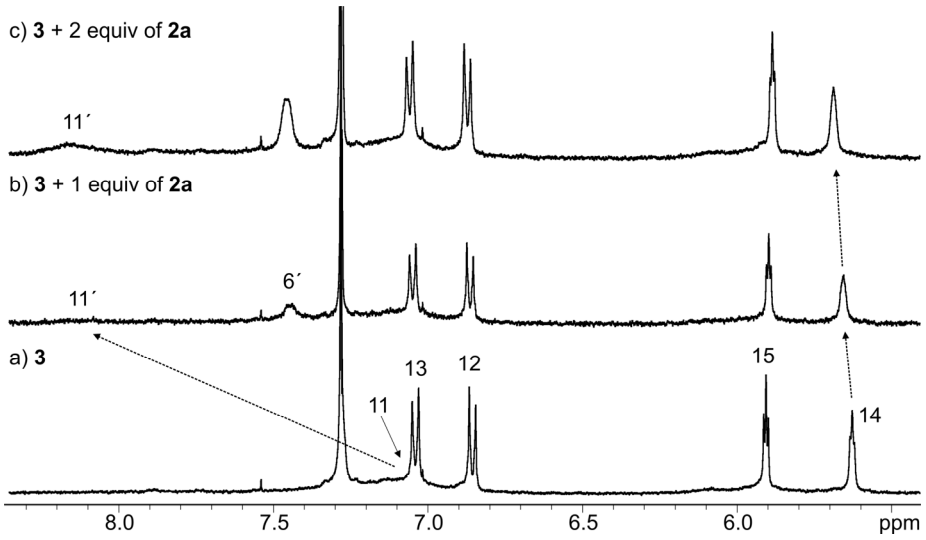

Figure 3.17 Downfield region of the ^{1}H NMR titration experiment (500 MHz, $CDCl_3$, 298 K) of ditopic macrotricycle **3**, [**3**]= 3.0 mM, with **2a**. See also Figure 3.16 for proton assignments. Primed numbers correspond with complex species.

3.4.4 Calculation of the energetic barriers

- 2D NOESY exchange experiments.

The 2D phase sensitive NOESY spectra were acquired on a 1mM solution of **2c⊂1** at 253K. The spectral width was 5 ppm and 1s of relaxation delay. The final size of the spectra was 2048 x 256 points and 16 scans were taken for each data set. The 2D NOESY experiment was acquired to calculate the energy barrier of the change of the NHs diastereotopic pyrrolic protons in the **2c⊂1** complexe at 253K.

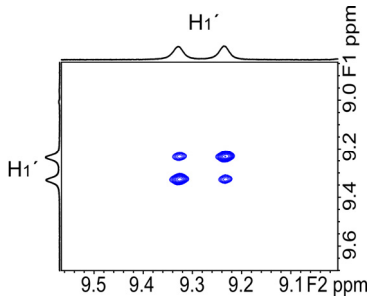

Figure 3.18 Selected region of the $^{1}H,^{1}H$-2D EXSY experiment (500MHz, $CDCl_3$, 253K) of the inclusion complex **2c⊂1**. The chemical exchange cross peaks of the NHs diastereotopic pyrrolic protons $H_1´$ is observed

The spinlock was 0.4s. The rate constants were calculated using the D2DNMR software.[18] This program performs a kinetic matrix analysis of the cross-peaks intensities. This analysis provides a first-order rate constant for multisite exchange directly for the 2D EXSY spectrum peak volumes.

The 2D-EXSY experiment shows cross-peaks due to chemical exchange between the two NH signals. Consequently, the rate constant *k* for the exchange process can be calculated using the equation [2]. From the integration of the cross-peaks it is possible to obtain the intensities (I_{AB}, I_{BA}). From the integration of the diagonal peaks the intensities (I_{AA}, I_{BB}) as well as the molar fractions (X_A, X_B) of two diastereotopic NH protons that are in exchange.

$$k = \frac{1}{\tau_m} \ln \frac{r+1}{r-1} \qquad [2]$$

Where *r* is:

$$r = 4(\chi_a\chi_b)\ \frac{(I_{AA} + I_{BB})}{(I_{AB} + I_{BA})} - (\chi_a-\chi_b)^2$$

- DNMR (Dynamic NMR) Line-shape Analysis

This program implemented in Topspin software allows the simulation of temperature dependent 1D NMR spectra and interactively refine the model parameters to get the best fit of the measured and simulated 1D NMR spectra.

3.5 References and notes

[1] Mugridge, J. S.; Szigethy, G.; Bergman, R. G.; Raymond, K. N. *J. Am. Chem. Soc.* **2010**, *132*, 16256.
[2] Yoshizawa, M.; Klosterman, J. K.; Fujita, M. *Angew. Chem.,Int. Ed.* **2009**, *48*, 3418.
[3] Iwasawa, T.; Hooley, R. J.; Rebek, J. *Science* **2007**, *317*, 493.
[4] Ajami, D.; Rebek, J. *Nature Chem.* 2009, *1*, 87.
[5] Pluth, M. D.; Bergman, R. G.; Raymond, K. N. *J. Org. Chem.* **2008**, *73*, 7132.
[6] Salvio, R.; Moisan, L.; Ajami, D.; Rebek, J. *Eur. J. Org. Chem.* **2007**, 2722.
[7] Tarkanyi, G.; Jude, H.; Palinkas, G.; Stang, P. *J. Org. Lett.* **2005**, *7*, 4971.
[8] Valderrey, V.; Escudero-Adan, E. C.; Ballester, P. *J. Am. Chem. Soc.* **2012**, *134*, 10733.
[9] Baytekin, H. T.; Sahre, M.; Rang, A.; Engeser, M.; Schulz, A.; Schalley, C. A. *Small* **2008**, *4*, 1823.
[10] Rebek, J.; Costello, T.; Wattley, R. *J. Am. Chem. Soc.* **1985**, *107*, 7487.
[11] Gibson, H. W.; Lee, S. H.; Engen, P. T.; Lecavalier, P.; Sze, J.; Shen, Y. X.; Bheda, M. *J. Org. Chem.* **1993**, *58*, 3748.
[12] Zhang, W.; Yamamoto, H. *J. Am. Chem. Soc.* **2007**, *129*, 5298.
[13] Zheng, H. Y.; Zhou, W. D.; Lv, J.; Yin, X. D.; Li, Y. J.; Liu, H. B.; Li, Y. L. *Chem-Eur J* **2009**, *15*, 13253.
[14] This section has been done in collaboration with Albano Galán Coca
[15] Wolf, C.; Konig, W. A.; Roussel, C. *Liebigs Ann.* **1995**, 781.
[16] Even if the **2c⊂1** complex is quantitatively assembled at the working concentration, the calculation of the thermodynamic constants of the racemization process has to be done considering the equilibrium involved in the host-guest process. To solve this limitation, the thermodynamic constants of the racemization process have to be determined in a sample containing an excess of macrocycle **1**.
[17] Geometries of the complexes were refined by performing an optimize geometry calculation with Molecular Mechanics using augmented MM3 parameters as implemented in the software CAChe WorkSystem Pro Version 6.1.12.33, Fujitsu Limited. A conjugate gradient method was used for energy minimization with a convergence energy criterion of 0.001 kcal/mol.
[18] Abel, E. W.; Coston, T. P. J.; Orrell, K. G.; Sik, V.; Stephenson, D. *J. Magn. Reson.* **1986**, *70*, 34.

Chapter 4

Binding of Ion Quartets by a Bis-calix[4]pyrrole Macrotricyclic Receptor*

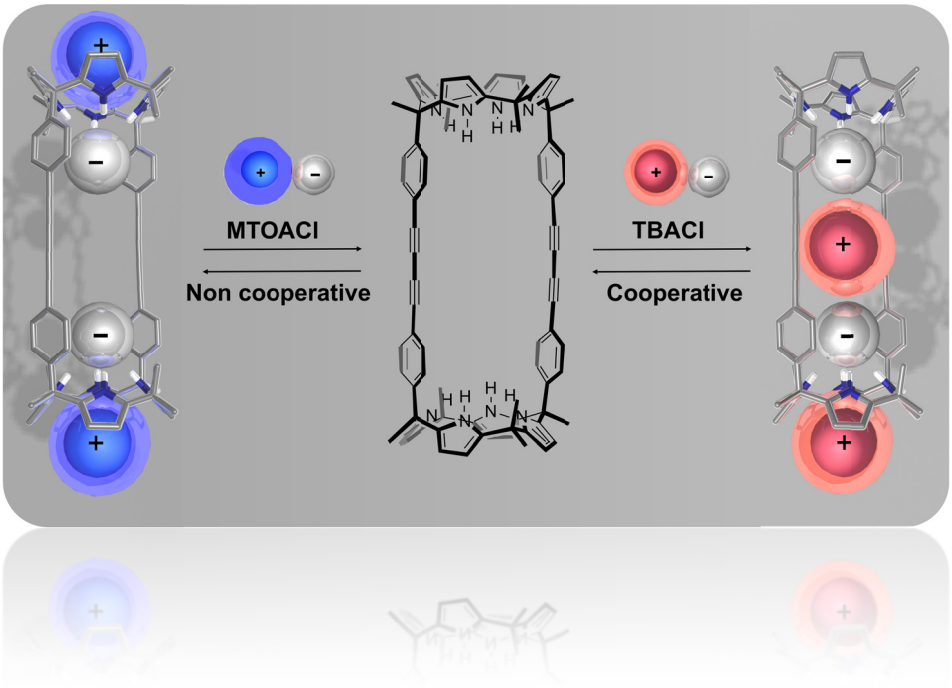

*Most of the contents of this chapter were publish in: Valderrey, V.; Escudero-Adán, E. C.; Ballester, P., *Angew. Chem. Int. Ed.* **2013**, 52, 6898 –6902

4.1 Introduction

In solvents of low dielectric constant, ion pairs tend to associate into aggregates of different stoichiometry stabilized mainly by electrostatic forces. Aggregates such as ion-pair dimers or ion-pair tetramers have been detected in solution.[1] However, the ion-pair aggregation constants are demonstrated to be in all the cases lower than the ion pair constants.[2] Invariably, the electrostatic interaction of a receptor with an ion has to be influenced for its counterion. To that basis, single receptors capable of complexation with both a cation and an anion, the so-called heteroditopic receptors, should offer, compared to monotopic versions, sensible advantages, in terms of affinity and specificity.[3,4] These receptors possess covalently connected binding sites for the anion and the cation. Cooperative and allosteric effects are claimed to play an important role in the binding of ion-pairs by heteroditopic receptors. As detailed in *Chapter 1*, depending on the relative spatial location of the binding sites and/or the choice of ion-pair components, the resulting 1:1 complexes exhibit different binding geometries: *close*-contact, *solvent*-separated or *receptor*-separated (Figure 4.1). The relative arrangement of the bound ions depends on the spatial location and nature of the binding sites, the choice of the ion-pair components, and the fashion in which the binding takes place (sequential/concurrent).[5,6] Ion-triplets are the result of the interaction of one cation with two anions, or one anion and two cations.[7] The formation of *cascade* complexes constitutes an alternative strategy for ion pair binding and produces the net binding of ion-triplets in close contact binding mode. The idea is to use a homoditopic receptor, which is rendered into heteroditopic by the first complexation of an ion into one of its two identical binding sites. The subsequent binding of an ion-pair, either in sequential or concurrent fashion, also benefits from cooperative and allosteric effects providing a bound ion-triplet in *close*-contact binding mode. Surprisingly to us, examples of efficient complexation of dimers of ion-pairs or quartets of ions by synthetic receptors have not been described in the literature despite the known existence of these species in solution.[1,2]

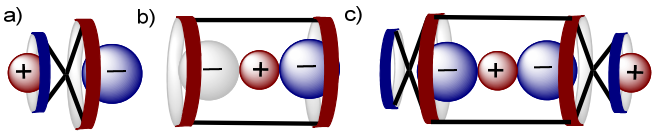

Figure 4.1 Schematic representations of ion-paired complexes: a) a heteroditopic receptor binding the ion-pair in *host*-separated mode; b) a homoditopic receptor forming a *cascade* complex and displaying a *close*-contact binding geometry; c) a bis-heteroditopic receptor forming a *cascade* complex of two ion-pairs and displaying both *close*-contact and *host*-separated binding modes.

Calix[4]pyrroles are known to be not only good anion receptors but also ion pair receptors through an ion-separated binding mode.[3,8,9,10] When a calix[4]pyrrole interact with an ion-pair, the initial coordination of the anion by stabilising four H-bond interactions with the NH pyrrolic protons of the calix[4]pyrrole, induces a conformational change that results in an electron-rich bowl-cavity able to coordinate the ion-pair cation. On that basis, we envisaged that the two walls bis-calix[4]pyrrolic macrotricyclic receptor **1** described in the previous chapters, having two calix[4]pyrrole binding sites built into a three-dimensional and rigid molecular scaffold could be an ideal candidate for the effective binding of ion-pair dimers through the formation of *cascade* complexes.

4.2 Results and discussion

4.2.1 Design and synthesis of receptor **1**

The synthesis of the cylindrical homoditopic receptor **1**[11] and the two walls calix[4]pyrrole **3** used as a model have been described in *Chapter 2*. The receptor **1** was designed with two 1,3-diynyl linkers which provide conformational rigidity and avoid the collapse of its macrocyclic structure (Figure 4.2). According to molecular modelling studies, these spacers locate the two distal heteroditopic binding sites (calix[4]pyrrole units) at an ideal distance and in an optimal relative orientation to achieve the cooperative/allosteric binding of two identical or distinct ion pairs. Due to its similar structural properties to a single hemisphere of the macrotricycle **1**, two walls calix[4]pyrrole **3** has been selected as model system to determine reference binding constants.

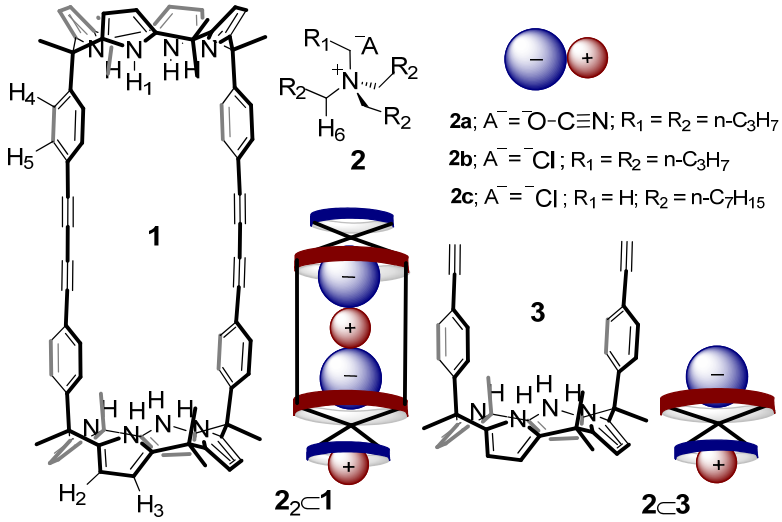

Figure 4.2 Molecular structures of receptors **1** and **3** and ion pairs **2**. Schematic representations of ion pairs **2**, a cascade complex of receptor **1** with two ion-pairs displaying *close*-contact and *host*-separated binding modes (**2_2⊂1**) and a complex of receptor **3** with an ion-pair in *host*-separated mode (**2⊂3**).

4.2.2 ^{1}H NMR binding studies of receptor **1** with the ion pairs **2**

The initial addition of 1 equiv. of **2a** (TBAOCN) to a $CDCl_3$ solution of **1** (1 mM) resulted the appearance of a new set of proton signals that were assigned to bound **1** (Figure 4.3b). The signal for the bound NH protons (1') resonates at δ = 11.4 ppm indicating their involvement in hydrogen-bonding interaction with the cyanate. The methylene protons *alpha* to the nitrogen of the TBA cation (6') appear as a broad hump at δ = 2.5 ppm significantly upfield shifted with respect to free TBA (6). The ratio of integral values for the protons signals assigned to free and bound receptor is 1:1. These results indicate that 50% of the receptor is bound to both components of the ion-pair and that the chemical exchange between the free and bound **1** is slow on the ^{1}H NMR chemical shift timescale. However, they do not allow for an unequivocal assignment of the number of species involved in the bound state of **1**. The existence of a fast exchange on the ^{1}H NMR chemical shift timescale between two complexes **2a⊂1** and **$2a_2$⊂1**, formed in a 50% overall extent, or the exclusive formation of the **$2a_2$⊂1** complex could explain this experimental observations. The addition of more than 1.0 equiv. of **2a** did not induce further changes in the chemical shifts of the signals assigned to bound **1** but

only increased their intensities relative to the signals of free **1**. When 2 equiv. of **2a** were added only the signals assigned to bound **1** were detected (Figure 4.3c). Adding an excess of **2a** (2.7 equiv.) simply produced sharpening and a moderate downfield shift to the broad signal assigned to the methylene protons (6') *alpha* to the nitrogen of the TBA cation. Taken together, these observations suggest that the new set of signals must correspond to the protons of bound receptor **1** in the $\mathbf{2a}_2\subset\mathbf{1}$ complex and that the stability constant of the complex can be estimated as $K_{2:1}(\mathbf{2a}_2\subset\mathbf{1}) > 10^8\ M^{-2}$. In addition, the free and bound TBA cations are involved in a fast chemical exchange on the ^{1}H NMR chemical shift timescale.

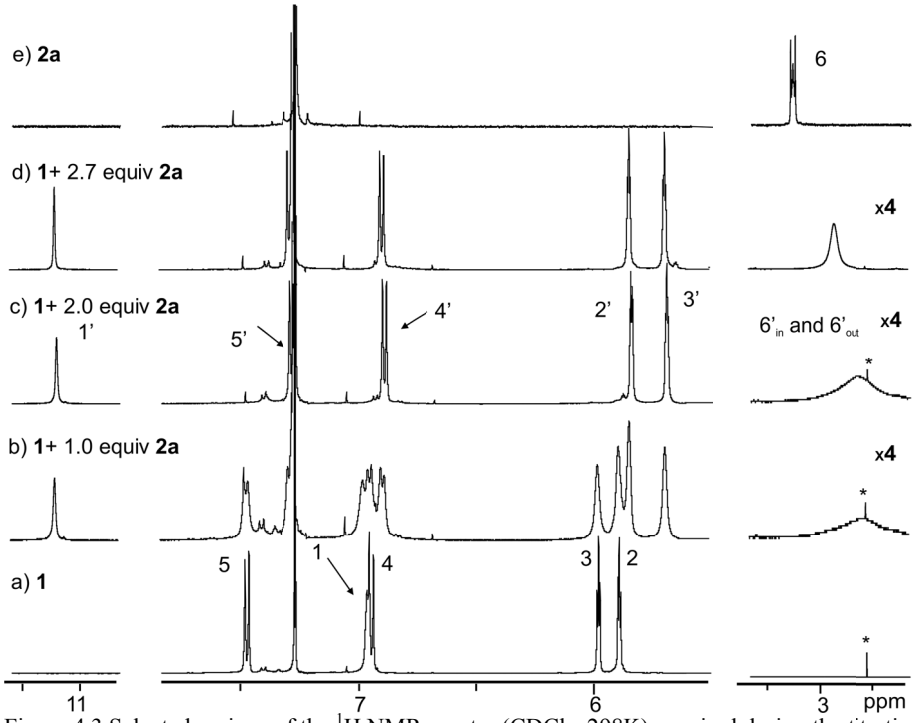

Figure 4.3 Selected regions of the ^{1}H NMR spectra ($CDCl_3$, 298K) acquired during the titration of **1** with incremental amounts of **2a**: b) 1.0; c) 2.0; and d) 2.7 equiv. of **2a** added. The ^{1}H NMR spectra of **1** and **2a** are shown in a) and e), respectively. Primed numbers correspond to the $\mathbf{2a}_2\subset\mathbf{1}$ complex. For proton assignments see Figure 4.1and Figure 4.5. * = Impurity

A variable temperature ^{1}H NMR experiment (Figure 4.4) performed on the sample containing 2 equiv. of **2a** revealed that at 278 K the broad signal assigned to bound TBA protons (6') splits into two signals of equal intensity. It is worthy to notice that the

chemical shift values of these two signals are upfield shifted with respect the same protons in free TBA that resonate at 3.3 ppm at 238 K (Figure 4.22).

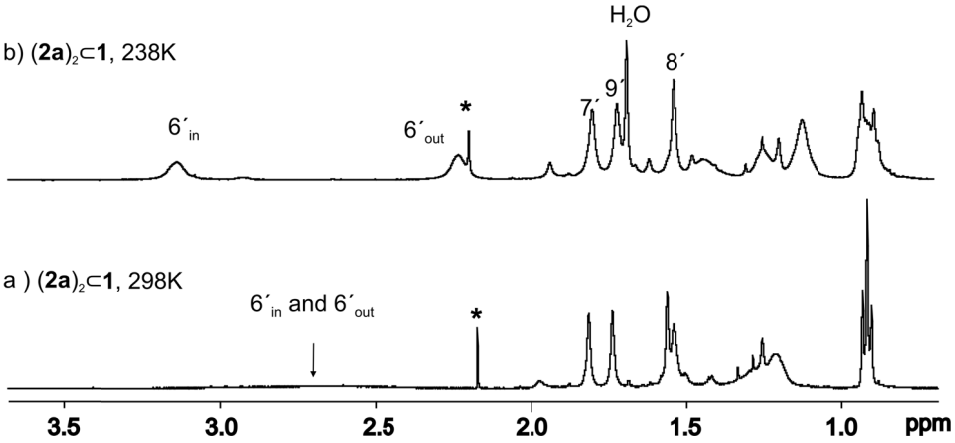

Figure 4.4 ^{1}H NMR spectra (500 MHz) acquired in a variable temperature experiment of a $CDCl_3$ solution containing receptor **1** and 2 equivalents of **2a.** The coalescence of the signal of the methylene protons α to the nitrogen of the tetrabutylammoniun takes place at 298 K.

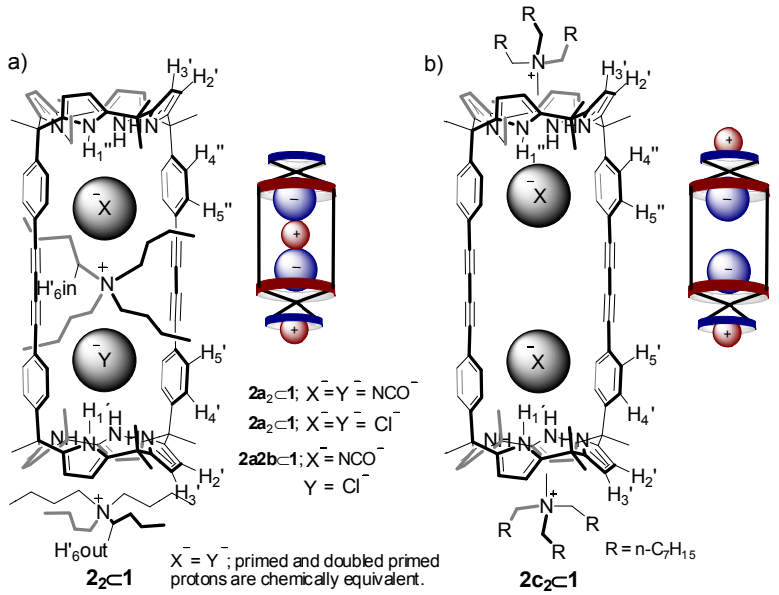

Figure 4.5 Molecular structure of the homo- and hetero-dimeric ion-pair complexes derived from the TBA and MTOA salts.

Molecular modelling studies advocated for a *cascade* complex, as depicted, for the probable structure of the **2a**$_2$⊂**1** complex in a low dielectric medium like chloroform.

The modelled structure serves to explain the existence of two chemically non-equivalent TBA cations and the splitting of the N-*alpha* methylene signals. At 238 K the two TBA cations (referred as "in" and "out") are in chemical exchange, as revealed by the detection of a cross peak between them in an EXSY experiment (Figure 4.6). At this low temperature a ROESY experiment allowed the assignment of the more upfield shifted methylene signal to the TBA_{out} cation, which is included in the electron rich cup provided by the outer calix[4]pyrrole core in *cone* conformation. Even at 238 K, the TBA_{out} cation shows fast chemical exchange on the ^{1}H NMR chemical shift timescale with free TBA in excess (experimental section Figure 4.23).

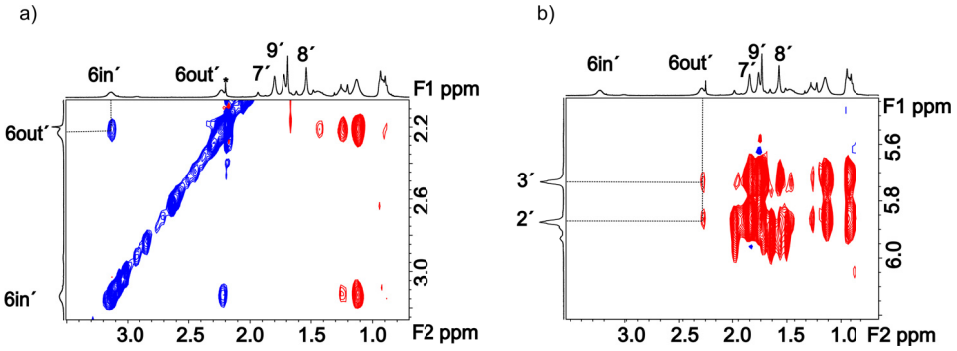

Figure 4.6 ROESY experiment (500 MHz, p15, 0.3 s, $CDCl_3$, 1.6 × 10^{-3}M) of $\mathbf{2a}_2\subset\mathbf{1}$ at 238K showing a) chemical exchange between the methylene protons α to the nitrogen of the tetrabutylammonium cyanate H_{6in}´ and H_{6out}´. Cross-peaks indicating intermolecular close contacts between the α-protons (H_{6in}´ and H_{6out}´) and the β-protons and γ-protons of the tetrabutylammoniun cation. b) Cross-peaks indicating intermolecular close contacts between H_{6out}´ and the β-pyrrolic protons of the bis-calix[4]pyrrole macrocycle H_2´ and H_3´.

In contrast, the TBA_{in} cation that is sandwiched between the two cyanates display slow exchange with free TBA. This result is in agreement with the proposed five-particle structure and the different location of the two TBA components.

Analogous results to those described above were obtained during the ^{1}H NMR studies of the complexation of TBACl, **2b**, by receptor **1** (experimental section Figure 4.24). Receptor **1** showed similar behaviour with other tetrabutylammonium salts as bromide and azide.

The ^{1}H NMR spectrum of a $CDCl_3$ solution containing an equimolar mixture of **2a**, **2b** and **1** showed a set of proton signals that did not coincide either with those assigned to $\mathbf{2a}_2\subset\mathbf{1}$ or $\mathbf{2b}_2\subset\mathbf{1}$ (Figure 4.7).

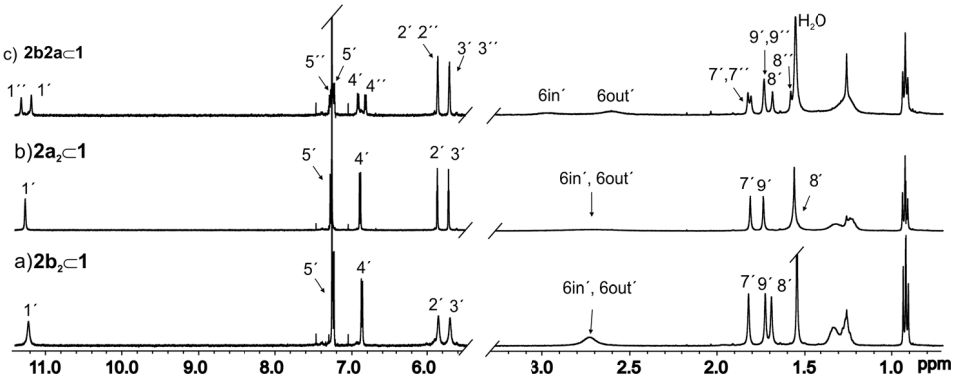

Figure 4.7 ^{1}H NMR (500 MHz, $CDCl_3$, 298K) spectra of a) **2b**$_2$⊂**1**, b) **2a**$_2$⊂**1** and c) **2b2a**⊂**1**. At room temperature, it is possible to distinguish the CH_2 α-protons of the tetrabutylammonium included between the anions H_{6in}´ and one positioned in the shallow aromatic cavity of the calix[4]pyrrole H_{6out}´ in the complex **2b2a**⊂**1**.

Two different and highly downfield shifted signals for the NH protons (1' and 1'') of **1** indicated their participation in different hydrogen bonding interactions. Four different set of proton signals for the aromatic protons (4',5',4'' and 5'') supported the existence of different interaction in each of the two binding sites of **1**. Clearly, these observations point to the exclusive and quantitative formation of the unsymmetrical assembly **2a2b**⊂**1**. Even at 298 K the methylene protons alpha to the nitrogen of the TBA cation resonate as separate downfield signals in complete agreement with the presence of two chemically non-equivalent bound TBA cations in the **2a2b**⊂**1** complex. A ROESY experiment at 248 K allowed the assignment of all the ^{1}H NMR signals of the complex **2a2b**⊂**1** and showed chemical exchange between the methylene protons α to the nitrogen of the tetrabutylammonium cyanate H_{6in}´ and H_{6out}´ (Figure 4.25). Finally, we were interested in the evaluation of the thermodynamic stability of the hero-dimer **2a2b**⊂**1**. The addition of excess **2a** to the $CDCl_3$ solution containing **2a2b**⊂**1** induced the appearance of the proton signals corresponding to **2a**$_2$⊂**1**. Conversely, the addition of excess **2b** to the preformed **2a2b**⊂**1** complex did not induce the appearance of any new proton signal for bound **1**. Based on these results we can conclude that the thermodynamic stability of **2a2b**⊂**1** lies between that of the two homo-dimers **2a**$_2$⊂**1** or **2b**$_2$⊂**1** (experimental section Figure 4.26 and Figure 4.27).

The use of ion pair **2c** containing a methyl trioctylammonium cation (MTOA) produced significantly different results (Figure 4.5b). The ^{1}H NMR spectra of a $CDCl_3$ solution containing equimolar amounts of **2c** and **1** shows three different sets of signals for the protons of **1** (Figure 4.8c). One of the sets corresponds to free **1** while the other two sets, based on the number of proton signals contained and their chemical shifts, are assigned to the protons of **1** in the **2c⊂1** and **2c**$_2$**⊂1** complexes. By integration of selected proton signals in the three different sets it was possible to determine the ratio of species **1**:**2c⊂1**:**2c**$_2$**⊂1** as approximately 0.23:0.44:0.33 (Figure 4.9 d). This ratio is close to that expected from an equimolar mixture of substrates at 1 mM concentration yielding a 2:1 complex through a non-cooperative binding process ($K_m \sim 10^4$ M^{-1}).

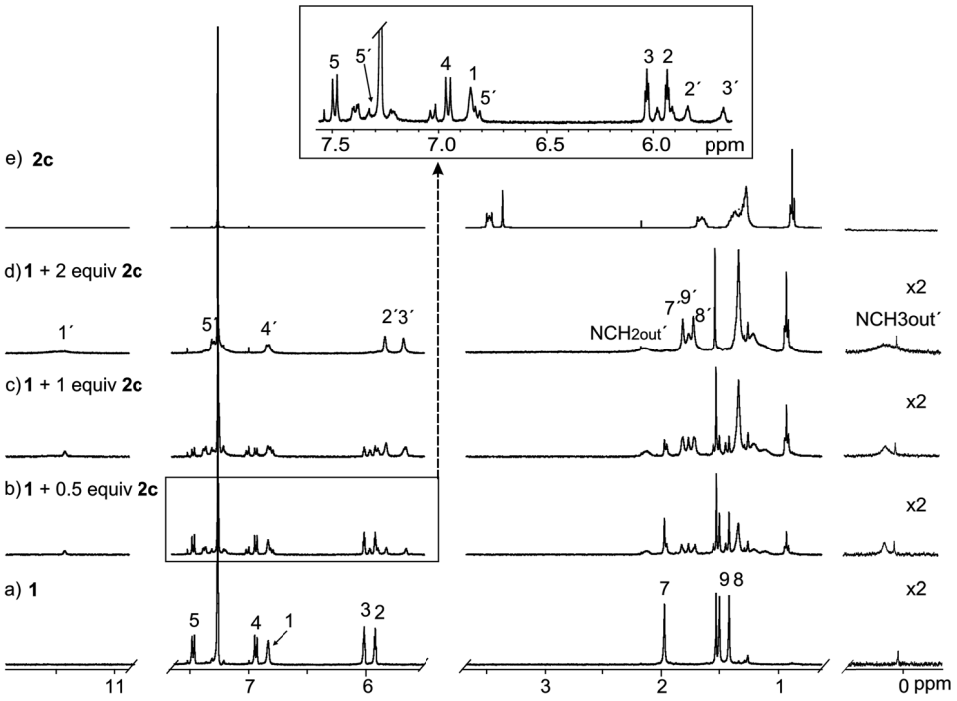

Figure 4.8 ^{1}H NMR (500 MHz, 298 K, $CDCl_3$) spectra acquired during the titration of bis-calix[4]pyrrole macrocycle [**1**]= 2.9 mM with methyl trioctylammonium chloride **2c**.

Two different signals are assigned for the non-chemically equivalent protons α to the nitrogen of the MTOA, NCH_{2out}´and NCH_{3out}´ resonating at 2.2 ppm and 0.2 ppm, respectively. The upfield shift respect to the free MTOA (Figure 4.8e) (where NCH_2 and NCH_3, 3.4 ppm and 3.3 ppm, respectively) remarks on the interaction of the cation

with the external electron rich cavity of the calix[4]pyrrole. When 2 equiv. of **2c** are added a single set of proton signals corresponding to the **2c**$_2$⊂**1** complex were detected. The methyl and methylene protons alpha to the nitrogen of the MTOA cation only increased their intensities indicating they are interacting with receptor **1** throw the same kind of interactions. These results indicate that **1** binds **2c** through a process that is not significantly cooperative and yields a homo-dimeric **2c**$_2$⊂**1** complex having both ion-pairs bound in a *receptor*-separated binding geometry, instead of the *cascade* arrangement assigned to the homo- and hetero-dimeric complexes of **2a** and **2b** with **1**.

These different behaviour can be explain taking into account that the methyl group of the MTOA cation is a better fit than the TBA cation for the shallow cup opposite to the bound anion. This is the expected result for a calix[4]pyrrole unit acting as ion-pair receptor and affording a *receptor*-separated binding geometry in the ion-paired complex. Second, and more importantly, the complexation process of **2c** by **1** displayed diminished signs of cooperativity, if any.

Finally, the addition of 1 equiv. of **2b** to an equimolar $CDCl_3$ solution of **2c** and **1** induced the quantitative formation of the corresponding hetero-dimer **2a2c**⊂**1** complex as judged by the simplification of the ^{1}H NMR spectrum of the mixture (Figure 4.9b).

Similarly, the ^{1}H NMR spectra of a $CDCl_3$ solution containing equimolar amounts of **2a**, **2c** and **1** shows all the expected proton signals for the quantitative assembly of the **2a2c**⊂**1** complex (Figure 4.9c) In the latter case, the desymmetrization of the two binding sites in **1** upon complexation with **2c** and **2a** becomes evident and must be due to the presence of two different bound anions. In the two hetero-dimeric complexes **2a2c**⊂**1** and **2b2c**⊂**1**, as well as in homo-dimer **2c**$_2$⊂**1,** the methyl protons for the bound MTOA cation are highly shifted upfield at $\delta = 0.2$ ppm.

The addition of excess **2a** to a $CDCl_3$ solution containing the **2a2c**⊂**1** complex resulted in the selective exchange of the bound chloride by cyanate while the bound MTOA remains intact (Figure 4.28).

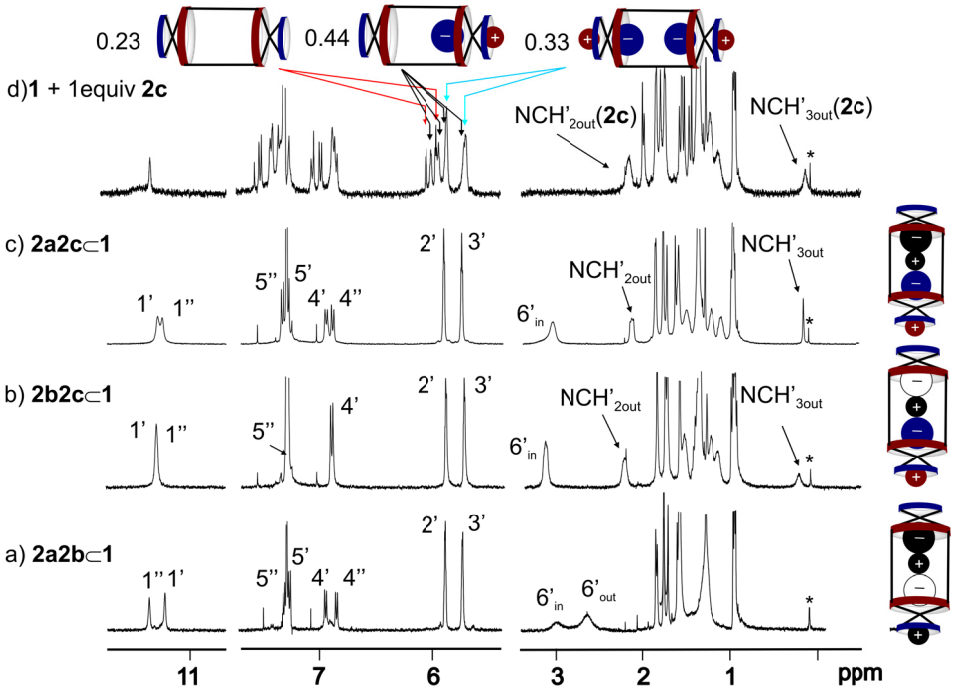

Figure 4.9 Selected regions of the ^{1}H NMR spectra (298 K, 500 MHz) of $CDCl_3$ solutions of **1** (1 mM) containing: a) 1 equiv. of **2a** and 1 equiv. of **2b** ; b) 1 equiv. of **2b** and 1 equiv. of **2c**; c) 1 equiv. of **2a** and 1 equiv. of **2c** ; d) 1 equiv. of **2c**. See Figure 5.4 for molecular structures and proton assignments. Schematic representations of the complexes and binding geometries of the ion-pair are also shown. The ion-pairs are color coded **2a** (-black/+black), **2b** (-white/+black) and **2c** (-blue/+red). The position of the anions in all hetero-dimeric complexes is interchangeable. The MTOA cation of **2c** is selectively located in the "out" position.

This observation together with the existence of exclusive intermolecular contacts between its methylene protons and the β-pyrrole protons of **1** provides strong support for the selective placement of the MTOA cation in the "out" position of the complex and included in the shallow cup formed by the pyrrole rings (Figure 4.10 b). Taken together this results we can conclude that both the cooperativity of the assembly process and the binding geometry of the final aggregates can be controlled by the nature of the cations present in the ion pair components.

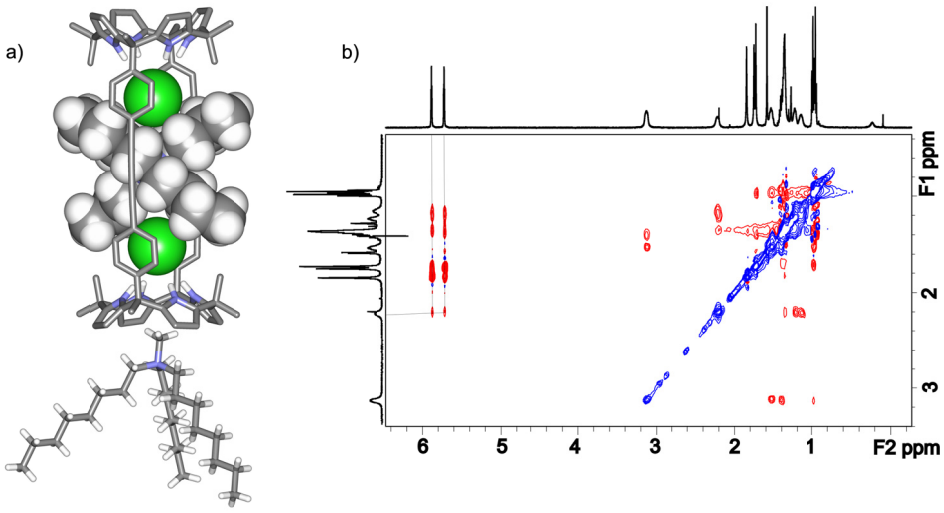

Figure 4.10 a) Energy-minimized structure of the hetero-dimer **2b2c⊂1.** Receptor **1** and the MTOA "out" cation are shown stick representation. The anions and the "in" TBA cation included in the cavity of **1** are displayed as CPK representations; b) ROESY experiment (500 MHz, p15, 0.3 s, $CDCl_3$, 2.9 × 10^{-3}M) of **2b2c⊂1** at 298K. There is no chemical exchange between the methylene protons α to the nitrogen of the tetrabutylammonium H_{6in}´ and the ones of the methyl trioctylammonium NCH_{2out}´. Cross-peaks indicating intermolecular close contacts between the methylene protons α to the nitrogen of the methyl trioctylammonium cation (NCH_{2out}´) and the β-pyrrolic protons of the bis-calix[4]pyrrole macrocycle H_2´and H_3´.

4.2.3 Study of the cooperativity involved in the formation of the ion-quartet complexes

As revealed the ^{1}H NMR titration experiments described in the previous section, the formation of the **2a**$_2$⊂**1** and **2b**$_2$⊂**1** *cascade*-like complexes resulting from the interaction between **1** and the ion pairs **2a** and **2b** seems to involve highly cooperative effects. On the contrary, the interaction between **1** and the ion pair **2c** affords to complexes with the same stoichiometry but with a complete different rearrangement of the ion pair dimers through a non-cooperative process.

To characterize thermodynamically the **2**$_2$⊂**1** complexes and gain insights into the cooperative factors that govern the formation of the ion quartets, we performed isothermal titration calorimetry (ITC) and proton NMR titration experiments.

First, it is necessary to describe which equilibria are involved in the formation of the dimeric ion-pair complexes, define its thermodynamic constants and its relationships

taking into account statistical factors (Figure 4.11). The cooperative factor (α) is defined as the cooperativity in the entrance of the second ion-pair in the preformed **2b⊂1**.

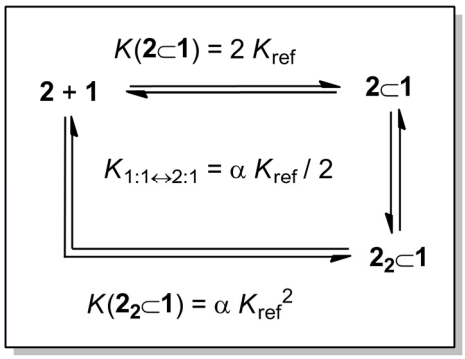

Figure 4.11 Equilibria involved in the complexation of ion pairs **2a**, **2b** and **2c** with **1**. The overall binding constant $K(\mathbf{2}_2\subset\mathbf{1})$ and the stepwise binding constants $K(\mathbf{2}\subset\mathbf{1})$ and $K_{1:1\leftrightarrow2.1}$ are shown as well as their relationship with K_{ref} (reference constant), α (cooperativity factor), and statistical corrections.

Ideally, the reference constant provide the value of the interaction between a calix[4]pyrrole unit and an ion pair, that is the interaction of one hemisphere of the receptor **1** with an ion pair. However, the mathematically correlation of K_{REF} with the stepwise binding constant $K(\mathbf{2}\subset\mathbf{1})$ have to consider statistical corrections. The **2⊂1** complex has two possibilities to be form and one to be destroy, so $K(\mathbf{2}\subset\mathbf{1}) = 2K_{ref}$. In the next step, to form the complex $\mathbf{2}_2\subset\mathbf{1}$ from **2⊂1** there is one possibility to be formed and two possibilities to destroy it, then $K_{1:1\leftrightarrow2:1} = \alpha K_{ref} / 2$. In this equilibrium we have to consider the cooperativity factor (α) to quantify whether the preformed 1:1 complex induce a positive, negative or has not influence in the formation of the 2:1 complex. Finally, the overall binding constant $K(\mathbf{2}_2\subset\mathbf{1})$ can be calculated as the product of the stepwise binding constants $K(\mathbf{2}\subset\mathbf{1})$ and $K_{1:1\leftrightarrow2.1}$ resulting $K(\mathbf{2}_2\subset\mathbf{1}) = \alpha K_{ref}^{\ 2}$.

In order to quantify the reference constant K_{ref} of the systems we selected reference models. The ideal receptor used as a reference should have an hydrogen bonding binding pocket for the anion as similar as the ones of receptor **1** and the corresponding pyrrolic electron rich cavity able to provide cation-π interactions with the cation of the ion pair. A priori, the octamethyl calix[4]pyrrole heteroditopic receptor would be an ideal candidate. With the introduction of two *meso*-aromatic substituents in the calix[4]pyrrole core of the reference, we also take into account, the expected repulsive

effect of the aromatic walls in the binding of anions within receptor **1**. However, to perfectly resemble the homoditopic receptor **1** the axial direction of the aryl substituents of **3** is mandatory. To achieve such axial direction, calix[4]pyrrole **3** has to be locked in the *cone* conformation which is not well populated in chloroform solution. Then, the better solvated open conformation of **3** can exhibit a diminished binding affinity for the guest. With these considerations in mind, we selected the two walls calix[4]pyrrole receptor **3** as a the best accessible candidate to be our model system. Being receptor **3** a synthetic precursor of **1** it is easily accessible to us and we consider that the slightly lower binding affinity is going to be negligible in the final results. Initially, we studied the interaction of **3** with the ion pairs **2a** and **2b,** separately by ^{1}HNMR titrations experiments.

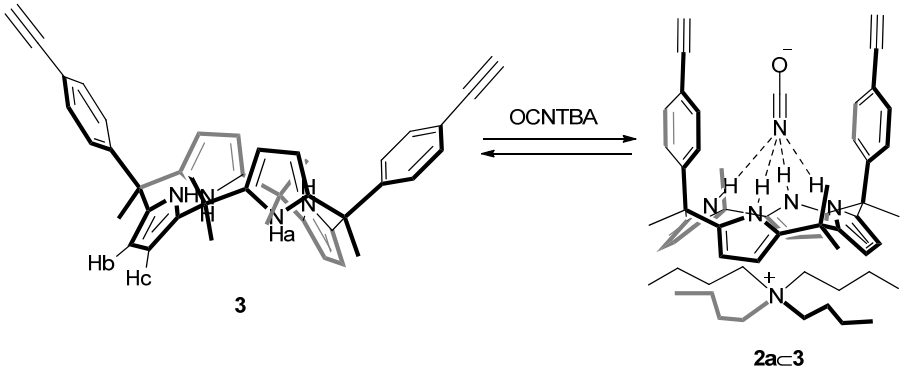

Figure 4.12 Equilibrium involved in the interaction between the calix[4]pyrrole **3** and the ion pair tetrabutylammonium cyanate **2a**.

We carried out a ^{1}H NMR study to estimate the association constant between **3** and **2a** in $CDCl_3$. Addition of 5.8 equiv of **2a** induced a downfield shift of the NH pyrrolic protons **a** indicating its participation in H-bond interactions and the *para* system of the aromatic walls was upfield shifted (Figure 4.13). The two different signals of the β pyrrolic protons move in opposite directions up **2a** addition. This different tendency in the movement of the β pyrrolic protons can be explain in base to the conformational flexibility of the calix[4]pyrrole core. It is well known that in non-polar solvents as chloroform, the α,α isomer of the two walls aryl-extended calix[4]pyrrole feature a *1,3-alternate* conformation as the most favourable one in which, any molecule of solvent is hydrogen bound to the NH pyrrolic protons. Upon anion binding, the calix[4]pyrrole

core changes the *1,3-alternate* conformation to cone conformation in order to maximize the number of hydrogen bond interactions between the four NHs pyrrolic protons and the anion. In that cone conformation, the β-pyrrolic protons **b** do not fall anymore into the shielding area of the aryl-substituent of the calix[4]pyrrole core explaining its downfield shift observed during the titration.

Even working at 6.3 mM concentration, it was necessary to add more than 20 equiv of **2a** to observe the saturation of the receptor **3** which means we are in the presence of a small binding constant.

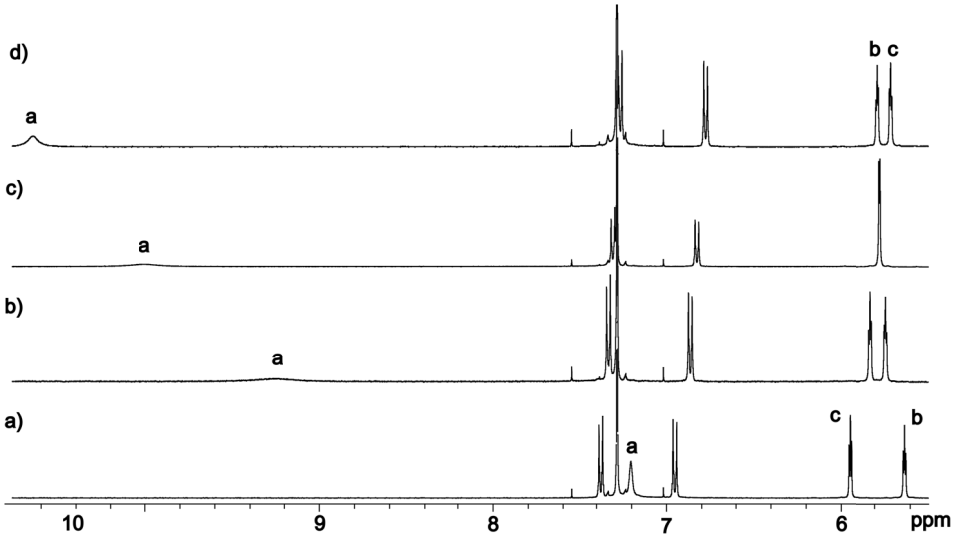

Figure 4.13 Selected regions of the ^{1}H NMR titration of **3** ([**3**] = 6.3 mM) with **2a** in $CDCl_3$ at 298K. a) **3**; b) **3** + 5.8 equiv **2a**; c) **3** + 10.9 equiv **2a**; d) **3** + 20.9 equiv **2a**.

The fit of the ^{1}H NMR titration data to a 1:1 binding model afforded to an association constant $K_{1:1}$(**2a**⊂**3**) = 33±7 M^{-1} (Figure 4.14). This result is in agreement with an association constant value of 5.4×10^2 M^{-1} reported for the 1:1 complex of TBACl and octamethylcalix[4]pyrrole in CD_2Cl_2 solution.[9]

The high thermodynamic stability estimated for the **2a**$_2$⊂**1** complex ($K_a > 10^8$ M^{-2}) is in striking contrast with the low binding affinity measured for **2a** and the "two wall" calix[4]pyrrole **3** ($K_{1:1}$(**2a**⊂**3**) = K_m = 33±7 M^{-1}).

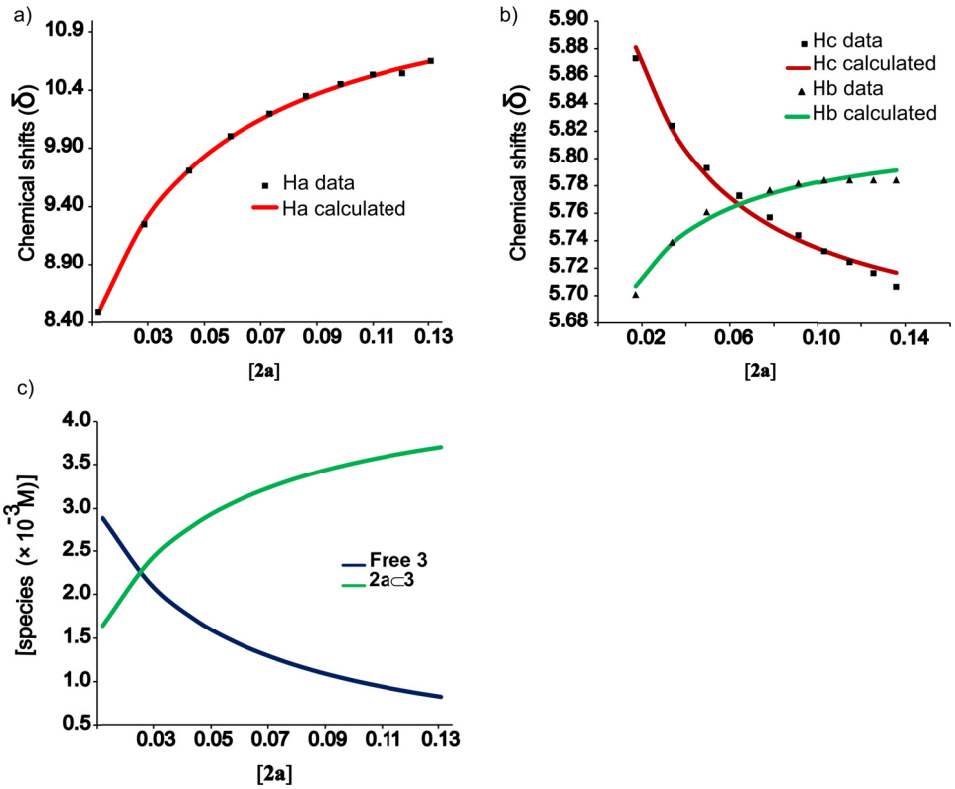

Figure 4.14 a) Fit of the chemical shifts changes experienced by the proton Ha of **3** during the titration with **2a** using a 1:1 binding model; b) Fit of the chemical shifts changes experienced by the protons Hc and Hb of **3** during the titration with **2a** using a 1:1 binding model $K_{\mathbf{2a}\subset\mathbf{3}}$ = 33±7 M^{-1}. c) Speciation distribution profiles during the titration.

Consequently the formation of the $\mathbf{2a}_2\subset\mathbf{1}$ complex must involve an impressive cooperative effect possibly dictated by the *cascade* arrangement of the two ion-pairs: one bound as an intimate contact ion-pair and the other as a *host*-separated ion-pair. The existence of a highly cooperative binding process also explains why the intermediate complex **2a**⊂**1** (1:1) was not detected during ^{1}H NMR titration, *vide supra*. The binding of ion pairs by **1** is likely to occur in a stepwise fashion. Initially, as proposed by Sessler et al. for calix[4]pyrrole receptors[9], one of the two units of **1** binds one chloride anion. This locks the calix[4]pyrrole core of one site in the *cone* conformation and generates an electron-rich bowl-shaped cavity opposite to the bound anion. This cavity is possibly the most preferred binding site for the TBA_{out} cation yielding the ternary **2a**⊂**1** complex displaying an *host*-separated binding mode for the ion pair. The formed **2a**⊂**1** complex

features an internal cavity that is complementary in size and function to another ion pair **2a** bound in *close*-contact mode. The components of the second ion pair **2a** can be taken up concurrently or in a stepwise manner. In order to assess the cooperative factor of the binding process, we probed the interaction of **1** with **2a** using isothermal titration calorimetry (ITC) experiments. The stepwise injection of a $CHCl_3$ solution of macrocycle **1** (6 mM) to a solution of **2a** (0.6 mM) in the same solvent resulted in a gradual release of heat due to the binding process (exothermic process). The normalized integrated data produced a single sigmoideal binding isotherm (Figure 4.15a).

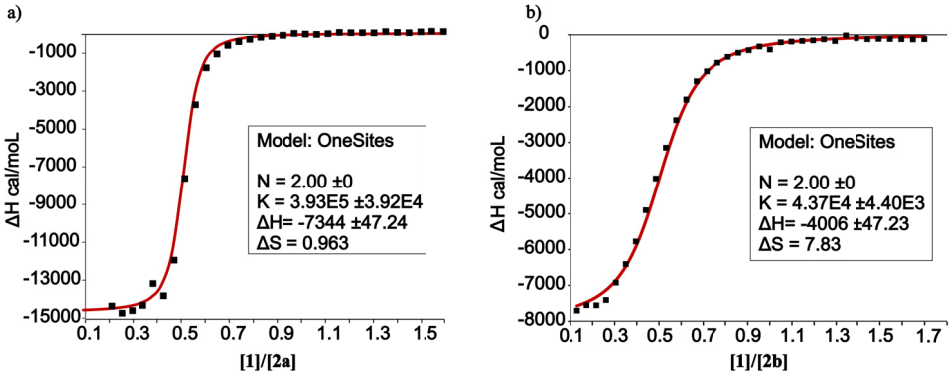

Figure 4.15 a) Binding isotherm of the calorimetric titration experiment of a $CHCl_3$ solution of **1** over **2a**; b) Binding isotherm of the calorimetric titration experiment of a $CHCl_3$ solution of **1** over **2b**. The continuous red line represents the least-squares-fit of the data to a one set of sites binding model.

On one hand, the observation of a single inflection point in the binding isotherm at a molar ratio **1**/**2a** = 0.5 gave evidence for the formation of the $\mathbf{2a}_2\subset\mathbf{1}$ complex. On the other hand, the lack of a second inflection point at a molar ratio **1**/**2a** = 1, which corresponds to the formation of the **2a**⊂**1** complex, is indicative of either of the existence of two almost identical binding events for the two ion-pairs by **1** or, as it is most likely in the present case, that the **2a**⊂**1** complex is formed to a negligible extent during the ITC experiment. For simplicity, the ITC data were fitted to the theoretical isotherm derived from the one set of sites binding model implemented in the Microcal ITC Data Analysis software.[12] By using this simple model, the fitting procedure returns averaged enthalpy change ($\Delta H_{average}$) and microscopic binding constant ($K_{average}$) values for the two binding events affording the $\mathbf{2a}_2\subset\mathbf{1}$ complex. The values for the overall stability constant and enthalpy change for the $\mathbf{2a}_2\subset\mathbf{1}$ complex are obtained by simply

squaring the value of $K_{average}$ and doubling that of $\Delta H_{average}$. Using this procedure we determined $K_{2:1}$(**2a**$_2$⊂**1**) = 1.5±0.3 × 10^{11} M^{-2} and ΔH(**2a**$_2$⊂**1**) = -14.6±0.2 kcal/mol. When K(**2a**⊂**3**) = K_{ref} (**2a**⊂**3**) = 33 M^{-1} is used as reference for the binding affinity of one of the sites in **1**, the value of the calculated cooperativity factor is α = K(**2a**$_2$⊂**1**)/K_{ref}^2 = 1.3 × 10^8. Analogous results to those described above were obtained during the ^{1}H NMR studies of the complexation of TBACl, **2b**, by receptor **1**. ITC titrations revealed that the thermodynamic stability of the *cascade* complex with the chloride anion, **2b**$_2$⊂**1**, is reduced by two orders of magnitude with respect to the cyanate analogue $K_{2:1}$(**2b**$_2$⊂**1**) = 1.9 × 10^9 M^{-2} (Figure 4.15b). This results is in agreement with the decrease in binding affinity measured for the reference calix **3** and **2b** ($K_{1:1}$(**2b**⊂**3**) = K_{ref} = 10±2 M^{-1} (Figure 4. 29 and Figure 4.30). Nevertheless, the cooperativity factor value calculated for **2b**$_2$⊂**1** is of a similar order of magnitude than for **2a**$_2$⊂**1**. To the best of our knowledge, this represents the discovery of one of the highest allosteric binding processes reported to date using a synthetic receptor.

Next, we studied the thermodynamic properties of the interaction between **1** and the ion pair **2c**. Initially, we determined the association constant for the reference system K_{ref}(**2c**⊂**3**). By ^{1}H NMR titration experiments we observed a slow chemical exchange on the proton NMR time scale which suggest that the association constant between **3** and **2c** has to be higher than 10^4M^{-1}. Since association constants with 10^4 or higher orders of magnitude cannot be accurately determined by ^{1}H NMR titrations, we decided to performed ITC experiments in $CHCl_3$. Titration of **3** with methyltrioctylammonium chloride **2c** was performed by adding aliquots of 10 μL of a chloroform solution of **3** over a solution of the ion pair **2c**. The solution of the receptor **3** ([**3**] = 7.2 mM) was approximately ten times more concentrated than the one of **2c** ([**2c**] = 0.68 mM). The complexation process resulted to be exothermic. The fitting of the data to a 1:1 binding model returned a reference binding constant K_{ref}(**2c**⊂**3**) = K_m = 8.3±2 × 10^3 M^{-1} and ΔH_{ref}(**2c**⊂**3**) = -5.5±0.1 kcal/mol) (Figure 4.16).

In complete agreement with previous reports for the simple octamethylcalix[4]pyrrole[9], reference calix[4]pyrrole **3** shows a remarkable increase in binding affinity for **2c** compared to **2a** or **2b**. Because the methyl group of the MTOA cation is a better fit than the TBA cation for the shallow cup opposite to the bound anion this is the expected

result for a calix[4]pyrrole unit acting as ion-pair receptor and affording a *receptor-separated* binding geometry in the ion-paired complex.

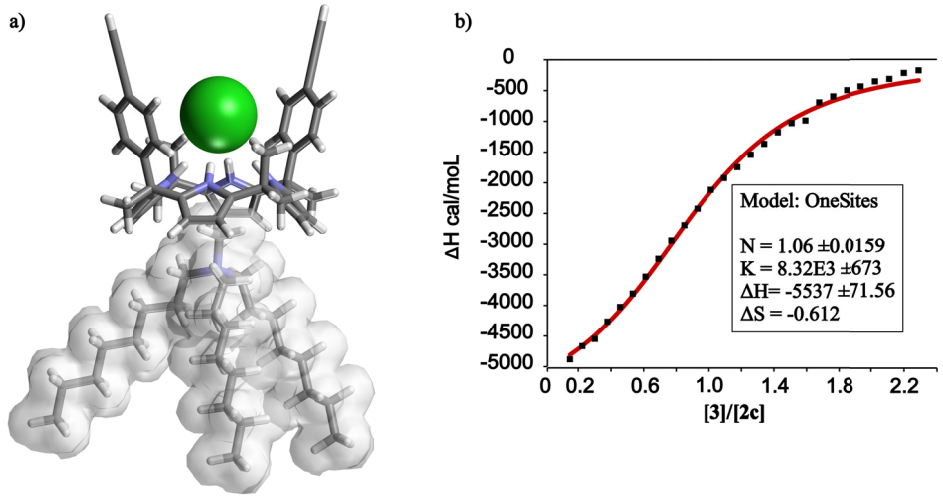

Figure 4.16 a) Energy-minimized structure of **3**⊂**2c**; b) Binding isotherm of the calorimetric titration experiment of a $CHCl_3$ solution of **3** over **2c**. The continuous red line represents the least-squares-fit of the data to a one set of sites binding model.

Titration of **1** with methyltrioctylammonium chloride **2c** was performed by adding aliquots of 6 μL of a chloroform solution of 1 over a solution of the ion pair **2c**. The solution of the receptor **1** ([**1**] = 7.0 mM) was approximately twelve times more concentrated than the one of **2c** ([**2c**] = 0.57 mM).

In addition, the ITC data for **2c** with **1** returned $K_{average}$ = 4.9±1.0 × 10^4 M^{-1} and $\Delta H_{average}$= -8.4±0.2 kcal/mol when fitted to the one set of sites model (Figure 4.17).

The magnitudes of these constants are in very good agreement with the values obtained for the reference **3**. The α value calculated for **1** binding **2c** is only 35**,** (using the same procedure employed for **2a** and **2b**), which represents a drop in the cooperativity factor of almost six orders of magnitude. Taken together, these results indicate that **1** binds **2c** through a process that is not significantly cooperative and yields a homo-dimeric $\mathbf{2c}_2$⊂**1** complex having both ion-pairs bound in a *receptor-separated* binding geometry, instead of the *cascade* arrangement assigned to the homo- and hetero-dimeric complexes of **2a** and **2b** with **1**. Second, and more importantly, the complexation process of **2c** by **1** displayed diminished signs of cooperativity, if any.

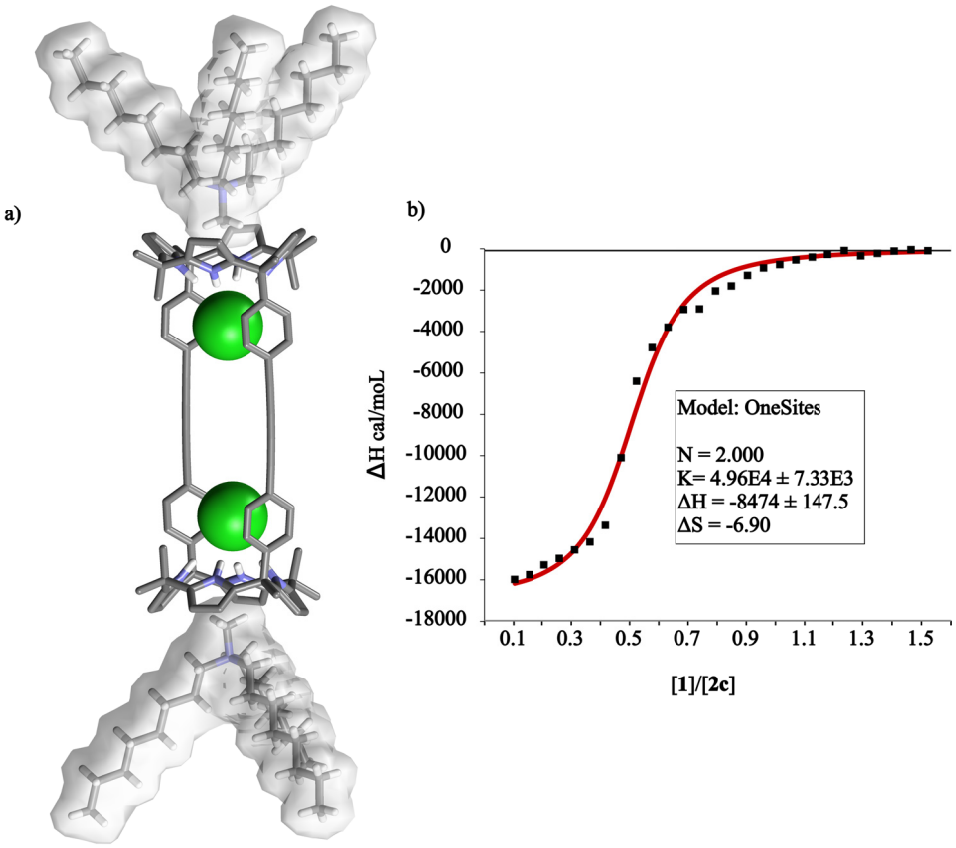

Figure 4.17 a) Cache minimized structure **2c**$_2$⊂**1**; b) Binding isotherm of the calorimetric titration experiment of a $CHCl_3$ solution of **1** over **2c**. The continuous red line represents the least-squares-fit of the data to a one set of sites binding model.

The binding processes for forming the **2a2c⊂1** and **2b2c⊂1** complexes are also expected to be highly cooperative ($\alpha > 10^3$) based on their estimated thermodynamic constant ($> 10^8\ M^{-2}$) and the values calculated for the corresponding K_{ref}.

4.2.4 Solid state studies: X-ray structures of **2a**$_2$⊂**1**, **2b**$_2$⊂**1** and **2a2b⊂1**

The structures of the aggregates proposed in solution are supported by X-ray diffraction results of single crystals. X-ray diffraction of single crystals grown from slow evaporation of $CDCl_3$ solutions containing: **2a** and **1** in a 2:1 molar ratio (Figure 4.18a), **2b** and **1** in a 2:1 molar ratio (Figure 4.18b) and a equimolar mixture of **2a, 2b** and **1**

(Figure 4.18c) revealed the formation of the corresponding five components *cascade* structures in the solid state.

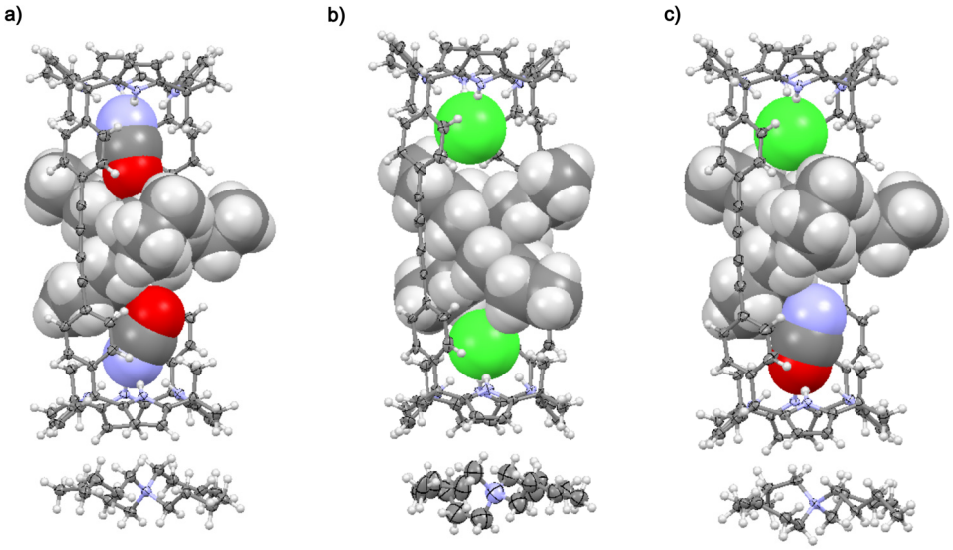

Figure 4.18 X-ray structures of cascade complexes: a) **2a**$_2$⊂**1**, b) **2b**$_2$⊂**1,** and c) **2a2b**⊂**1**. Receptor **1** and the "out" cations are shown as ellipsoids at 50% probability. The anions and the "in" TBA cation included in the cavity of **1** are displayed as CPK representations.

The solid state structure of the **2b**$_2$⊂**1** complex reveals that the two chloride anions are perfectly centered in the long C_2 axis of macrocycle **1** suggesting that the ion triplet $Cl^-TBA^+Cl^-$ possesses a size that perfectly matches the dimensions of the cavity in **1**. However, the solid state structure of the **2a**$_2$⊂**1** shows one of the cyanate anion slightly out of the C_2 axis due to its higher size compared with chloride. It is worthy to note that in all the solved structures the tetrabutylammonium cations positions its aliphatic chains threading the macrotricycle acquiring a pseudorotaxane-like topology.

4.2.5 Gas-phase characterization

Aggregates of ion-pair dimers within receptor **1** were also detected in gas phase. One of the advantages of mass spectrometry is the low quantity of sample required for the analysis. As described in *Chapter 2*, the synthesis of receptor **1** involves low yield reactions being not straightforward the obtainment of high quantities of final product. For this reason, we selected mass spectrometry to test the applicability of this ion-pair

dimeric recognition strategy toward a pool of monoatomic and polyatomic tetrabutylammonium salts (Figure 4.19).

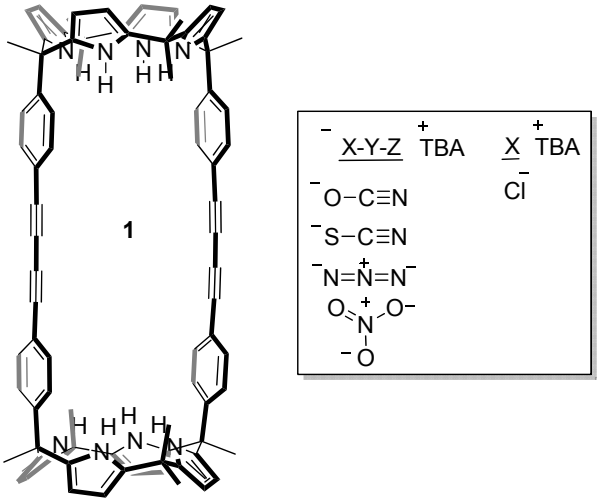

Figure 4.19 Molecular structures of receptor **1** and ion-pairs derived of tetrabutylammonium cations that have been analysed by mass spectrometry.

Experiments in solution and in solid state indicated that TBA^+ is bound to the external shallow aromatic cup of one calix[4]pyrrole through weak cation-π interactions in a *host*-separated binding mode. The release of the coordinated cation in the dimeric *cascade* complexes formed in dichloromethane solution allowed the detection in gas phase of the negatively mono-charged $(ANION^-TBA^+ANION^-)\subset 1$ complex by means of Electrospray Fourier-transform ion-cyclotron-resonance (ESI-FTICR) mass spectrometry in negative mode. A mixture of **1** with **2** equiv. of ClTBA **2b** provided a mass spectrum that exhibited a unique signal at m/z 1510.8 corresponding to the adduct $[\mathbf{1}+\mathbf{TBA}+2Cl]^-$ (Figure 4.20). The experimental isotope pattern perfectly matches the theoretical one and adducts of higher stoichiometry were not detected. This result is in complete agreement with ITC and ^1H NMR experiments performed in solution for the interaction of **1** and **2b**. In solution as well as in gas-phase, the complex $[\mathbf{1}+Cl]^-$ is formed in a negligible extent giving support to the highly strong positive cooperative effect that the coordination of the first ion-pair induces in the interaction of the second one within bis-cali[4]pyrrole macrotricyclic receptor **1**.

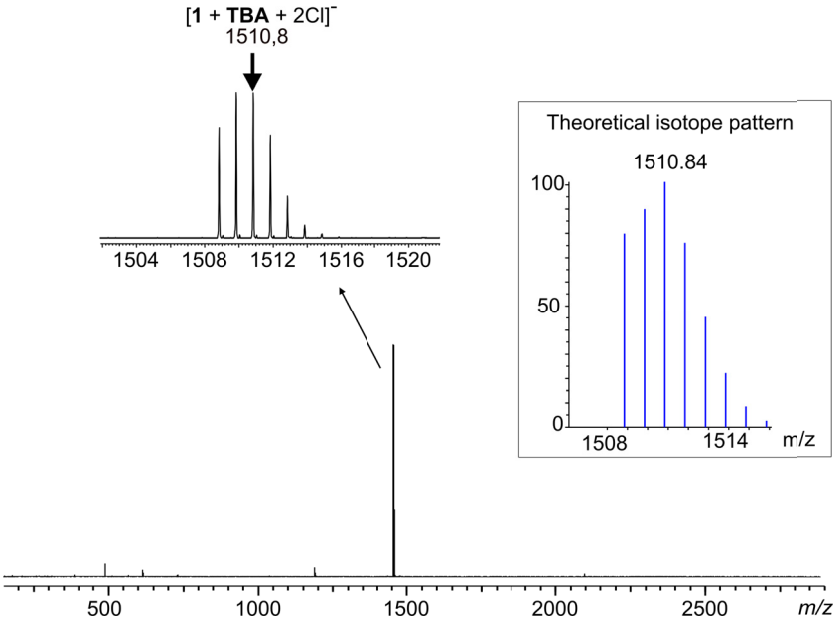

Figure 4.20 ESI-FTICR mass spectrum in negative mode of a solution containing one equivalent of **1** and 2 equiv of ClTBA **2b**.

The results obtained in the same experimental conditions with tetrabutylammonium cyanate **2a** ion pair revealed the formation of the homo-dimeric *cascade* complex [**1**+**TBA**+2OCN]$^-$ but also the formation of the hetero-dimeric *cascade* complex [**1**+**TBA**+OCN+Cl]$^-$ (Figure 4.31). Solution experiments demonstrated that the formation of the homo-dimeric complex was thermodynamically more favourable. Most likely, the excessive presence of chloride during the experimental manipulation of the sample induces the formation of the hetero-complex in the gas-phase. The cascade complexes for other tetrabutylammonium ion-pairs were also detected in gas-phase. In the case of the tetrabutylammonium azide, only the heterocomplex [**1**+**TBA**+N_3+Cl]$^-$ was detected as unique specie in the mass spectrum suggesting the high thermodynamic stability of this complex compared with the homo-dimeric cascade complex [**1**+**TBA**+2N_3]$^-$ which was not detected (Figure 4.32). Tetrabutylammonium nitrate and thiocyanate provide a mixture of complexes in the gas-phase being possible to detect the signals of the homo-dimeric and the hetero-dimeric complexes but also [**1**+SCN,NO_3]$^-$ complexes. This is probably an indication that the positive cooperative effects with this tetrabutylammonium salts are not as strong as in the cases of the cyanate or chloride

(Figure 4.33, Figure 4.34) due to size, shapes or other features of the anions. Unfortunately, experiments in solution using these ion-pairs have not been yet done and further comparisons between studies in solution and gas-phase cannot be established.

4.2.6 Binding of a tetrabutylammonium cation by homo-dimeric ion-pair complex **2c**$_2$⊂**1**.

We conclude this chapter by introducing our preliminary results in the use of ion-pair dimeric complexes as supramolecular receptors for tetrabutylammonium cations. The idea here is to make use of the different coordination properties of MTOA and TBA cations toward the bis-calix[4]pyrrole macrotricyclic receptor **1** to achieve the formation of six particles supramolecular aggregates.

As we described in previous sections, the addition of 2 equiv of ClTMOA **2c** to a millimolar solution of receptor **1** produces the formation of a new set of proton signals that we assigned to the formation of the complex **2c**$_2$⊂**1**. Ion pairs containing MTOA cation bind to receptor **1** through a non- cooperative process being both ion-pairs units independently coordinated to the calix[4]pyrrole moieties of **1** in a *host*-separated mode. This symmetrical homo-dimer ion-pair complex **2c**$_2$⊂**1** (Figure 4.17a) possess an electron rich cavity limited by two chloride anions at a fixed distance where a tetrabutylammonium cation can be included. A non-coordinating anion like PF_6 was selected as the salt counterion.

The addition of 1 equiv. of PF_6TBA to the previously formed **2c**$_2$⊂**1** did not produce significant changes in the signals of the macrotricyclic receptor however all the signals corresponding to the aliphatic protons of the tetrabutylammonium cations are shifted 0.1 ppm upfield respect to the ones of the PF_6TBA free in solution. Excess of PF_6TBA only produces a downfield shift of protons 6′ towards the free tetrabutylammonium indicating a fast chemical exchange on the ^{1}H NMR timescale between the free and bound TBA^+. This result, together with molecular modelling studies (Figure 4.21a), point to an interaction of the tetrabutylammonium cation with the electron rich cavity of **2c**$_2$⊂**1**. However, more studies are necessary to have a better understanding about this kind of supramolecular aggregates.

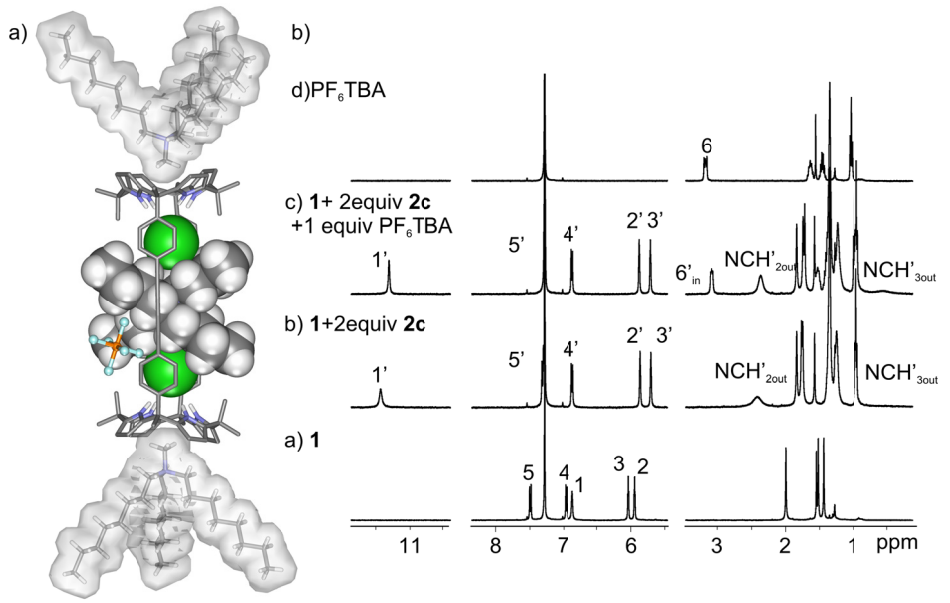

Figure 4.21 a) Energy-minimized structure of the ion sextuplet aggregate within bis-calix[4]pyrrole macrotricyclic receptor **1**. The ions included inside the receptor cavity are represented in CPK mode and the counterion of the positively charged six members agreggate; b) ^{1}H NMR spectra (298 K, 500 MHz) of $CDCl_3$ solutions of a) **1** (1 mM); b) **1** + 2 equiv. of **2c**; c) **1** + 2 equiv. of **2c** and 1 equiv. of PF_6TBA; c) free PF_6TBA. See Figure 4.2 and Figure 4.5 for proton assignments.

4.3 Conclusion

We have described the formation in solution of highly stable thermodynamically and kinetically complexes of ion-pair dimers and quartets of ions with the bis-calix[4]pyrrole macrotricyclic receptor **1**. We demonstrate that bis-calix[4]pyrrole macrocyclic receptor **1** binds two chloride or cyanate tetrabutylammonium ion-pairs **2** (a quartet of ions) yielding $\mathbf{2_2}\subset\mathbf{1}$ complexes through a highly cooperative process ($\alpha > 10^5$). The complexes have a structure with a cascade-like arrangement of the ion pairs. One ion-pair is bound in a close contact geometry while the other in a receptor-separated arrangement. The solution structures for the complexes are supported by an array of ^{1}H NMR experiments and have been corroborated in the solid state by single crystal X-ray diffraction analysis. Additionally, the exclusive and quantitative formation of the ion-pair hetero-dimers $\mathbf{2a2b}\subset\mathbf{1}$ can also be achieved. Most of the ion-pair dimers

were also detected in the gas-phase complex by means of Electrospray Fourier-transform ion-cyclotron-resonance (ESI-FTICR) mass spectrometry in negative mode. The use of the ion-pair **2c** containing a methyltrioctylammonium cation instead of tetrabutylammonium renders the binding process significantly less cooperative. This finding together with the results of ^{1}H NMR experiments suggest that in the homodimeric complex **2c**$_2$⊂**1** both bound ion-pairs feature a *receptor*-separated binding mode. The equimolar combination of TBA and MTOA salts allows the self-assembly of hetero ion-pair dimer complexes with *cascade* arrangement by means of a cooperative binding processes. Importantly, in the **2a2c**⊂**1** and **2b2c**⊂**1** complexes the MTOA cation seems to be selectively located in the "out" position. The interwoven structure of the described ion quartet complexes can be consider as a novel strategy for the assembly of pseudorotaxanes and their further application in the supramolecularly assisted synthesis of new interlocked structures. Finally, our first attempts toward the rational design of ion complexes of higher stoichiometry were also described.

4.4 Experimental section

4.4.1 General information and instrumentation

All reagents were obtained from commercial suppliers and used without further purification. Anhydrous solvents were obtained from a solvent purification system SPS-400-6 from Innovative Technologies, Inc. All solvents were of HPLC grade quality, commercially obtained and used without further purification.

Routine ^{1}H NMR spectra were recorded on a Bruker Avance 400 (400.1 MHz for ^{1}H NMR) and Bruker Avance 500 (500.1 MHz for ^{1}H NMR) ultrashield spectrometer. The deuterated solvents (Aldrich) used was in all the experiments $CDCl_3$; chemical shifts are given in ppm, relative to TMS.

Isothermal titration calorimentry experiments were performed using a Microcal VP-ITC Microcalmeter.

Crystal structure determinations were obtained by slow evaporation of dichloromethane for **2a**$_2$⊂**1** and **2a2b**⊂**1** chloroform in the case of **2b**$_2$⊂**1**. The measured crystals were unstable under atmosphere conditions; they were prepared under inert conditions

immersed in perfluoropolyether as protecting oil for manipulation. Measurements were made on a Bruker FR591 diffractometer equipped with an APPEX 2 4K CCD area detector, a rotating anode with $Mo_{K\alpha}$ radiation and an Oxford Cryostream 700 low temperature device (T = 100K). Full-sphere data collection was used with ω and φ scans. Programs used: Data collection Apex2 V2010.7-0 (Bruker AXS 2010), data reduction Saint + Version 7.60A (Bruker AXS 2008) and absorption correction SADABS V. 2008-1 (2008). Crystal structure solution was done using methods implemented in SHELXTL version 6.14 (Sheldrick, G.M. (2008)).

4.4.2 Experimental section: Figures

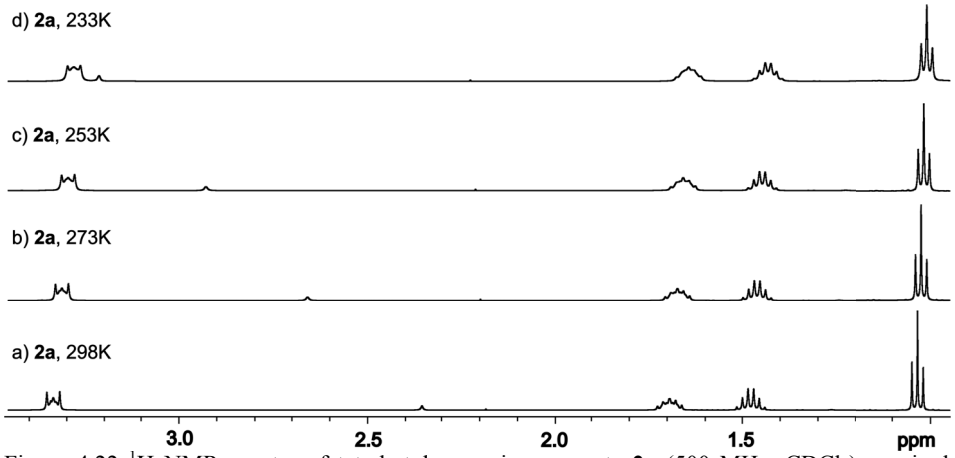

Figure 4.22 ^{1}H NMR spectra of tetrabutylammonium cyanate **2a** (500 MHz, $CDCl_3$) acquired during a variable temperature experiment.

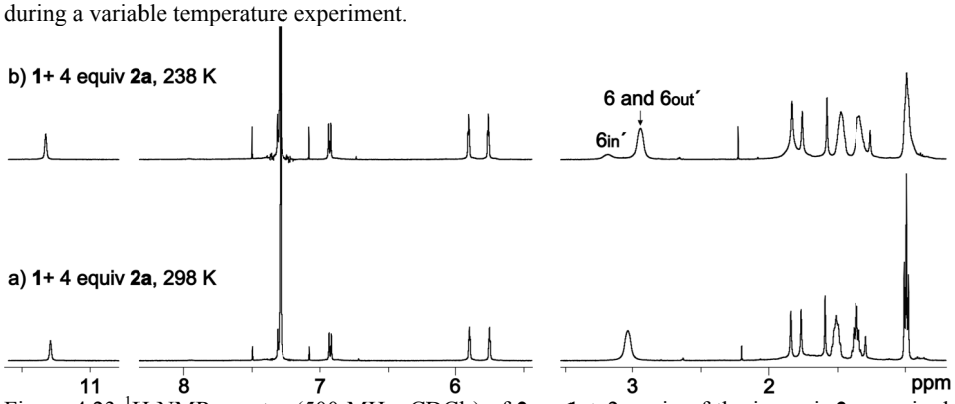

Figure 4.23 ^{1}H NMR spectra (500 MHz, $CDCl_3$) of $\mathbf{2a}_2\subset\mathbf{1}$ + 2 equiv of the ion pair **2a** acquired during a variable temperature experiment. At 238K fast exchange on the NMR time scale is observed between the "out" TBA cation and the cation of the free **2a**.

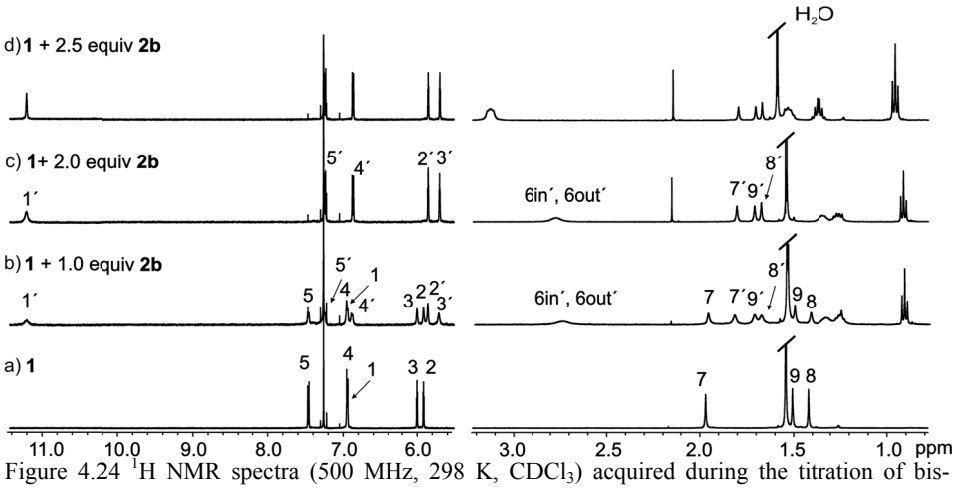

Figure 4.24 ^{1}H NMR spectra (500 MHz, 298 K, $CDCl_3$) acquired during the titration of bis-calix[4]pyrrole macrocyle **1**= 2.9 mM with tetrabutylammonium chloride **2b**.

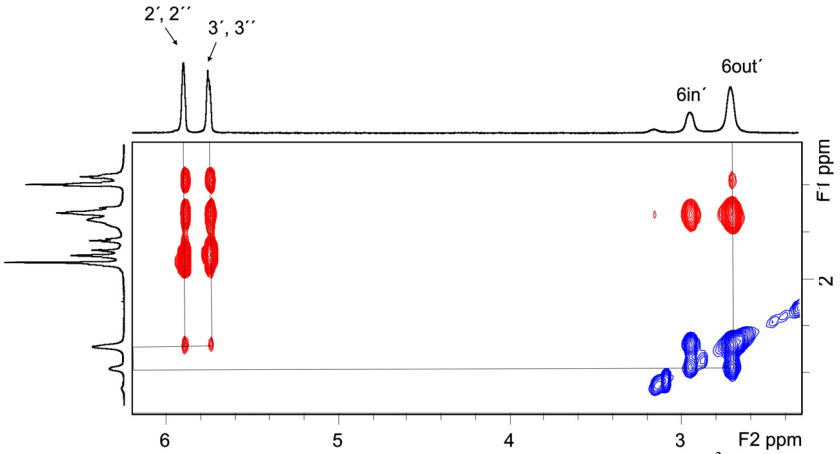

Figure 4.25 ROESY experiment (500 MHz, p15, 0.3 s, $CDCl_3$, 1.6 × 10^{-3}M) of **2a2b⊂1** at 248K showing chemical exchange between the methylene protons α to the nitrogen of the tetrabutylammonium cyanate $H_{6in´}$ and $H_{6out´}$. Cross-peaks indicating intermolecular close contacts between H6out´ and the β-pyrrolic protons of the bis-calix[4]pyrrole macrocycle $H_2´$, $H_2´´$, $H_3´$ and $H_3´´$.

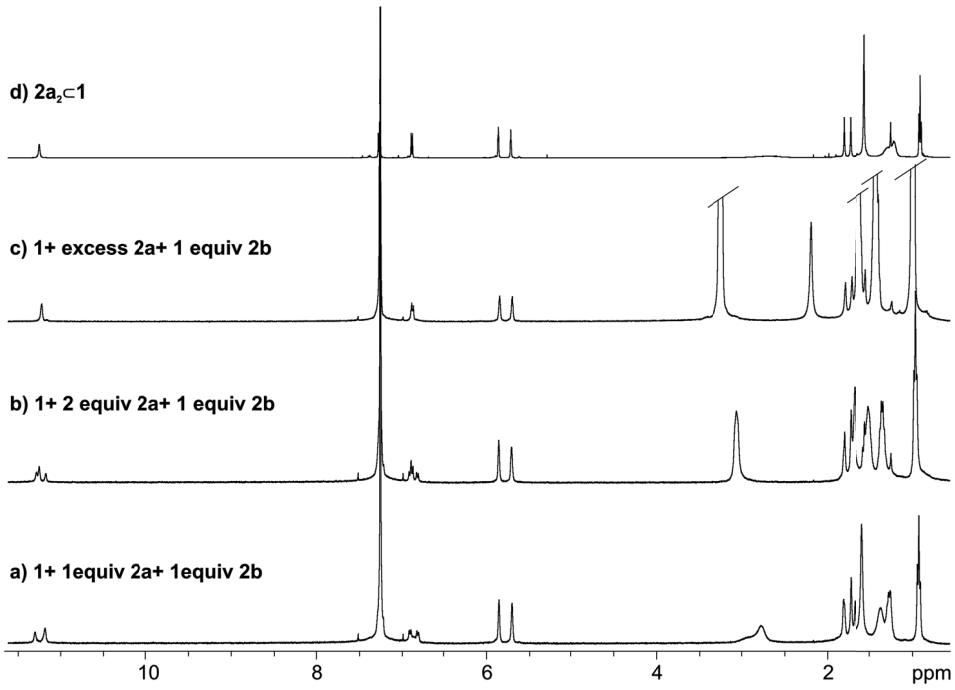

Figure 4.26 ^{1}H NMR (500 MHz, $CDCl_3$) spectra of the addition of increasing quantities of **2a** over a solution containing **2a2b⊂1**.

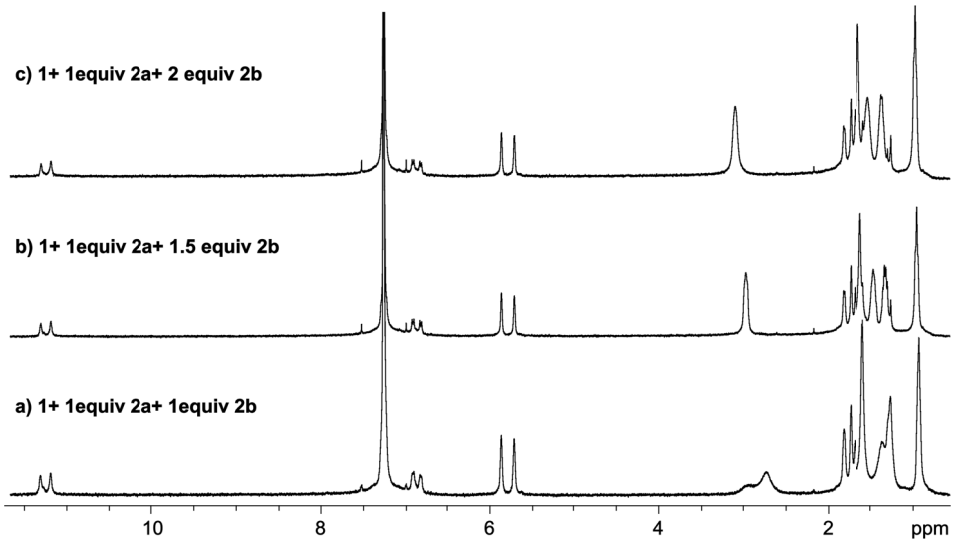

Figure 4.27 ^{1}H NMR (500 MHz, $CDCl_3$) spectra of the addition of increasing quantities of **2b** over a solution containing **2a2b⊂1**.

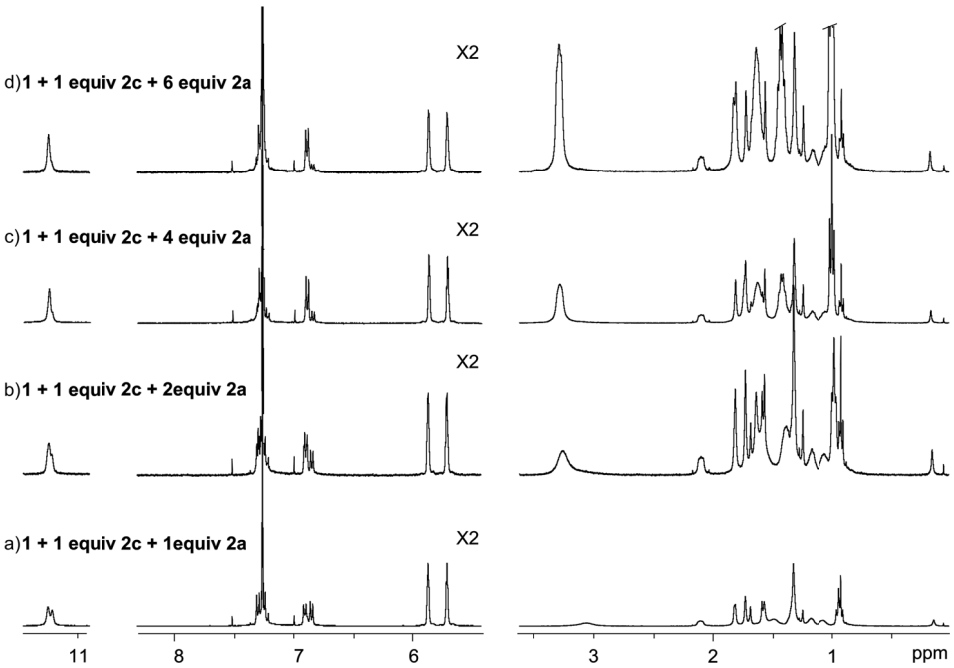

Figure 4.28 ^{1}H NMR (500 MHz, 298 K, $CDCl_3$) spectra of: a) **1** + 1 equiv of **2c** +1 equiv **2a**; b) **1**+ 1 equiv **2c** + 2 equiv **2a**; c) **1**+ 1 equiv **2c** + 4 equiv **2a**; d) **1**+ 1 equiv **2c** + 6 equiv **2a**.

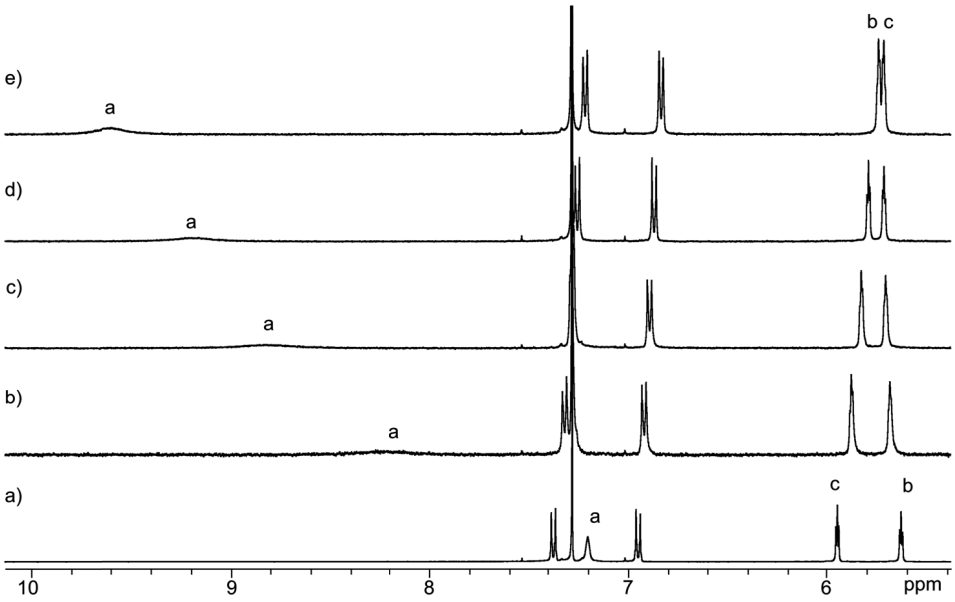

Figure 4. 29 Selected regions of the ^{1}H NMR titrations of **3** ([**3**] = 6.5 mM) with **2b** in $CDCl_3$ at 298K. a) **3**; b) **3** + 5.03 equiv **2b**; c) **3** + 9.3 equiv **2b**; d) **3** + 14.8 equiv **2b**; e) **3** + 19.4 equiv **2b**.

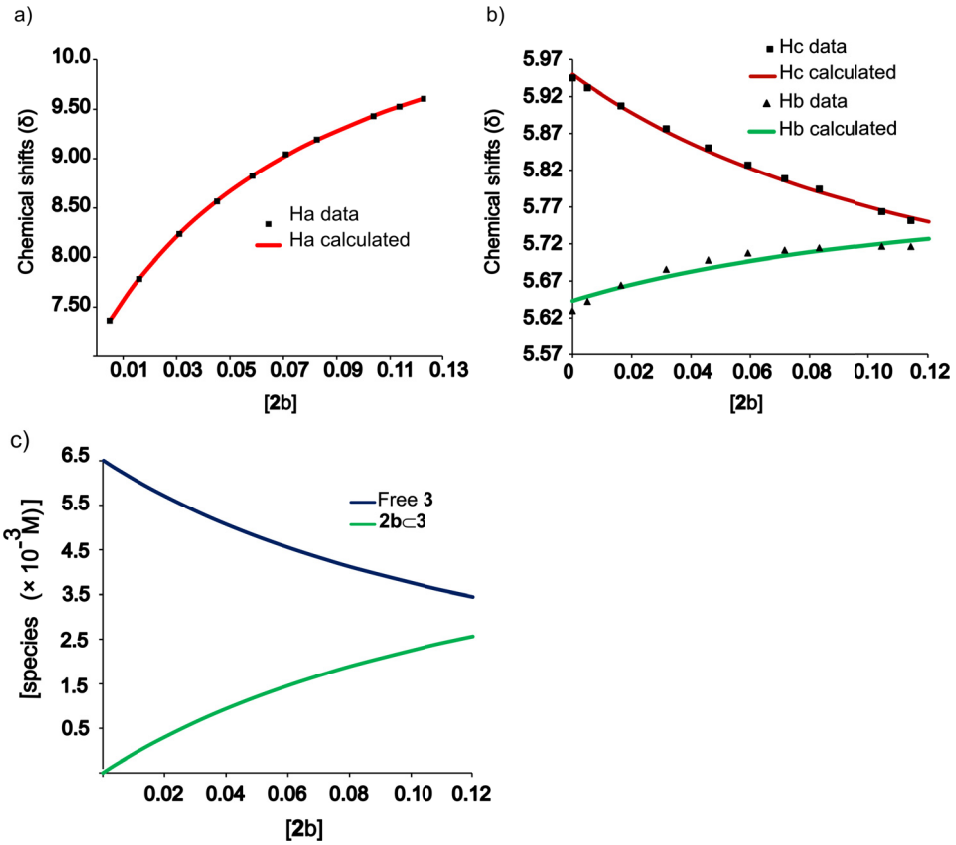

Figure 4.30 a) Fit of the chemical shift changes experienced by the proton Ha of **3** during the titration with **2b** using a 1:1 binding model. b) Fit of the chemical shifts changes experienced by the proton Hc and Hb of **3** during the titration with **2b** using a 1:1 binding model. $K_{\mathbf{2b}\subset\mathbf{3}}$ = 10±2 M^{-1}. c) Speciation distribution profiles during the titration.

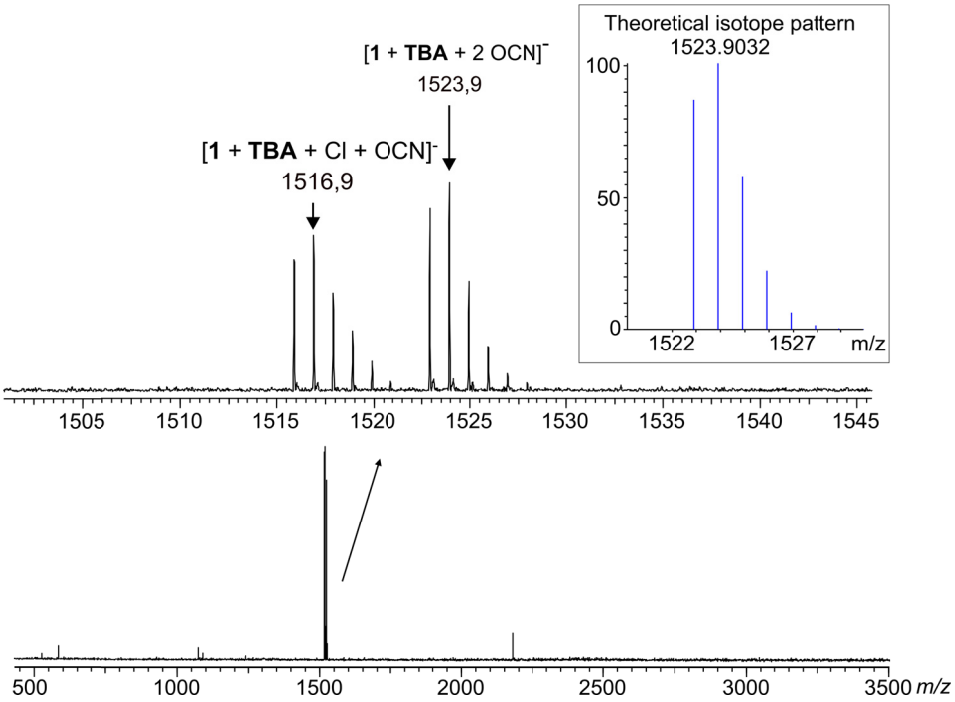

Figure 4.31 ESI-FTICR mass spectrum in negative mode of a solution containing one equivalent of **1** and 2 equiv of OCNTBA **2a**.

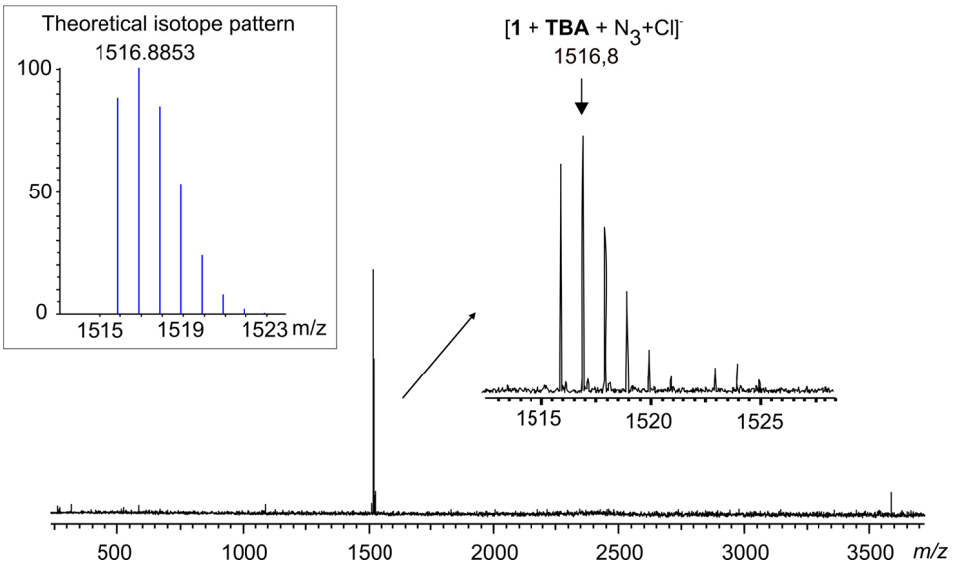

Figure 4.32 ESI-FTICR mass spectrum in negative mode of a solution containing one equivalent of **1** and 2 equiv of N_3TBA.

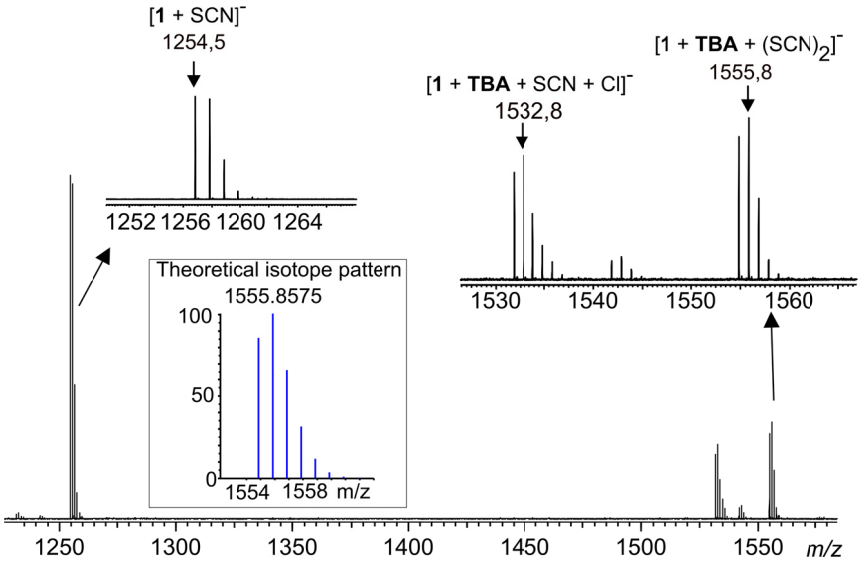

Figure 4.33 ESI-FTICR mass spectrum in negative mode of a solution containing one equivalent of **1** and 2 equiv of SCNTBA.

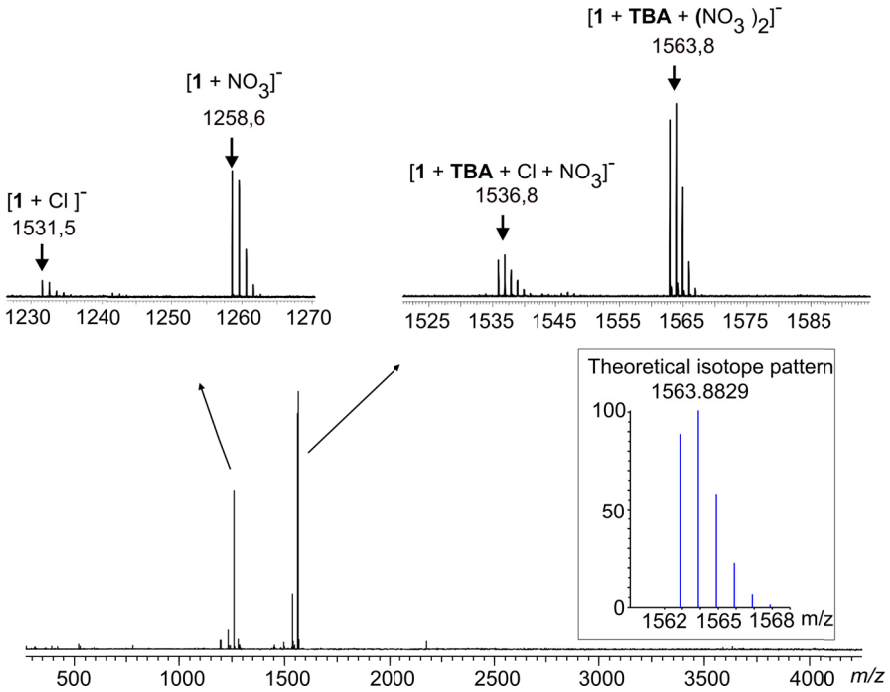

Figure 4.34 ESI-FTICR mass spectrum in negative mode of a solution containing one equivalent of **1** and 2 equiv of NO_3TBA **2b**.

4.5 References and notes

[1] Goralski, P.; Chabanel, M. *Inorg. Chem.* **1987**, *26*, 2169.
[2] Hunter, C. A.; Low, C. M. R.; Rotger, C.; Vinter, J. G.; Zonta, C. *Chem. Commun.* **2003**, 834.
[3] Kim, S. K.; Sessler, J. L. *Chem. Soc. Rev.* **2010**, *39*, 3784.
[4] McConnell, A. J.; Beer, P. D. *Angew. Chem.* **2012**, *51*, 5052.
[5] Kim, S. K.; Lynch, V. M.; Young, N. J.; Hay, B. P.; Lee, C. H.; Kim, J. S.; Moyer, B. A.; Sessler, J. L. *J. Am. Chem. Soc.* **2012**, *134*, 20837.
[6] Soberats, B.; Martinez, L.; Sanna, E.; Sampedro, A.; Rotger, C.; Costa, A. *Chem-Eur J* **2012**, *18*, 7533.
[7] Fuoss, R. M.; Kraus, C. A. *J. Am. Chem. Soc.* **1935**, *57*, 1.
[8] Kim, S. K.; Vargas-Zuniga, G. I.; Hay, B. P.; Young, N. J.; Delmau, L. H.; Masselin, C.; Lee, C. H.; Kim, J. S.; Lynch, V. M.; Moyer, B. A.; Sessler, J. L. *J. Am. Chem. Soc.* **2012**, *134*, 1782.
[9] Gross, D. E.; Schmidtchen, F. P.; Antonius, W.; Gale, P. A.; Lynch, V. M.; Sessler, J. L. *Chem-Eur J* **2008**, *14*, 7822.
[10] Custelcean, R.; Delmau, L. H.; Moyer, B. A.; Sessler, J. L.; Cho, W. S.; Gross, D.; Bates, G. W.; Brooks, S. J.; Light, M. E.; Gale, P. A. *Angew. Chem.* **2005**, *44*, 2537.
[11] Valderrey, V.; Escudero-Adan, E. C.; Ballester, P. *J. Am. Chem. Soc.* **2012**, *134*, 10733.
[12] The use of binding models considering two set of sites or sequential binding sites afforded multiple mathematical solutions providing sensible fits due to the optimization of at least four fitting variables ($K_{1:1}$, $K_{2:.1}$, $\Delta H_{1:1}$, $\Delta H_{2:1}$).

Chapter 5

Binding of Tetrabutylammonium [6,6]-phenyl-C_{61}-butyric Carboxilate by Porphyrin Tweezer Receptors

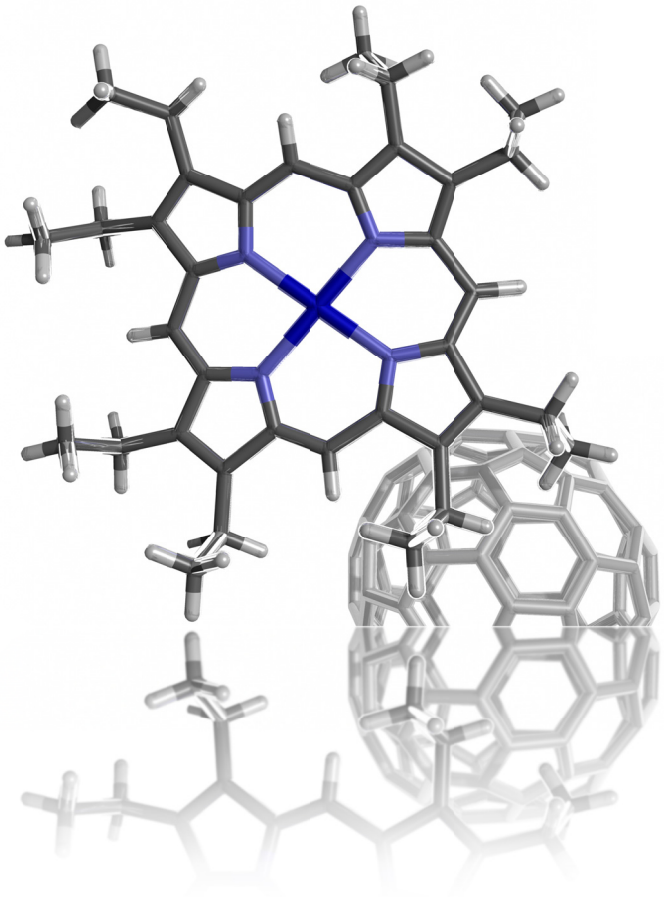

5.1 Introduction

The supramolecular complementarity between π-electron donor aromatic monoporphyrins and π-electron acceptor fullerenes was evidenced for the first time in the solid state.[1,2] Since then, many receptors of fullerenes based on this attractive interaction have been designed. The number of covalently attach porphyrin units and its relative disposition are key factors to lead high binding affinities in the design of efficient receptors. Cyclic face-to-face bis-porphyrin receptors[3,4] as well as acyclic bis-porphyrin tweezers have demonstrated to form thermodynamically stable complexes with fullerenes. In both cases, the nature of the spacer that links the two porphyrin units is the main factor that confers unique recognition properties to the different types of fullerene receptors. In order to achieve the formation of highly thermodynamically stable complexes between fullerenes and porphyrin tweezers it is required the use of spacers capable of preorganizing the host in a conformation close to that attained in the complex. In doing so, metal coordination-based spacers[5] or hydrogen bound pre-organized aromatic spacers[6] has been used to arrange the pair of chromophores in a relative disposition that is adequately suitable for the recognition of fullerenes. Macrocyclic compounds such as calix[4]arenes are also efficient spacers enabling an appropriate spatial arrangement of the porphyrin to coordinate fullerenes.[7] Porphyrin tweezer receptors for the recognition of fullerene derivatives are still scarce. Two examples of Zn(II) bis-porphyrin tweezer receptors effective in the complexation of bis-pyridine functionalized fullerenes were recently described. In this case, the fullerene is recognized by metal coordination bonds established between the porphyrin metal centers and both pyridine-fullerene functional groups.[8,9] Interestingly, in addition to their application as molecular receptors, the assembly of these supramolecular systems resulted to be suitable for the study of light-triggered electron and energy transfer processes. Our contribution to the recognition of fullerene derivatives by porphyrin tweezer receptors is described in this chapter. Two synthetic approaches for the synthesis of porphyrin tweezers containing two walls calix[4]pyrrole spacers are detailed. Moreover, the recognition properties of this novel porphyrin-based receptor

towards alkylammonium salts derived from [6,6]-phenyl-C_{61}-butyric carboxylic acid are introduced.

5.2 Results and discussion

5.2.1 Design and synthesis

This relatively new family of porphyrin-based molecular tweezers is formed by two porphyrin units covalently linked to a macrocyclic calix[4]pyrrole spacer. Its synthesis could be potentially achieved using a wide variety of reactions starting with the adequate functionalization of the starting materials; porphyrins and calix[4]pyrroles.

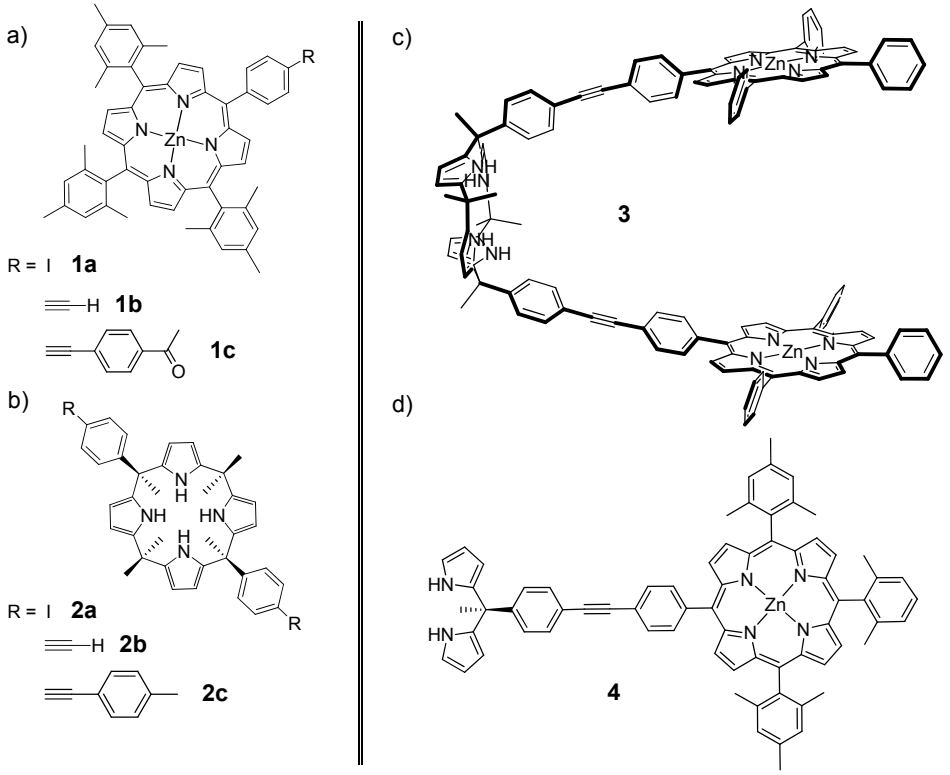

Scheme 5.1 Molecular structures of: a) Zn(II) metallated *mesityl*-substituted porphyrins **1a**, **1b** and **1c**, b) α,α-*aryl* extended calix[4]pyrroles **2a**, **2b** and **2c**, c) Zn metallated *mesityl*-substituted bisporphyrins tweezer with a calix[4]pyrrole spacer **3** and d) dipyrromethane derived from a zinc metallated *mesityl*-substituted porphyrin **4**.

Palladium catalysed coupling reactions have been successfully applied to attach metallated porphyrin units to a wide variety of rigid spacers.[10,11,12] The triple bonds that result from the palladium coupling connects both porphyrin units with the spacer and confers linearity to the linker. Moreover, it serves to force a co-facial orientation of both porphyrin units. Additionally, the mandatory use of *aryl*-halides in Sonogashira couplings produces the formation of a relatively rigid system that positions the spacer and the binding sites at enough distance to avoid its stearic hindrance. With these considerations in mind, our initial design consisted in the use of Zn(II) metallated *mesityl*-substituted porphyrins derivatives **1a** and **1b** (Scheme 5.1). Such porphyrins have been prepared according to described procedures.[13,14] The tested calix[4]pyrrole spacers were the *aryl*-extended α,α-calix[4]pyrroles **2a** and **2b** described in *Chapter 1*.[15] Model systems were used in order to select the most adequate conditions for the Sonogashira coupling between the porphyrin and calix[4]pyrrole units. For the Pd-coupling reactions we have used a mixture of toluene and triethylammine being the first one the solvent that provides solubility to the *mesityl*-substituted porphyrins and the second one the requisite base. Monoethynyl Zn-porphyrin **1b** reacts with the commercially available 4-iodoacetophenone in the presence of bis(triphenylphosphine)palladium(II) dichloride and a catalytic amount of CuI in a 1:1 mixture of dry toluene/triethylammine to obtain compound **1c** in 60% yield. Single crystals suitable for X-ray analysis were obtained from the slow evaporation of chloroform/methanol solution (Figure 5.1a). Afterwards, the same conditions were applied for the synthesis of compound **2c** from the reaction of calix[4]pyrrole **1a** with the commercially available 4-ethynyltoluene to afford compound **2c** in a 75% yield. Single crystals for X-ray analysis were obtained from the slow evaporation of a dimethylformamide saturated solution of **2c** where the calix[4]pyrrole core displays a *1,2-alternate* conformation (Figure 5.1b). Once we had fully characterized the model systems, we applied the same reaction conditions for the double Sonogashira reaction between the di-iodo calix[4]pyrrole **1a** and porphyrin **2a** to prepare the porphyrin-based tweezers receptor **3** (Scheme 5.1c). Unfortunately, even when those conditions worked well for the model systems; all our attempts to synthesize receptor **3** failed.

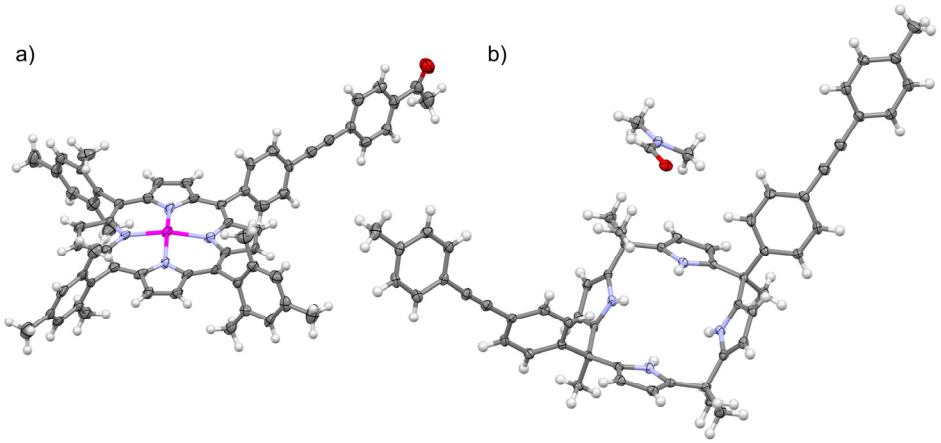

Figure 5.1 X-ray structures of a) Zn metallated *mesityl*-substituted porphyrin **1c** and b) α,α-*aryl* extended calix[4]pyrrole **2c**. Thermal ellipsoids are drawn at the 50% of probability.

The ^{1}H NMR spectrum of the reaction mixture showed the total consumption of the calix[4]pyrrole **2a**. However, it did not show any characteristic signal of *β*-pyrrolic protons expected for a product containing a calix[4]pyrrole unit. A preparative thin layer chromatography of the reaction mixture allowed us to isolate the *homo*-coupling product of the acetylene porphyrin units. Additionally, a very polar product was recovered. The ^{1}H NMR spectrum of the isolated compound showed broad and ill-defined signals that could not be assigned to the desired product or any other product containing a calix[4]pyrrole unit. Similar results were obtained for the reaction between porphyrin **1b** and calix[4]pyrrole **2b** using the same reaction conditions or even trying other solvents or palladium catalysts. An alternative synthetic strategy was designed relying on the preparation of the porphyrin-based dipyrromethane **4** using as starting material the model system **1c**. The Zn-porphyrin *aryl*-methyl ketone **1c** was reacted with an excess of freshly distilled pyrrole in the presence of trifluoroacetic acid. Unfortunately, the isolation of the expected dipyrromethane product **4** was not possible. We surmise that photoinduced electron-tansfer processes between the the electron rich aromatic porphyrin units and the electron acceptor calix[4]pyrrole/dipyrrole components are taking place in solution producing the structural degradation of the anion-radicals centered on the pyrrole rich components. Coinciding with our synthetic efforts in the preparation of porphyrin-based tweezers having calix[4]pyrrole spacers, Mamardashvili *et al*. reported the first example of such family of tweezers.[16,17] The authors employed

an identical calix[4]pyrrole spacer as synthetic precursor. However, the porphyrin units were simple Zn(II) 5-ethynyloctaethylporphyrins lacking the *meso*-phenyl susbstituents and incorporating ethyl substituted pyrroles. We decided to reproduce the reported methodology and for this reason we synthetized Ni-metallated 5-ethynyloctaethylporphyrin **5e** following analogous procedures to the ones described in literature.[18,19,20,21,22,23] Octaethylporphyrin (OEP) **5a** was obtained after five synthetic steps following the procedure reported by Sessler *et al*.[18] Free-base OEP was first metallated with nickel and later subjected to a Vilsmeier formylation obtaining the porphyrin derivative **5c**.[21] Our attempts to perform the formylation in a Zn-OEP scaffold were not successful. By performing a Takai reaction at 0ºC in the formylated Ni-OEP we obtained a *trans*-iodovinyl derivative **5d**. However, the Takai reaction in our hands progressed with noticeably lower yields comparing to the reported ones (40% compared with 75% reported in the literature).[19,20] Surprisingly, the same Takai conditions failed completely to produce iodovinyl derivatives from analogous aldehydes, namely free base, Zn(II) or Cu(II).[22] Finally, the dehydroiodination of **5d** proceeded in the presence of *t*-BuOK to produce the ethynyl-OEP derivative **5e** that was directly used in the next reaction without further purification.

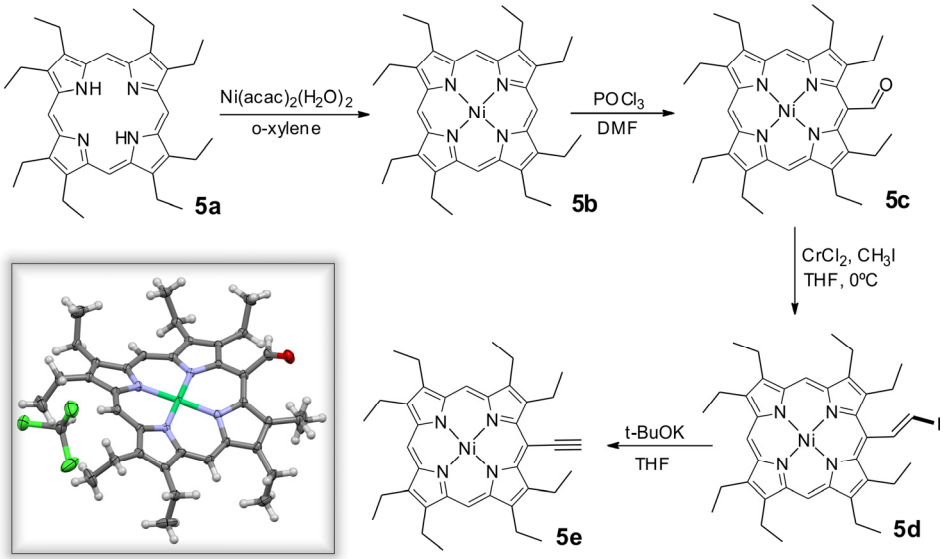

Scheme 5.2 Synthetic scheme for the obtention of Ni metallated ethynyl-octaethylporphyrin **5e**. X-ray structure of *meso*-formyloctaethylporphyrinatonickel(II) **5c**. Thermal ellipsoids are drawn at the 75% of probability.

Ni-bisporphyrin tweezer receptor **6a** was obtained in a 4% yield by reacting three equivalents of the ethynyl-OEP **5e** with one equivalent of α,α-diiodocalix[4]pyrrole **2a** in the presence of $Pd(Ph_3)_2Cl_2$ and CuI and in a 1:1 mixture of dry toluene/triethylamine at 50ºC during 12 hours. Additionally, the mono reacted product **6b** was isolated in 12% yield.

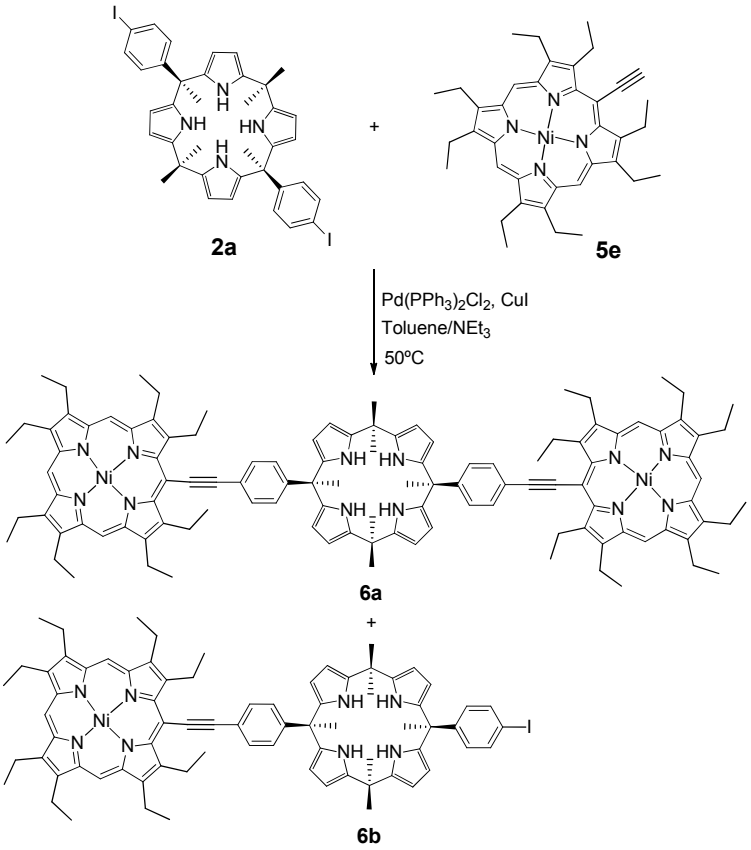

Scheme 5.3 Synthetic scheme for the preparation of bis-Ni-octaethylporphyrin containing a calix[4]pyrrole spacer **6a** using a Sonogashira bis-coupling reaction. The *mono*-Sonogashira product **6b** is also depicted.

The ^{1}H NMR spectra of the obtained reaction products are depicted in Figure 5.2. The *mono*-Sonogashira product (Figure 5.2a) presents a *C*s symmetry and shows four different signals for the *β*-pyrrolic protons (H_9, H_{10}, H_{13} and H_{14}). Additionally, as result of the non-symmetrical functionalization of the two calix[4]pyrrole *meso*-phenyl walls, two different NHs pyrrolic protons (H_{11} and H_{12}) and four different aromatic proton

signals (H_7, H_8, H_{15} and H_{16}) are observed. Conversely, *double*-Sonogashira product presents C_{2v} symmetry displaying two different signals corresponding to two *β*-pyrrolic protons (H_9 and H_{10}) and only one broad signal for NHs pyrrolic protons H_{11} in its ^{1}H NMR spectrum. In *non*-polar solvents as CH_2Cl_2, the favoured conformation for the calix[4]pyrrole core is the *1,3-alternate* conformation. In that conformation the *β*-pyrrolic protons H_9 appear upfield shifted compared with H_{10} due to the ring current influence of the aromatic ring.

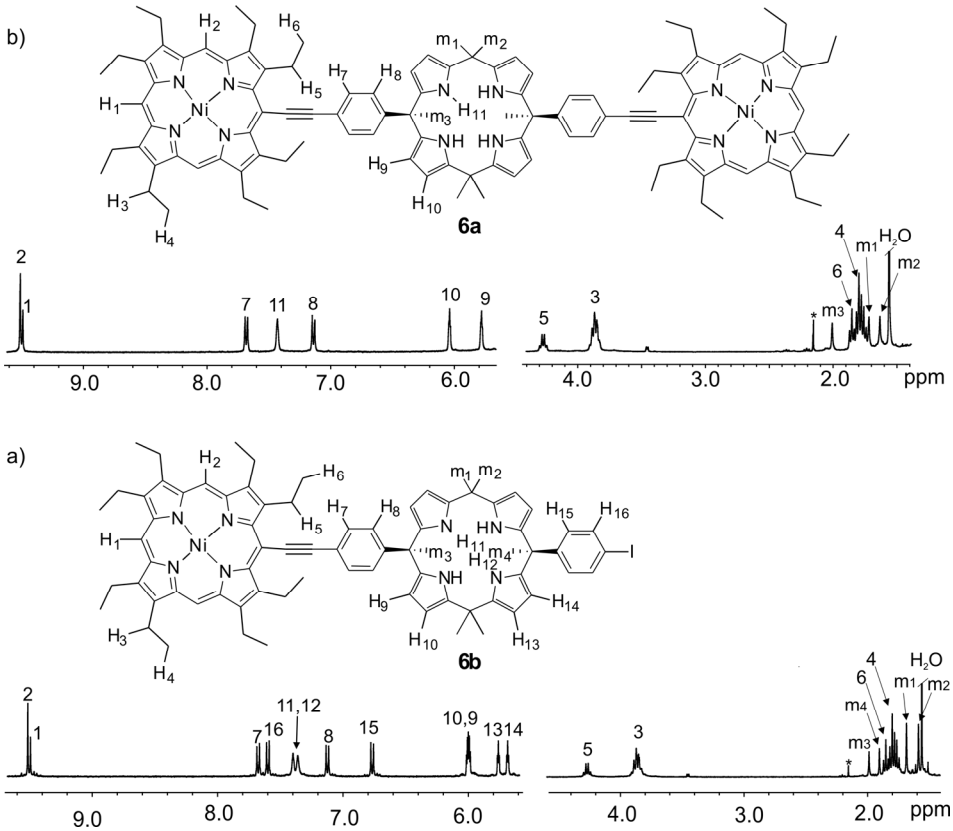

Figure 5.2 Selected regions of the ^{1}H NMR (400 MHz, CD_2Cl_2, 298K) of a) *mono*-Sonogashira porphyrin product **6b** and b) *double*-Sonogashira porphyrin product **6a**.* =acetone

As previously demonstrated by our group, the covalent framework of the porphyrin tweezer receptors can be tunned to control the three dimensional architectures of the supramolecular complexes deriving from a common guest.[24,25] Additionally, the complementarity between the tweezers cavity and the guest´s shape and size has strong

influence in the binding affinity. Inspired by the findings reported above, we considered the use of the copper(I)-catalyzed azide-alkyne cycloaddition (CuAAC) to covalently attach two porphyrin units to a calix[4]pyrrole spacer.[26] Most likely, triazol moieties connecting calix[4]pyrrole and porphyrin units are going to provide porphyrin tweezers containing cavities with different size and shape compared to the ones described above (*vide supra*).

Calix[4]pyrrole **7** (Scheme 5.4) was synthesized following a procedure recently described in our group.[27]

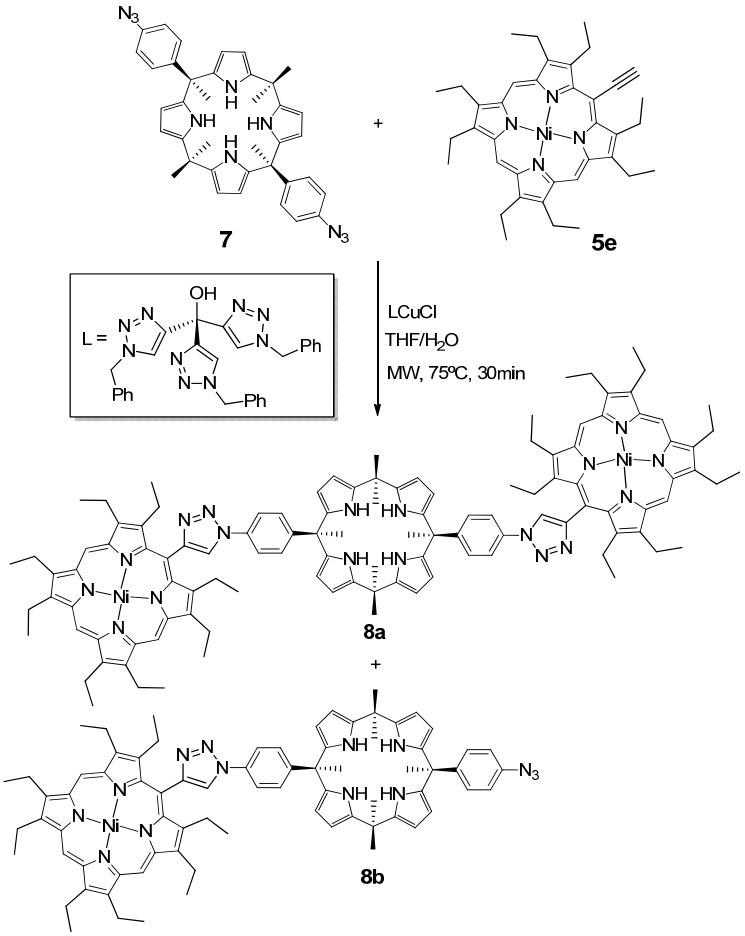

Scheme 5.4 Synthetic scheme for the preparation of bis-Ni-octaethylporphyrin containing a calix[4]pyrrole spacer **8a** using a copper(I)-catalyzed azide-alkyne cycloaddition "*click* reaction". The *mono*-porphyrin product **8b** is also depicted.

We applied a microwave-assisted (75ºC during 30 min) CuAAC strategy to porphyrin-tweezer **8a** formation by adding 4 equivalents of ethynyl-OEP **5e** to calix[4]pyrrole **7** in the presence of a tris(triazolyl)methanol-Cu(I) catalyst[28] with a 4:1 mixture of THF/water. Bis-porphyrin **8a** was obtained in a 42% yield and *mono*-porphyrin product **8b** was isolated in 22% yield (Scheme 5.4).

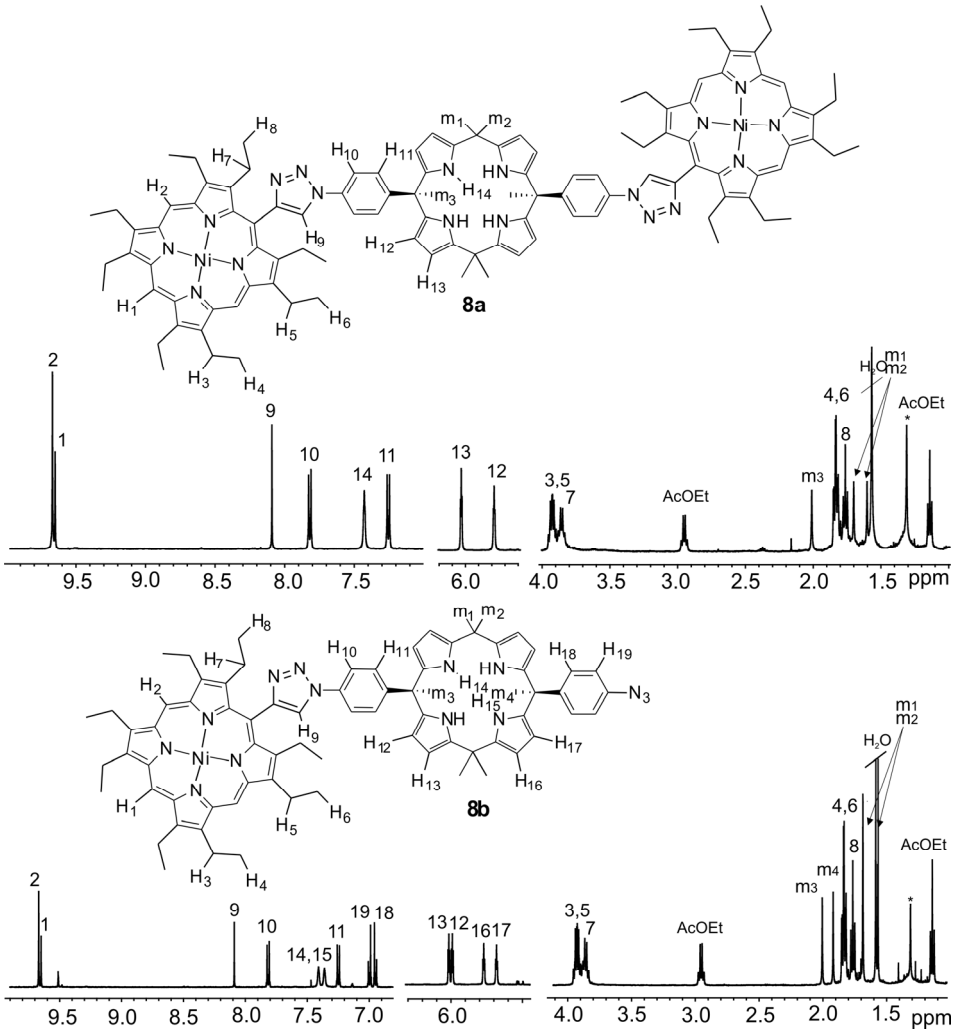

Figure 5.3 Selected regions of the ^{1}H NMR (400 MHz, CD_2Cl_2, 298K) of a) *mono*-porphyrin product **8b** and b) *double*-porphyrin product **8a**.

The ^{1}H NMR spectra of **8a** and **8b** porphyrin-calix[4]pyrrole products are depicted in Figure 5.3. As expected the proton signals and its chemical shifts are similar to the ones obtained for **6a** and **6b**.

Ni-bisporphyrin **6a** and **8a** possess three binding sites: two porphyrin units able to establish metal coordination bonds or van der Walls interactions and one calix[4]pyrrole unit able to recognize electron-rich molecules by establishing four hydrogen-bond interactions. Moreover, as we described in *Chapter 1*, the coordination of the calix[4]pyrrole core locks the unit in the *cone* conformation featuring an additional electron-rich bowl-shape cavity defined by the pyrrole rings able to coordinate cations.

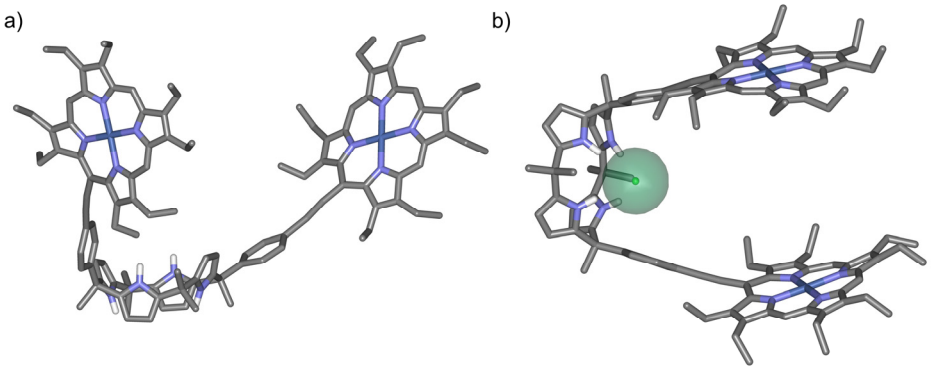

Figure 5.4 Energy-minimized structure[29] of two possible tweezer conformational states: a) 1,3-*alternate* and b) *cone* conformation.

Such molecular tweezers are expected to present at least two well defined conformational states depending on the conformation adopted by the calixpyrrole unit (1,3-*alternate* and *cone* conformation). The conformational equilibrium between the two states can be controlled by complexation of an adequate guest by establishing hydrogen-bond interactions. When the α,α-calix[4]pyrrole is locked in the *cone* conformation, the co-facial disposition of the porphyrin units is induced. This conformation; is the most suitable to establish guest interactions with tweezer binding mode. It is worthy to mention that both, the conformational equilibrium and the host-guest interactions are likely to be affected by the nature of the solvent i.e. polar solvents would favour that the calix[4]pyrrole core is adopting the *cone* conformation.

5.2.2 Binding studies involving the bis-porphyrin twezeer receptor **6a** and tetrabutylammonium salt of [6,6]-phenyl-C_{61}-butyric carboxylic acid.

Porphyrin tweezers designed for the recognition of functionalized and non-functionalized fullerenes described so far contained more or less conformationally flexible spacers which play mainly a simple structural role. It is well establish that the kind of spacer used to hold together the two binding units of the tweezer receptors, and most importantly, its conformational flexibility are key factors in controlling the binding affinity. To the best of our knowledge, besides that structural role, there are not examples of tweezer receptors in which the spacer constitutes an additional binding site able to participate in the recognition of fullerene derivatives. We envisaged that porphyrin tweezer receptors **6a** and **8a** could be useful in the recognition of [6,6]-phenyl-C_{61}-butyric acid carboxylate (PCBA). Thus, the tetrabutylammonium salt derived from [6,6]-phenyl-C_{61}-butyric carboxylate was prepared in our lab from the corresponding acid obtained by hydrolysis of the commercially available methyl ester PCBM. Initially, the calix[4]pyrrole spacer of the porphyrin tweezer is able to establish hydrogen-bond interactions with the carboxylate of the PCBA ammonium salt. This first interaction has a two-fold effect: it locks the calix[4]pyrrole in *cone* conformation creating a pyrrolic electron-rich aromatic cavity able to coordinate the alkylammonium cation of the ion pair and constitutes the switch that induces the co-facial orientation of the two porphyrin rings. Importantly, the calix[4]pyrrole spacer will also contribute to the thermodynamic stability of the 1:1 complex cooperating through the establishment of hydrogen-bonds to the π,π-interactions between the aromatic surfaces of fullerene and porphyrins. Thus, we expect an enhancement of the magnitude of the association constant of this family of porphyrin tweezers towards fullerenes compared to related examples reported in literature. Preliminary studies of the interaction of Ni-porphyrin tweezers **6a** with tetrabutylammonium [6,6]-phenyl-C_{61}-butyric carboxylate **9** (Figure 5.5a) were performed by means of ^{1}H NMR spectroscopy in d^8-THF.

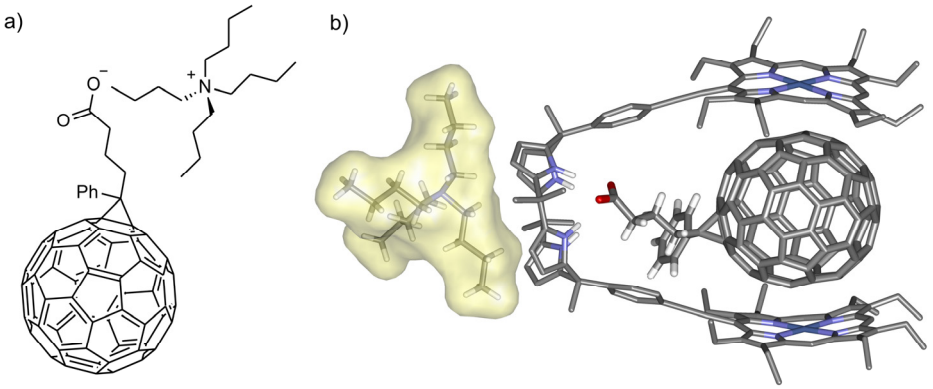

Figure 5.5 a) Molecular structure of tetrabutylammonium [6,6]-phenyl-C_{61}-butyric carboxylate **9** and b) energy-minimized structure[29] of the 1:1 sandwich complex, **9**⊂**6a**.

The addition of 0.5 equiv of **9** to a 0.5 mM solution of **6a** produced the observation of two different signals for the NH pyrrolic protons of the calix[4]pyrrole unit of tweezer **6a**. These signals were assigned to the free (11) and the bound (11´) bis-porphyrin tweezer (Figure 5.6b). The signal for the bound NH protons (11') resonates at δ = 12.0 ppm indicating their involvement in hydrogen-bonding interaction with the carboxylate.[30]

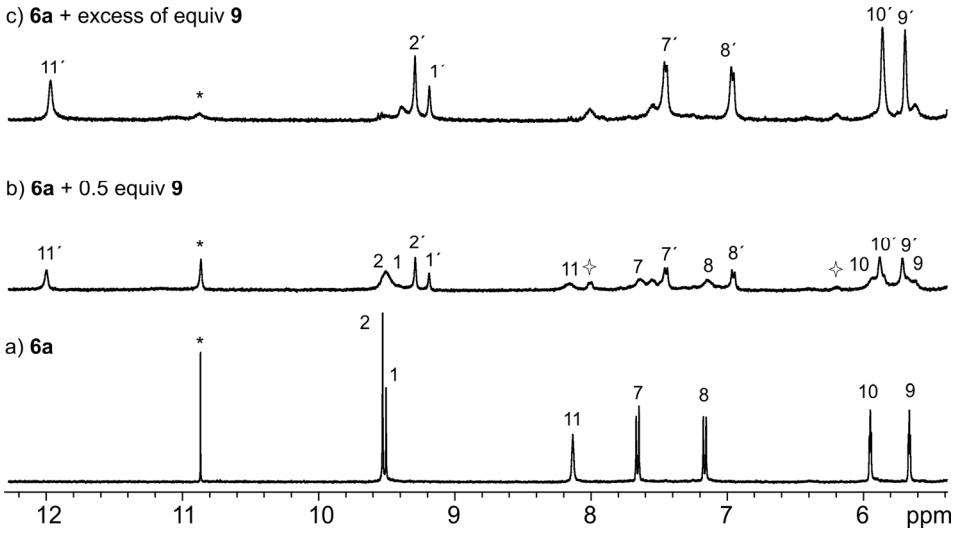

Figure 5.6 Downfield region of the ^{1}H NMR experiment (500 MHz, d^8-THF, 298 K) of a) porphyrin tweezer receptor **6a**; [**6a**]= 0.5 mM, b) **6a** + 0.5 equiv of **9** and c) **6a** + excess of **9**. Primed numbers correspond to bound **6a**.

The observation of two different set of signals for the aromatic protons (7, 8, 7' and 8') is in complete agreement with the existence of free and bound **6a**. The two signals assigned to the *β*-pyrrolic protons of bound **6a** are shifted in opposite directions respect to the unbound receptor, as expected for the conformational switch. A new set of signals are also observed for the *meso*-protons of the bound porphyrin rings that are upfield shifted with respect to the ones assigned to the free chromophores. When an excess of **9** is added only the signals that correspond to the bound receptor are detected. It is worthy to highlight that tetrabutylammonium [6,6]-phenyl-C_{61}-butyric carboxylate **9** is not soluble in THF, however complex **9⊂6a** is soluble at the working concentration conditions. These preliminary results provide strong support for the formation of a 1:1 inclusion complex **9⊂6a** (Figure 5.5b) but did not allow an unequivocal assigment of the aromatic protons of bound **9**.

5.3 Conclusion

We have synthesized two Ni metallated bisporphyrin tweezer receptors **6a** and **8a** containing calix[4]pyrrole spacers. The two receptors possess slightly different orientation of the porphyrin rings as a result of the different linkers used to connect the porphyrin and the calix[4]pyrrole units. In both cases, however, the porphyrin moiety used is the octaethylporphyrin unit. Our attempts to use Zn metallated *mesityl*-substituted porphyrins in the synthesis of related bisporphyrins were unsuccessful. We have presented preliminary results of the use of one of the bisporphyrins as porphyrin tweezer receptor in the recognition of the tetrabutylammonium salt of [6,6]-phenyl-C_{61}-butyric carboxylic acid **9**. The obtained NMR data suggest the formation of a 1:1 inclusion complex **9⊂6a**. In this complex the calix[4]pyrrole spacer orients the porphyrin units in a co-facial disposition and also participates as an additional binding site in the recognition of the [6,6]-phenyl-C_{61}-butyric carboxylate. Further studies are necessary in order to characterize thermodynamic and kinetically the complex.

5.4 Experimental section

5.4.1 General information and instrumentation

All reagents were obtained from commercial suppliers and used without further purification. Anhydrous solvents were obtained from a solvent purification system SPS-400-6 from Innovative Technologies, Inc.All solvents were of HPLC grade quality, commercially obtained and used without further purification. Routine ^{1}H NMR spectra were recorded on a Bruker Avance 400 (400.1 MHz for ^{1}H-NMR) and Bruker Avance 500 (500.1 MHz for ^{1}H NMR) ultrashield spectrometer. The deuterated solvents (Aldrich) used are indicated in the experimental part; chemical shifts, δ, are given in ppm, relative to TMS.

5.4.2 Synthetic procedures

4-(3-Methyl-3-hydroxybut-1-yn-1-yl)benzaldehyde; procedure adapted from reference[13]
^{1}H NMR (400 MHz, CD_3CN) δ (ppm) 8.74 (s, broad 2H), 7.42 (d, J~ 8.7 Hz, 2H), 6.95 (d, J~ 8.7 Hz, 2H), 6.65 (m, 2 H), 6.02 (m, 2H), 5.79 (m, 2 H), 1.96 (s, 3 H)

5-[4-(3-Methyl-3-hydroxybut-1-yn-1-yl)phenyl]-10,15,20-trimesitylporphirinato-zinc (II); procedure adapted from reference[14]
^{1}H NMR (400 MHz, CD_2Cl_2) δ 8.88 (d, J ~ 4.6 Hz, 2H), 8.77 (d, J~ 4.6 Hz, 2H), 8.73 (s, 4H), 8.22 (d, J~ 8.0 Hz, 2H), 7.84 (d, J ~ 8.7 Hz, 2H), 7.34 (s, 6H), 2.66 (s, 9H), 2.26 (s, 1H), 1.87 (s, 6H), 1.86 (s, 12H),1.75 (s, 6H).
HR-MS (ESI +ve) m/z calculated for $C_{58}H_{52}N_4OZn$: $[M+H]^+$ 885.34, found $[M+H]^+$ 885.2, $[M+Na]^+$ 907.2 , $[M+Na+MeOH]^+$ 939.2

5-(4-Ethynylphenyl)-10,15,20-trimesitylporphinatozinc(II) **1a** synthetic procedure adapted from reference[14]
^{1}H NMR (400 MHz, CD_2Cl_2) δ 8.84 (d, J ~ 4.6 Hz, 2H)), 8.78 (d, J ~ 4.6 Hz, 2H), 8.7 (s, 4H), 8.20 (d, J ~8.05 Hz, 2H), 7.9 (d, J ~ 8.0 Hz, 2H), 7.32 (s, 6H), 3.4 (s, 1H), 2.64 (s, 9H), 1.87 (s, 6H),1.86 (s, 12H).

MS (ESI +ve) m/z calculated for C_{55} H_{46} N_4 Zn: $[M+H]^+$ 827.3, found $[M+H]^+$ 827.2, $[M+Na]^+$ 849.2.

5-(4-Iodophenyl)-10,15,20-trimesitylporphinatozinc(II) **1b** synthetic procedure adapted from reference[14]

^{1}H NMR (400 MHz, CD_2Cl_2) δ 8.84 (d, J ~ 4.5 Hz, 2H)), 8.77 (d, J ~ 4.5 Hz, 2H), 8.71 (s, 4H), 8.08 (d, J ~8.4 Hz, 2H), 7.96 (d, J ~ 8.7 Hz, 2H), 7.29 (s, 6H), 2.65 (m, 9H), 1.85 (s, 6H), 1.84 (s, 12H).

Trimesitylporphinatozinc(II) derivative **1c**

Under Ar atmosphere, 5-(4-Ethynylphenyl)-10,15,20-trimesitylporphinatozinc(II) **1a** (84mg, 0.101mmol) and 4-iodoacetophenone (100 mg, 0.406mmol) were disolved in 20 ml of a 1:1 mixture of dry toluene and triethylamine freshly distilled. Then, $[Pd(PPh_3)_2Cl_2]$ (9.96 mg, 0.014 mmol) and CuI (2.7 mg, 0.014 mmol) were added. The reaction was let stirred at 45ºC for three hours. After that, the reaction crude was concentrated and the residue was subjected to silica column chromatography with dichloromethane as mobile phase. A purple product was obtained (42.4 mg, 44% yield)

^{1}H NMR (400 MHz, CD_2Cl_2) δ 8.93 (d, J ~ 4.6 Hz, 2H)), 8.79 (d, J ~ 4.6 Hz, 2H), 8.74 (s, 4H), 8.29 (d, J ~8.24 Hz, 2H), 8.06 (d, J ~8.50 Hz, 2H), 7.99 (d, J ~8.22 Hz, 2H), 7.82 (d, J ~8.37 Hz, 2H), 7.33 (s, 6H), 2.68 (s, 3H), 2.65 (s, 6H), 1.88 (s, 6H),1.87 (s, 12H).

MS (MALDI +ve) m/z calculated for $C_{63}H_{52}N_4OZn$: 946.4, found: 946.3.

The structure is also confirmed by X-ray diffraction analysis.

α,α-aryl extended calix[4]pyrrole **2c**

Under Ar atmosphere, iodo α,α-calix[4]pyrrole **2a** (40mg, 0.057mmol) and 4-ethynyltoluene (0.029ml, 0.228mmol) were dissolved in 8 ml of a 1:1 mixture of dry toluene and triethylamine freshly distilled. Then, $[Pd(PPh_3)_2Cl_2]$ (6.42 mg, 0.007 mmol) and CuI (1.59 mg, 0.007 mmol) were added. The reaction was let stirred at 50ºC overnight. After that, the reaction crude was concentrated and the residue was subjected

to silica column chromatography eluting with CH_2Cl_2/hexane 1:1 as mobile phase to obtain a yellowish solid (33 mg, 74% yield)

^{1}H NMR (400 MHz, CD_2Cl_2) δ 8.93 (d, J ~ 4.6 Hz, 2H)), 8.79 (d, J ~ 4.6 Hz, 2H), 8.74 (s, 4H), 8.29 (d, J ~8.24 Hz, 2H), 8.06 (d, J ~8.50 Hz, 2H), 7.99 (d, J ~8.22 Hz, 2H), 7.82 (d, J ~8.37 Hz, 2H), 7.33 (s, 6H), 2.68 (s, 3H), 2.65 (s, 6H), 1.88 (s, 6H),1.87 (s, 12H).

MS (MALDI +ve) m/z calculated for $C_{56}H_{52}N_4^{+\cdot}$: 780.4, found: 780.5. The structure is also confirmed by X-ray diffraction analysis.

Meso-monoformyloctaethylporphyrin Ni (II) synthetic procedure from references[19,20]

^{1}H NMR (400 MHz, $CDCl_3$) δ 11.9 (s, 1H), 9.35 (s, 1 H), 9.32 (s, 2H), 3.75 (m, 16 H), 1.74 (m, 24 H).

MS (MALDI +) m/z calculated for $C_{37}H_{44}N_4NiO$ 618.29, found $[M]^+$ 618.4. The structure is also confirmed by single crystal X-ray diffraction analysis.

5-*trans*-(2´-iodoethenyl)-2,3,7,8,12,13,17,18-octaehtylporphyrinatonickel(II) following procedures described in reference[22]

^{1}H NMR (400 MHz, $CDCl_3$) δ 9.74 (d, J~ 14 Hz, 1H), 9.49 (s, 1H), 9.48 (s, 1 H), 5.56 (d, J~ 14 Hz, 1H), 3.84 (m, 16 H), 1.77 (m, 24 H).

5-ethynyl-2,3,7,8,12,13,17,18-octaethylporphyrinatonickel(II) **5e** following standard procedures[22]

^{1}H NMR (400 MHz, $CDCl_3$) δ 9.42 (s, 2H), 9.41 (s, 1H), 4.49 (s, 1H), 4.16 (q, 4H), 3.84 (m,12H),1.75 (m, 24H).

Ni-bisporphyrin tweezer **6a**

Iodo α,α-calix[4]pyrrole **2a** (11 mg, 0.014 mmol) and 5-ethynyl-2,3,7,8,12,13,17,18-octaethylporphyrinatonickel(II) **5e** (24 mg, 0.406 mmol) were dissolved in 2 ml of a 1:1 mixture of dry toluene and triethylamine freshly distilled. Then, $[Pd(PPh_3)_2Cl_2]$ (3.38 mg, 0.005 mmol) and CuI (1.04 mg, 0.005 mmol) were added. The reaction was let stirred at 50ºC overnight. The crude was purify after two preparative thin layer silica

chromatography. The first preparative TLC was done in hexane/CH_2Cl_2 6:4 as mobile phase. The second isolated fraction was subjected to a second preparative TLC eluted with hexane/acetone 9:1. Then, the second isolated fraction corresponded with the *mono*-porphyrin product **6b** (2.2mg, 12.83%yield) and the third one to the *double*-Sonogashira product being a red-violet product **6a** (1.1 mg, 4.52% yield)

6b ^{1}H NMR (500 MHz, CD_2Cl_2) δ 9.51 (s, 2H), 9.49 (s, 1H), 7.67 (d, ^3J~8.63 Hz, 2H), 7.59 (d, ^3J~8.63 Hz, 2H), 7.43 (broad signal, 2H), 7.35 (broad signal, 2H), 7.12 (d, ^3J~8.32 Hz, 2H), 7.76 (d, ^3J~8.32 Hz, 2H), 5.99 (m, 2H), 5.75 (dd, ^4J~2.99 Hz ^3J~3.06 Hz, 2H), 5.68 (dd, ^4J~2.90 Hz ^3J~3.17 Hz, 2H), 4.27 (q, ^3J~7.35 Hz, 4H), 3.86 (m, 12H), 1.98 (s, 3H), 1.90 (s, 3H), 1.85 (t, ^3J~7.61 Hz, 6H), 1.77 (m, 18H), 1.68 (s, 6H), 1.58 (s, 6H).

HR-MS (MALDI +) m/z calculated for $C_{76}H_{81}IN_8Ni$ $[M]^{+}$ 1290.4977, found: 1290.4655.

6a ^{1}H NMR (500 MHz, CD_2Cl_2) δ 9.50 (s, 4H), 9.48 (s, 2H), 7.68 (d, ^3J~8.37 Hz, 4H), 7.43 (broad signal, 4H), 7.14 (d, ^3J~8.37 Hz, 4H), 6.03 (dd, ^4J~2.99 Hz ^3J~3.06 Hz, 4H), 5.77 (dd, ^4J~2.90 Hz ^3J~3.17 Hz, 4H), 4.27 (q, ^3J~6.85 Hz, 8H), 3.86 (m, 24H), 2.01 (s, 6H), 1.85 (t, ^3J~7.61 Hz, 12H), 1.77 (t, ^3J~7.61 Hz, 36H), 1.72 (s, 6H), 1.63 (s, 6H).

HR-MS (MALDI+) m/z calculated for $C_{114}H_{124}N_{12}Ni_2$ $[M]^{+}$ 1776.8773, found: 1776.8883.

Ni-bisporphyrin tweezer **8a**

Azida α,α-calix[4]pyrrole **7** (9mg, 0.063mmol), 5-ethynyl-2,3,7,8,12,13,17,18-octaethylporphyrinatonickel(II) **5e** (39mg, 0.063mmol) and copper (II) catalyst (2.86 mg, 5.67 µmol) were added to a 0.5-2 mL microwave reaction vessel. The vessel was placed in a 2-neck round bottom flask and the system purged with Ar three times. Freshly degassed THF (0.4 mL) was added and the reaction stirred until all the material was dissolved. Freshly degassed water was added producing a yellowish oily precipitate that rests on top of the reaction mixture. The reaction is heated in the microwave at 75ºC for 30 min. The reaction mixture is extracted into CH_2Cl_2 and washed two times with water and dried over Na_2SO_4. A preparative thin layer chromatography eluted with

a mobil phase hexane/AcOEt 8:2 was performed to obtain a second fraction that correspond to the *mono*-porphyrin product **8b** (3.8 mg, 21.4 % yield) and a third fraction as a red-violet solid that corresponds with the desired product (11mg, 41 % yield).

8b ^{1}H NMR (500 MHz, CD_2Cl_2) δ 9.66 (s, 2H), 9.68 (s, 1H), 8.09 (s, 1H), 7.81 (d, ^{3}J~8.86 Hz, 2H), 7.40 (broad signal, 2H), 7.36 (broad signal, 2H), 7.24 (d, ^{3}J~8.80 Hz, 2H), 6.99 (d, ^{3}J~9.07Hz, 2H), 6.94 (d, ^{3}J~9.07 Hz, 2H), 6.01 (dd, ^{3}J~3.11 Hz ^{4}J~2.98 Hz, 2H), 5.98 (dd, ^{3}J~2.11 Hz ^{4}J~2.98 Hz, 2H), 5.76 (dd, ^{3}J~2.99 Hz ^{4}J~2.93 Hz, 2H), 5.68 (dd, ^{3}J~2.99 Hz ^{4}J~2.93 Hz, 2H), 3.93 (q, ^{3}J~5.45 Hz, 4H), 3.91 (q, ^{3}J~5.58 Hz, 4H), 3.85 (q, ^{3}J~7.76 Hz, 8H), 2.00 (s, 3H), 1.91 (s, 3H), 1.83 (m, 14H), 1.76 (t, ^{3}J~8.08 Hz, 8H), 1.68 (s, 6H), 1.58 (s, 6H).
MS (ESI -ve) m/z calculated for $C_{76}H_{82}N_{14}Ni$ $[M+Cl]^{-}$1285.5, found: 1285.6.
8a ^{1}H NMR (500 MHz, CD_2Cl_2) δ 9.67 (s, 4H), 9.65 (s, 2H), 8.09 (s, 2H), 7.82 (d, ^{3}J~8.84 Hz, 4H), 7.42 (broad signal, 4H), 7.25 (d, ^{3}J~8.84 Hz, 4H), 6.03 (dd, ^{4}J~2.99 Hz ^{3}J~3.06 Hz, 4H), 5.78 (dd, ^{4}J~2.90 Hz ^{3}J~3.17 Hz, 4H), 3.930 (q, ^{3}J~7.5 Hz, 8H), 3.918 (q, ^{3}J~7.5 Hz, 8H), 3.85 (q, ^{3}J~ 7.53Hz, 8H), 2.95 (q, ^{3}J~7.53 Hz, 8H), 2.01 (s, 6 H), 1.837 (t, ^{3}J~7.61 Hz, 12H), 1.76 (t, ^{3}J~7.61 Hz, 12H), 1.70 (s, 6H), 1.60 (s, 6H), 1.142 (t, ^{3}J~7.61 Hz, 12H).
MS (ESI -ve) m/z calculated for $C_{114}H_{126}N_{18}Ni_2$ $[M+Cl]^{-}$1899.8, found: 1899.8.

5.5 References and notes

[1] Sun, Y. P.; Drovetskaya, T.; Bolskar, R. D.; Bau, R.; Boyd, P. D. W.; Reed, C. A. *J. Org. Chem.* **1997**, *62*, 3642.
[2] Boyd, P. D. W.; Hodgson, M. C.; Rickard, C. E. F.; Oliver, A. G.; Chaker, L.; Brothers, P. J.; Bolskar, R. D.; Tham, F. S.; Reed, C. A. *J. Am. Chem. Soc.* **1999**, *121*, 10487.
[3] Tashiro, K.; Aida, T.; Zheng, J. Y.; Kinbara, K.; Saigo, K.; Sakamoto, S.; Yamaguchi, K. *J. Am. Chem. Soc.* **1999**, *121*, 9477.
[4] Hernandez-Eguia, L. P.; Escudero-Adan, E. C.; Pintre, I. C.; Ventura, B.; Flamigni, L.; Ballester, P. *Chem-Eur J* **2011**, *17*, 14564.
[5] Sun, D. Y.; Tham, F. S.; Reed, C. A.; Chaker, L.; Boyd, P. D. W. *J. Am. Chem. Soc.* **2002**, *124*, 6604.
[6] Wu, Z. Q.; Shao, X. B.; Li, C.; Hou, J. L.; Wang, K.; Jiang, X. K.; Li, Z. T. *J. Am. Chem. Soc.* **2005**, *127*, 17460.
[7] Hosseini, A.; Taylor, S.; Accorsi, G.; Armaroli, N.; Reed, C. A.; Boyd, P. D. W. *J. Am. Chem. Soc.* **2006**, *128*, 15903.
[8] D'Souza, F.; Amin, A. N.; El-Khouly, M. E.; Subbaiyan, N. K.; Zandler, M. E.; Fukuzumi, S. *J. Am. Chem. Soc.* **2012**, *134*, 654.
[9] Eggenspiller, A.; Takai, A.; El-Khouly, M. E.; Ohkubo, K.; Gros, C. P.; Bernhard, C.; Goze, C.; Denat, F.; Barbe, J.-M.; Fukuzumi, S. *J. Phys. Chem. A* **2012**, *116*, 3889.
[10] Jokic, D.; Asfari, Z.; Weiss, J. *Org. Lett.* **2002**, *4*, 2129.
[11] Kim, D.; Lee, S.; Gao, G. H.; Kang, H. S.; Ko, J. *J. Organomet. Chem.* **2010**, *695*, 111.
[12] Kubo, Y.; Murai, Y.; Yamanaka, J.; Tokita, S.; Ishimaru, Y. *Tetrahedron Lett.* **1999**, *40*, 6019.
[13] Gryko, D.; Li, J. Z.; Diers, J. R.; Roth, K. M.; Bocian, D. F.; Kuhr, W. G.; Lindsey, J. S. *J. Mater. Chem.* **2001**, *11*, 1162.
[14] Thamyongkit, P.; Muresan, A. Z.; Diers, J. R.; Holten, D.; Bocian, D. F.; Lindsey, J. S. *J. Org. Chem.* **2007**, *72*, 5207.
[15] Valderrey, V.; Escudero-Adan, E. C.; Ballester, P. *J. Am. Chem. Soc.* **2012**, *134*, 10733.
[16] Kulikova, O. M.; Mamardashvili, N. Z. *Russ. J. Org. Chem.* **2010**, *46*, 1246.
[17] Mamardashvili, G. M.; Mamardashvili, N. Z.; Koifman, O. I. *Russ. J. Coord. Chem.* **2011**, *37*, 872.
[18] Sessler, J.L; Mozaffari, A; Johson, M.R. *Organic Syntheses* **1992**, 70, 68-78
[19] Arnold, D. P.; Johnson, A. W.; Mahendran, M. *J. Chem. Soc., Perkin Trans. 1* **1978**, 366.
[20] Arnold, D.; Johnson, A. W.; Winter, M. *J. Chem. Soc., Perkin Trans. 1* **1977**, 1643.
[21] Chen, Y. H.; Medforth, C. J.; Smith, K. M.; Alderfer, J.; Dougherty, T. J.; Pandey, R. K. *J. Org. Chem.* **2001**, *66*, 3930.
[22] Arnold, D. P.; Hartnell, R. D. *Tetrahedron* **2001**, *57*, 1335.
[23] Pognon, G.; Mamardashvilli, N. Z.; Weiss, J. *Tetrahedron Lett.* **2007**, *48*, 6174.
[24] Gomila, R. M.; Quinonero, D.; Rotger, C.; Garau, C.; Frontera, A.; Ballester, P.; Costa, A.; Deya, P. M. *Org. Lett.* **2002**, *4*, 399.

[25] Ballester, P.; Costa, A.; Castilla, A. M.; Deya, P. M.; Frontera, A.; Gomila, R. M.; Hunter, C. A. *Chem-Eur J* **2005**, *11*, 2196.
[26] The synthesis of bisporphyrins **8a** and **8b** have been done in collaboration of Dr. Louis Adriaenssens
[27] Adriaenssens, L.; Estarellas, C.; Jentzsch, A. V.; Belmonte, M. M.; Matile, S.; Ballester, P. *J. Am. Chem. Soc.* **2013**, *135*, 8324.
[28] Ozcubukcu, S.; Ozkal, E.; Jimeno, C.; Pericas, M. A. *Org. Lett.* **2009**, *11*, 4680.
[29] Geometries of the complexes were refined by performing an optimize geometry calculation with Molecular Mechanics using augmented MM3 parameters as implemented in the software CAChe WorkSystem Pro Version 6.1.12.33, Fujitsu Limited. A conjugate gradient method was used for energy minimization with a convergence energy criterion of 0.001 kcal/mol.
[30] Cafeo, G.; Kohnke, F. H.; Valenti, L.; White, A. J. P. *Chem-Eur J* **2008**, *14*, 11593.

Chapter 6

Heterodimeric Rhodium(III) Porphyrin Macrocycles for the Assembly of Pseudorotaxane and Rotaxane-like Structures

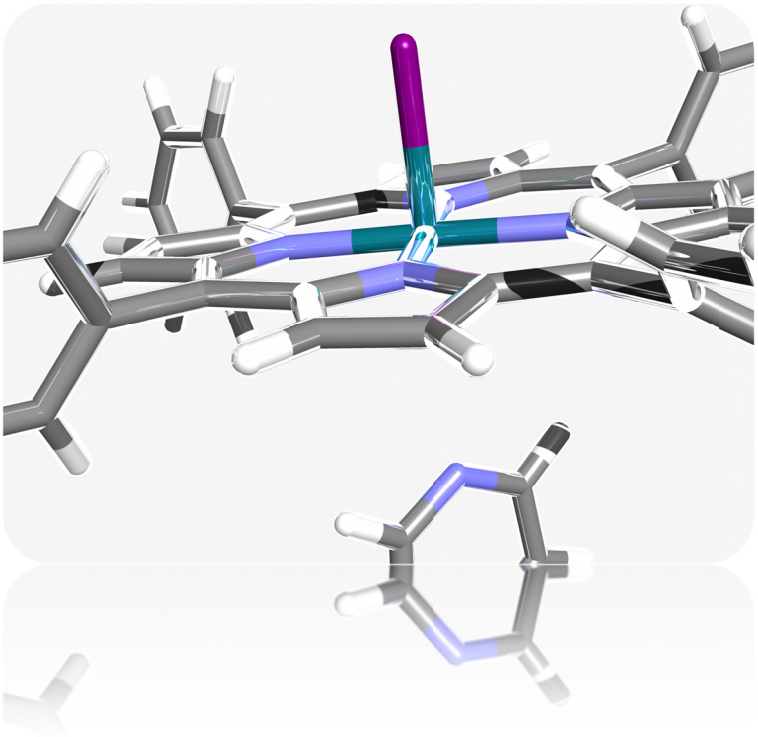

*This chapter has been done with the help of Dra. Gemma Aragay.

6.1 Introduction

Rotaxanes and catenanes have been widely studied owing to their interesting physical and chemical properties compared to their non-interlocked analogues.[1] The synthesis of [2]pseudorotaxanes and [2]rotaxanes employing non-covalent interactions (i.e. hydrogen bonding) to self-assemble the interlocked topologies of these supramolecules offers an easier and a faster alternative compared to the use of just covalent synthesis. The most common strategy for the construction of such molecular architectures implies the use of a "two-molecule approach" involving the threading of a macrocycle by a linear component. However, alternative synthetic strategies based on "three-molecules approach" have also been described for the construction of non-covalent [2]rotaxane assemblies.[2,3] Various templated synthetic approaches have been described for the preparation of rotaxane and pseudorotaxane topologies involving rhodium metallated porphyrin units as stoppers of the linear component.[4] Nevertheless, examples of interlocked assemblies containing Rh(III) porphyrins in the macrocyclic component are scarce.[5] To the best of our knowledge, there are no reported examples of the use of the metal coordination abilities of rhodium porphyrins towards pyridine ligands for the self-assembly of the macrocyclic unit in mechanically interlocked structures. Our group described the construction of [2]pseudorotaxane and [2]rotaxane structures using a series of self-assembled heterodimeric tetralactam macrocycles. The macrocycles were assembled by the formation of two kinetically labile zinc porphyrin-pyridine interactions.[6] Zn(II) porphyrins and *N*-donor ligands are known to form complexes which have weak thermodynamic stability and are kinetically quite labile. In consequence, the chemical exchange between the free and the bound states of the molecular components of the rotaxane assembly structure is fast on the ^{1}H NMR timescale. The existence of a fast exchange process complicates the analysis of the assemblies using NMR spectroscopy. One of the motivations of our work with rhodium porphyrins as building blocks is to make use of the high thermodynamic and kinetic stability of the Rh(III)-porphyrin-nitrogen bond compared to the Zn(II) analogs.[7] Hence, kinetically and thermodynamically more stable rotaxane-like structures will be assembled. Herein, we report our findings on the construction of pseudorotaxane and

rotaxane assemblies based on Rh(III) bisporphyrins. The Rh(III) centers are basic interaction sites for the assembly of supramolecular macrocycles through the formation of two coordination bonds with suitable pyridyl ditopic ligands. Subsequently, the results obtained in the study of the threading process of linear diamides through the macrocyclic supramolecular assembly are discussed.

6.2 Results and discussion

6.2.1 Design and synthesis

Monoporphyrins **1**•H_2 and **1**•Rh, pyridyl and bispyridyl-based ligands **2** and **3** and bisporphyrin **4**•H_4 were prepared according to similar methods described in the literature (Figure 6.1).[8,9]

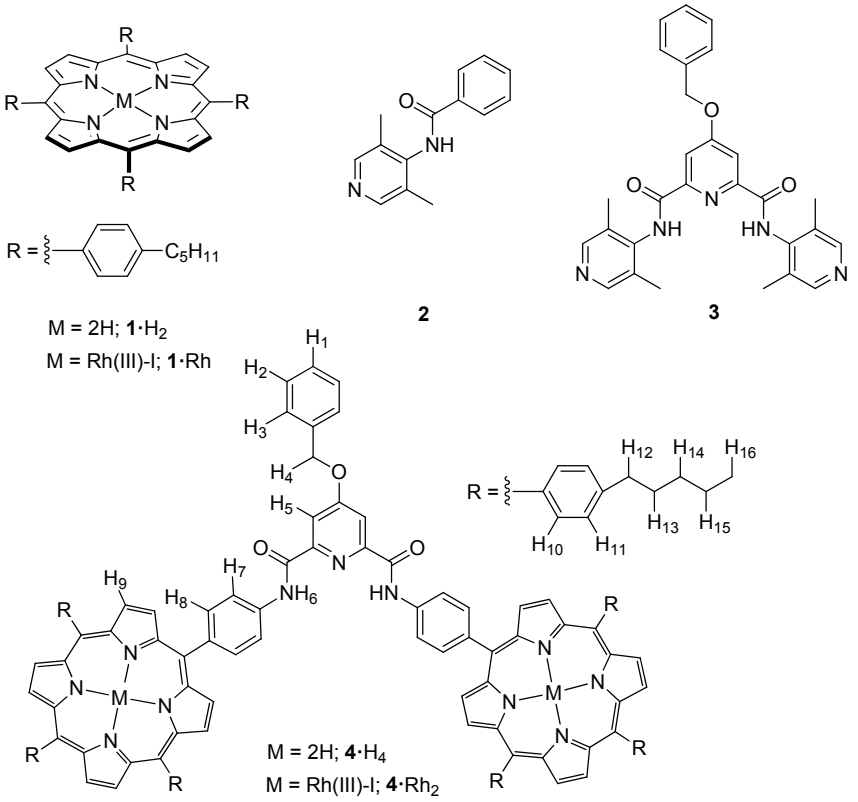

Figure 6.1 Schematic representation of the porphyrins and amines used in this study.

Metallation of free base bisporphyrin **4**•H_4 was accomplished by the reaction with the dimeric complex $[Rh(CO)_2Cl]_2$ in dichloromethane at room temperature followed by "in situ" oxidation with iodine. Column chromatography purification using neutral alumina of the reaction crude yielded the bisporphyrin **4**•Rh_2 in approximately 90 % yield (Figure 6.1).

Interestingly, the ^{1}H NMR spectra of the rhodium porphyrins **1**•Rh and **4**•Rh_2 in $CDCl_3$ (experimental section: Figure 6.9 and Figure 6. 10) show broad signals for the aromatic protons of the *meso*-phenyl substituents. This effect is likely to be provoked by the slow rotation, on the NMR time scale, of the C_{meso}-C_{phenyl} bond and by the fact that the coordination of the iodine to the metal six-coordinated Rh(III) centre renders the two faces of the porphyrin unit chemically non-equivalent.

6.2.2 Model Systems: Binding studies of monoporphyrin **1**•Rh with pyridyl derivatives.

Binding studies of monoporphyrin **1**•Rh with mono- and bispyridyl ligands **2** and **3**, respectively, were performed in order to be used as reference systems in the thermodynamic characterization of the macrocyclic assembly involving bispyridyl ligand **3** and Rh(III) bisporphyrin **4**•Rh_2.

The binding of rhodium porphyrin **1**•Rh with monopyridine **2** and bispyridyl ligand **3** was probed at room temperature using UV-Vis spectroscopy and toluene as solvent (experimental section: Figure 6.11 and Figure 6.12). Our first attempts to determine the binding constants in chloroform solution failed. Most likely, traces of acid present in $CHCl_3$, even after careful deacidification, affected the metallated porphyrin units at the low concentration used in these experiments (10^{-6} M) and produced non-symmetrical Soret bands in the UV-Vis absorption spectra.

In individual and separated experiments, solutions of **1**•Rh (4×10^{-6} M), maintained at constant concentration, were titrated by adding incremental amounts of monopyridine **2** or bispyridyl ligand **3**. In both cases, the maximum of the Soret band, initially at 415 nm, experienced a red-shift to 433 nm ($\Delta\lambda$ 18 nm) upon addition of the ligand. The titration spectra also showed the existence of an isosbestic point centred at 423 nm. A red shift of 18 nm for the Soret band of the Rh(III) porphyrin is characteristic of the

axial coordination of a pyridyl ligand.[9] The UV-Vis data obtained during the titration of **1**•Rh with **2** were analysed using a simple 1:1 binding model.[10] Conversely, when bispyridine **3** was used a binding model that considers the formation of 1:1 and 1:2 complexes was considered.

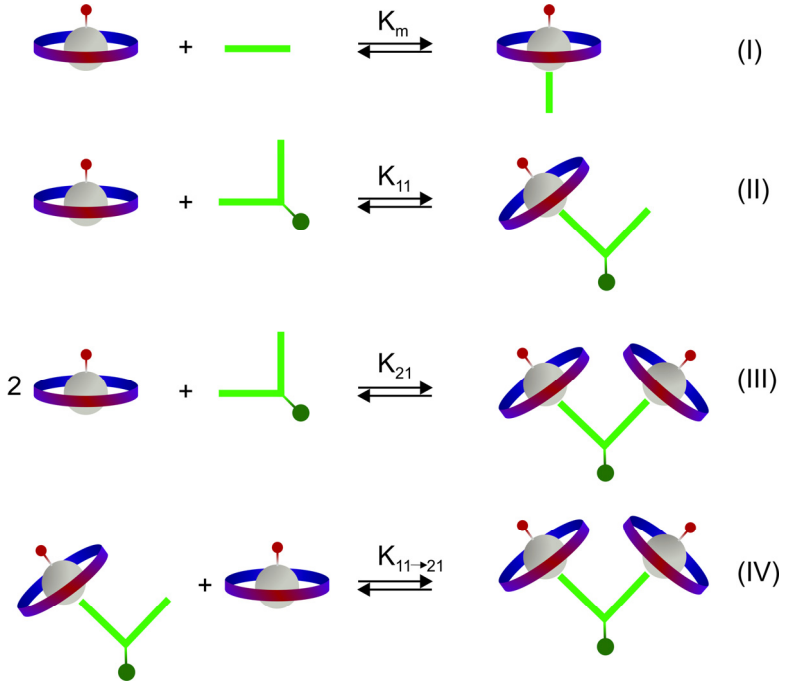

Scheme 6.1 Schematic representation of the possible equilibria involved in the binding of a porphyrin with monotopic (I) and ditopic (II)-(IV) amines. (K_{11} = $2K_m$; K_{21}=$K_m^2\alpha_P$; $K_{11\rightarrow21}\alpha_P$ = $K_m/2$) where α_P is the cooperative factor of the rhodium porphyrin **1**•Rh.

As previously reported by our group for other complexation processes involving Rh(III) porphyrins and amines,[9] the mathematical analysis of the titration data using the described binding models demonstrated that the association constants for the 1:1, **1**•Rh@**2** and **1**•Rh@**3** or the 2:1 (**1**•Rh)$_2$@**3** complexes were too high to be accurately measured at the concentrations used for the UV-Vis absorption titrations (~ 10^{-6} M). Thus, we decided to simply estimate the binding constant of K_{11} **1**•Rh@**2** as 7.0 x 10^8 M^{-1}. This is the value used as reference for the microscopic constant (K_m) of the interaction between Rh(III) and the pyridine nitrogen atom. For the Rh(III)-N interaction of **1**•Rh with bispyridyl ligand **3** we fixed the stability constant of the 1:1 complex to the statistically estimated value (K_{11} = $2K_m$, 1.4 x 10^9 M^{-1}). The value

returned from the fit of the titration data for K_{21} was 1.9 x 10^{17} M^{-2}. The magnitude calculated for K_{21} is somewhat lower than the statistical estimate ($K'_{21} = K_m^2$), 5.0 x 10^{17} M^{-2}. This result can be easily explained by assuming a decrease in the binding affinity for the second interaction of the bispyridyl ligand **3** with an additional monoporphyrin. We ascribe this anticooperative binding behaviour to the existence of unfavourable steric interactions between the two adjacent monoporphyrin units bound in the 2:1 complex (experimental section: Figure 6.13). A negative cooperativity factor (α_P) of 0.038 was calculated from the ratio between the statistically estimated and the calculated values of the stability constant of the 2:1 complex (**1**•Rh)$_2$@**3** ($K_{21} = K'_{21}\alpha_P$). The formation of the 2:1 (**1**•Rh)$_2$@**3** complex was confirmed by ^{1}H NMR spectroscopy. Upon addition of 0.5 equiv of **3** to a millimolar chloroform solution of monoporphyrin **1**•Rh (4 x 10^{-3} M) the 2:1 complex, which has two porphyrins linked to the bispyridyl ligand **3**, is the predominant species in solution (experimental section: Figure 6.14). The signals of the protons of **3** are highly affected by the current of the porphyrin rings appearing upfield shifted with respect to those for the free ligand. The signals that show the highest upfield shifts correspond to the protons *alpha* to the nitrogen atom of the pyridine residue and its methyl substituents which resonate at 0.68 ($\Delta\delta$ = -7.7 ppm) and 0.50 ppm ($\Delta\delta$ = -1.7 ppm), respectively. The magnitude of the shielding effects indicates the location of the ligand on-top of the porphyrin ring. The addition of more than 0.5 equivalent of ligand **3** produces the destruction of 2:1 (**1**•Rh)$_2$@**3** complex and the concomitant formation of the 1:1 **1**•Rh@**3** complex. The ^{1}H NMR spectrum of a solution containing an excess of **3** (> 3 equiv) with respect to **1**•Rh shows separate signals for the protons of free **3** in solution and those involved in the 2:1 and the 1:1 complexes. The integration of these signals allowed the calculation of the molar ratio **3:**(**1**•Rh)$_2$@**3:1**•Rh@**3** as 0.14 : 0.09 : 1 (experimental section: Figure 6.14). This observation is in complete agreement with the speciation calculated using the calculated/estimated association constants and the experimental **3** to **1**•Rh ratio at the concentration used for the ^{1}H NMR experiment (4 mM) (experimental section: Figure 6.15).

6.2.3 Binding studies involving **4**•Rh_2 and bispyridyl ligand **3**

The binding of **4**•Rh_2 bisporphyrin with ditopic ligand **3** in solution was studied by means of ^{1}H NMR spectroscopy at room temperature. The addition of 0.5 equiv of **3** to a millimolar solution of **4**•Rh_2 produced the observation of two separated signals for the NH amide protons of the bisporphyrin. These signals were assigned to the protons in the free (H_6) and the bound ($H_{6'}$) bisporphyrin (experimental section: Figure 6.16). In addition, a new set of signals for the *β*-pyrrolic protons of the bound bisporphyrin was detected. These signals are slightly upfield shifted with respect to the singlet of the *β*-pyrrolic protons in the free porphyrin and they split into four doublets ($H_{11'}$) corresponding to the two chemically non-equivalent protons of the *endo* and *exo* pyrrole rings of the porphyrin core in the self-assembled macrocycle (experimental section: Figure 6.16). When 1 equiv of ligand **3** is added only the signals that correspond to the protons of the bound bisporphyrin are detected. It is worth noting, the change experienced by the signals corresponding to the *ortho* and *meta* aromatic protons H_7 and H_8 of the *meso*-phenyl groups connecting the porphyrin core to the spacer. In the bound bisporphyrin, these protons appear as four well-defined doublets ($H_{7'}$, $H_{8'}$, $H_{9'}$, $H_{10'}$) owing to the slow rotation, on the ^{1}H NMR timescale, of *meso*-phenyl substituents around the single C_{meso}-C_{phenyl} bond. All the signals of the protons in the bound bispyridyl **3** appear upfield shifted compared to the free ligand. This is the expected behaviour caused by the magnetic anisotropy of the porphyrin ring-current effect to the axially bound ligand. The signals that are most affected by the magnetic anisotropy are the ones corresponding the protons *alpha* to the coordinated pyridine nitrogen atom of **3**. These aromatic protons resonate at δ = 0.69 ppm ($H_{12'}$) ($\Delta\delta$ = -7.6 ppm) in the self-assembled macrocycle (Figure 6.2). The amide NH protons of the bound ligand **3** ($H_{13'}$) are also upfield shifted as a consequence of the proximity of the porphyrin ring and appear at 6.6 ppm ($\Delta\delta$ = -3.3 ppm). Finally, the signal corresponding to the protons of the *β*-methyl substituents of the pyridyl groups of bound **3** also experience the magnetic anisotropy of the porphyrin core and shifted upfield ($H_{14'}$) ($\Delta\delta$ = -1.7 ppm) indicating that the pyridyl is axially oriented and located on top of the porphyrin ring.

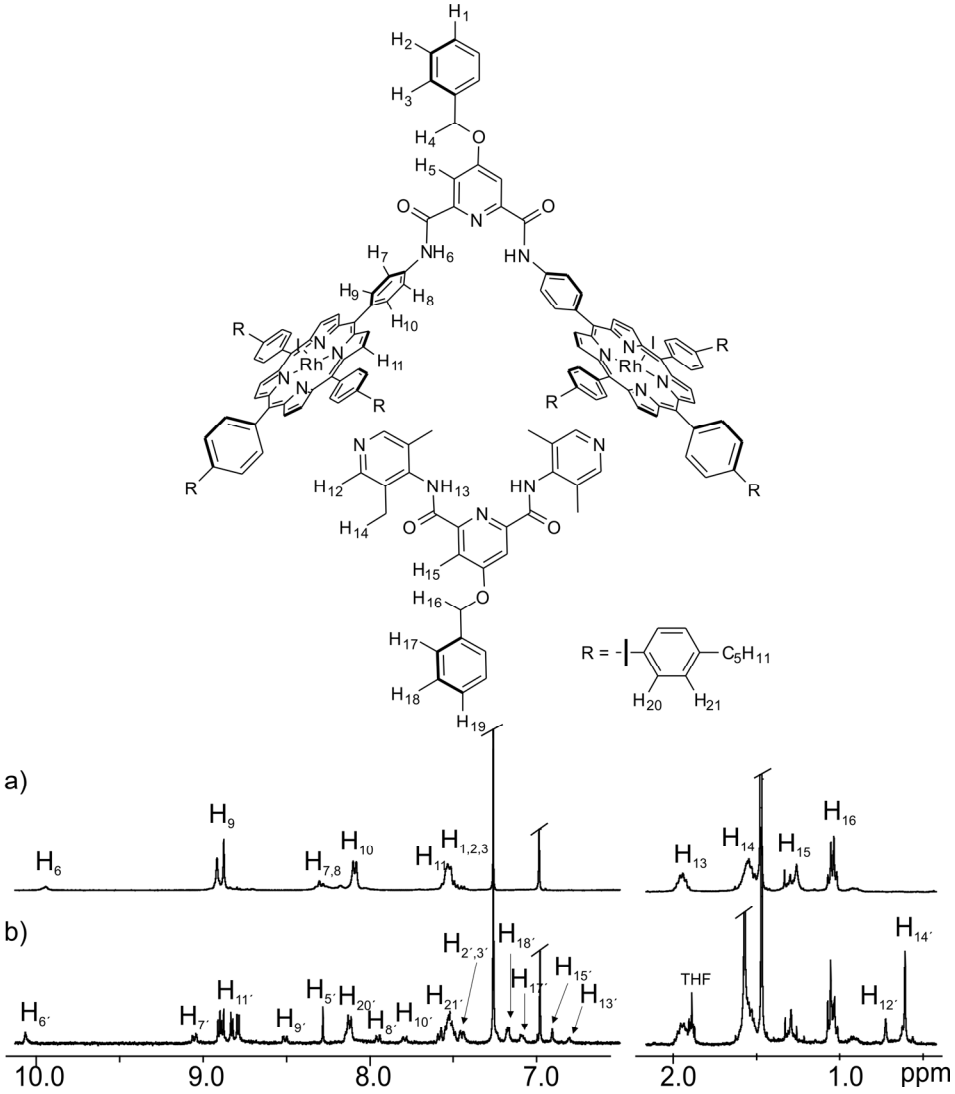

Figure 6.2 (Top) Molecular structure of the macrocycle (**4**•Rh_2)@**3** with the corresponding proton assignment. (Bottom) ^{1}H NMR spectra (500 MHz, $CDCl_3$, 298 K) of **4**•Rh_2 bisporphyrin (see Figure 6.1 for proton assignments) (a) and the macrocycle (**4**•Rh_2)@**3**. Primed numbers correspond to the complex structure (b).

ROESY experiments were very useful in assigning each signal observed in the ^{1}H NMR spectrum to the corresponding protons of (**4**•Rh_2)@**3** (experimental section: Figure 6.17). Intermolecular contacts (cross peaks) were detected between the *α*- and *β*-methyl protons of the terminal pyridines ($H_{12'}$ and $H_{14'}$) and the *β*-pyrrolic protons ($H_{11'}$) and

the aromatic protons of the *meso*-phenyl rings of the bisporphyrin **4**•Rh_2 ($H_{20'}$). This observation is in complete agreement with the formation of the proposed macrocyclic structure (**4**•Rh_2)@**3**.

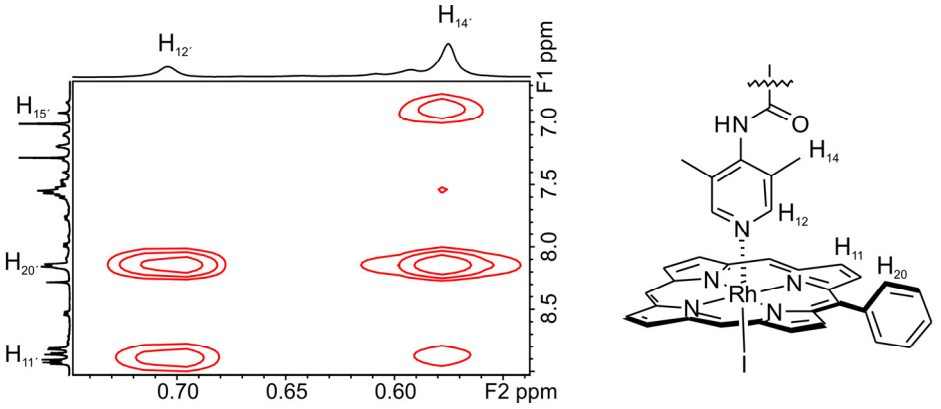

Figure 6.3 Selected region of ROESY experiment (500 MHz, p15: 0.3 s, $CDCl_3$, $1.0 \cdot 10^{-3}$M) of the 1:1 complex (**4**·Rh_2)@**3** showing correlations between the pyridine methyl protons ($H_{14'}$) and the *β*-pyrrolic protons ($H_{11'}$) and the aromatic protons of the *meso*-phenyl rings of the porphyrin ($H_{20'}$). Protons *alpha* to the pyridine ($H_{12'}$) show also correlation with *β*-pyrrolic protons ($H_{11'}$) and the aromatic protons of the *meso*-phenyl rings of the porphyrin ($H_{20'}$).

Compared to the self-assembly of a similar macrocycle involving zincated porphyrins instead of rhodium ones, the described macrocycle shows a completely different dynamic behaviour when studied by ^{1}H NMR. In the case at hand, we can clearly see two different sets of signals in the ^{1}H NMR spectrum of the mixture of **4**•Rh_2 and 0.5 equiv of **3**, (i.e. 0.5 equiv), one corresponds to the protons of the assembled macrocycle (**4**•Rh_2)@**3** and the other to the same protons in the free bisporphyrin **4**•Rh_2. The existence of a binding process in slow exchange on the ^{1}H NMR time scale between free **4**•Rh_2 and the macrocycle (**4**•Rh_2)@**3** is responsible of the duplicity of the signals. Conversely, when Zn(II) bisporphyrins were involved in the self-assembly process of macrocycles, the equilibrium showed fast chemical exchange between free and complexed species on the ^{1}H NMR time scale. The observed change in the dynamics of the self-assembly processes of the macrocycles supports the expected higher kinetic and thermodynamic stability of the macrocycles based on Rh(III)-N coordination bonds compared to the more labile Zn(II)-N counterparts. Addition of 1 equiv of **3** to a chloroform solution of **4**•Rh_2 bisporphyrin (5×10^{-3} M) produces the quantitative self-assembly of the macrocycle. This observation indicates that the binding constant of the

self-assembled macrocycle is too high to be determined by ^{1}H NMR spectroscopy. For this reason, we decided to use UV-Vis spectroscopy in the thermodynamic characterization of the self-assembly process (experimental section: Figure 6.18). We performed titration experiments in toluene solution due to problems related to traces of acid in $CHCl_3$ solutions (*vide supra*). Similarly to the results obtained with the model system (**1**•Rh), addition of **3** to a solution of **4**•Rh_2 resulted in a red shift of the maximum of the Soret band in the UV-Vis spectra of 16 nm (from 416 to 432 nm) and the appearance of a single isosbestic point centred at 423 nm. These observations are indicative of the complexation of the bispyridyl ligand **3** and the metallated bisporphyrin in axial geometry and support the existence of a two species equilibrium. The fit of the UV-Vis titration data to a 1:1 theoretical binding model only allowed us to estimate that the binding constant must be higher than 10^7 M^{-1} because in the presence of 1 equiv of **3** the shift of the Soret band achieved saturation.[10] The sensitivity of the UV-Vis titrations does not allow to perform experiments at concentrations lower than 0.5×10^{-6} M for **4**•Rh_2. The unavailability of an accurate value for the stability constant of the supramolecular macrocycle eliminated the possibility to determine the effective molarity (EM) value of the assembly. We are very much interested in comparing EM values for structurally analogous assemblies based on intermolecular interaction of significantly different strength. Our aim is to find out if the strength of the intermolecular interactions is related to the EM value. The comparison of EM values for assemblies based on Zn-N and Rh-N interaction seemed to be a suitable model system. Unfortunately, the high thermodynamic stability of the Rh-N interaction hampered the accurate determination of the EM value. We expect to determine this EM value in further studies directed towards the thermodynamic characterization of the destruction process of the supramolecular macrocycle yielding the open 2:1 complex. Taken together, the results described above indicate that the combination of an equimolar mixture of bisporphyrin **4**•Rh_2 and ditopic ligand **3** induces the quantitative self-assembly of the macrocycle (**4**•Rh_2)@**3** (Figure 6.4) owing to the formation of two kinetically and thermodynamically highly stable Rh(III)-N metal coordination bonds.

The spacer in the bisporphyrin component **4**•Rh_2 was selected based on the previous experience of the group. The 2,6-dicarboxamide linker provided the thermodynamically

most stable self-assembled macrocycles in our studies with the analogous Zn(II) bisporphyrin. The intramolecular hydrogen bond interactions established between the amide NH's and the pyridine nitrogen of the spacer favour the *cis* disposition of the porphyrins in an almost perpendicular orientation and yielding a preorganized system ideal for a ditopic interaction with nitrogen ligands with a similar angle (~96º) between the heteroatoms. Simple molecular modelling studies of the macrocyclic structure shows that rhodium bisporphyrins are indeed oriented almost perpendicularly displaying a distorted rectangular geometry upon interaction with the bispyridyl ligand. The parallel sides of the distorted rectangle are slightly different in length (Figure 6.4).

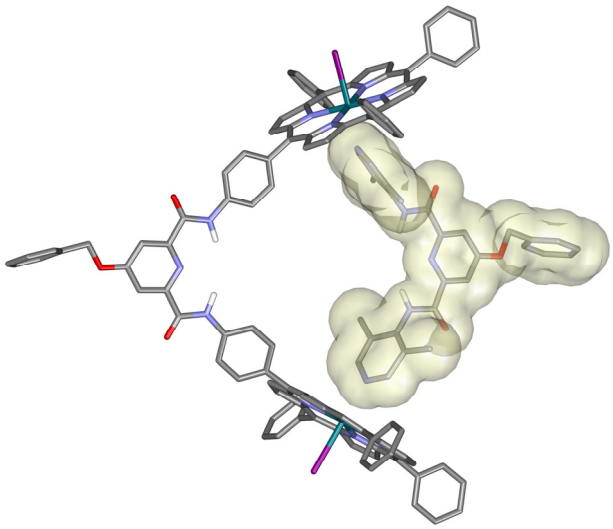

Figure 6.4 Energy-minimized[11] structure of the (**4**•Rh_2)@**3** macrocycle.

In order to achieve a perfect ditopic interaction, the geometry of the rectangular assembly requires that the linkers are distorted from the ideal 90º. The assembled macrocycle (**4**•Rh_2)@**3** features four hydrogen-bond groups (amides) with the NH donor units converging towards the interior of the cavity. Two amide groups belong to the bisporphyrin **4**•Rh_2 and the other two to the bispyridyl ligand **3**. The macrocycle was designed as a new "non-covalent" cyclic component through which linear components can be threaded yielding supramolecular structures with rotaxane or pseudorotaxane topologies.

6.2.4 Pseudorotaxane and rotaxane-like structures based on the (**4**•Rh_2)@**3** macrocycle.

Once the macrocycle (**4**•Rh_2)@**3** was characterized, we studied its binding properties with linear diamines **5** and **6**.[6] The interaction of diamine **5** with an equimolar mixture of **4**•Rh_2 and **3**, which provide the assembled macrocycle, was proven by ^{1}H NMR titration experiments. The addition of incremental amounts of **5,** induced downfield shifts in the signals of the NH amide protons of both components, **4**•Rh_2 and **3,** of the macrocycle. When 2 equiv of the linear diamine **5** were added to the solution of the pre-formed (**4**•Rh_2)@**3** macrocycle, the signals of the NH amide protons of the bisporphyrin ($H_{6'}$) and the bispyridyl ligand ($H_{13'}$) appeared downfield shifted $\Delta\delta$ = 0.27 and 0.75 ppm, respectively, compared to the free macrocycle

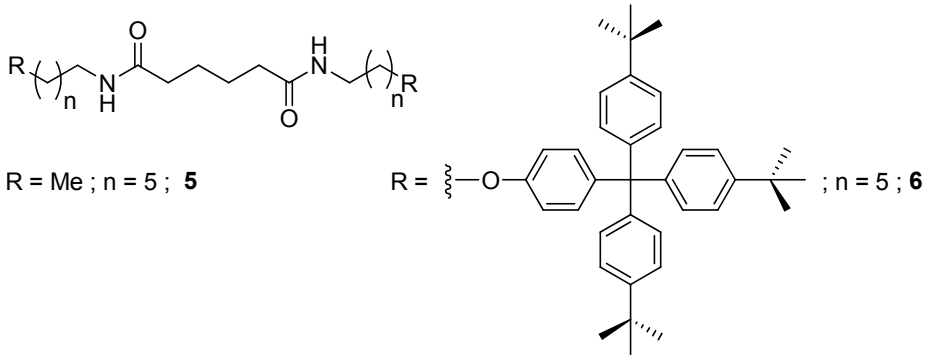

Figure 6.5 Molecular structures of linear diamides **5** and **6**.

These observations suggest the formation of hydrogen-bonding interactions between the four amide groups of (**4**•Rh_2)@**3** and the carbonyl oxygen's of **5** (Figure 6.6). In agreement with this hypothesis, the signals of the NH protons of the linear diamide **5** did not display significant chemical shift changes during the titration experiment. In short, the amide NHs of the linear component are not involved in the hydrogen bonding recognition event. The observation of a single signal for the amide NHs of the macrocyclic component that shift downfield upon increasing the amount of **5** supports the existence of a fast chemical exchange process on the NMR time scale between free and bound state.[2] The association constant value for the interaction between (**4**•Rh_2)@**3** and **5** was calculated to be 180 M^{-1}.[12] The value of the association constant is of the

same order of magnitude than the one reported for the analogous Zn(II) porphyrin systems.[6] This finding indicates that the strength of the metal coordination bonds used to template the formation of the macrocycle does not have a significant effect on the thermodynamic stability of the complexes formed with the linear diamide **5**. Thus, the thermodynamic stability of the formed aggregates is mainly determined by the four intermolecular hydrogen bonds established between the assembled macrocycle and the linear diamide. It is worth noting that the adipic amide ligand **5** can bind the macrocycle (**4**•Rh_2)@**3** and form four hydrogen bonds by means of non-threaded geometry or it can be threaded through the macrocycle. In other words, the interaction of the macrocyclic cavity and ligand **5** can either yield a pseudorotaxane-like complex or not. In both cases, the need of dissociation of the Rh(III)-N coordination bonds is not required for the disassembly of the complex.

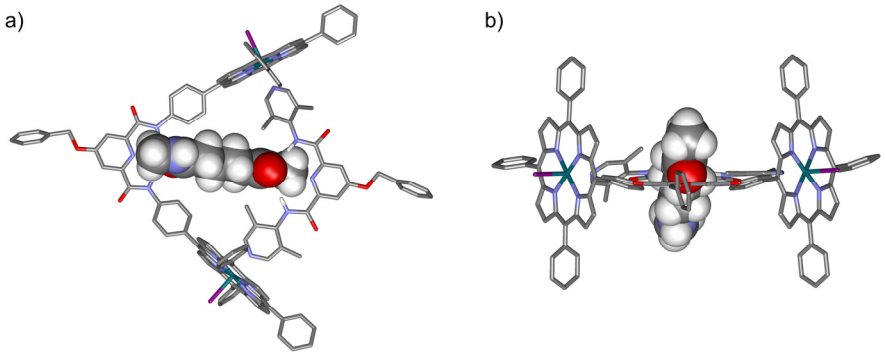

Figure 6.6 Energy-minimized[11] structure of complex (**4**•Rh_2)@**3**⊂**5**; front (a) and side (b) views.

A different dynamic behavior was observed during the complexation studies of the linear diamide **6** with (**4**•Rh_2)@**3**. Two separated signals for the amide NH protons ($H_{6'}$) of the bisporphyrin unit of the macrocycle resonated at 10.4 ppm and 10.9 ppm in the ^{1}H NMR spectrum of a solution of (**4**•Rh_2)@**3** and 2 equiv of **6**. Both signals are downfield shifted compared to the same protons in the free macrocycle (10.1 ppm) (Figure 6.7, left). We attributed the observed splitting of the NH protons to the existence of a chemical exchange process between the free and the bound macrocycle that is slow on the NMR time scale. The slow exchange dynamics observed for the binding process do not relate well kinetic stability with the thermodynamic stability measured for the complex. Consequently, the high kinetic stability detected for the complex must be the

result of other forces controlling guest dissociation than the simple host-guest interaction.

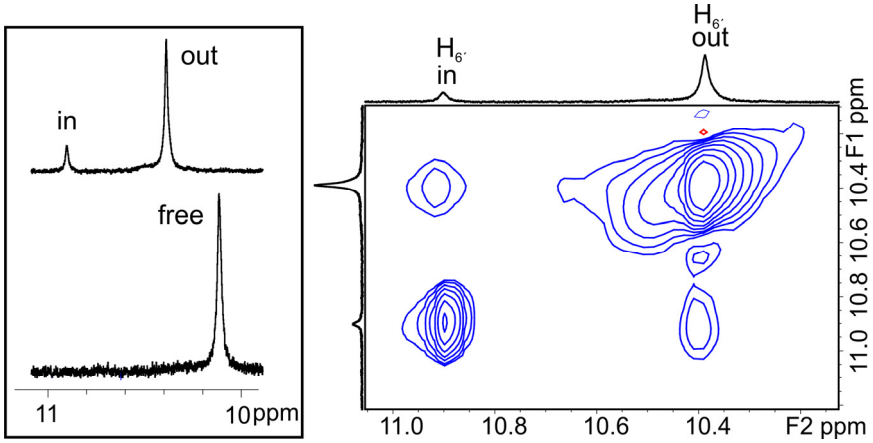

Figure 6.7 Left. Selected region of the ^{1}H NMR (400MHz, $CDCl_3$ and 298K) spectra of free (**4**•Rh_2)@**3** (bottom) and (**4**•Rh_2)@**3** with 2 equiv ligand **6** (top). Right. Expansion of the EXSY experiment at 298 K; [(**4**•Rh_2)@**3**] = 7 mM; 2 eq of **6**.

If one assigns a [2]rotaxane topology to some of the complexes formed by the interaction of (**4**•Rh_2) and **3**, then the complex dissociation implies the breaking of at least one of the two Rh-N coordination bonds used for the assembly of the macrocycle (Figure 6.8). If this was the case, the dissociation of the complex is mainly controlled by the thermodynamic stability of the macrocycle explaining the observed slow exchange dynamics for the binding process.

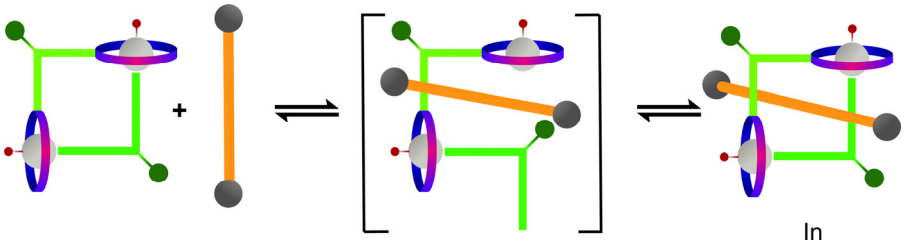

Figure 6.8 Process involved in the **6**⊂[(**4**•Rh_2)@**3**] rotaxane formation. The key intermediate is represented in brackets.

Moreover, while the intensity of the NH signal resonating at 10.9 ppm increases upon addition of excess of **3**, which represents the expected behaviour for an increase in the concentration of the complex with [2]rotaxane topology, quite unexpectedly the second signal of the NH protons initially centered at 10.4 ppm shifts downfield. We ascribed

the initial downfield shift of this signal compared to free macrocycle (**4**•Rh_2)@**3** and its unexpected chemical shift change on addition of excess **6** to the existence of the second binding geometry for the complex **6**⊂(**4**•Rh_2)@**3.** In this alternative geometry of the complex, the interaction between the linear diamide **6** and the macrocycle (**4**•Rh_2)@**3** also takes place through the formation of four hydrogen bonds but does not require the threading of the linear component through the macrocycle**.** Thus, two different binding equilibria between (**4**•Rh_2)@**3** and **6** are occurring simultaneously in solution: (a) one featuring fast exchange dynamics on the NMR time scale and involving the interaction of the linear component and the macrocycle affording a non-threaded complex geometry and (b) the other showing slow exchange dynamics on the NMR timescale and implying the formation of a complex with [2]rotaxane topology (Figure 6.8 and Figure 6.21). Additionally, the signals corresponding to the methylene protons *alpha* to the amide groups of the linear amide **6** experience a downfield shift. Most likely, this is caused by the magnetic shielding exerted by the aromatic groups that shape the internal cavity of the macrocycle on the threaded diamide. The small difference in chemical shift that exists between the free and threaded signals of the *alpha* protons in the linear diamide provokes the observation of the binding process as a fast chemical exchange on the NMR timescale.

In striking contrats to the results discussed above, when Zn(II) bisporphyrins are involved in the assembly of the macrocyclic component, at room temperature, the ^{1}H NMR spectrum in the presence of an excess of linear diamide ligand **6** showed a time-averaged signal for the NH bisporphyrin protons ($H_{6'}$). Lowering the temperature of the solution mixture at 253 K allowed the observation of two separate signals for the NH protons of the Zn(II) bisporphyrin that were assigned to the free and bound macrocycle involved in a slow chemical exchange on the ^{1}H NMR timescale. Taken in concert, these results indicate that the kinetic stability of the macrocyclic structure has been significantly increased when the bisporphyrin unit of the macrocyclic assembly is metallated with Rh(III) instead of Zn(II). At room temperature the rate constant for the dissociation of the [2]rotaxane assembly **6**⊂(**4**•Rh_2)@**3** was determined using two dimensional exchange spectroscopy (2D-EXSY) as $k_{(\mathbf{4}\bullet Rh2)@\mathbf{3}\subset\mathbf{6}} = 0.36\ s^{-1}$. The areas of the diagonal and the cross-peaks corresponding to the NH signals ($H_{6'}$) for the exchange

process between the [2]rotaxane and the free/externally bound macrocycle were used in the calculation (Figure 6.7, right). The value of the dissociation rate constant corresponds to an energy barrier ($\Delta G^{\neq}$) of 18.5 kcal/mol at 298 K. Analogous [2]rotaxane-like assemblies based on Zn(II)-bispophyrins showed a dissociation rate constant of $k_{rotaxane}$ = 13 s^{-1} that translates into an energy barrier of 14.4 kcal/mol at 253 K.[6] Even at room temperature, the difference of 4.1 kcal/mol in the energy barrier for the dissociation of the two different [2]rotaxane assemblies (Rh(III)-based rotaxane vs Zn(II)-based rotaxane) highlights the increase in the kinetic stability of the threaded architecture provoked by the change of the metal center at the porphyrin core, from Zn(II) to Rh(III).

6.3 Conclusion

In conclusion, we have demonstrated the quantitative self-assembly of a macrocycle formed by the interaction between a rhodium bisporphyrin **4**•Rh_2 and a bispyridyl ligand **3** through two Rh(III)-N coordination bonds. The use of rhodium porphyrins for the self-assembly of the macrocycle provides a sensible increase in the thermodynamic stability of the cyclic structure compared to their Zn(II) counterparts. Unfortunately, UV-Vis spectroscopy studies did not allow the accurate determination of the stability constant of the macrocyclic assembly due to its large estimated magnitude (> 10^7 M^{-1}). The threading of the self-assembled macrocycle with linear neutral diamides through the establishment of four intermolecular hydrogen bonding interactions has been accomplished and yields complexes with [2]pseudorotaxane and [2]rotaxane like topologies. The use of Rh(III) metallated porphyrin instead of Zn(II) analogue induces a sensible increase in the kinetic stability of the rotaxane-like structure but has an almost negligible effect in its thermodynamic stability. Due to the existence of bulky stoppers in the linear ligand **6**, the formation/dissociation of the [2]rotaxane **6**⊂(**4**•Rh_2)@**3** assembly requires the rupture of one of the coordination Rh(III)-N bonds that are holding the cyclic structure. The higher kinetic/thermodynamic stability featured by the (**4**•Rh_2)@**3** macrocycle compared to the Zn(II) counterpart allowed to study at room temperature of the dynamic properties of the binding process with the linear diamide **6** yielding the interwoven assembly **6**⊂(**4**•Rh_2)@**3**. EXSY experiments were useful to

determine the rate constant for the dissociation of the [2]rotaxane based on Rh(III) metal centers and confirmed a significant increase in its kinetic stability compared to the Zn(II) analogues. However, the higher kinetic and thermodynamic stability provided by the (**4**•Rh_2)@**3** macrocycle compared with the Zn(II) counterpart does not have a significant effect on the thermodynamic stability of the [2]rotaxane assembly that derives from it. The thermodynamic stability of **6**⊂ (**4**•Rh_2)@**3** is mainly controlled by the formation of four hydrogen-bonding interactions between the linear component and the amide groups of the macrocyclic assembly. These intermolecular interactions are identical in the two [2]rotaxane architectures constructed using Rh(III) or Zn(II) metal centers in the bisporphyrin unit of the macrocyclic component.

6.4 Experimental section

6.4.1 General information and instrumentation

All solvents and reagents (analytical grade and spectroscopic grade) were obtained from Sigma-Aldrich and used as received. All solvents were HPLC grade quality commercially obtained and used without further purification. deuterochloroform and chloroform were deacidified by passing through a short column of aluminium oxide 90 active, neutral (Merck).

^{1}H NMR spectra were recorded on a Bruker Avance 400 and 500 ultrashield spectrometers. Chemical shifts (δ) are reported in ppm, relative to TMS. UV-Vis titrations were carried out on a Shimadzu UV-2401PC. UV-Vis spectrophotometric titrations were analyzed by fitting the whole series spectra using the software SPECFIT 3.0 from Spectrum Software Associates.

6.4.2 Synthetic procedures

Synthesis of **4**·Rh_2

To a dichloromethane solution of **4**·H_2 (148 mg, 0.077 mmol) and sodium acetate (127 mg, 1.54 mmol) was slowly added a solution of $[Rh(CO)_2Cl]_2$ (72 mg, 0.185 mmol) in CH_2Cl_2. The mixture was stirred for 4 hours at room temperature under argon

atmosphere. Afterwards, iodine (118 mg, 0.465 mmol) was added and the mixture was stirred at room temperature overnight. The solvent was evaporated and the residue was taken up in CH_2Cl_2 and washed 3 times with a KI solution, once with water and dried with Mg_2SO_4. The residue was purified by column chromatography eluting with a mixture 8:2 CH_2Cl_2:THF to yield a purple-red solid residue (90 % yield).

^{1}H-NMR δ (400 MHz, $CDCl_3$): 9.67 (br, 2H), 8.92 (m, 16H), 8.22 (m, 8H), 8.1 (m, 12H), 7.55 (m, 17H), 5.43 (s, 2H), 2.95(m, 12H), 1.94 (m, 16H), 1.56 (m, 16H), 1.03 (m, 24H).

MS (MALDI+) *m/z* calculated for $C_{132}H_{125}I_2N_{11}O_3Rh_2$ $[M-I]^+$ 2245.7; found 2245.9.

Synthesis of **2**

A solution of 3,5-dimethylpyridin-4-amine and *N*-ethyl-*N*-isopropylpropan-2-amine in dry CH_2Cl_2 under argon atmosphere was cooled down to 0ºC. Benzoyl chloride was added dropwise over it and the mixture was stirred overnight at room temperature under inert atmosphere. The white precipitate was filtered and washed three times with CH_2Cl_2. The product was purified by chromatography eluting with AcOEt. Finally a white solid was obtained in a 15% yield.

^{1}H-NMR δ (400 MHz, $CDCl_3$): 8.27 (br, 2H), 8.13 (br, 2H), 7.92 (m, 2H), 7.57 (m, 1H), 7.46 (m, 2H), 2.19 (s, 6H).

HR-MS (ESI+) *m/z* calculated for $C_{36}H_{32}N_2O_2$ $([M+Na])^+$ 547.2361; found 547.2353.

Synthesis of **7**

Over an ethanol solution (5 mL) of *N*-(2,2-diphenylethyl)hydroxylamine (0.2g, 0.938 mmoL) was added dropwise during 20 min a solution of isophthalaldehyde (0.06g, 0.447 mmol) in 3 mL of ethanol. The solution was stirred at room temperature overnight under inert atmosphere. The white precipitate was filtered, washed with cold ethanol and dried under vacuum to give the desired product as a white powder.

^{1}H-NMR δ (400 MHz, $CDCl_3$): 8.69 (s, 1H), 8.21 (d, 8.0 Hz, 2H), 7.3 (t, 8.0 Hz, 1H), 7.29 (m, 20H), 7.04 (s, 2H), 5.02 (t, 7.8 Hz, 2H), 4.50 (d, 7.8 Hz, 4H).

HR-MS (ESI+) *m/z* calcd for $C_{14}H_{14}N_2O$ $([M+H])^+$ 277.1184; found 227.1186.

6.4.3 Experimental section: figures

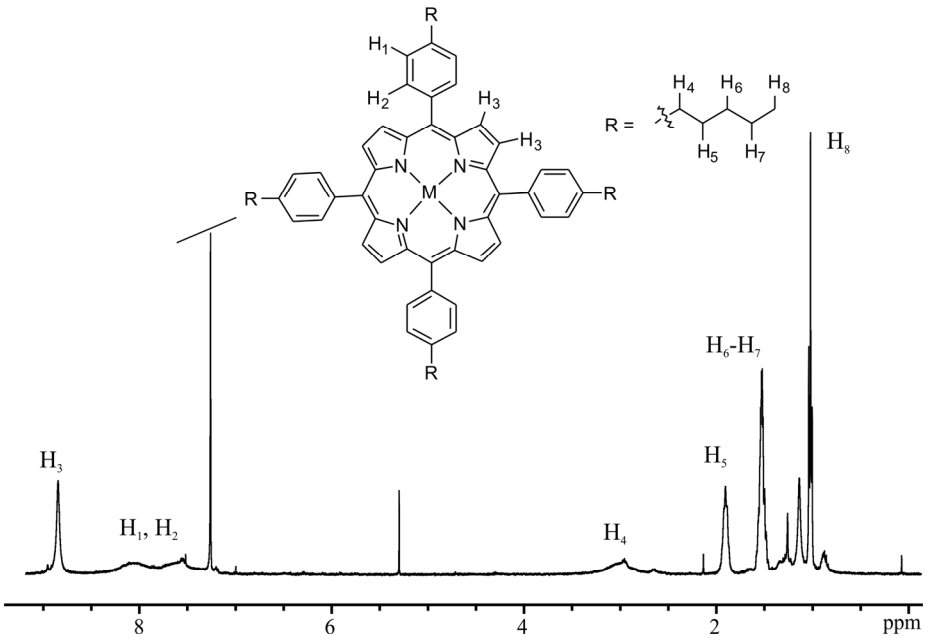

Figure 6.9 ^{1}H NMR (400 MHz, 298 K) spectrum of monoporphyrin **1**·Rh in $CDCl_3$.

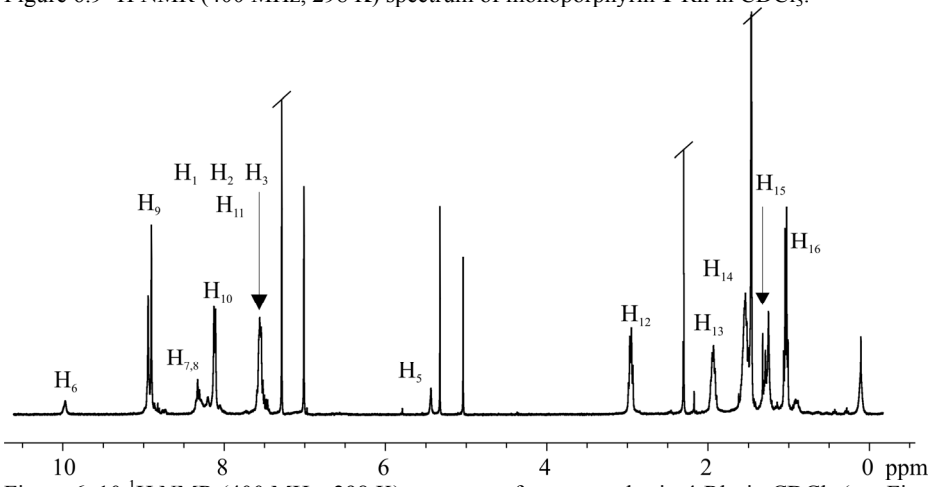

Figure 6. 10 ^{1}H NMR (400 MHz, 298 K) spectrum of monoporphyrin **4**·Rh_2 in $CDCl_3$ (see Figure 6.1 for proton assigments).

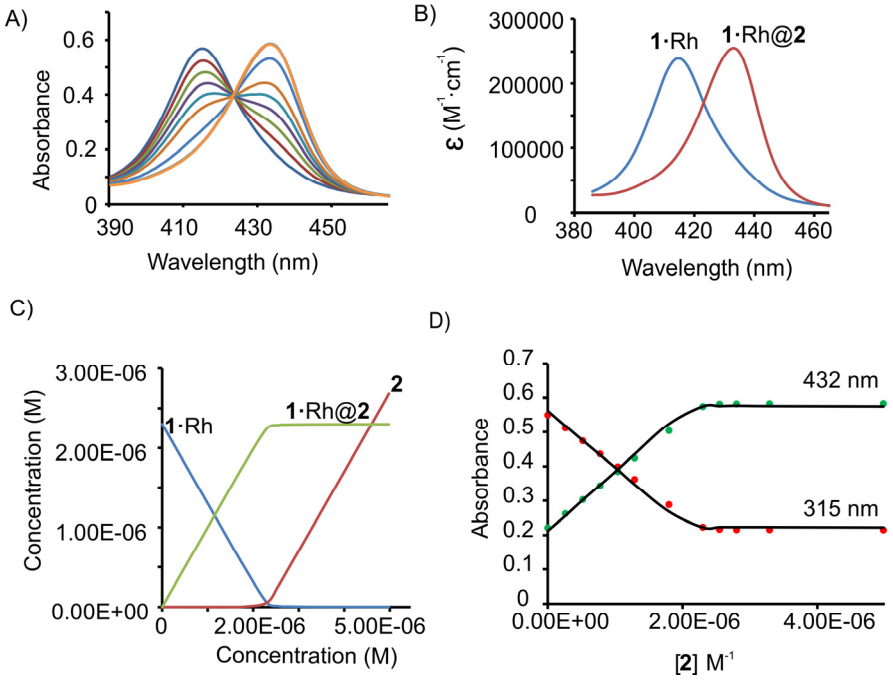

Figure 6.11 Spectra of the UV-Visible titration of **1**•Rh with **2** in toluene at 298 K for the calculation of K_m Rh(III)-N. The concentration of the porphyrin was maintained constant throughout the titration (4.0×10^{-6} M in a 10 mm path cell). Measured UV-Visible spectra (a) and predicted spectra (b) of the free porphyrin and 1:1 complex formed. Speciation curves during titration (c) and fitting of the titrations data at selected wavelengths (d) to the theoretical binding model considering the porphyrin in two different stoichiometric states (free and 1:1 complex).

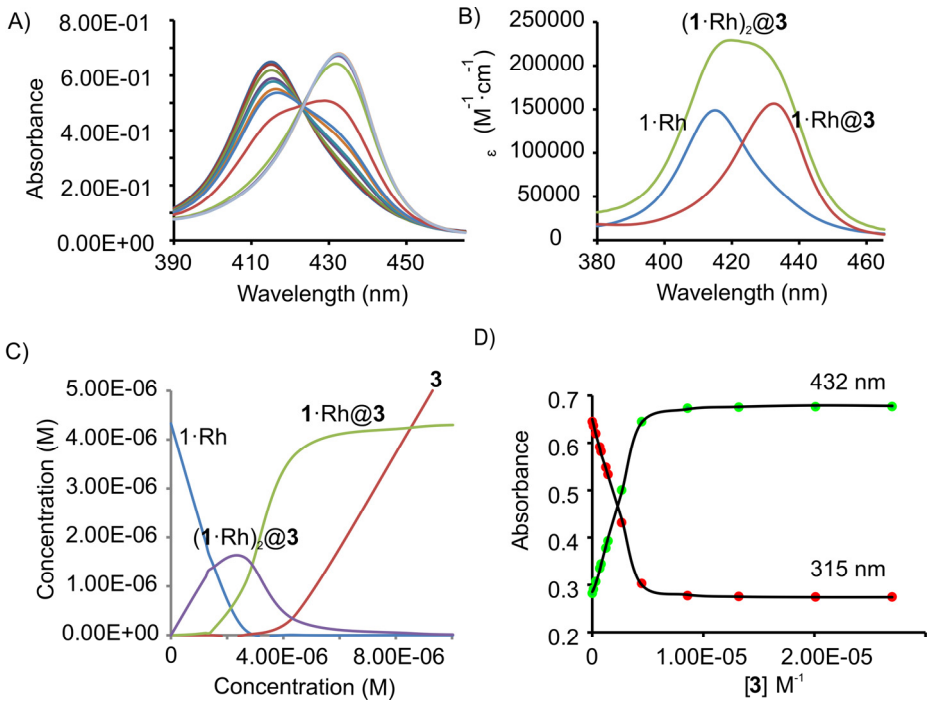

Figure 6.12 Spectra of the UV-Visible titration of **1**•Rh with **3** in toluene at 298 K. The concentration of the porphyrin was maintained constant throughout the titration (4.0×10^{-6} M in a 10 mm path cell). Measured UV-Visible absorption spectra (a) and predicted spectra (b) of the free porphyrin, the 2:1 and the 1:1 complex formed. Speciation curves during titration (c) and fitting of the titrations data at selected wavelengths (d) to the theoretical binding model.

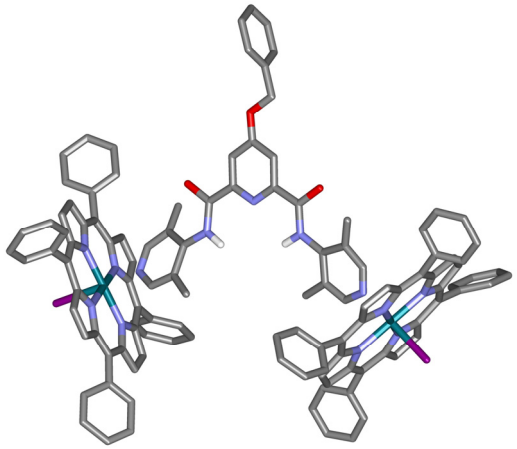

Figure 6.13 Energy-minimized structure[11] of the interaction of **1**•Rh with **3** in (**1**·Rh)$_2$@**3**. Aliphatic pentyl chains of the *meso*-aromatic rings have been omitted for clarity.

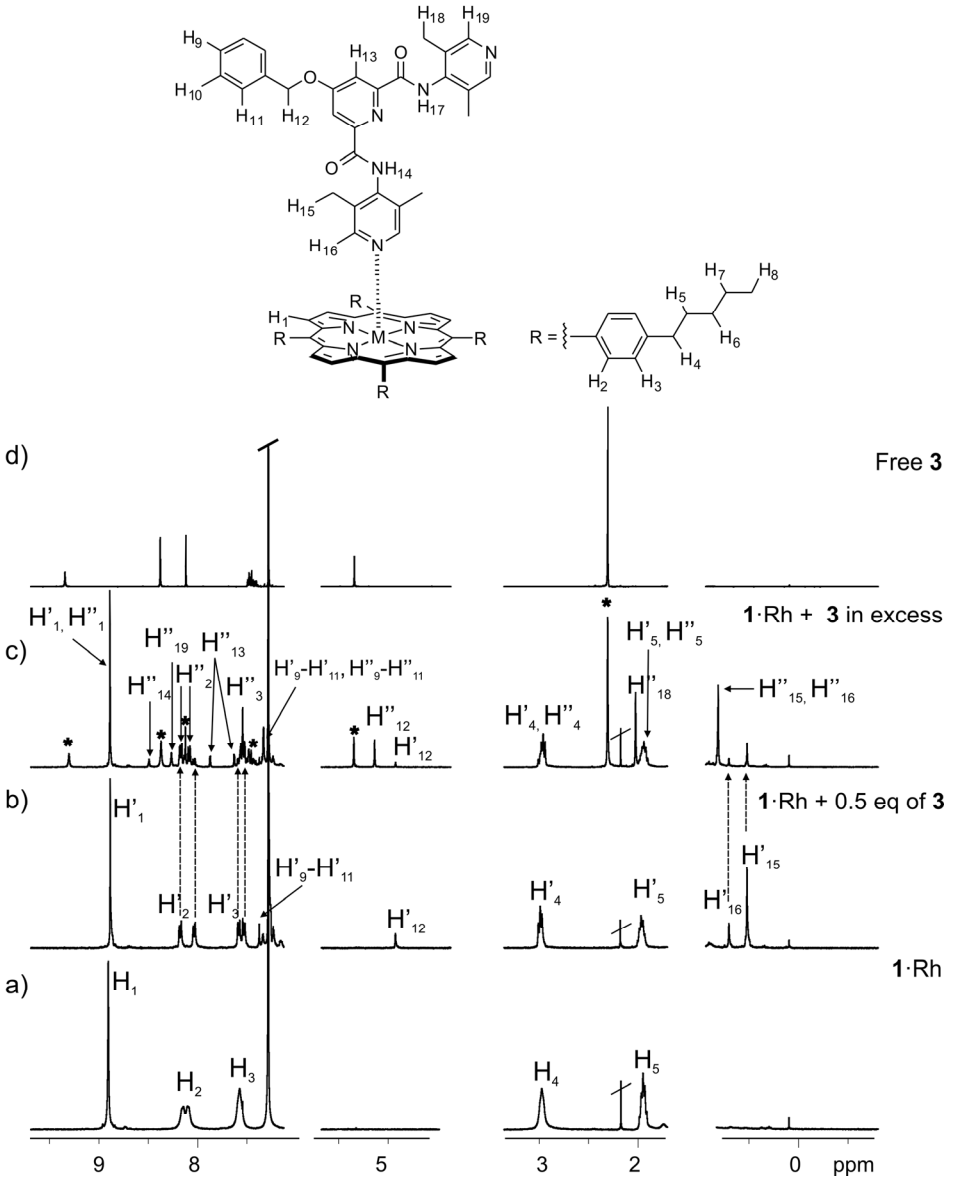

Figure 6.14 ^{1}H NMR spectra of free **1**·Rh (a), 2:1 complex (**1**·Rh)$_2$@**3** (b) and a mixture of 2:1 complex (**1**·Rh)$_2$@**3**, 1:1 complex (**1**·Rh)@**3** and free **3** (c). d) ^{1}H NMR spectra of free **3**. Protons H are referred to the free **1**·Rh, protons H' are referred to the 2:1 complex (**1**·Rh)$_2$@**3**, and protons H'' are referred to the 1:1 complex (**1**·Rh)@**3**. * Signals corresponding to free **3**.

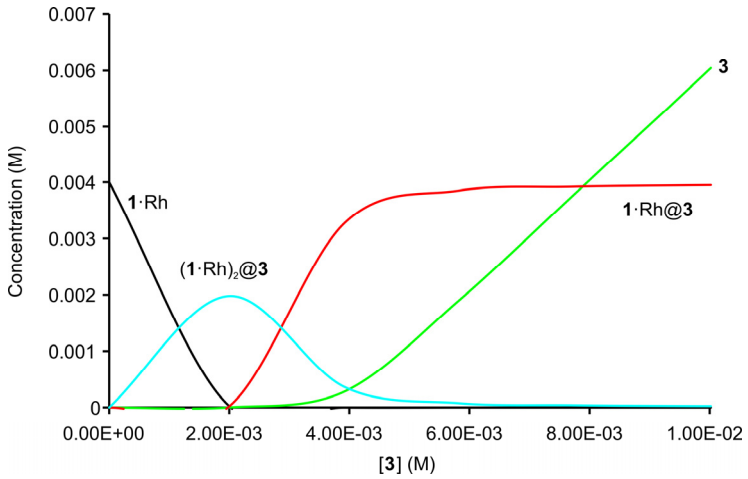

Figure 6.15 Theoretical speciation curves for a titration of **1**·Rh with bispyridyl ligand **3** considering the estimated association constants.

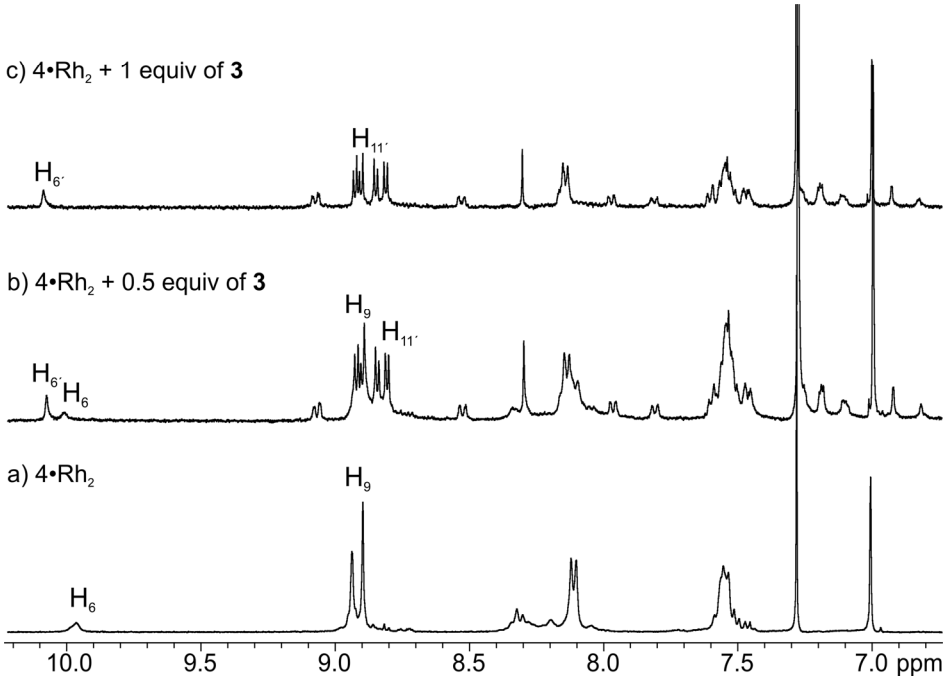

Figure 6.16 Selected region of the ^{1}H NMR titration (400MHz, $CDCl_3$) of a) (**4**•Rh_2)@**3**; b) (**4**•Rh_2)@**3** + 0.5 equiv of **3** and c) (**4**•Rh_2)@**3** + 1 equiv of **3**. See Figure 6.1 and Figure 6.2 for proton assigments.

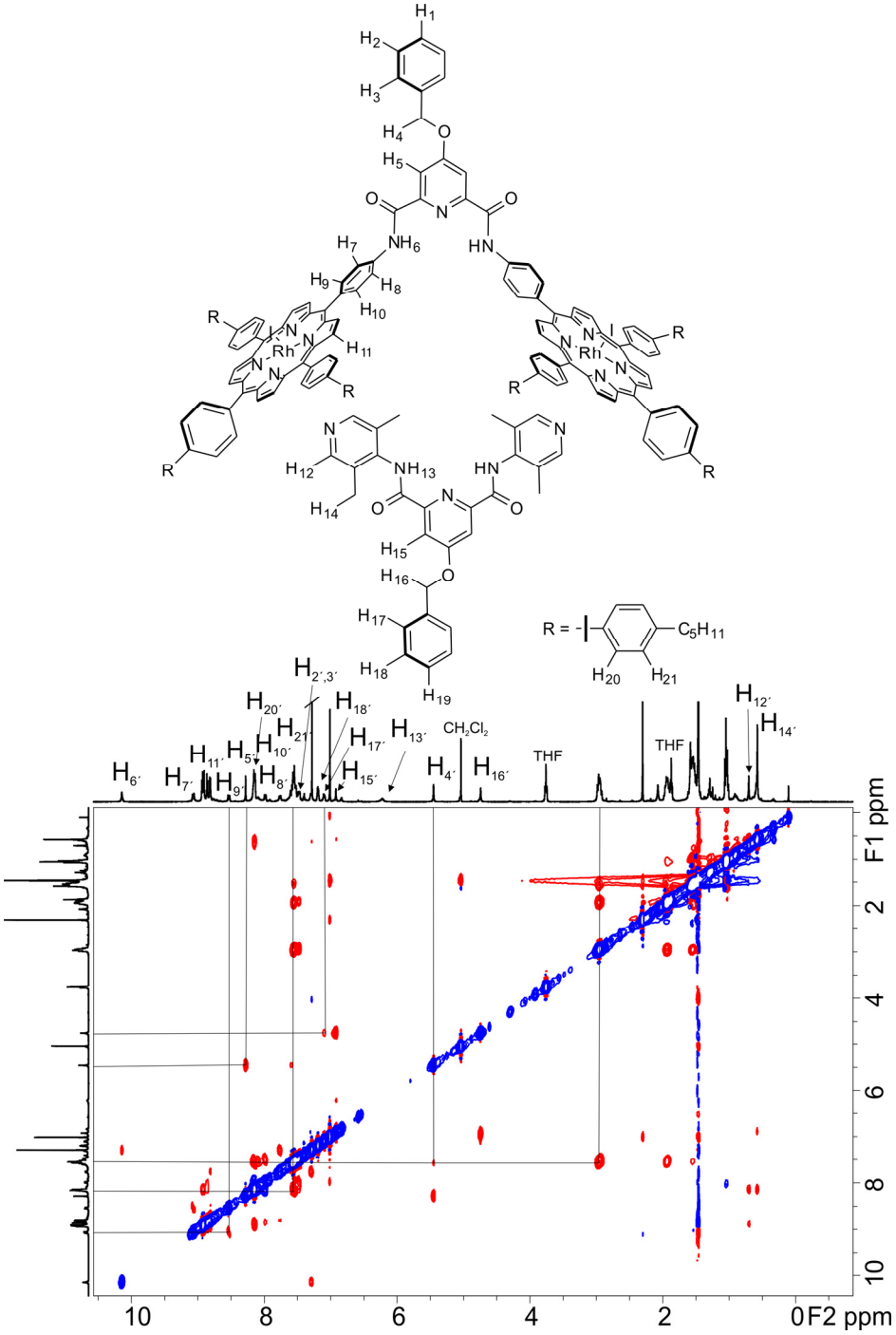

Figure 6.17 ROESY experiment (500 MHz, p15: 0.3 s, $CDCl_3$, $1.0 \cdot 10^{-3}$M) of (**4**·Rh_2)@**3**.

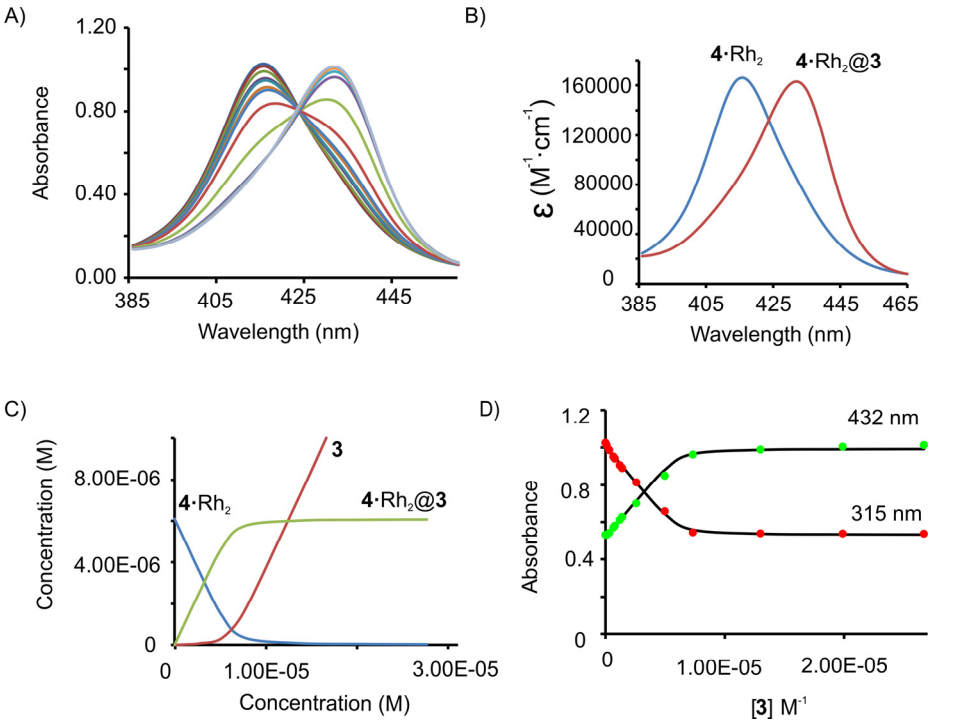

Figure 6.18 Spectra of the UV-visible titration of **4**•Rh_2 with **3** in toluene at 298 K. The concentration of the porphyrin was maintained constant throughout the titration (4.3×10^{-6} M in a 10 mm path cell). Measured UV-visible spectra (a) and predicted spectra (b) of the free porphyrin, and the 1:1 complex formed. Speciation curves during titration (c) and fitting of the titrations data at selected wavelengths (d) to the theoretical binding model.

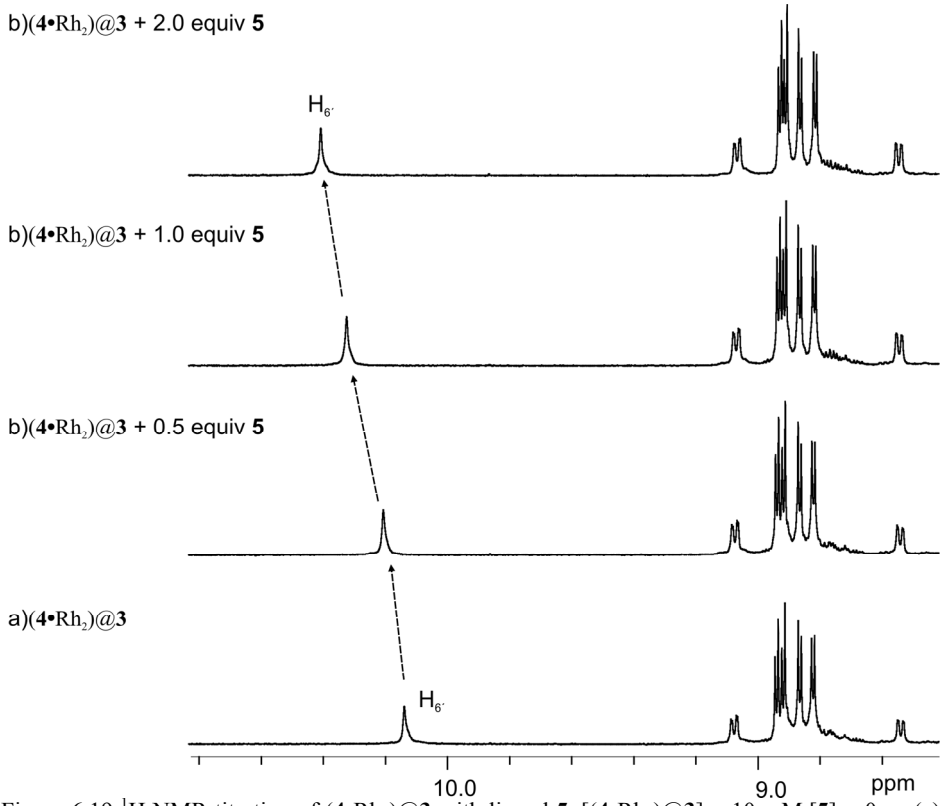

Figure 6.19 ^{1}H NMR titration of (**4**•Rh_2)@**3** with ligand **5**. [(**4**•Rh_2)@**3**] = 10 mM.[**5**] = 0 eq (a), 0.5 eq (b), 1 eq (c), 2 eq (d).

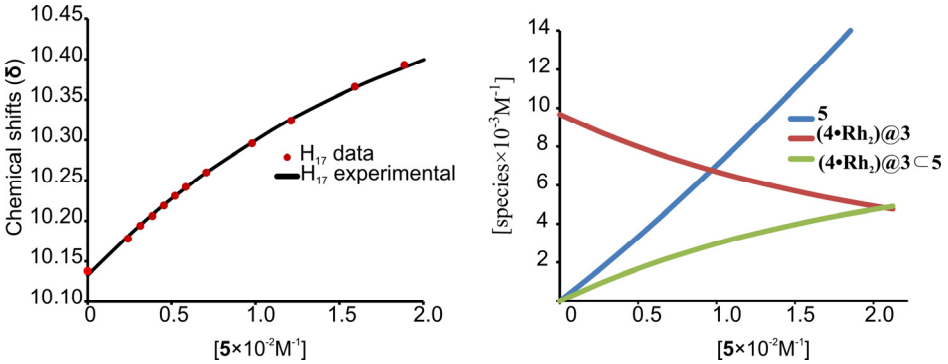

Figure 6.20 Fit of the ^{1}H NMR titration data of the interaction between the linear diamine **5** and the macrocycle (**4**•Rh_2)@**3**. b) Speciation distribution profiles of the species involved in the equilibrium along the titration.

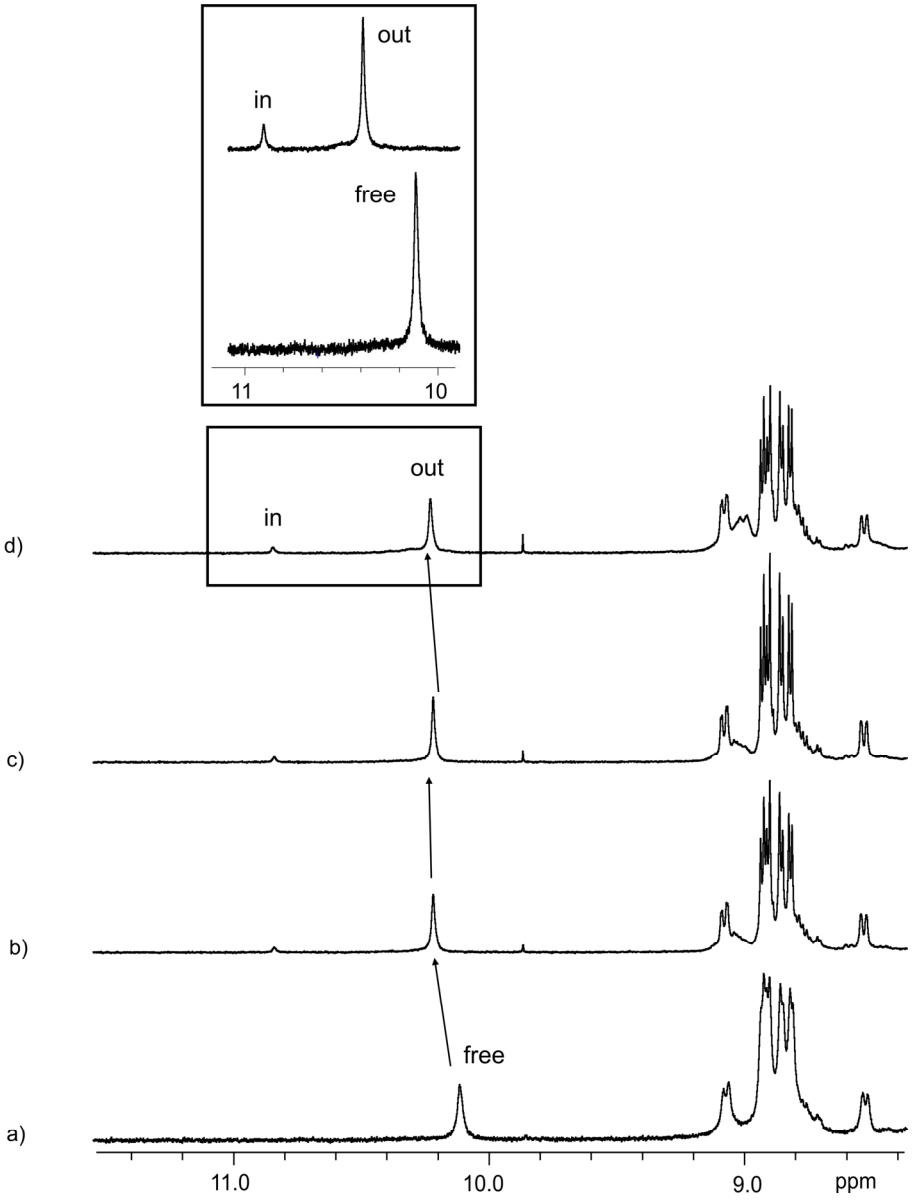

Figure 6.21 ^{1}H NMR titration of (**4**•Rh_2)@**3** with ligand **7**. [(**4**•Rh_2)@**3**] = 7 mM. [7] = 0 eq (a), 0.25 eq (b), 0.5 eq (c), 1 eq (d), 2 eq (e).

6.5 References and notes

[1] J.P. Sauvage, Molecular machines and motors; Springer-Verlag: Berlin, 2001; Vol. 99.
[2] Jeong, K. S.; Choi, J. S.; Chang, S. Y.; Chang, H. Y. *Angew. Chem. Int. Edit.* **2000**, *39*, 1692.
[3] Hunter, C. A.; Low, C. M. R.; Packer, M. J.; Spey, S. E.; Vinter, J. G.; Vysotsky, M. O.; Zonta, C. *Angew. Chem. Int. Edit.* **2001**, *40*, 2678.
[4] Ikeda, T.; Asakawa, M.; Goto, M.; Nagawa, Y.; Shimizu, T. *Eur. J. Org. Chem.* **2003**, 3744.
[5] Mullen, K. M.; Gunter, M. J. *J. Org. Chem.* **2008**, *73*, 3336.
[6] Ballester, P.; Costa, A.; Deya, P. M.; Frontera, A.; Gomila, R. M.; Oliva, A. I.; Sanders, J. K. M.; Hunter, C. A. *J. Org. Chem.* **2005**, *70*, 6616.
[7] Beyler, M.; Heitz, V.; Taesch, J.; Sauvage, J. P. *J. Porphyrins Phthalocyanines* **2011**, *15*, 848.
[8] Planells, M.; Pelleja, L.; Ballester, P.; Palomares, E. *Energ Environ Sci* **2011**, *4*, 528.
[9] Pintre, I. C.; Pierrefixe, S.; Hamilton, A.; Valderrey, V.; Bo, C.; Ballester, P. *Inorg. Chem.* **2012**, *51*, 4620.
[10] SPECFIT, version 3.0; Spectra Software Associates.
[11] Geometries of the complexes were refined by performing an optimize geometry calculation with Molecular Mechanics using augmented MM3 parameters as implemented in the software CAChe WorkSystem Pro Version 6.1.12.33, Fujitsu Limited. A conjugate gradient method was used for energy minimization with a convergence energy criterion of 0.001 kcal/mol.
[12] HyNMR2008

Chapter 7

General Conclusions and Future Perspectives

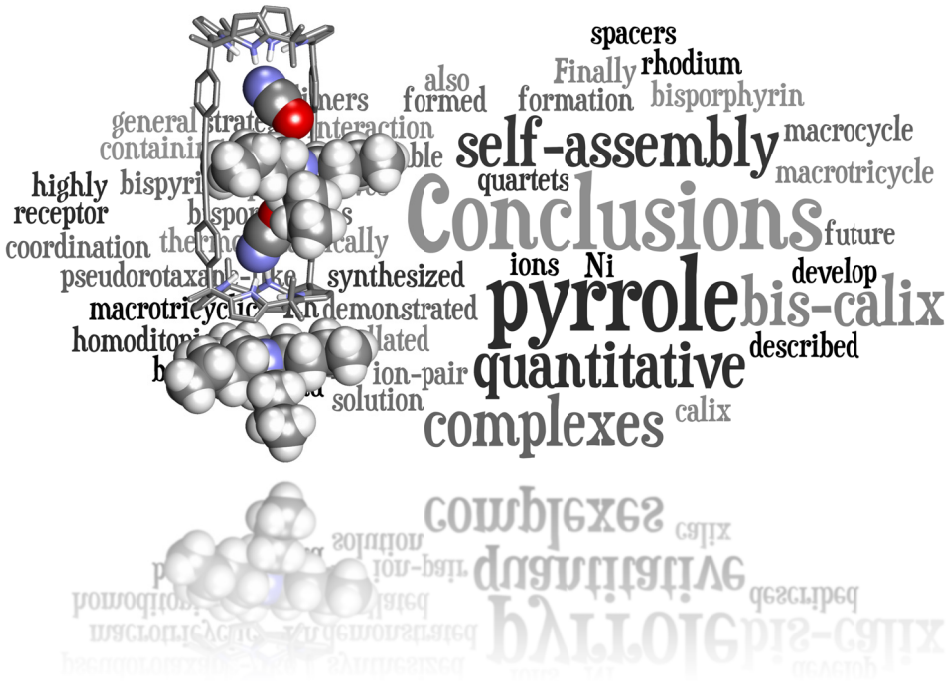

The work herein presented was focused on the study of molecular assemblies based on calix[4]pyrrole and porphyrins and this chapter summarizes the general conclusions that can be deduced from this doctoral thesis.

A homoditopic bis-calix[4]pyrrole macrotricycle was synthetized and its topology and binding properties were used to develop three general strategies for the quantitative self-assembly of pseudorotaxane-like complexes. In one of this strategies, the polyatomic anion of an ion pair is recognized by the supramolecular complex that results when a neutral heteroditopic 3,5-pyridinecarboxamide-*N*-oxide linear molecule threads the homoditopic macrotricycle. The counter ion is coordinated externally to the macrocyclic structure. This [2]pseudorotaxanes were structurally and thermodynamically fully characterized. The same templating strategy was applied to other bis-amidepyridine *N*-oxide derivatives to produce similar self-assembled structures. Different polyatomic anions derived from tetrabutylammonium (TBA) salts were used to template the assembly of analogous [2]pseudorotaxanes and these structures are unprecedented examples of four particle aggregates with interwoven topology. Attempts in exploiting this methodology of pseudorotaxane assembly in the synthesis of mechanically interlocked molecules (i.e. rotaxanes) through a "capping" approach were also presented.

Additionally, this bis-calix[4]pyrrole macrotricyclic receptor has been used in the assembly of various thermodynamically stable 1:1 inclusion complexes with different bipyridine bis-*N*,*N*′-oxides in apolar solvents. Interestingly, it was found that when axially chiral bipyridine bis-*N*,*N*′-oxides are included into the receptor, the enantiomer interconversion of the chiral ligand is facilitated by the reduction of its racemization barrier in 2.2 kcal/mol. Studies in solution and in the solid state evidence that the hydrogen bond interactions established in the *host-guest* complexes force the elongation of the bipyridine bis-*N*,*N*′-oxide ligand. Such elongation most probably stabilizes the transition state of the racemization process. The influence of the coordination of bipyridine bis-*N*,*N*′-oxides ligands within shorter versions of the macrocycle is currently under study. In that case, the destabilization of the transition state of the racemization process is expected due to the compression of the bipyridine bis-*N*,*N*′-

oxides ligands. Additionally, *ortho* substituted bipyridine bis-*N*,*N*´-oxides were used as linear components for the preparation of interlocked molecular architectures as [2]pseudorotaxanes. This methodology opens the possibility to use *ortho* substituted bipyridine bis-*N*,*N*´-oxides as linear components for the preparation of different mechanically-interlocked molecular architectures.

The formation of thermodynamic and kinetically highly stable complexes of ion-pair dimers and quartets of ions by a bis-calix[4]pyrrole macrotricyclic receptor has been also achieved. It was demonstrated that this receptor binds either two chloride or cyanate tetrabutylammonium ion-pairs (a quartet of ions) yielding five component assembled complexes through a highly cooperative process ($\alpha > 10^5$). This is one of the highest cooperative binding process reported to date using a synthetic receptor. The complexes have a structure with a *cascade*-like arrangement of the ion pairs where one ion-pair is bound in a *close*-contact geometry while the other in a *host*-separated arrangement. The proposed structures in solution for the complexes are supported by an array of ^{1}H NMR experiments and also by single crystal X-ray diffraction analysis. Additionally, the exclusive and quantitative formation of the ion-pair hetero-dimers was also achieved. Importantly, most of the ion-pair dimeric complexes were also detected in the gas-phase. The use of a ion pairs containing a methyltrioctylammonium cation (MTOA) instead of tetrabutylammonium rendered the binding process significantly less cooperative. This finding together with the results of ^{1}H NMR experiments suggest that in the homodimeric complex involving MTOA cations both bound ion-pairs feature a *host*-separated binding mode. The equimolar combination of TBA and MTOA salts allowed the self-assembly of hetero ion-pair dimeric complexes with *cascade* arrangement by means of cooperative binding processes. Remarkably, in these latest complexes the MTOA cation seems to be selectively located in the outer position of the receptor. The interwoven structure of the aforementioned ion quartet complexes can be considered as a novel strategy for the assembly of pseudorotaxanes.

The previously described templating strategies for the assembly of [2]pseudorotaxanes open the possibility to the design of diverse mechanically interlocked molecules such as catenanes, rotaxanes or molecular shuttles based on rotaxanes. Such interlocked

molecules are expected to possess interesting dynamic features that could be controlled by external chemical stimuli, i.e. presence or absence of anions.

We have also synthesized two Ni metallated bisporphyrins containing calix[4]pyrrole spacers. The two receptors possess slightly different orientation of the porphyrin rings as a result of the different linkers used to connect the porphyrin and the calix[4]pyrrole units. However, in both cases, the porphyrin moiety used was the octaethylporphyrin unit. The attempts to use Zn metallated *mesityl*-substituted porphyrins in the synthesis of related bisporphyrins were unsuccessful. Preliminary results for the use of one of these bis-porphyrins as porphyrin tweezer receptors in the recognition of the tetrabutylammonium salt of the [6,6]-phenyl-C_{61}-butyric carboxylic acid were presented. In this complex the calix[4]pyrrole spacer oriented the porphyrin units in a co-facial disposition and also participates as an additional binding site in the recognition of the [6,6]-phenyl-C_{61}-butyric carboxylate. Further studies are necessary in order to characterize the complex thermodynamically and kinetically.

Finally, we have demonstrated the quantitative self-assembly of a macrocycle formed by the interaction between a rhodium bisporphyrin and a bispyridyl ligand through two Rh(III)-N coordination bonds. The use of rhodium porphyrins for the self-assembly of the macrocycle provided a sensible increase in the thermodynamic stability of the cyclic structure compared to their Zn(II) counterparts. Unfortunately, UV-Vis spectroscopy studies did not allow the accurate determination of the stability constant of the macrocyclic assembly due to its large estimated magnitude ($> 10^7$ M^{-1}). The threading of the self-assembled macrocycle with linear neutral diamides through the establishment of four intermolecular hydrogen bonding interactions has been accomplished and yielded complexes with [2]pseudorotaxane and [2]rotaxane like topologies. The use of Rh(III) metallated porphyrin instead of Zn(II) analogue induces a sensible increase in the kinetic stability of the rotaxane-like structure, but has an almost negligible effect in its thermodynamic stability. In this case, the thermodynamic stability of the [2]rotaxanes is mainly controlled by the formation of four hydrogen-bonding interactions between the linear component and the amide groups of the macrocyclic assembly. These intermolecular interactions were identical in the two [2]rotaxane

architectures constructed using Rh(III) or Zn(II) metal centers in the bispophyrin unit of the macrocyclic component.

Abreviation List

ACN	-	Acetonitrile
B3LYP	-	Becke. Three parameter, Lee-Yang-Parr
Cl	-	Chlorine
DMF	-	Dimethylformamide
DMAP	-	4-Dimethylaminopyridine
DOSY	-	Difussion-Ordered SpectrocopY
EM	-	Effective molarity
ESI	-	Electrospray ionization
EtOAc	-	Ethylacetate
EXSY	-	EXchange SpectroscopY
ITC	-	Isothermal titration Calorimetry
kcal	-	kilocalorie
MTOA	-	Methyltrioctylammonium
MS	-	Mass spectrometry
NMR	-	Nuclear Magnetic Resonance
NOE	-	Nuclear Overhauser Effect
NOESY	-	Nuclear Overhauser Effect SpectroscopY
Oxone®	-	Potassium peroxymonosulfate
Pd/C	-	Palladium on carbon
ROESY	-	Rotating frame Overhauser Effect SprectroscopY
r.t.	-	Room temperature
TBA	-	Tetrabutylammonium
THF	-	Tetrahydrofurane
TLC	-	This Layer Chromatography
UV	-	Ultraviolet